



---

**THE EFFECT OF METAL SULFIDES ON HOLE AND ELECTRON  
TRANSPORT BUFFER LAYERS IN ORGANIC PHOTOVOLTAICS:  
EXPERIMENTAL AND NUMERICAL DEVICE SIMULATION  
INVESTIGATIONS.**

---

Author:  
**Michael Adepelumi Adedeji**

Supervised by:  
**Prof. Geneve Tessema Mola**

A thesis presented for the award of  
Doctor of Philosophy in Physics (Materials Sciences)

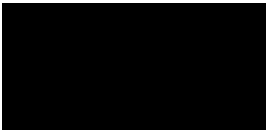


School of Chemistry and Physics  
University of Kwazulu-Natal, Pietermaritzburg campus  
South Africa  
November 2022

# Preface

The research was carried out by the candidate under the supervision and guidance of Professor Genee Tessema Mola, of the School of Chemistry and Physics in the College of Agriculture, Engineering, and Science, University of Kwazulu-Natal, Pietermaritzburg Campus. This research was financially supported by UKZN, National Research Foundation (NRF) funds - South Africa, the Commonwealth Scholarships Commission in the United Kingdom (CSC-UK) and the University of Lagos, Nigeria. This project has not been submitted for degree award in any other University, and all results reported herein are due to the investigations by the candidate.

Signature (Student): .....  ..... Date: 12<sup>th</sup> November, 2022.

Signature (Supervisor):.....  ate: .....2022.

# Abstract

Organic solar cells (OSCs) are promising alternative renewable energy sources that often suffer from insufficient absorption of solar radiation, short exciton lifetimes and small diffusion length of their charge carriers. Several strategies are being investigated to overcome these challenges in a move towards the commercialization of this solar cell technology. Increasing the path-length of incident electromagnetic radiation within the photo-absorbing layer of the solar cell, may elongate the time that light spends within the solar cell, thereby increasing the light-matter interaction time and consequently the photo-absorption within the photo-active material of the solar cell. The process described may be accomplished if suitable plasmonic metal nano-structures are added into the solar cell matrix. This intervention may also enhance the collection of the photo-generated charge carriers.

The effects of metal sulphide nanoparticles incorporation in organic solar cells were studied and presented in this thesis. The metal sulphide nanoparticles were characterized and introduced into the hole- and electron- transport layers of fullerene and non-fullerene electron acceptors based solar cells, to elicit improved photo-absorption via the localized surface plasmon effects and facilitate better charge collection at the electrodes. Devices were fabricated both in an ambient environment and in a controlled environment (Nitrogen filled glovebox). The metal sulphide nanoparticles were incorporated in the fabricated solar devices using both the conventional and inverted device architectures. The power conversion efficiencies of the devices improved significantly after the incorporation of these nanoparticles. Device numerical simulation studies were also performed to reproduce some of the experimental results with a view to further investigating the devices and discussing their charge transport characteristics. The simulation results show improved charge carrier characteristics from the metal-sulphide doped devices by way of improved conductivity and shifted Fermi level offsets which were aided by the presence of the metal-sulphides.

Asides from successfully achieving improved device performances in the investigations and simulations carried out in this thesis, this thesis successfully demonstrated the incorporation of nano-composites in non-fullerene acceptors-based organic solar cells for the first time to the best of our knowledge.

# Dedication

To the Almighty God for His mercies and the gift of eternal life - Psalm 136:1  
To the loving memories of my parents

## Declaration - Plagiarism

**I, Michael A. Adedeji, declare that:**

1. The research reported in this thesis, except where otherwise indicated, is my original research.
2. This project has not been submitted for any degree or examination at any other university.
3. This project does not contain other persons data, pictures, graphs or other information, unless specifically acknowledged as being sourced from other persons.
4. This project does not contain other persons' writing, unless specifically acknowledged as being sourced from other researchers. Where other written sources have been quoted, then:
  - Their words have been re-written but the general information attributed to them has been referenced.
  - Where their exact words have been used. then their writing has been placed in italics and inside quotation marks, and referenced.
5. This project does not contain text, graphics or tables copied and pasted from the Internet, unless specifically acknowledged, and the source being detailed the thesis and in the references sections.

Signed:  \_\_\_\_\_

Date: 12<sup>th</sup> November, 2022

## Publications

### Declaration - Publications

I declare that the contents of this dissertation are from the research papers indicated below.

1. **Michael A. Adedeji**, M.S.G Hamed, G.T.Mola. Light trapping using copper decorated nano-composite in the hole transport layer of organic solar cell, *Solar Energy* 195 (2020) 310-317. My role in this article included designing the experiment, fabrication of the solar cells, data analysis and manuscript writing. The manuscript was thereafter sent to the co-authors for editing before submitting for publication. I later on addressed most of the reviewers' comments as well.

2. **Michael A. Adedeji** and Genevieve Tessema Mola, Numerical investigation of the effects of copper sulfide nanoparticles on hole transport layer of thin-film organic solar cells, *Journal of Computational Electronics* 21.1 (2022): 128-136. doi.org/10.1007/s10825-021-01843-z. My role in this article simulation design and execution, data analysis and manuscript writing. The manuscript was thereafter sent to the co-author for editing before submitting for publication. I addressed all of the reviewers' comments for this publication

3. **Michael A. Adedeji**, Rodrigo Garcia-Rodriguez, Matthew L. Davies, Yong Zhang, and Genevieve Tessema Mola, Plasmon-Enhanced Charge Transport Processes for Improved Collection of Photo-Current in Polymer Solar Cells. *ACS Applied Energy Materials* 2022 5 (10), 12503-12512. doi: 10.1021/acsaem.2c02146. My role in this published article included designing the experiment, fabrication of the solar cells, data analysis and interpretation. I also designed and executed the numerical simulation sequences. I thereafter summarized the experimental and the simulations into a manuscript report before sending to the co-authors and subsequently submitted for journal publication. I answered most of the reviewers' comments for this publication as well.

4. **Michael A. Adedeji**, Abiodun Kazeem Ogundele, Matthew L. Davies, Genevieve Tessema Mola, The effect of silver-sulfide on charge transport buffer layers in fullerene based polymer solar cell, Manuscript submitted for publication at *Solar Energy*. My role in this article included designing the experiment, fabrication of the solar cells, data analysis. My role in this manuscript included designing the experiment, fabricating the thin film solar cells, data analysis and interpretation. I also designed and executed the numerical simulation sequences. I thereafter summarized the experimental and the simulations into a manuscript report before sending

to the co-authors and subsequently submitted for journal publication.

## Publications that are not included in this thesis

1. M.S.G.Hamed, **Michael A. Adedeji**, Y.Zhang, and G.T.Mola, Silver-sulphide nano-composite assisted photons capture in thin-film polymer solar absorber, *Applied Physics A* (2020) 126(3)1-9. doi.org/10.1007/s00339-020-3389-8. My role in this article was to assist the main author during the experiments, characterizations, and data analysis. I edited the manuscript before it was sent out for publication.

2. G.T Mola, M.C Makhosazane, M.S.G Hamed, **Michael A. Adedeji**, G.M. Xolani, K. Amit, S. Gaurav, and Y. Zang. Local surface plasmon resonance assisted energy harvesting in thin film organic solar cells, *Journal of Alloys and Compounds* 856 (2021): 158172. My role in this article was to assist the main authors during the experiments, characterizations, and data analysis. I interpreted some of the results and edited the manuscript before it was sent out for publication.

3. Mohammed S.G. Hamed, **Michael A. Adedeji** and Geneve Tessema Mola, Rare-Earth-Metal-induced plasmon resonances for enhanced photons harvesting in inverted thin film organic solar cells, *Energy Fuels* (2021), 35, 15010-15017. My role in this article was to assist the main authors during the experiments, characterizations, and data analysis. I interpreted some of the results and edited the manuscript before it was sent out for publication.

# Acknowledgment

I give God the glory for seeing me through. He's been a very present help in times of need - Psalm 46:1.

I wish to say a big thank you to my supervisor, **Prof Genene Tessema Mola** for his constant support throughout my doctoral studies. Thank you for your patience, motivation, enthusiasm, knowledge and mentorship. I've become a better researcher by learning under you. Thank you for encouraging to go for new things, for your total support during my commonwealth scholarship application and facilitating the link with Prof. Mathew Davies. God bless you real good Prof.

I would like to thank the University of KwaZulu Natal, Pietermaritzburg Campus, the School of Chemistry and Physics - UKZN for the free tuition for three years, making it easy for me to study without financial worries. Appreciation to the University of Lagos, Nigeria and the Physics department, Unilag for my study leave, enabling me to come to South Africa for the PhD program.

I want to appreciate the Commonwealth Scholarships Commission in the United Kingdom for the Split-site scholarship I was offered to Swansea University, Swansea, UK where I spent 10months at the Applied Photochemistry Lab, SPECIFIC, School of Engineering with Professor Mathew Davies. Many thanks to the Applied photochemistry group members (Rodrigo, Emmanuel, Rhys and the others) and great guys from other groups (Ram Datt, Michael spence, Suzanne and very many others too numerous to finish mentioning). Thank you all.

Huge thanks to my friends and lab members here in the Materials science group (Xolani, Mohammed, Yotasha, Makose, Jude, Abiodun, Abdallah and Solomon). Thank you for the good times, the advice, invaluable support, discussions, patience and encouragement during the entire research period.

I would like to thank the National Research Foundation (NRF) for their financial assistance and the UKZN Microscopy and Microanalysis Unit(MMU) for several SEM and TEM measurements.

I want to say a big thanks to all my friends, colleagues in other departments,

neighbours, church members, prayer partners and church members (in South Africa, Swansea and Nigeria) for all the emotional, financial and other forms of supports. Drs Abiola Ilori, Abidemi Adebayo, Adeleye, Abimbola, Akomolafe and Bro Johnson, Sis Funke etc... Thank you all, God bless you.

I can not thank you enough, my darling and lovely wife, fragrance mixed with the warmth of tenderness, **Mrs. Morenike A. Adedeji**, for your emotional, and psychological support, and sacrifices. Thank you for taking care of the homefront while I've been away. God bless you. I also appreciate the sacrifices of my children Emmanuel and EbunOluwa, who had to cope with daddy's absence.

————— - SI YA BONGA JESU —————

# List of Abbreviations

A	Acceptor
Ag	Silver
Au	Gold
Ag <sub>2</sub> S	Silver sulphide
Al	Aluminum
BHJ	Bulk heterojunction
CuS	Copper sulphide
D	Donor
DSSCs	Dye-sensitized solar cells
EDX	Energy dispersive X-ray
$E_g$	Energy gap
ETL	Electron transport layer
FF	Fill factor
FWHM	Full width at half maximum
GPDVM	General-purpose Photovoltaic Device Model
HTL	Hole transport layer
HOMO	Highest occupied molecular orbital
ITO	Indium tin oxide
ITIC-Th	3,9-bis(2-methylene-(3-(1,1-dicyanomethylene)-indanone))-5,5,11,11-tetrakis(5-hexylthienyl)-dithieno[2,3-d:2',3'-d']-s-indaceno[1,2-b:5,6-b']dithiophene
$J_{SC}$	Short circuit current density
J-V	Current density-voltage Curve
LiF	Lithium fluoride
LUMO	Lowest unoccupied molecular orbital
LSPR	Localized surface plasmon resonance
LWF	Low work function

MoO <sub>3</sub>	Molybdenum trioxide
NC	Nanocomposite
NFA	Non Fullerene Acceptor
NIR	Near-infrared
NPs	Nanoparticles
OFETs	Organic field-effect transistors
OLEDs	Organic light-emitting diodes
OSCs	Organic solar cells
OPV	Organic photovoltaic
P3HT	Poly (3-hexylthiophene)
PCE	Power conversion efficiency
PCBM	[6,6]-phenyl-C61-butyric acid methyl ester
PC71BM	[6,6]-Phenyl-C71-butyric acid methyl ester (PC71BM)
PEDOT:PSS	Poly(ethylene-3-4-dioxy thiophene):poly styrene sulphonate
PFN-Br	Poly(9,9-bis(3'-(N,N-dimethyl)-N-ethylammonium-propyl-2,7-fluorene)-alt-2,7-(9,9-dioctylfluorene))dibromide
PL	Photoluminescence
$P_{max}$	Maximum power
PSCs	Polymer solar cells
PTB7	poly4,6-(2-ethylhexyl-3-fluorothieno[3,4-b]thiophene-2-carboxylate)alt-2,6(4,8-bis(2-ethylhexyloxy) benzo[1,2-b:4,5-b]dithiophene)
PTB7-Th	Poly[4,8- bis(5-(2-ethylhexyl)thiophen-2-yl)benzo [1,2-b;4,5-b']dithiophene-2,6-diyl-alt-(4-(2- ethylhexyl)-3-fluorothieno[3,4-b] thiophene-)-2-carboxylate-2-6-diyl]
PV	Photovoltaic
PVP	Polyvinyl pyrrolidone
SCAPS	Solar Capacitance Software
SCLC	Space charge limited current
SEM	Scanning electron microscope/microscopy
SPP	Surface plasmon polariton
$R_s$	Series resistance
$R_{sh}$	Shunt resistance
TEM	Transmission electron microscope/microscopy
TFOPVs	Thin film organic photovoltaics
TMM	Transfer Matrix Method

UV-Vis	Ultra violet-visible
$V_{max}$	Maximum voltage
$V_{OC}$	Open circuit voltage
XRD	X-ray diffractometer/diffraction
ZnO	Zinc oxide

# List of Figures

1.1	World's carbon intensity of electricity [7]. . . . .	3
1.2	World's energy consumption by energy sources[7]. . . . .	4
2.1	(a) Single layer device schematics (b) Bilayer device schematics (c) Exciton dissociation at a D/A interface (d) Bulk heterojunction device schematics [16]. . . . .	13
2.2	Individual atomic orbitals often overlap with one another to create bonding and anti-bonding molecular orbitals[54] . . . . .	16
2.3	Ordered and Dis-ordered materials' Densities of energy states (DOS) displaying narrow and wide bandwidths respectively[54]. . . . .	16
2.4	Mechanisms of photo-current generation in organic solar cells[68]. . .	19
2.5	Current density - Voltage (J-V) characteristics of OPVs . . . . .	20
2.6	Solar cell's equivalent circuit diagram with series and shunt resistances included. . . . .	21
2.7	Conjugated polymers (donors), fullerenes (acceptors) and their derivatives, and non fullerene acceptors' chemical structures[89]. . . .	23
2.8	Photon-absorption enhancement in OPV devices via some plasmonic resonance mechanisms (a) Light scattering (b) Localized Surface Plasmon Resonance (LSPR)(c) Surface Plasmon Polariton Effect[120]. . .	25
2.9	(a)LSPR on a spherical nano-structure due to interaction with an electric field causing collective oscillation of the electronic cloud[47]. (b) LSPR sub-mechanisms: the far-field and the near-field coupling[117].	26
2.10	(a) Device structure of the solar cell embedded with bi-metallic NPs of Au and Ag (b) TEM images of Ag, Au, and bi-NPs (c) J-V curves of solar cells with and without NPs (d) EQE spectra of PTB7:PC70BM with and without NPs[163] . . . . .	30
2.11	Plasmonic nano-structures embedded in the rear charge transport layer[149]. . . . .	32

3.1	Typical device fabrication processes for inverted solar cells[15]	48
3.2	DoS diagram adopted in the model. The e/h capture and release processes for one electron trap. Similar processes take place in all electron and hole traps[24]	50
4.1	Schematics for P3HT:PC61BM photoactive layer BHJ OSC and CuS-nanoparticles doped PEDOT:PSS buffer HTL	57
4.2	CuS powder HRTEM images (a & b), HRSEM (c) and the Energy Dispersive X-ray (EDX) (d).	58
4.3	Absorption spectra of the solar devices prepared at different CuS concentrations in PEDOT:PSS (b)Optical absorption of CuS NPs suspension in deionized water	60
4.4	J–V plots of devices fabricated with/without CuS-doped PEDOT:PSS as HTLs at various CuS doping levels.	61
4.5	SCLC curves of devices fabricated with CuS-doped PEDOT:PSS as HTLs at various CuS doping levels	63
4.6	Stability of the solar cells fabricated with CuS and 0.05% CuS doped PEDOT:PSS hole transport layers stored in ambient laboratory conditions.	65
5.1	Various photoactivity that may be induced by the presence of plasmonic nanomaterials embedded in a semiconducting medium in the presence of electromagnetic field. Reproduced with permission from ref[26]. Copyright Elsevier, 2018.	76
5.2	Copper sulphide (CuS) nanoparticles-doped hole transport layer (PEDOT:PSS) in a P3HT/PCBM organic solar cell.	78
5.3	(a)Optical absorption profile of the OSC under investigation (b) Measured optical absorptions of the pristine and doped OSC devices (c) The modified device schematics showing the introduced modified hole selective layer (MHSL)	79
5.4	J-V characteristics of laboratory fabricated and simulated devices	81
5.5	J–V curves taken from simulated OSCs at different valence band’s DOS in the Modified Hole Selective Layer (MHSL) with values A, B and No MSHL giving results that are in close agreement to actual fabricated Cus-doped devices	82
5.6	CELIV plots for the three devices	83

5.7	Plots of recombination time constants as a function of MHSL thicknesses for the three devices . . . . .	84
5.8	Device performances plotted as a function of MHSL thicknesses. . . . .	85
5.9	(a) Average carriers density at $P_{max}$ and (b) recombination time constant of doped and undoped devices plotted as a function of fermi offsets at the anode. . . . .	86
5.10	Device performance characteristics for the devices as functions of fermi offsets at the anode. . . . .	87
6.1	(a) Collective displacement of electron cloud due to interaction of metal nanoparticle with the incident electric field. (b) Possible plasmonic processes that may occur in a semiconducting medium when plasmonic materials interact with incident electromagnetic fields (i) charge carriers excitation (ii) light scattering (iii) hot electron injection (iv) heat transfer (v) local electric field enhancement (iv) dipole resonance energy transfer. Reproduced with permission from refs[26, 27]. Copyrights MDPI, 2016 and RSC, 2020. . . . .	94
6.2	Schematics device diagram (a) and energy levels alignment (b) for organic solar cell whose ZnO ETL has been incorporated with silver sulfide NPs. . . . .	95
6.3	(a) XRD and (b) SEM of the silver sulfide powders. . . . .	97
6.4	(a) Normalized absorption (inset: bandgap extrapolation) of the silver sulfide powders. (b) Absorbency of the TFOPV films with/without NPs incorporation. . . . .	99
6.5	Photo-luminescence of thin film solar cells using ETL incorporated with $Ag_2S$ nanoparticles. . . . .	101
6.6	J-V plots of PTB7-Th:ITIC-Th solar cells fabricated at (a) different concentration of NPs incorporation in the ZnO ETL for the $0.1\text{ cm}^2$ devices and (b) different device effective areas at 0.33 wt% nanoparticle incorporation. . . . .	102
6.7	External quantum efficiency measured from solar cells that use ETL with/without $Ag_2S$ nano-particles. . . . .	103
6.8	Numerical investigation of the temperature dependence of device parameters via device simulation for NPs-doped and pristine HTL devices (a) $V_{oc}$ and $J_{sc}$ versus temperature (b) Fill factor and PCE, respectively. . . . .	106
6.9	J-V curves of the simulated $Ag_2S$ -doped devices with different doped-ETL/Active layer interface defect densities (inset: similar simulation with the pristine devices). . . . .	107

6.10	The photo-assisted capacitance–voltage characteristics of the a) pristine ETL and the b) NPs-incorporated ETL devices at various illumination intensities. . . . .	108
7.1	Schematic device structure of TFPSC . . . . .	118
7.2	(a) The SEM (b) The HR-TEM (Inset: HR-TEM showing fringes and lattice spacing) (c) The XRD of the silver sulfide nanoparticles and (d) Optical absorption of the silver sulfide nanoparticles in de-ionized water (inset: bandgap estimation from the tauc’s plot) . . . . .	120
7.3	Absorption spectrum of the devices thin films at varying silver sulfide NPs doping concentration of the PEDOT:PSS HTL . . . . .	123
7.4	Current density - Voltage characteristics of the devices containing varying conc. of $Ag_2S$ NPs doping in the PEDOT:PSS HTL . . . . .	124
7.5	Incident photon-to-current conversion efficiency (IPCE) curves for the PEDOT:PSS-doped devices . . . . .	125
7.6	Normalized UV-Vis absorption of PTB7-Th:PC71BM active layers coated on ZnO films that had been incorporated w/wo silver sulfide NPs . . . . .	126
7.7	Current density - Voltage curves for the devices containing varying concentration of nano-particle doping in the Zinc oxide ETL . . . . .	127
7.8	Comparison of the experimental and simulated current density - voltage (J-V) characteristics of the devices containing varying conc. of $Ag_2S$ NPs doping in the zinc oxide ETL . . . . .	130
7.9	CELIV plots for the $Ag_2S$ NPs-incorporated ETL devices . . . . .	132
7.10	(left panel) Average carriers density at $P_{max}$ and (right panel) Recombination time constant of $Ag_2S$ NPs -incorporated ETL devices plotted as a function of Fermi offsets at the cathode . . . . .	133
7.11	(left panel) Maximum Power - $P_{max}$ and (right panel) Average carriers density at $P_{max}$ of $Ag_2S$ NPs -incorporated ETL devices plotted as a function of Temperature . . . . .	134

# List of Tables

2.1	OPV devices with plasmonic nano-structures in the active layer. . . .	29
2.2	OPV devices with plasmonic nano-structures in the buffer layer. . . .	31
4.1	The solar cell parameters of the best performed devices. . . . .	63
4.2	The charge transport parameters of devices fabricated with CuS-doped PEDOT:PSS as HTLs various CuS doping levels . . . . .	66
5.1	Baseline parameters . . . . .	81
5.2	Device performance parameters for varying $N_V$ in the MHSL. . . . .	82
6.1	Silver sulfide NPs XRD analysis . . . . .	100
6.2	Device performance parameters for solar cells fabricated with/without silver sulfide-incorporated ZnO as the ETLs at various NPs loading levels and at various effective device areas. . . . .	104
6.3	Simulation device parameters . . . . .	105
6.4	Experimental and simulated solar cells parameters for the 0.15 cm <sup>2</sup> devices . . . . .	107
7.1	Device performance parameters for devices fabricated with/without Ag <sub>2</sub> S-doped PEDOT:PSS as the hole transport layers at various doping levels, the effective device area is 0.15 cm <sup>2</sup> . . . . .	123
7.2	Device performance parameters for devices fabricated with/without Ag <sub>2</sub> S-doped Zinc oxide as the electron transport layers at various doping levels, the effective device area is 0.035 cm <sup>2</sup> . . . . .	126
7.3	Charge transport properties of the doped-ETL thin film organic solar cell devices. . . . .	128
7.4	Baseline parameters for the simulation of NPs-incorporated ETL solar cell . . . . .	131

7.5	Experimental and simulated solar cells parameters for the 0.00 wt%, 0.11 wt% and 0.33 wt% doped-ETL devices. . . . .	131
-----	---	-----

# Contents

<b>1</b>	<b>Introduction</b>	<b>2</b>
1.1	Justification . . . . .	4
1.2	Aim of the thesis . . . . .	5
1.3	Objectives of the thesis . . . . .	5
1.4	Thesis outline . . . . .	7
<b>2</b>	<b>Literature review</b>	<b>12</b>
2.1	General Introduction . . . . .	12
2.2	Charge carrier transport theory . . . . .	15
2.2.1	Molecular energy levels in organic semiconductors . . . . .	15
2.2.2	Charge transport in organic semiconductors and devices . . . . .	17
2.3	Organic solar cells working mechanism . . . . .	18
2.4	Characterizing organic solar cells . . . . .	20
2.5	Photo-absorbing materials for organic solar cells . . . . .	22
2.6	Plasmon resonance as a strategy for improving solar energy harvesting and charge collection . . . . .	24
2.6.1	Light scattering . . . . .	25
2.6.2	Localized surface plasmon resonance (LSPR) . . . . .	26
2.6.3	Surface plasmon polariton (SPP) . . . . .	28
2.6.4	Applications of metal nanoparticles as plasmonic agents in OPVs . . . . .	30
2.7	Metal-sulphides as plasmonic materials in OPVs . . . . .	33

<b>3</b>	<b>Materials, Methods and Device Simulation Modelling</b>	<b>47</b>
3.1	Materials . . . . .	47
3.1.1	The metal-sulphide nano-structures . . . . .	47
3.1.2	Photo-active layer materials . . . . .	48
3.1.3	Charge transport layers . . . . .	48
3.2	Characterizations and characteristics . . . . .	49
3.3	The Simulation Model . . . . .	49
<b>4</b>	<b>Light trapping using copper decorated nano-composite in the hole transport layer of organic solar cells</b>	<b>55</b>
4.1	Abstract . . . . .	55
4.2	Introduction . . . . .	56
4.3	Experimental and Methods . . . . .	58
4.3.1	Materials . . . . .	58
4.4	Results and discussion . . . . .	59
4.4.1	Morphology studies . . . . .	59
4.4.2	Optical absorption of HTL films . . . . .	61
4.4.3	Characterization of TFOSC . . . . .	62
4.4.4	Charge transport properties . . . . .	64
4.4.5	Device degradation . . . . .	66
4.5	Conclusion . . . . .	67
<b>5</b>	<b>Numerical investigation of the effects of copper sulfide nanoparticles on hole transport layer of thin-film organic solar cells</b>	<b>74</b>
5.1	Abstract . . . . .	75
5.2	Introduction . . . . .	75
5.3	The simulation parameters . . . . .	78
5.4	Results and Discussion . . . . .	81
5.5	Conclusion . . . . .	84

<b>6</b>	<b>Plasmon enhanced charge transport processes for improved collection of photo-current in polymer solar cell</b>	<b>92</b>
6.1	Abstract . . . . .	93
6.2	Introduction . . . . .	93
6.3	Materials and methods . . . . .	95
6.3.1	Materials . . . . .	95
6.3.2	Methods . . . . .	95
6.4	Results and discussion . . . . .	96
6.4.1	Silver sulphide characterization . . . . .	96
6.4.2	Optical characteristics of the thin films . . . . .	98
6.4.3	Photovoltaic characteristics . . . . .	101
6.4.4	Device simulation . . . . .	104
6.5	Conclusion . . . . .	110
<b>7</b>	<b>The effect of silver-sulfide on charge transport buffer layers in fullerene based polymer solar cell</b>	<b>116</b>
7.1	Abstract . . . . .	117
7.2	Introduction . . . . .	117
7.3	Materials and methods . . . . .	119
7.3.1	Materials . . . . .	119
7.3.2	Methods . . . . .	119
7.4	Results and discussion . . . . .	121
7.4.1	Nano-particles (NPs) characterization . . . . .	121
7.4.2	Silver sulfide NPs in the HTL . . . . .	122
7.4.3	Silver sulfide NPs in the ETL . . . . .	125
7.4.4	Device simulation . . . . .	128
7.4.5	Discussion on the doped-HTL devices . . . . .	132
7.5	Conclusion . . . . .	134

<b>8 Conclusion and Recommendation</b>	<b>143</b>
8.1 Recommendations . . . . .	144

# Chapter 1

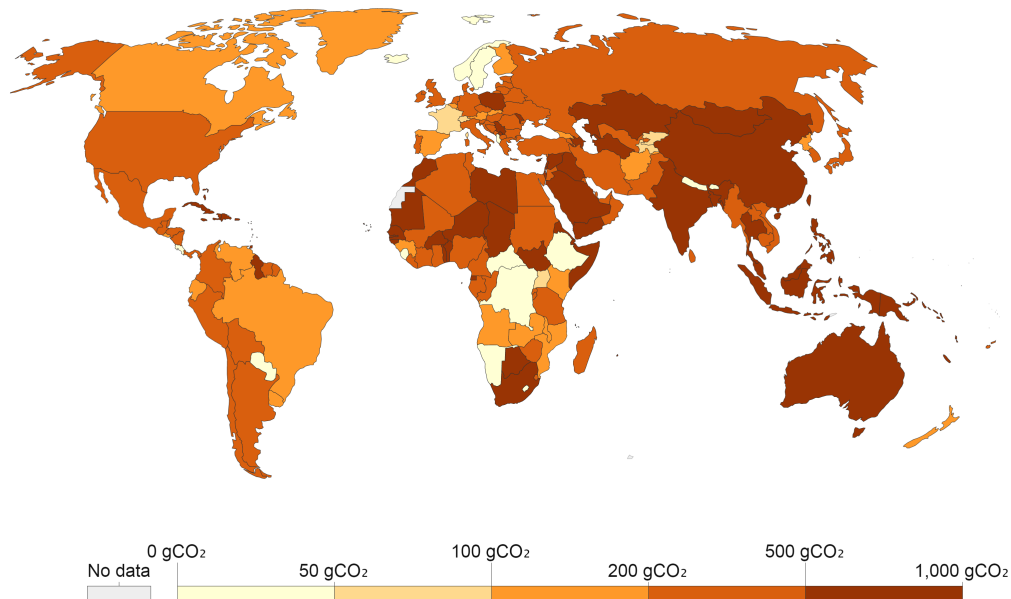
## Introduction

The socio-economic growth of economies all over the world is highly dependent on efficient energy delivery system for the provision of various energy services, as energy use for lighting, refrigerated storage, transportation, education, research, industrial manufacturing and a host of others are consequent upon efficient energy delivery services. The process chain to produce these services starts from the extraction or capture of a primary energy source, conversion into suitable energy carriers and transmission for various end-uses[1]. Fossil fuels, which are heavily carbon-based, had been the prominent traditional energy sources. Their use will eventually dwindle due to their running out at present usage rates. Their continued use also has negative impact on the environment such as severe environmental degradation, climate change and global warming emanating from continued emission of CO<sub>2</sub> into the environment (see Figure 1.1). These concerns have popularized global calls for carbon-neutral energy generation in recent years. The development of clean, environment-friendly alternative energy sources have therefore been at the fore of research and policy making in the last few decades[2, 3, 4, 5, 6].

Global energy consumption is continuously increasing in recent years and will continue to increase. Figure 1.2 shows the percentage distribution of the total energy consumption in 2021 by energy sources. It also shows electricity generation by different energy sources[7]. The renewable energies share in both scenarios has shown appreciable growth in twenty years with the most growth being recorded in the electricity sector. Electricity production from renewable resources has been lagging behind production from non-renewable sources primarily due to higher production cost and perhaps, also because these non-renewable sources are more established and thus more resistant to change. Obviously, more efforts are still needed to bring up the renewable energies share appreciably in the total energy mix. The photovoltaic conversion of solar energy appears to be one of the most promising ways of meeting the increasing energy demands of the future in a time when conventional sources of energy are being depleted. The present growing interest in photovoltaic conversion is a consequence of the concern to identify future sources of energy that will be inexpensive as well as consistent with the maintenance and safety of the environment. Solar energy is one of the most consistent and abundant renewable

## Carbon intensity of electricity, 2021

Carbon intensity measures the amount of greenhouse gases emitted per unit of electricity produced. Here it is measured in grams of CO<sub>2</sub> per kilowatt-hour of electricity.



Source: Ember Climate (from various sources including the European Environment Agency and EIA)

OurWorldInData.org/energy • CC BY

Figure 1.1: World's carbon intensity of electricity [7].

resource, as the sun's lifetime is effectively infinite with respect to human history, with solar energy being continuously radiated to the earth whether it's being used or not.

Photovoltaics or solar cells convert solar energy directly into electricity. They come in inorganic, organic or hybrid forms. Photovoltaic devices are solid state devices therefore they are rugged, simple in design and require little maintenance. Solar cells have been traditionally made with Silicon, Gallium Arsenide, Copper Indium Selenide (CIS) and some other materials[1, 8]. Solar modules are presently heavily Silicon technology based. The technology uses enormous energy and employs toxic, environment-unfriendly chemicals and processes, resulting in expensive, high embodied-energy solar panels and environmental pollution. Organic photovoltaics on the other hand are easier to set-up, employ environmentally benign processes and promise much cheaper modules due to less material usage, low energy for production and versatile applicability[9, 10, 11, 12, 13].

There are several fundamental differences between solar cells made from inorganic and organic semiconducting materials. Inorganic semiconductors typically have much higher charge carriers mobility than polymers and other organic semiconductors[14]. This has remarkable impact on design strategies and efficiency of organic devices. Conversely, the absorption coefficient of organic semiconductors is relatively stronger which partly makes up for their lower mobilities. Hence or-

# More than one-third of global electricity comes from low-carbon sources; but a lot less of total energy does Our World in Data

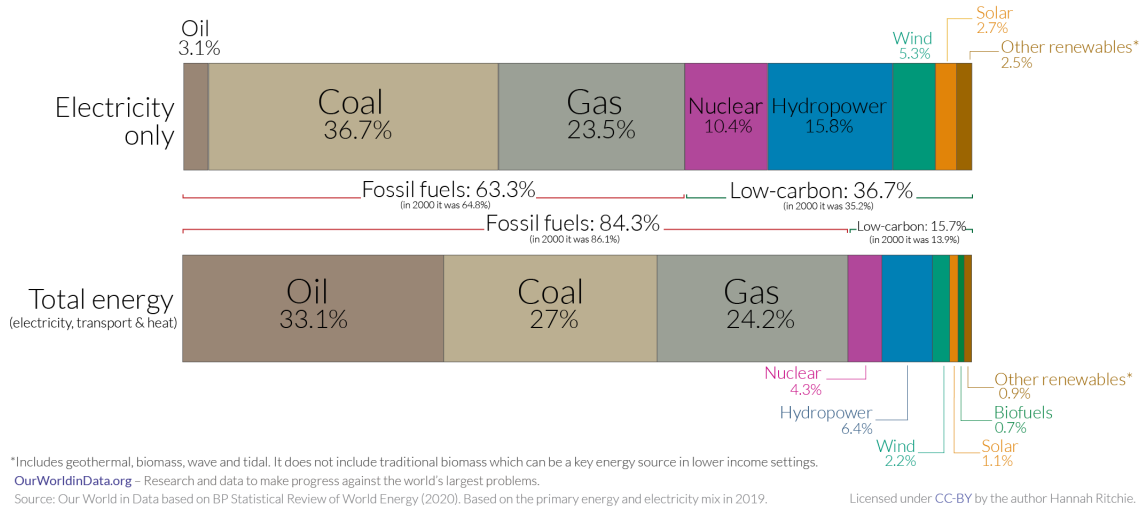


Figure 1.2: World's energy consumption by energy sources[7].

organic materials can record high absorption even in thin film devices, a feat that is not easily achieved in inorganic photovoltaics. The diffusion length of excitons in crystalline, inorganic semiconductors is much longer than same in the organic semiconductors due to the amorphous and disordered arrangement of molecules in these materials[15, 16, 17, 18, 19, 20, 21, 22, 23], this limits the thickness of organic devices to few a few 100 nm, while the inorganic solar cells could be micrometer thick. Moreover, the nature of the excitons in these two classes of solar cells is different with excitons from organic semiconductors requiring more energy for dissociation than those from inorganic semiconductors[24, 25]. Novel low band gap organic materials synthesis, the introduction of charge selective and/or charge blocking layers, the introduction of varied device architectures, and the incorporation of optical spacers are among techniques researchers have explored to improve the performance of organic solar cells, despite their low charge-carrier mobility. Reported power conversion efficiencies that is as high as 13%[26] have been reported from some of these interventions[27, 28, 29, 30, 31]. Moreover, the addition of metal nano-composites in the charge transport layers of the solar cell is also a promising approach for improving both the device charge-collection and efficiency in organic solar cells.

## 1.1 Justification

Increased incidences of natural disasters indicate the world may be approaching ecological catastrophe. Failure to respond to climate change and environmental degradation will reverse international efforts to reduce poverty and no nation will be immune to the impact of global warming. The need to develop sustainable and economical alternatives to fossil energy becomes apparent and calls for expansion in sustainable energy studies into areas of design, operations and maintenance. Silicon-based solar cells and other similar inorganic materials photovoltaic panels are being

deployed for electricity generation. However, these have a high production cost, leading to slow uptake of solar in the total electricity generation mix. Organic-based PV systems are now emerging as alternatives (and complementary in some cases). Organic photovoltaics implementation can address the socio-economic and environmental challenges from various fronts, as energy projects designed to promote access to cleaner and affordable energy are critical elements for overcoming poverty in Africa. Fossil energy usage will reduce drastically, greatly benefitting the environment and jobs will be created. The promised affordability of organic solar energy systems will facilitate easier stand-alone and mini-grids installations by individuals and rural communities.

## 1.2 Aim of the thesis

Improving the power conversion efficiency (PCE) of organic solar cells through enhanced photo-absorption, and more effective charge collection through enhanced buffer layer incorporation is the overall aim of this Ph.D. research. Interfacial layers were doped with Silver- and Copper- Sulphides in different experiments and used to fabricate enhanced solar cells. The devices were fabricated in ambient and controlled (glove-box) environments to study the charge generation, transport and collection processes. Poly (3-hexylthiophene) (P3HT) and Poly[4,8- bis(5-(2-ethylhexyl)thiophen-2-yl)benzo [1,2-b;4,5-b']dithiophene-2,6-diyl-alt-(4-(2- ethylhexyl)-3-fluorothieno[3,4-b] thiophene)-2-carboxylate-2-6-diyl)] (PTB7-Th) were the donor materials used in this research, while [6,6]-phenyl-C61-butyric acid methyl ester (PC60BM), [6,6]-Phenyl-C71-butyric acid methyl ester (PC71BM) (PC71BM) and 3,9-bis(2-methylene-(3-(1,1-dicyanomethylene)-indanone))-5,5,11,11-tetrakis(5-hexylthienyl)-dithieno[2,3-d:2',3'-d']-s-indaceno[1,2-b:5,6-b']dithiophene (ITIC-Th) were the acceptors used in this Ph.D. research. This Ph.D. work conducted one of the first investigations in which a metal nano-composite was used to enhance the performance of non-fullerene acceptor (NFA) based organic solar cell on the one hand, and utilized an n-type plasmonic material to elicit stronger photo-absorption and charge collection in a p-type transfer medium in another hand. Numerical device simulations were also conducted on the various fabricated devices to provide more insight into the various photo-physical processes going-on within the solar cells.

## 1.3 Objectives of the thesis

The research was focused on fabricating binary system devices (PTB7-Th:PC71BM, PTB7-Th:ITIC-Th and P3HT:PC60BM). The specific objectives are as follows:

- (a) To obtain and characterize Silver sulphide and Copper sulphide nano-composite powders. The characterizations were in terms of optical and morphological properties of the synthesized nanoparticles by using X-Ray diffraction (XRD), high resolution scanning and electron transmission microscopy (HRSEM and HRTEM)

- (b) To fabricate, and characterize the thin-film organic solar cells.
- (c) To optimize the solar the performance of the devices by incorporating the metal nano-composites in either the anodic or the cathodic interfacial layer.
- (d) To conduct numerical device simulation and obtain more insight into the photo-physical processes within the solar cells.

## 1.4 Thesis outline

There are eight chapters in this thesis. Chapters one to three provides the general background and framework upon which the thesis is based. Chapters four to seven discuss the research results in terms of published (4 and 5) articles, along with submitted (6) and draft (7) manuscripts. Each chapter has its own abstract, introduction, experimental details, results and discussion as well as conclusion. The articles and the most recent submissions were submitted and published in different journals. Chapter eight is the conclusion.

### Chapter 1

General introduction: Solar energy was presented as being the panacea to world's energy crisis and mitigation of the global environmental challenges. This chapter also contain research justification, objectives and general description.

### Chapter 2

Literature review: A brief look at photovoltaics, materials for organic solar cells, plasmonic resonance, processes and its application to boosting solar cells performance, a brief look at buffer layers in organic solar cells and why they are important to the overall device performance.

### Chapter 3

Materials and Methods: Specific materials used for the various investigations conducted in this thesis are listed and discussed where applicable. Experimental methods, and characterization are also discussed.

### Chapter 4

The incorporation of Copper sulphide nanoparticles in a P3HT:PC60BM device was reported as published. The investigation included degradation studies on the devices.

### Chapter 5

This chapter discusses the numerical investigation of the effects of copper sulfide nanoparticles on hole transport layer of thin-film organic solar cells.

### Chapter 6

Plasmon-enhanced charge transport processes for improved collection of photo-current in polymer solar cells was discussed in this chapter. Here plasmonic resonance effect was elicited from a non-fullerene acceptor based device by suitable addition of silver sulphide to the ZnO electron transport layer. Computer-based simulation studies was also conducted to provide further insights into the charge transport processes and device characteristics.

## **Chapter 7**

The effect of silver-sulfide on charge transport buffer layers in fullerene based polymer solar cell. Plasmonic resonance effect was elicited in a fullerene-based solar cell by separately doping the hole transport- and the electron transport- layers of the devices with silver sulfide nanoparticles. The interesting ensuing charge-collection dynamics was reported in this chapter and plausible explanations provided. Simulation studies was also conducted to explain some features of the device characteristics.

## **Chapter 8**

Conclusions and recommendation for future research.

# Bibliography

- [1] *Sambo, A. S. (1997). Energy options for sustainable national development: Resources, issues, and the position of renewable energy technologies. University Inaugural Lecture delivered on, 17.*
- [2] *M.Z.Jacobson, M.A. Delucchi, Z.A.F. Bauer, S.C. Goodman, W.E. Chapman, M.A. Cameron, C.Bozonnat, L.Chobadi, H.A. Clonts, P.Enevoldsen, J.R. Erwin, S.N. Fobi, O.K. Goldstrom, E.M. Hennessy, J.Liu, J.Lo, C.B. Meyer, S.B. Morris, K.R. Moy, P.L. O’Neill, I.Petkov, S.Redfern, R.Schucker, M.A. Sontag, J.Wang, E.Weiner, and A.S. Yachanin, 100% Clean and Renewable Wind, Water, and Sunlight All-Sector Energy Roadmaps for 139 Countries of the World, Joule, 1(2017)108-121.*
- [3] *International Energy Agency Releases its World Energy Outlook(2017) <https://www.globalenergyinstitute.org/international-energy-agency-releases-its-world-energy-outlook>.*
- [4] *I.F.Roth and L.L.Ambs, Incorporating externalities into a full cost approach to electric power generation life-cycle costing, Energy, 29(2004) 2125-2144.*
- [5] *D.Yue, P. Khataev, F. You, and S. B. Darling, Deciphering the uncertainties in life cycle energy and environmental analysis of organic photovoltaics Energy Environ. Sci., 5(2012)9163-9172.*
- [6] *S.B.Darling, F.You, T.Veselka, and A.Velosa, Assumptions and the Levelized cost of energy for photovoltaics Energy Environ. Sci., 4(2011)3133-3139.*
- [7] *<https://ourworldindata.org/electricity-mix> accessed July 2nd, 2022.*
- [8] *R. Messenger and D. Y Goswami (2001). Handbook of Energy Efficiency and Renewable Energy, Taylor & Francis Group, LLC, FL Pg. 23-1*
- [9] *M.S.Dresselhaus, and I. L. Thomas, Alternative energy technologies. Nature 414 (2001) 332-337.*
- [10] *N.Grossiord, J.M. Kroon, R.Andriessen, P.W.M. Blom, Degradation mechanisms in organic photovoltaic devices. Org Electron 13 (2012) 432-456.*
- [11] *K.Branker, M.J.M.Pathak, J.M.Pearce, A Review of Solar Photovoltaic Levelized Cost of Electricity, Renewable Sustainable Energy Rev, 15 (2011) 4470-4482.*

- [12] B. Zimmermann, H.F.Schleiermacher, M.Niggemann, U.Wurfel, *Solar Energy Materials & Solar Cells* 95 (2011) 1587-1589.
- [13] M. Kaltenbrunner, M. S. White, E. D. G lowacki, T. Sekitani, T. Someya, N. S. Sariciftci & S.Bauer, *Nature Communications* (2012) DOI: 10.1038.
- [14] C.D. Dimitrakopoulos and D.J. Mascaro: *Organic thin-film transistors: A review of recent advances. IBM J. Res. Dev.* 45, 11 (2001).
- [15] P. Peumans, A. Yakimov, and S.R. Forrest: *Small molecular weight organic thin-film photodetectors and solar cells. J. Appl. Phys.* 93, 3693 (2003).
- [16] J.J.M. Halls, K. Pichler, R.H. Friend, S.C. Moratti, and A.B. Holmes: *Exciton diffusion and dissociation in a poly(pphenylenevinylene)/C60 heterojunction photovoltaic cell. Appl. Phys. Lett.* 68, 3120 (1996).
- [17] J.J.M. Halls and R.H. Friend: *The photovoltaic effect in a poly(p-phenylenevinylene)/ perylene heterojunction. Synth. Met.* 85, 1307 (1997).
- [18] H.R. Kerp, H. Donker, R.B.M. Koehorst, T.J. Schaafsma, and E.E. van Faassen: *Exciton transport in organic dye layers for photovoltaic applications. Chem. Phys. Lett.* 298, 302 (1998).
- [19] T.J. Savanije, J.M. Warman, and A. Goossens: *Visible light sensitization of titanium dioxide using a phenylene vinylene polymer. Chem. Phys. Lett.* 287, 148 (1998).
- [20] A. Haugeneder, M. Neges, C. Kallinger, W. Spirkl, U. Lemmer, J. Feldmann, U. Scherf, E. Harth, A. Gugel, and K. Mullen: *Exciton diffusion and dissociation in conjugated polymer/fullerene blends and heterostructures. Phys. Rev. B* 59, 15346 (1999).
- [21] L.A.A. Pettersson, L.S. Roman, and O. Inganas: *Modeling photocurrent action spectra of photovoltaic devices based on organic thin films. J. Appl. Phys.* 86, 487 (1999).
- [22] M. Stoessel, G. Wittmann, J. Staudigel, F. Steuber, J. Blassing, W. Roth, H. Klausmann, W. Rogler, J. Simmerer, A. Winnacker, M. Inbasekaran, and E.P. Woo: *Cathode-induced luminescence quenching in polyfluorenes. J. Appl. Phys.* 87, 4467 (2000).
- [23] T. Stubinger and W. Brutting: *Exciton diffusion and optical interference in organic donor-acceptor photovoltaic cells. J. Appl. Phys.* 90, 3632 (2001).
- [24] *Primary Photoexcitations in Conjugated Polymers: Molecular Exciton versus Semiconductor Band Model*; edited by N.S. Sariciftci (World Scientific, Singapore, 1997).
- [25] B.A. Gregg and M.C. Hanna: *Comparing organic to inorganic photovoltaic cells: Theory, experiment, and simulation. J. Appl. Phys.* 93, 3605 (2003).
- [26] He, Y., & Li, Y. (2011). *Fullerene derivative acceptors for high performance polymer solar cells. Physical chemistry chemical physics*, 13(6), 1970-1983.

- [27] *C.C. Chen, W.H. Chang, K. Yoshimura, K. Ohya, J. You, J. Gao, Z. Hong and Y. Yang, Adv. Mater. 26 (2014) 5670-5677.*
- [28] *Y. Liu, J. Zhao, Z. Li, C. Mu, W. Ma, H. Hu, K. Jiang, H. Lin, H. Ade and H. Yan, Nat. Commun. 4 (2014) 6293.*
- [29] *L. Nian, W. Zhang, N. Zhu, L. Liu, Z. Xie, H. Wu, F. Wurthner and Y. Ma, J. Am. Chem. Soc. 137 (2015) 6995-6998.*
- [30] *I. Constantinou, T-H. Lai, D. Zhao, E. D. Klump, J. J. Deiningner, C. K. Lo, J. R. Reynolds, and F. So, Appl. Mater. Interfaces 7 (2015) 4826-4832.*
- [31] *N. Li and C.J. Brabec, Energy Environ. Sci. 8 (2015) 2902-2909.*

# Chapter 2

## Literature review

### 2.1 General Introduction

Sunlight, often viewed as the most promising, cheapest and most abundant naturally occurring energy resource can be converted directly into electricity without any intervening heat engine through photovoltaic conversion. Photovoltaic devices are of simple designs, requiring low maintenance because they are mostly solid state and hence are compact and rugged. Research on photovoltaic materials, which has increased greatly in the past few decades, has impacted significantly on reducing dependence on fossil energy. It is believed that this trend will continue to increase as individuals and nations continue to embrace the solar energy harnessing technologies that have entered the energy mix. Crystalline Silicon (c-Si), Compound semiconductors (CIGS, CdTe, CIS, CZTS etc.), Thin Film Solar Cells (TFSC), Organic Photovoltaics (OPV), Dye-Sensitized Solar Cells (DSSC), Perovskite Solar Cells (PSC) and their hybrids are the various solar cell technologies presently available for solar energy capture and electricity generation. Some of these technologies are utilized in the form of solar panels. Some are set up in solar concentration mode for solar electricity generation or solar heating applications amongst various other modes of energy capture and use. The c-Si technologies, which could be mono- or poly- crystalline, currently have the largest market share of the solar cells. However, Si-based solar cells are expensive due to high cost of Silicon wafers preparation and the device fabrication processes. Si-based devices also have huge thickness translating to high embodied energy and energy payback time. Moreover, Silicon extraction and wafer making process utilizes environment-unfriendly chemicals and processes.[1, 2, 3, 4].

The Organic Photovoltaics (OPV) are made from organic semiconductors and small molecules. Their low fabrication cost, ease of mass production coupled with large-area fabrication capability, solution processing at low temperatures, mechanical flexibility and semi-transparency along with tunable optical and electronic properties makes them highly attractive to researchers. Combining the above desirable qualities, OPVs turn out to have low embodied energy, low energy payback and has

potential to be cheap when fully matured for market entry[5, 6, 7, 8, 9, 10, 11, 12]. Moreover, Organic photovoltaics (OPVs) can serve as both alternative solar energy harvesters or complementary to other technologies due to the abundance of the raw materials used for the production and the ease of turning these constituents to the needed forms in environment-friendly fashion. The ability to finetune the optical properties of OPVs has enabled production of semi-transparent OPV devices which could be easily be used on windows and other such frames due to their robust mechanical flexibility, making them ideal candidate for integrated PV applications[13, 14, 15].

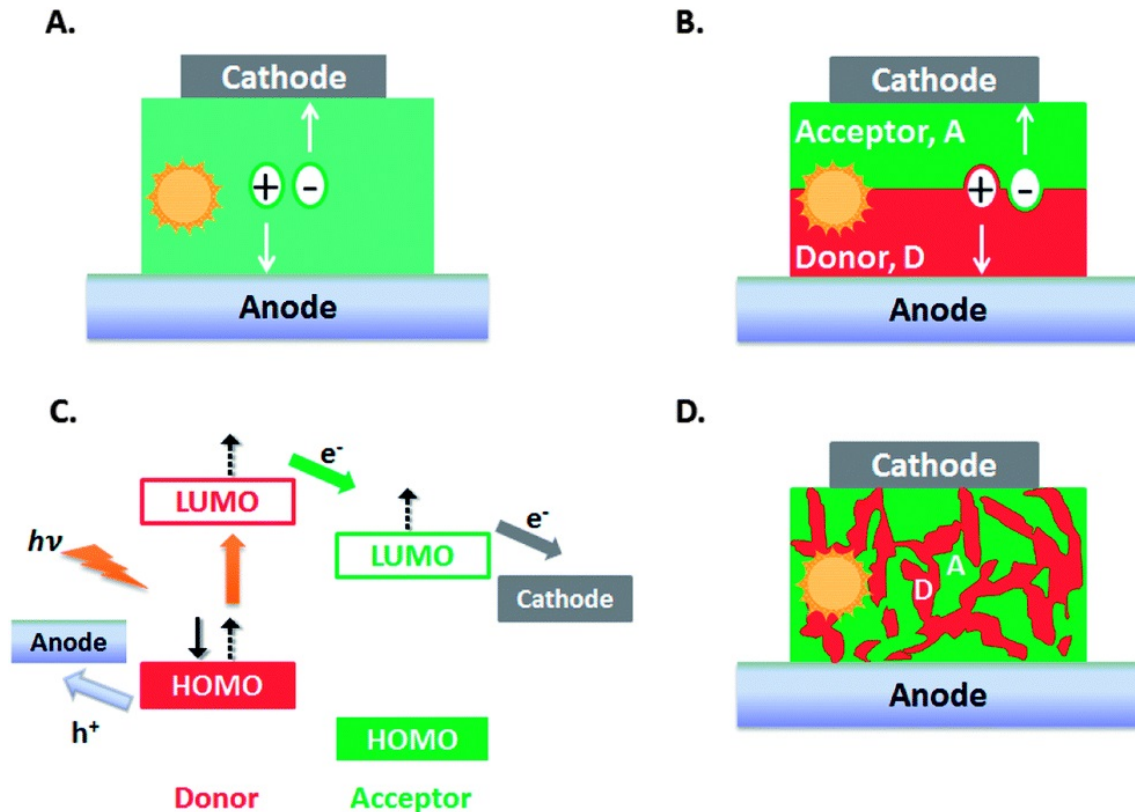


Figure 2.1: (a) Single layer device schematics (b) Bilayer device schematics (c) Exciton dissociation at a D/A interface (d) Bulk heterojunction device schematics [16].

Organic photovoltaic cells typically consist of carbon-based semiconductors. These semiconductors are classified according to their electron donating or accepting nature into Donors and Acceptors. The use of these photoactive materials started with the single layer devices in which a single organic semiconductor is sandwiched between two electrodes that serve to collect photo-generated charge carriers from the device. However, these cells perform poorly due to high exciton recombination because of insufficient electric field for exciton dissociation[17, 18]. Bilayer devices were introduced thereafter to cater for the deficiency of the single layer devices. In bilayer devices, two organic semiconductors with different electron affinity and ionization energy (acceptor and donor) are deposited on top of each other, with both sandwiched between two electrodes as in the single layer devices. Electrostatic forces are induced at the interface between the two materials which creates a local

electric field for the exciton dissociation, leading to better efficiency being recorded than the single layer devices[19, 20]. However, the extremely short diffusion length of photo-generated excitons in organic semiconductors limit exciton dissociation in the bilayer structure to the interface between the donor and the acceptor materials, as excitons generated within the bulk of either material will likely recombine before getting to the interface. In order to address this limitation, the bulk heterojunction (BHJ) device preparation mode was introduced. This preparation mode has grown to become the most widely adopted preparation mode for OPV devices. Figure 2.1 shows the schematics of the three structures. The BHJ devices consist of a mixture of donor and acceptor materials in a continuous blend matrix as illustrated in Figure 2.1d. The continuous interpenetration of the donor and acceptor materials presents a much greater interfacial area for exciton dissociation. Moreover, the distance that the dissociated charge carriers will travel to their respective collection electrodes is much smaller thereby reducing the recombination probability appreciably, leading to generally improved photo-currents being extracted from the solar cells and consequently improved efficiency over the bilayer devices[21, 22, 23]. Most BHJ devices comprise of two components only (binary-OPVs) though three-component devices (ternary BHJ-OPVs) have also been explored. Due to the interpenetrating nature of the photo-active layer in the BHJ devices, attaining good miscibility of the D-A materials is essential for good nano-morphology to reduce incidences of large phase segregation, heavy traps and other related features that may promote geminate and non-geminate recombination of the charge carriers. The nano-morphology is usually controlled by the use of solvent additives, solvent vapour annealing and thermal annealing to name a few[24, 25].

Insufficient solar energy absorption by the polymer medium, low charge carrier mobility and short exciton lifetimes are issues that need to be resolved before the commercialization of organic photovoltaic solar cells. The thin film nature of the BHJ devices severely limits the achievable photocurrents as most incident solar radiation simply pass through the device without interacting with the absorption layer, thus various mechanisms are being put in place to trap or absorb more solar radiations in the organic thin films. Some of these techniques include the use of optical spacers[26, 27, 28, 29], device symmetry adjustment, ternary device implementation[30, 31] and introducing periodic nanostructures[32, 33, 34, 35]. Incorporating metallic nanostructures in the active layer or the charge transport layers of thin film organic photovoltaic devices is also a means of trapping solar radiation in the solar cells to enhance their optical absorption[36, 37]. These nanostructures assist with the nano-scale light-matter interaction to improve the absorption of the solar photons and lessen recombination[38, 39, 40, 41]. The technique of enhancing optical absorption through the incorporation of metallic nanostructures in a medium is known as localized surface plasmon resonance (LSPR) and the nanostructures are said to be plasmonic. LSPR occurs when an incident electromagnetic field produces non-propagating excitations of the conduction electrons at the surface of a metallic nanostructure [42, 43]. The LSPR characteristics of several metal and metallic nanocomposites are interesting due to their resonance frequency in the visible and near-infrared range of the EM spectrum and have been utilized in various applications such as information technology and data storage, energy and photo-catalysis

as well as biomedical applications (biosensing, bioimaging and nanosurgery to name a few)[44, 45, 46, 47, 48, 49].

## 2.2 Charge carrier transport theory

### 2.2.1 Molecular energy levels in organic semiconductors

In organic semiconductors, the molecules are composed of atoms that are principally joined by covalent bonds. The bonding atoms create molecular orbitals by the combinatorial linking of their overlapping atomic orbitals, having varying orbital energies due to the bonding and anti-bonding orbitals. In Fig 2.2 for instance, a single electron cloud comprising of the first two electrons, one from each of the interacting atoms, make up the bonding orbital to form a bonding molecular orbital whose energy is lowered because of the increased electron density, greater columbic force between the electrons and the nuclei and thus are the more tightly bound electrons[50]. The Pauli Exclusion Principle constrains that additional electrons cannot occupy the bonding orbital of a full-shell atom but the anti-bonding orbital. Thus the next sets of electrons from the interacting atoms form the anti-bonding molecular orbitals. There is reduced atomic charge shielding in the anti-bonding orbital since electrons there are farther from the nuclei as can be seen from the figure, leading to a higher energy but less stable molecule[50]. Organic semiconductors are also often  $\pi$ -conjugated polymers comprised chiefly of carbon and hydrogen atoms. These materials possess alternating single and double carbon-carbon bonds which result from the hybridization of carbon atoms, yielding  $\sigma$ -bonds and  $\pi$ -bonds. The  $\pi$ -bonds results in delocalized states over significant segments of the polymer chains[51, 52, 53].

Individual interacting atoms in a bulk semiconductor film are not the only determining factors that affect the distribution of molecular orbital energies. Individual molecules in the film typically experience varying packing environments, resulting in varied degrees of molecular deformation by virtue of the inter-molecular interactions. This ultimately leads to a realization of different bond lengths, bond angles and energy levels within individual molecules[55, 56]. This varying environmental thermodynamic nature also play a role in altering the molecular orbital energies as both internal molecular interaction and thermodynamic factors slightly shifts molecular orbital energies, affecting both the HOMO and the LUMO levels. The variation in the HOMO and LUMO energy levels within a material is often regarded as the energetic disorder[5, 57, 58]. For instance, the polymer crystallinity can induce the nature of the inter-molecular interaction that leads to changes in the shape and width of LUMO and HOMO levels (see Figure 2.3). Crystalline organic semiconductors usually possess higher charge mobility than their amorphous counterparts because of their ordered molecular packing which greatly aid electronic coupling. In poly-crystalline or amorphous structures however, several perturbations are expected which gives rise to a wide band in energy level distribution than

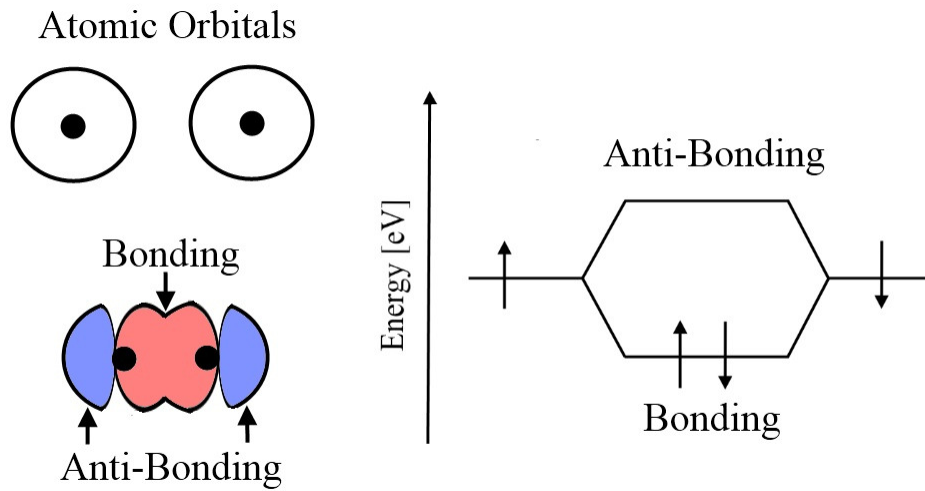


Figure 2.2: Individual atomic orbitals often overlap with one another to create bonding and anti-bonding molecular orbitals[54]

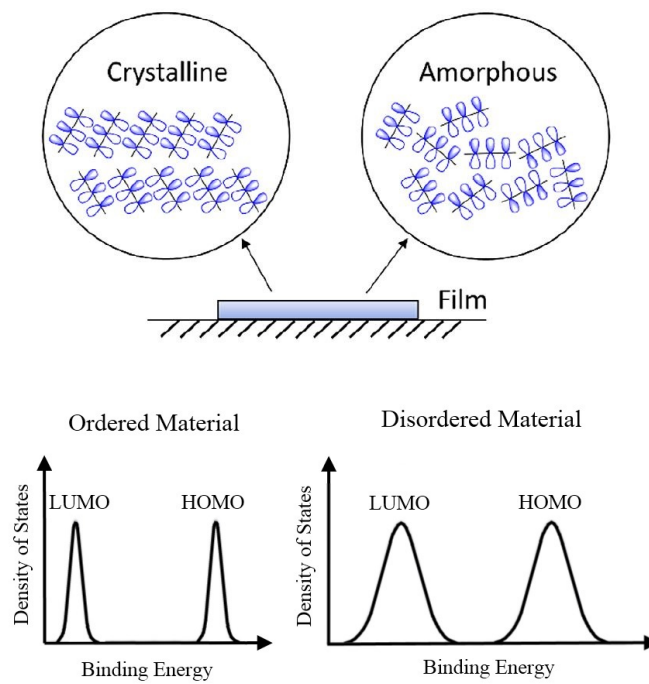


Figure 2.3: Ordered and Dis-ordered materials' Densities of energy states (DOS) displaying narrow and wide bandwidths respectively[54].

in crystalline medium (Figure 2.3). These variations would eventually cause changes in the optical and electrical properties of the semiconductor polymer.

## 2.2.2 Charge transport in organic semiconductors and devices

Charge carriers transport in organic semiconductors occur via their frontier molecular orbitals, namely the highest occupied molecular orbitals (HOMO) and the lowest unoccupied molecular orbital (LUMO), which are responsible for holes and electrons transport respectively. The synchronization of these molecular energy orbitals across the various interfaces greatly affects or determines the ensuing charge transport dynamics. In most organic semiconductor devices, interfacial electron and hole transport layers (ETL and HTL respectively), are also often incorporated to play very important role in pinning the energy levels for effective charge transport. In organic photovoltaic solar cells (OPVs), the electron- and hole- transporting layers (ETL and HTL respectively) extract the charges to the external circuit rather than inject them. The HOMOs in the HTL should lie above the donor's HOMO while the LUMOs of the ETL lie below the acceptor LUMO to provide the necessary force for preferentially harvesting the photo-generated charges. In a D-A molecules blend bulk-heterojunction (BHJ) medium, the LUMO levels energy difference between molecules determines the effective dissociation of excitons at the molecular interface and is called the LUMO energy level offset [59, 60, 61]. Organic semiconductors-based devices are often made by the sequential deposition of thin film layers of the different materials on rigid or flexible substrates and the devices performance strongly depend on how the charge carriers transport across the several interfaces. The devices thus often consist of several metal-organic and/or organic-organic interfaces which significantly influence device performance and lifetime, as several heterogeneous electronic processes like charge injection/extraction, exciton dissociation and/or recombination as well as charge recombination often take place at these interfaces [62, 63, 64].

Generally speaking, the drift and diffusion of charge carriers in semiconducting devices is responsible for the extracted currents from the devices. The current density drift-diffusion equations [65, 66, 67] describes the charge carriers transport mechanism:

$$J_{total} = J_{drift} + J_{diffusion} \quad (2.1)$$

$$J_n = q\mu_n\xi + qD_n\nabla n \quad (2.2)$$

$$J_p = q\mu_p\xi + qD_p\nabla p \quad (2.3)$$

$$J_{cond.} = J_n + J_p \quad (2.4)$$

in the equations above, the medium induced traps are not considered.  $n$  and  $p$  are electrons and holes concentration,  $q$  is the elementary charge, the applied electric field is  $\xi$ ,  $\mu_n$  and  $\mu_p$  are the electrons and holes mobilities respectively, while  $D_n$  and  $D_p$  are the diffusion constants for the electrons and the holes respectively. The one dimensional current densities may hence be expressed according to the Poisson's and continuity equations as follows:

$$\frac{d\xi}{dx} = \frac{q}{\varepsilon}(p - n) \quad (2.5)$$

The diffusion constants,  $D_{n,p}$  may be expressed as:

$$D_{n,p} = \left(\frac{K_B T}{q}\right)\mu_{n,p} \quad (2.6)$$

where  $K_B$  is the Boltzmann's constant and  $T$  is the absolute temperature. By substituting the above relation in Equations 2.2 and 2.3 in the one dimensional Einstein diffusion equations, the current densities flow of charges due to electrons and holes may respectively be expressed in the x-direction:

$$J_n = q\mu n(x)\xi(x) + qD_n \frac{dn}{dx} = q\mu_n(n(x)\xi(x) + \frac{KT}{q} \frac{dn}{dx}) \quad (2.7)$$

$$J_p = q\mu p(x)\xi(x) + qD_p \frac{dp}{dx} = q\mu_p(p(x)\xi(x) + \frac{KT}{q} \frac{dp}{dx}) \quad (2.8)$$

## 2.3 Organic solar cells working mechanism

Four fundamental processes are involved in the operation of organic solar cells. The performance of any given organic photovoltaic system depends on the overall efficiencies of these processes which are photon absorption, exciton generation and diffusion, exciton dissociation into free charge carriers and their subsequent collection at the electrodes as illustrated in Figure 2.4.

The light-absorbing layer in the organic solar cell is composed of donor polymers, small molecules, fullerenes and non-fullerene molecules. Traditionally, incident solar radiation is usually absorbed by the electron donating moieties until recently when non-fullerene acceptors which can also absorb solar photons were developed to extend the possible range of absorption spectrum. Typical donor materials include the popular P3HT, PTB7 and PCDTBT. The high absorption coefficient (as high as  $10^5 \text{cm}^{-1}$ ) of these organic semiconductors affords the possibility of making

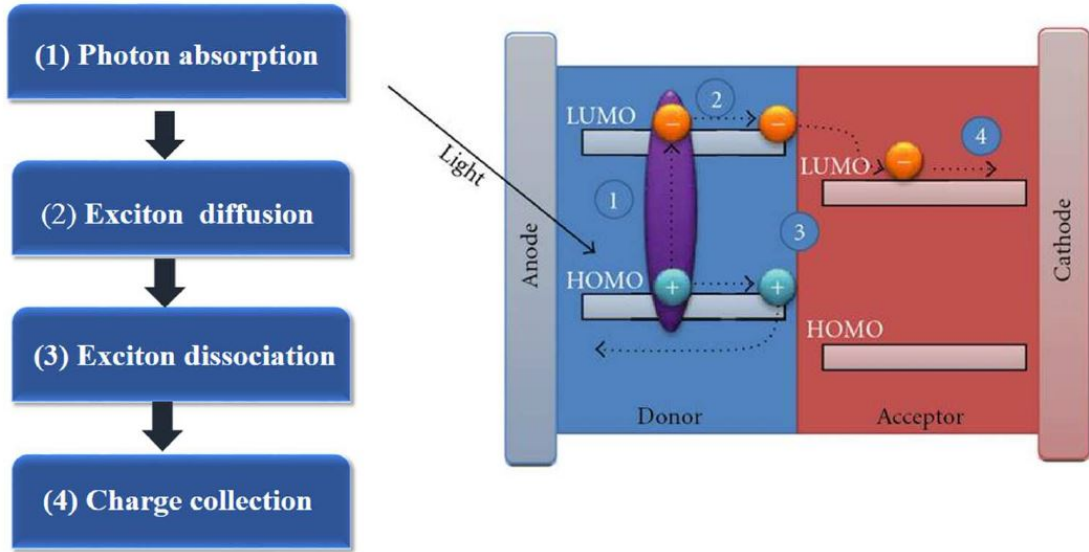


Figure 2.4: Mechanisms of photo-current generation in organic solar cells[68].

them in thin films to counter the short lifetimes of their photo-generated excitons. Photo-absorption in semiconducting polymers is dependent on the bandgap. Higher bandgap polymers absorb less and hence generate low photo-current than low bandgap organic semiconductors, since these overlap better with the solar spectrum[68, 69, 70, 71]. However, Optical interference due to absorption profile modification in the multi-layer thin film device may lead to some photo-absorption losses[72]. Moreover, the incident photon energy should be more than the absorbing semiconductor's bandgap for absorption and the consequent electronic excitation to occur while excess photon energy becomes lost to thermal processes. The photo-absorption leads to excitation of electrons from the HOMO to the LUMO of the semiconductors. The excitation of an electron simultaneously leaves a hole behind in the HOMO levels, effectively leading to the creation of an electron-hole pair which are bound by coulombic attractive forces. This quasi-particle is referred to as an exciton.

The photo-generated excitons must overcome their binding energy so as to dissociate into free electrons and holes. Excitonic migration to the nearest donor/acceptor interface within a limited time-frame and diffusion length is crucial for dissociation to occur successfully, failure of which will lead to the excited electron relaxing into the vacant hole (recombination). Typical exciton diffusion length in most organic semiconducting polymers is 10 - 20 nm. The exciton diffusion length is related to the exciton lifetime and diffusion coefficient ( $D_{exciton}$ ) by the following relations:

$$L_{exciton} = (\tau_{exciton} \cdot D_{exciton})^{\frac{1}{2}} \quad (2.9)$$

The energetic driving force, due to differences in the ionization energy and electron affinity of the donor (D) and acceptor (A) respectively, present at the D/A interface overcomes the binding energy holding the exciton together, effectively sep-

arating them into free charge carriers. The more this interfacial driving force is greater than the exciton binding energy, the easier the exciton dissociation becomes. The electron continues to travel in the acceptor material domain while the hole travels in the donor polymer chain backbone for collection at their respective electrodes. The charge carriers' motion is driven by the electrodes' Fermi level energy difference with the acquired drift velocity ( $V$ ) due to this field given by:

$$V = \mu_i E \quad (2.10)$$

where  $\mu_i$  is the carriers' mobility. Charge collection at the electrodes may be affected by non-geminate recombination due to traps before the charges reach the electrodes[73].

## 2.4 Characterizing organic solar cells

Solar cells are characterized by measuring their current (or current density) - voltage relationships, popular called I-V (J-V) curves. The curves facilitate the estimation of the most basic and/or fundamental parameters for making a general assessment of device performance. These basic parameters are the short-circuit current density ( $J_{sc}$ ), the open-circuit voltage ( $V_{oc}$ ), the Fill factor (FF) and the Power conversion efficiency (PCE) (Figure 2.5).

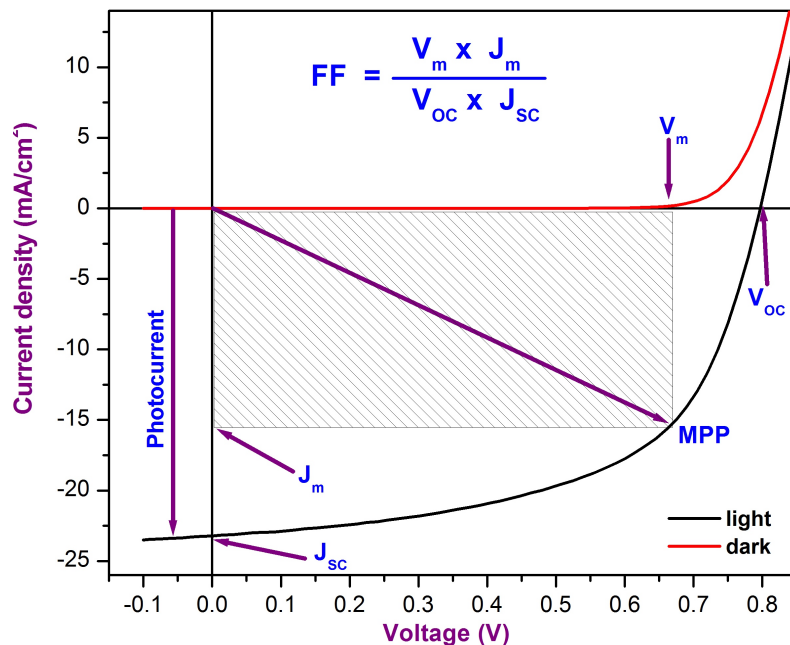


Figure 2.5: Current density - Voltage (J-V) characteristics of OPVs

A non-linear I-V relation is generally used to describe the curves using various models, the simplest of which is a simple diode equation, in which the applied voltage and current are related by:

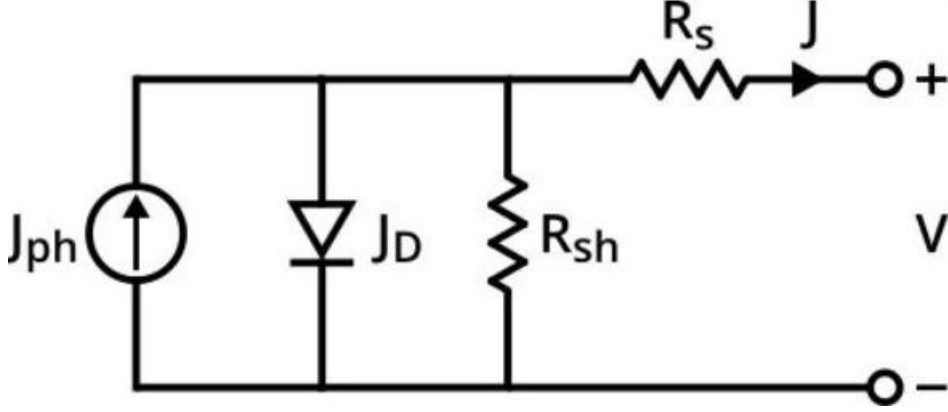


Figure 2.6: Solar cell's equivalent circuit diagram with series and shunt resistances included.

$$I_{dark} = I_0(e^{\frac{qV}{kT}} - 1) \quad (2.11)$$

$I_0$ ,  $q$ ,  $k$  and  $T$  refer to a constant, the electronic charge, Boltzmann constant and the absolute temperature respectively. The current due to the solar cell is the difference between the dark current and the current that flows as a result of the applied potential difference:

$$I(V) = I_{SC} - I_{dark} = I_{SC} - I_0(e^{\frac{qV}{kT}} - 1) \quad (2.12)$$

Real solar cells are affected by resistances hence the ideal Shockley equation is extended to include series and parallel resistances ( $R_s$  &  $R_p$ ), as depicted in Figure 2.6. The J-V characteristic then becomes the generalized Shockley equation:

$$J = \frac{1}{1 + \frac{R_s}{R_{sh}}} J_s \left( \exp\left(\frac{q(V - JR_s)}{nK_B T}\right) - 1 \right) - \left( J_{PH} - \frac{V}{R_{sh}} \right) \quad (2.13)$$

$J_s$  and  $n$  refer to the saturation current density, and the diode's ideality factor respectively while  $q$ ,  $k_B$  and  $T$  maintain their earlier definitions.  $J_{ph}$  is an optional photo-current added due to the I-V curve shifting downwards on the current axis. The open-circuit voltage and the short-circuit current density may then be calculated, and expressed as:

$$V_{OC} = \frac{nK_B T}{q} \ln \left[ 1 + \frac{J_{PH}}{J_s} \left( 1 - \frac{V_{OC}}{J_{PH} R_{sh}} \right) \right] \quad (2.14)$$

$$J_{SC} = \frac{1}{1 + R_s/R_{sh}} J_{PH} - J_s \left[ \exp\left(\frac{|J_{SC}| R_s}{nK_B T/q}\right) - 1 \right] \quad (2.15)$$

The solar cell power conversion efficiency (PCE) is the percentage of the maximum output of electrical power to the incident solar power, given by:

$$PCE = \frac{P_m}{P_{in}} = \frac{V_{OC} * J_{SC} * FF}{P_{in}} \quad (2.16)$$

where  $P_m$ ,  $P_{in}$ ,  $V_{OC}$ ,  $J_{sc}$  and  $FF$  are the maximum power point, the incident solar power density, the open-circuit voltage, the short-circuit current density and the fill factor respectively. Solar cells characteristics are routinely measured at standard Air Mass 1.5 (AM 1.5), incident power density of  $\approx 100 \text{ mW.cm}^{-2}$  and absolute temperature 298K[74].

The  $J_{sc}$  is proportional to the extent of absorbed photons, which a consequence of the absorption intensity and the spectral capture capacity of the photo-absorbing medium. Exciton generation and dissociation, charge transport in the medium and collection at the electrodes greatly affect the  $J_{sc}$  value as well. The fill factor ( $FF$ ) is the ratio of the maximum power  $P_m$  to the product of the  $J_{sc}$  and the  $V_{OC}$ . The  $FF$  is greatly affected by the solar cell's series and shunt resistances ( $R_s$  &  $R_{sh}$ ). Generally, the  $R_s$  is the sum of resistances due to bulk of the active layer, the electrodes and contact between them, while the leakage currents due to pinholes in the device or at the edges is responsible for the  $R_{sh}$ .

$$FF = \frac{P_m}{V_{OC} * J_{SC}} \quad (2.17)$$

The open-circuit voltage  $V_{OC}$  is highest voltage in the solar cell when current is not being drawn from the device. The bandgap of the donor and acceptor in the BHJ blend and the device's electrodes workfunction determines the  $V_{OC}$ . It is often roughly estimated by the energy difference of the donor's HOMO and the acceptor's LUMO. The need for adequate alignment of energy levels amongst the various device components; acceptor, donor, transport layers, and the electrodes are important to the overall device performance in organic solar cells[75, 76, 77].

## 2.5 Photo-absorbing materials for organic solar cells

The power conversion efficiency of organic solar cells is highly dependent on properties of the materials used, the device structure as well as processes at the interfaces.  $\pi$ -conjugated polymers are the major donor materials used for device fabrication due to the ability to easily finetune their properties, the most popular ones being Poly(phenylene) and Polythiophenes (PPVs and PTs). The PTs and their derivatives have been receiving immense research consideration for solar cells[78, 79]. The first BHJ-OSC was made with MEH-PPV donor which has a wide bandgap of 2.2 eV and UV absorption up to 600nm, limited charge mobility and some luminescence[80].

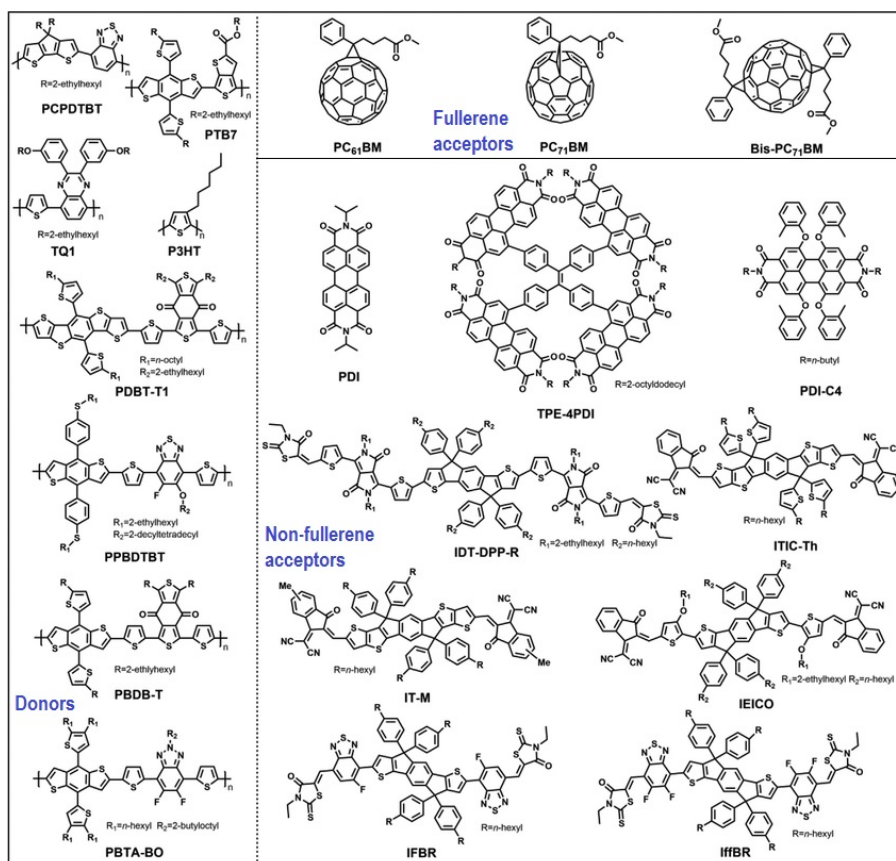


Figure 2.7: Conjugated polymers (donors), fullerenes (acceptors) and their derivatives, and non fullerene acceptors' chemical structures[89].

The Poly (3-hexylthiophene) (P3HT) is presently perhaps the most popular donor material under thin-film OPV research investigation today. It is highly soluble in several solvents, possess higher charge mobility and relatively more stable under ambient conditions leading to better photovoltaic performance[81]. The P3HT can be used with several electron acceptor materials. The poly 4,6-(2-ethylhexyl-3-fluorothieno[3,4-b]thiophene-2-carboxylate) alt-2,6(4,8-bis(2-ethylhexyloxy) benzo[1,2-b:4,5-b]dithiophene) (PTB7) is another important electron donating polymer known for its stable thin films and high efficiency solar cells[82, 83]. The Benzothiadiazole (BT), PCPDTBT possess a narrow bandgap and can absorb broadly even into the NIR region and has been demonstrated to exhibit high hole mobility. Others donors are the diketopyrrolopyrrole (DPP), and the Benzo[1,2-b;4,5-b']dithiophenes (BDT) among others[84, 85, 86].

Donor polymers are typically used with electron-deficient moieties that serve to withdraw or accept electrons, creating pathway for charge transport. The C60 buckminsterfullerene derivatives are the most popular acceptors in use for OPV and allied researches with PC60BM and PC71BM being the mostly used ones among the derivatives. Although both show moderate absorption in the UV-Vis region, the PC70/71BM absorbs better, outputs a higher current density, resulting in a better power conversion efficiency[87]. ICMA, ICBA and IC70MA are other fullerene derivatives routinely used as acceptors in OPV fabrications[88]. The optical absorp-

tion band of fullerene-based acceptors is however narrow and they have a rather low tunable energy band structure which makes them prone to energy loss and relatively weak external quantum efficiency (EQE) in comparison to photovoltaic technologies[89, 90, 91, 92]. Thus, Non fullerene acceptors (NFAs) were introduced in recent years to address the aforementioned challenges. The NFAs bandgaps can be easily tuned to cover a broader range of the EM spectrum to consequently achieve higher device PCEs (as high as 19%)[2, 89, 93]. The NFAs have high extinction coefficient, excitons travel longer before recombination due to a higher diffusion length and lifetime. Moreover in BHJ blends, they possess a better energy levels matching with donor polymers along with a low driving force for exciton splitting[10, 96]. Chemical structures of some donor polymers, fullerene acceptors and non-fullerene acceptors are depicted in Figure 2.7.

## 2.6 Plasmon resonance as a strategy for improving solar energy harvesting and charge collection

The effective capture of solar energy has been of a continuing research interest with the organic solar cell technologies being more interesting due to the limited thickness of their light-absorbing layers. Thus, organic solar cells research is continuously interested in improving photo-absorption despite the thickness limitation. Some of the strategies that have been developed included synthesis of new organic materials with a wider absorption range in the electromagnetic spectrum, adjusting the device architectures, and incorporating optical spacers in the device fabrication[97, 98, 99]. Charge transport is equally an important component of solar energy harvesting in thin film organic PV, which is dependent on the film conductivity, morphology of the absorber medium, and energy level alignment of the molecules at the interfaces. The use of charge selective layers to facilitate better charge removal and transport[100, 101] has been introduced to achieve better charge transport. However, the nature of the transport layers critically determines the effectiveness of the photo-generated charge collection from the solar cell devices. Thus, fine-tuning the properties of the transport layers using impurity doping has brought significant successes in device performance from the limited choices of charge transport materials available today in organic photovoltaic preparation [102]. This complements with the efforts of retaining some of the absorption losses as a consequence of using very thin absorber layers in TFOPVs (less than 200 nm) [103, 104, 105, 106].

In addition to methods earlier enumerated for enhancing solar radiation absorption and charge collection in OPVs, the incorporation of plasmonic nano-structures in OPV devices has equally been introduced[104, 107]. The use of plasmonic nanocomposites is popular, having been successfully used in various applications such as in LEDs, photon counting and detection, sensing (biological and chemical), OPVs and other optoelectronic applications[41, 108, 109]. Metal or metallic-composites nano-structures are explored for plasmonic applications due to their interesting

optical and electrical properties. For example, the strong absorption and scattering efficiency of the gold (Au) and silver (Ag) nanoparticles is because of their ability for localized surface plasmon resonance (LSPR) when suitably stimulated[110, 111].

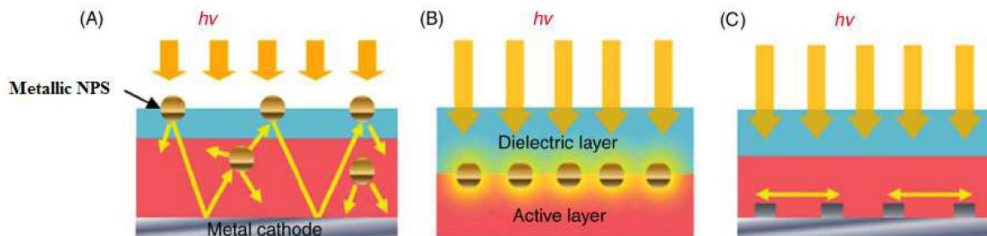


Figure 2.8: Photon-absorption enhancement in OPV devices via some plasmonic resonance mechanisms (a) Light scattering (b) Localized Surface Plasmon Resonance (LSPR)(c) Surface Plasmon Polariton Effect[120].

Plasmon-induced enhancements arises from the favourable interaction of the solar electromagnetic (EM) spectrum with the surface electron-cloud of favorably pre-disposed elements at the nano-scale through a number of physical mechanisms, leading to light-trapping and local field enhancements in the nano-structures' surrounding media. The realization of plasmonic effects by virtue of the incorporation of plasmonic nano-structures in solution-processed organic solar cells, leading to improved device performance have been severally demonstrated to result from mechanisms such as the localized surface plasmon resonance (LSPR), surface plasmon polariton (SPP) and light scattering as illustrated in Figure 2.8.

### 2.6.1 Light scattering

Light scattering can occur in a dielectric medium if the direction of the incoming EM beam is changed due to their encountering scattering centres. Metal and metallic-nanocomposites can behave like a scattering centre if their size is sufficiently large to cause such deflections. The change in the direction of the incident beam causes the beam to persist longer in the dielectric medium, thus increasing the photo-absorption rate if the medium is a suitable absorbing media. Light scattering is highly dependent on the size, shape and relative abundance of the introduced nano-structures[113]. The particles sizes and shapes depends on the material synthesis while the relative nano-structures abundance depends on the device preparation conditions. Moreover, relatively large-sized ( $>40$  nm diameter) nano-composites are required for effective light spreading through multiple scattering in OPV devices. One of the popular means of eliciting scattering response in OPV devices is to introduce the metal nano-composites into a suitable buffer layer so that the light absorption may be enhanced through forward and backward sunlight scattering, increasing the photon absorption rate and subsequently the exciton generation. Additionally, the light scattering plasmonic mechanism indirectly reduces reflection losses [114, 115, 116].

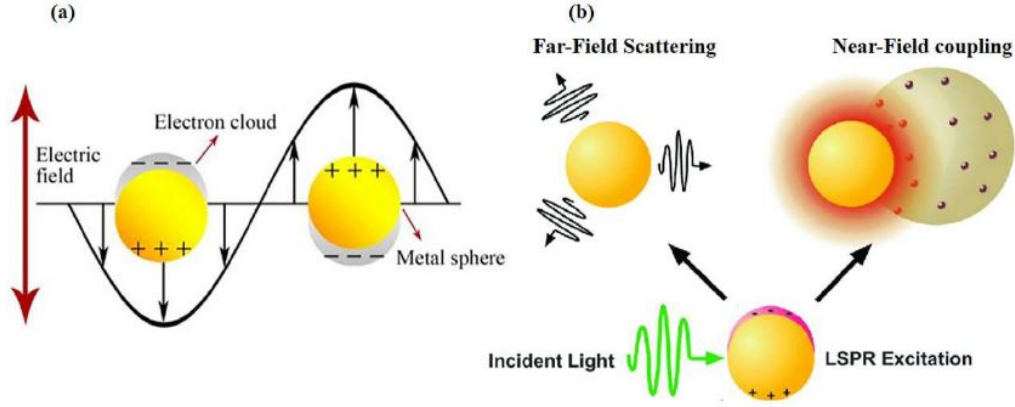


Figure 2.9: (a) LSPR on a spherical nano-structure due to interaction with an electric field causing collective oscillation of the electronic cloud[47]. (b) LSPR sub-mechanisms: the far-field and the near-field coupling[117].

## 2.6.2 Localized surface plasmon resonance (LSPR)

The incoming solar radiation's EM field may cause the surface electron cloud in metallic nano-structures to oscillate collectively, leading to heightened electromagnetic fields around the nano-particles, often over a range of characteristic wavelengths and frequency. The increased EM field consequently interacts more intensely with the surrounding dielectric media. If the photo-absorption profile of the dielectric media is consistent with the nano-structure's resonance wavelengths, photo-absorption in the media will be appreciably increased improving exciton generation. The resonance wavelengths of some metal nano-particles span over wide spectral range from the ultraviolet (UV) and visible to the near-infrared (NIR) region. The resonance frequency is a function of the particles' shapes, sizes, geometries, and the dielectric medium in which they are dispersed[118, 119, 120, 121]. The entire process is known as the localized surface plasmon resonance (LSPR) and is possibly the most dominant plasmonic resonance mechanism being explored in various applications. Figure 2.9 provides an illustration for the LSPR processes: The incident radiation, possessing wavelength much larger than the particle size, interacts with the metallic nano-structure, creating strong LSPR excitations within the immediate vicinity of the particles[122]. The mathematical relation for expressing the polarizability ( $P$ ) of a spherical nanoparticle is given by:

$$P = 4\pi\epsilon_0\epsilon_m a^3 \frac{\epsilon_p - \epsilon_m}{\epsilon_p + 2\epsilon_m} E_0 \quad (2.18)$$

$$\alpha = 4\pi a^3 \frac{\epsilon_p - \epsilon_m}{\epsilon_p + 2\epsilon_m} \quad (2.19)$$

where  $\alpha$ ,  $\epsilon_p$  and  $\epsilon_m$  are the particle's diameter, the medium's dielectric constant and the particle's dielectric constant respectively. From the eqn (2.18), as  $|\epsilon_p + 2\epsilon_m|$  approaches small value,  $\epsilon_p(\omega)$  will be equal to  $-2\epsilon_m$  and the particle polarizability will be large. The dielectric response of the metallic nano-structure is a complex

number according to Drude's model for metal-nanoparticles. The real part of which is frequency-related by the following expression:

$$\varepsilon_p(\omega) = 1 - \frac{\omega_p^2}{\omega^2 + \gamma^2} \quad (2.20)$$

$\gamma = 1/\tau$  in the above equation.  $\tau$ ,  $\omega$  and  $\omega_p$  refer to the electron's relaxation time, the metal nano-structure's electric field, and the plasmonic frequency of the bulk longitudinal electronic excitations. Furthermore, the plasmonic frequency is expressed as:

$$\omega_p = \sqrt{\frac{n_e e^2}{\varepsilon_0 m_{e*}}} \quad (2.21)$$

$e$ ,  $m_{e*}$ ,  $\varepsilon_0$ , and  $n_e$  are the electronic charge, the electron's effective mass, free-space permittivity and the electron number density respectively. The surface plasmon resonance frequency ( $\omega_{LSPR}$ ) may hence be obtained from equation (2.20) and (2.21) [123, 124, 125, 126]. to be:

$$\omega_{LSPR} = \omega_p \sqrt{\frac{1}{1 + 2\varepsilon_m} - \frac{1}{\omega_p^2 \tau^2}} \quad (2.22)$$

suggesting that the plasmon resonance frequency is highly dependent on the dielectric medium. The equation (2.21) shows that for the metal, the resonance frequency,  $\omega_p$ , depends on the density of free electrons in the particle. Thus both the dielectric medium and the metallic-nanostructure may be adjusted to achieve desired shifts in resonance frequencies[126, 127, 128].

## Near-field effect

The incident EM interaction with plasmonic nanostructures creates local field perturbations around the nano-structures. These perturbations may moreover be accompanied by enhanced polarizability. Since the initial interaction creates EM fields that are internal and external to the nanoparticles, these internal and external EM fields may be inferred using the Laplace equation:

$$E_{in} = \frac{3\varepsilon_m}{\varepsilon_p + 2\varepsilon_m} E_0 \quad (2.23)$$

$$E_{out} = E_0 + \frac{3\hat{n}(\hat{n} \cdot \vec{p}) - \vec{p}}{4\pi\varepsilon_0\varepsilon_m} \frac{1}{r^3} \quad (2.24)$$

$r$  is distance to nanostructure's center and  $\hat{n}$  is a unit vector. The first term at RHS of equation(2.24) is the incident EM field while the second term is the induced EM field within the nanostructure[123]. Near-field enhancements due to plasmonic nano-materials is morphology dependent.

## Far-field scattering effect

Incident light on plasmonic nano-structures may also be scattered into the far-field, depending on size, shape and material properties of the nano-structures[117]. Plasmonic nano-materials extinction process is dependent on their extinction coefficient, which is addition of the scattering and absorption processes. The cross-sections for the scattering  $C_{sca}$  and the absorption  $C_{abs}$  events are expressed as:

$$C_{sca} = \frac{1}{6\pi} * \left\{ \frac{2\pi}{\lambda} \right\}^4 |\alpha|^2 \quad (2.25)$$

$$C_{abs} = \frac{2\pi}{\lambda} Im[\alpha] \quad (2.26)$$

For enhanced absorption in OPV devices, the nano-structure's light scattering events must outweigh their parasitic light absorption events. Thus, we define respective efficiencies for the scattering and the absorption events in order to adequately rate the scattering and absorption performances of the nanoparticles:

$$Q_{abs} = \frac{C_{abs}}{C_{abs} + C_{sca}} \quad (2.27)$$

$$Q_{sca} = \frac{C_{sca}}{C_{abs} + C_{sca}} \quad (2.28)$$

The size, geometry, particle type and the dielectric medium all determines the scattering and absorption efficiency of plasmonic nano-structures nanoparticle. Ideally, it is advisable that nano-structures size for photovoltaic applications should not exceed 50 nm to elicit LSPR responses.

### 2.6.3 Surface plasmon polariton (SPP)

The surface plasmon polariton effects occur when the collective oscillation of surface electrons induces an intense, oscillating field which travels along the surface. The field may propagate along the metallic-nanostructure surface and/or the dielectric medium surface. This effect obviously improves the dielectric response and enhances the photovoltaic process[129]. As illustrated in Figure 2.8c, the electromagnetic propagation may travel a few micrometers along the dielectric surface or few nanometers into the dielectric medium if the plasmonic nano-structure is situated at the interface between the dielectric medium and the metal electrode. The propagating energy eventually gets attenuated due to absorption by the electrode or the bulk of the dielectric layer. Metal/dielectric SPP excitations usually occur if the momentum component of the photon's energy coincides with those of the SPP. SPPs contributes to enhanced interfacial EM absorption and is very useful in thin-film OPVs [130, 131].

Table 2.1: OPV devices with plasmonic nano-structures in the active layer.

Device structures	Plasmonic nano-structures	$V_{oc}$ (V)	$J_{sc}$ ( $mA/cm^2$ )	FF	PCE	Year	Ref
ITO/PEDOT:PSS/P3HT:PCBM-Ag@Cu/ LiF/Al	Ag@Cu NPs	0.60	11.90	54.40	3.87	2019	[132]
ITO/PEDOT:PSS/P3HT:PCBM: Au:Ag /LiF /Al	Au:Ag	0.52	15.40	51.00	3.29	2019	[133]
ITO/PEDOT:PSS/Ag@SiO <sub>2</sub> /PTB7:PC70BM /Al	Ag@SiO <sub>2</sub>	0.74	16.65	68.00	8.92	2013	[134]
ITO/PEDOT:PSS/Au@SiO <sub>2</sub> /P3HT:PCBM /Al	Au@SiO <sub>2</sub>	0.62	10.60	57.00	3.80	2013	[135]
ITO/PEDOT:PSS/P3HT:ICBA-Au /Ca /Al	Au NPs	0.84	11.56	68.83	6.68	2015	[136]
ITO/PEDOT:PSS/P3HT:PCBM: Au/Al	Au-NPs	0.60	9.45	56.65	3.20	2015	[136]
ITO/ZnO/P3HT:PCBM:Ag@SiO <sub>2</sub> /MoO <sub>3</sub> /Ag	Ag@SiO <sub>2</sub>	0.61	9.72	66.50	3.94	2015	[121]
ITO/PEDOT:PSS/P3HT:PCBM-Au/Al	Au NPs	0.60	9.77	63.38	3.71	2012	[122]
ITO/TiO <sub>2</sub> /PBDTTT-C-T:PC <sub>71</sub> BM+Au /MoO <sub>3</sub> /Ag	Au	0.76	18.39	62.87	8.79	2012	[?]
ITO/PEDOT:PSS/Ag@SiO <sub>2</sub> /PTB7:PC <sub>71</sub> BM /Ca /Al	Ag@SiO <sub>2</sub>	0.75	17.05	67.30	8.61	2018	[137]
ITO/PEDOT:PSS/PCDTBT:PC <sub>71</sub> BM-Ag/ TiO <sub>x</sub> /Al	Ag NPs	0.86	11.61	69.00	7.10	2011	[160]
ITO/PEDOT:PSS/P3HT:PCBM-Ag /Ca /Al	Ag NPs	0.64	9.93	64.08	4.07	2013	[161]
ITO/PEDOT:PSS/PTB7:PC <sub>71</sub> BM-Au@Ag@SiO <sub>2</sub> /Ca /Al	Au@Ag@SiO <sub>2</sub> NC	0.75	18.07	70.8	9.56	2016	[162]
ITO/PEDOT:PSS/PBDTTT-C-T:PC <sub>71</sub> BM-Ag@SiO <sub>2</sub> /Ca /Al	Ag@SiO <sub>2</sub> NPs	0.76	16.94	62.0	7.77	2017	[138]
ITO/PEDOT:PSS/P3HT:PCBM-Ag:Zn:Ni /LiF /Al	Ag:Zn:Ni NC	0.56	12.36	47.70	3.33	2019	[139]
ITO/ZnO/PTB7:PCBM-Ag:Zn:Ni/MoO <sub>3</sub> / Al	Ag : Zn :Ni NC	0.73	14.76	46.93	5.06	2019	[140]
ITO/ZnO/PTB7:CdS:PCBM/MoO <sub>3</sub> /Ag	CdS-NPs	0.74	14.20	64.65	6.80	2016	[141]
ITO/PEDOT:PSS/P3HT:PCBM-Ag:Zn /LiF /Al	Ag:Zn NPs	0.55	14.00	47.00	3.60	2017	[142]
ITO/rGO/ZnO/P3HT:PCBM-Ag /MoO <sub>3</sub> /Ag	Ag-NPs	0.63	10.99	63.64	4.37	2016	[143]
ITO/rGO/ZnO/P3HT:PCBM-Au /MoO <sub>3</sub> / Ag	Au-NPs	0.63	11.17	63.70	4.44	2016	[143]
ITO/TiO <sub>2</sub> /PBDTTT-C-T:PC <sub>71</sub> BM+Au/ MoO <sub>3</sub> / Ag	Au-NPs	0.88	16.01	48.10	6.83	2015	[144]
ITO/PEDOT:PSS/P3HT:PCBM:Zn-SnS/ LiF/ Al	Zn-SnS NPs	0.55	12.65	54.00	3.75	2020	[145]

## 2.6.4 Applications of metal nanoparticles as plasmonic agents in OPVs

Plasmonic structures have been used by many researchers to enhance OPV device performances by incorporating various plasmonic nano-structures in the active layers of the solar cells. The optical absorption and charge collection processes were significantly improved through the various plasmonic mechanisms earlier discussed, leading to superior power conversion efficiencies being reported [160, 161, 162].

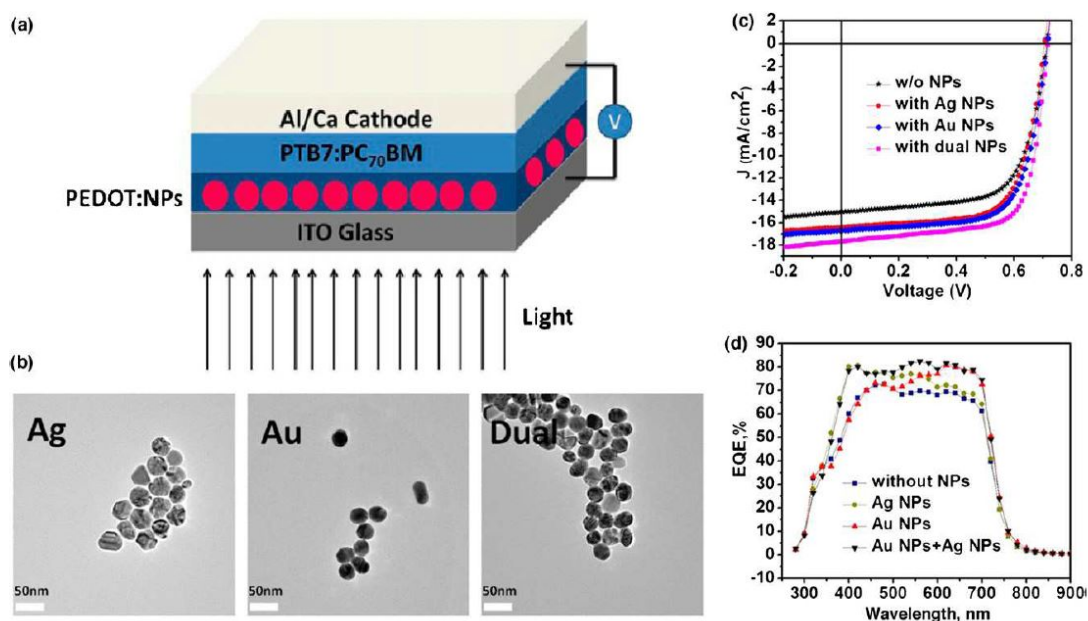


Figure 2.10: (a) Device structure of the solar cell embedded with bi-metallic NPs of Au and Ag (b) TEM images of Ag, Au, and bi-NPs (c) J-V curves of solar cells with and without NPs (d) EQE spectra of PTB7:PC<sub>70</sub>BM with and without NPs [163]

Li et al incorporated gold (Au) nanoparticles in the active layer of PTB7/PC<sub>70</sub>BM solar cell and reported increased plasmon-induced absorption with the absorption broadband ranging from 350 to 800 nm, resulting in enhanced power conversion efficiency of the devices to 9.62% [164]. Bimetallic Au@Ag(NPs) nano-particles were used in a P3HT:PCBM solar cell by Tzounis et al. to investigate their plasmonic performance. An improved PCE of 2.69% was obtained, while undoped devices recorded PCE of 2.24%. Oseni et al. studied two different bimetallic nano-composites, silver:zinc (Ag:Zn) and silver: magnesium (Ag:Mg), which were blended into PTB7:PCBM photo-active layers. Improved device performance was recorded for both cases in comparison to the pristine undoped devices due to enhanced optical and electrical properties of the doped devices [165]. More results of investigations by various research groups using different metal or metallic nano-composites in the photo-active layer of OPV devices have been summarized in Table 2.1.

Similarly, plasmonic effects can be induced by adding suitable metallic-nanocomposites to the transport layers of the organic solar cells. Plasmonic metal nano-structures incorporation in the electron- or hole- transport layers (ETL and HTL) of the solar

Table 2.2: OPV devices with plasmonic nano-structures in the buffer layer.

Device structures	Plasmonic nano-structures	$V_{oc}$ (V)	$J_{sc}$ ( $mA/cm^2$ )	FF	PCE	Year	Ref
ITO/PEDOT:PSS: Au@SiO <sub>2</sub> /PTB7:PC <sub>71</sub> BM/ LiF/ Al	Au@SiO <sub>2</sub> NPs	0.78	18.75	65.16	9.55	2020	[146]
ITO/Au:ZnO/PBDTTT-C-T:PC <sub>71</sub> BM /MoO <sub>3</sub> /Ag	Au NPs	0.75	15.81	66.20	7.86	2015	[147]
ITO/ZnO:Ag-SiO <sub>2</sub> /P3HT:PCBM /PEDOT:PSS/ Ag	Ag-NPs SiO <sub>2</sub>	0.58	14.14	46.00	3.54	2019	[148]
ITO/PEDOT:PSS: Au/PTB7:PC <sub>71</sub> BM/ TiO <sub>x</sub> :Au /Al	Au-NPs	0.76	17.17	61.40	8.01	2016	[149]
ITO/PEDOT:PSS: Au/PCDTBT:PC <sub>71</sub> BM/ TiO <sub>x</sub> :Au /Al	Au-NPs	0.89	12.03	62.90	6.75	2016	[149]
ITO/PEDOT:PSS: Au/P3HT:PCBM/ LiF/ Al	Au-NPs	0.63	8.94	62.00	3.51	2011	[150]
ITO/PEI/P3HT:ICBA/WO <sub>3</sub> :Cu/Ag	Cu-NPs	0.87	11.79	62.20	6.38	2016	[152]
ITO/PEDOT:PSS: Au/PBDT-TS1:PC <sub>70</sub> BM/ Ca/ Al	Au-NPs	0.82	18.72	67.34	10.29	2017	[153]
ITO/PEDOT:PSS: SiO <sub>2</sub> /P3HT:PC <sub>61</sub> BM /Al	SiO <sub>2</sub> NPs	0.52	12.10	36.00	2.27	2017	[154]
ITO/PEDOT:PSS: Ag/PTB7:PC <sub>71</sub> BM /Ca/ Al	Ag-NPs	0.68	14.70	63.20	6.40	2018	[155]
ITO/PEDOT:PSS: Cu/P3HT:PC <sub>60</sub> BM/ TiO <sub>x</sub> / Al	Cu-NPs	0.63	10.06	62.2	3.96	2014	[156]
ITO/PEDOT:PSS: Cu/PTB7:PC <sub>70</sub> BM/ TiO <sub>x</sub> / Al	Cu-NPs	0.63	10.06	62.2	3.96	2014	[156]
ITO/WO <sub>3</sub> : Au@SiO <sub>2</sub> /P3HT:PCBM/ LiF/ Al	Au@SiO <sub>2</sub>	0.61	4.72	54.00	1.58	2019	[157]
ITO/PEDOT:PSS: Ag/PTB7:PC <sub>70</sub> BM /Ca /Al	Ag-NPs	0.71	16.40	68.80	8.01	2013	[158]
ITO/PEDOT:PSS: Au/PTB7:PC <sub>70</sub> BM /Ca /Al	Au-NPs	0.71	16.70	68.80	8.16	2013	[158]
ITO/PEDOT:PSS: Au+Ag/PTB7:PC <sub>70</sub> BM /Ca /Al	Au+Ag NPs	0.71	17.70	69.00	8.67	2013	[158]
ITO/PEDOT:PSS: Ag:Zn/P3HT:PCBM /LiF/ Al	Ag:Zn-NPs	0.59	15.3	53.00	5.0	2019	[159]

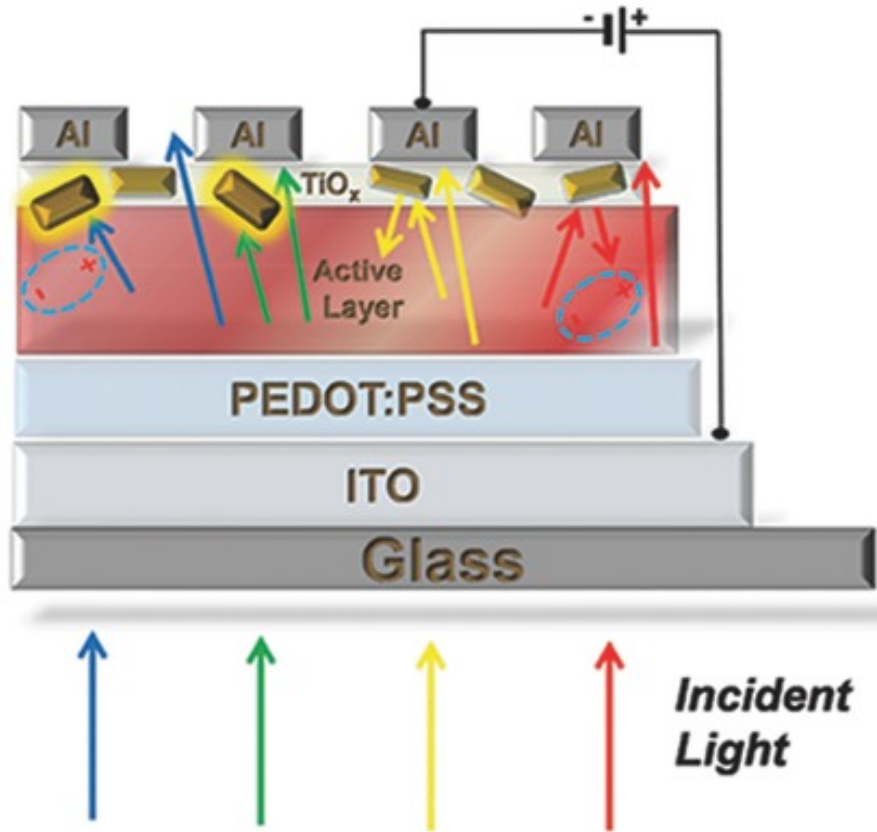


Figure 2.11: Plasmonic nano-structures embedded in the rear charge transport layer[149].

cells can enhance the incident light trapping through scattering and SPP processes, since these are more location dependent. Moreover, incorporation of plasmonic nano-structures aid in the collection of the charge carrier specie of the layer in which the nano-structures are added, thereby reducing recombination. Hence, holes collection may become easier with the addition of plasmonic structures in the holes transport layer of an organic solar cell and same for the electron transport layer[147]. For example, in Figure 2.9, the plasmonic nano-structures placed at the rear of the buffer layer scatters the light, inducing a cascade of total internal reflection events within the photo-absorbing layer of the device, effectively increasing the optical path length of the EM radiation. Obviously the radiation spends more time in the active-layer and thus interacts more with the medium and more photon absorption occurs[149]. D.S. Fung demonstrates that the incorporation of suitable plasmonic nanoparticles in PEDOT:PSS as HTL can enhance the HTL-Active layer interface roughness, reducing the series resistance and increasing the photo-current density[150]. Moreover, the conductivity of the medium is improved. Further reports of studies involving plasmonic nano-structures embedded in the charge transport layers of organic solar cells are included in Table 2.2.

## 2.7 Metal-sulphides as plasmonic materials in OPVs

Metal-sulphides are a group of semiconductor materials characterized by the presence of a sulfur being chemically bound to one or more metals, with the sulfur acting as anion in the compound. Metal-sulphide nano-structures have in recent years been attracting research attention for renewable energy applications because a myriad of compounds that can be easily synthesized, having easily adaptable optoelectronic, and physico-chemical properties. Their increasingly popular use is due to the wide range of bandgaps to which they could be tuned, band positioning[166]. Metal-sulphides have well-exposed active sites and are thus also encouraging for catalytic and photo-catalytic studies. These interesting materials have a range of potential unique properties that can be harnessed to harvest the solar light spectrum more effectively. Their small effective mass and shallow valence bands[167, 168, 172] makes them demonstrate quantum size effects in applications[169, 170, 171]. Metal-sulphides nano-composites have been reported to significantly enhance electrical conductivity, morphology and durability; conditions favorable for energy conversion and storage applications[174, 175, 173, 176, 177, 178].

# Bibliography

- [1] M.A.Green, K.Emery, Y.Hishikawa, W.Warta, and E.D. Dunlop, *Solar cell efficiency tables (Version 38)*, *Prog. Photovolt: Res. Appl.* 19(2011)565-572.
- [2] Cui, Y., Xu, Y., Yao, H., Bi, P., Hong, L., Zhang, J., Zu, Y., Zhang, T., Qin, J., & Ren, J. (2021). *Single-Junction Organic Photovoltaic Cell with 19% Efficiency*. *Advanced materials*, 33(41), 2102420.
- [3] L.Meng, Y.Zhang, X.Wan, C.Li, X.Zhang, Y.Wang, X. Ke, Z.Xiao, L.Ding, R.Xia, H.-L.Yip, Y.Cao, Y.Chen, *Organic and solution-processed tandem solar cells with 17.3% efficiency*, *Science* 14 (2018) 1094-1098.
- [4] A.Goetzberger, J.Knobloch, B.Voss, *Crystalline Silicon Solar Cells*. New York, (1998)114-118.
- [5] A.J.Heeger. *Bulk Heterojunction Solar Cells: Understanding the Mechanism of Operation*. *Adv Mater*, 26(2014)10-28.
- [6] H.Jin, C.Tao, M.Velusamy, M.Aljada, Y.Zhang, M.Hambsch, P.L. Burn, and P.Meredith, *Efficient, Large Area ITO-and-PEDOT-free Organic Solar Cell Sub-modules*, *Adv. Mater.* 24(2012)2572-2577.
- [7] G.Li, V. Shrotriya, J. S. Huang, Y. Yao, T. Moriarty, K. Emery, and Y. Yang, *High-efficiency solution processable polymer photovoltaic cells by self-organization of polymer blends*, *Nat. Mater*, 4 (2005)80-84.
- [8] H.Shirakawa, E. J. Louis, A. G. MacDiarmid, C. K. Chiang, A. J. Heeger, *Synthesis of electrically conducting organic polymers: halogen derivatives of polyacetylene, (CH)<sub>x</sub>*, *J. Chem. Soc. Chem. Comm.*, 16 (1977) 578-580.
- [9] T.D.Nielsen, C.Cruickshank, S.Forger, J.Thorsen, F.C.Krebs, *Business, market and intellectual property analysis of polymer solar cells*, *Solar Energy Materials and Solar Cells* 94(2010)1553-1571.
- [10] J.Kalowekamo, E.Baker , *Estimating the manufacturing cost of purely organic solar cells.*” *Solar Energy* 83 (2009) 1224-1231.
- [11] C.Powell, T.Bender, Y.Lawryshyn, Powell, Colin, *A model to determine financial indicators for organic solar cells*. *Solar Energy* 83(2009)1977-1984.
- [12] P.Kumaresan, S.Vegiraju, Y.Ezhumalai, S.L.Yau, C.Kim, W.-H.Lee, and M.-C.Chen, *Fused-Thiophene Based Materials for Organic Photovoltaics and Dye-Sensitized Solar Cells*, *Polymers*, 6(2014) 2645-2669.

- [13] *H.Hoppe and N.S.Sariciftci, Organic solar cells: An overview. Journal of materials research, 19(2004)1924-1945.*
- [14] *D.Wöhrle, and D.Meissner, Organic solar cells. Advanced Materials, 3(1991)129-138.*
- [15] *G.Dennler, N.S.Sariciftci, and C.J. Brabec, Conjugated polymer-based organic solar cells. Chemical reviews, 107(2007)1324-1338.*
- [16] *Alaa, F. E., Sun, J. P., Hill, I. G., & Welch, G. C. (2014). Recent advances of non-fullerene, small molecular acceptors for solution processed bulk heterojunction solar cells. Journal of Materials Chemistry A, 2(5), 1201-1213.*
- [17] *A.M.Bagher, Introduction to organic solar cells. Sustain. Energy 2 (2014)85-90.*
- [18] *A.G.Chamberlain, Organic solar-cells — a review, Sol Cells, 8(1983)47-83.*
- [19] *O.A.Abdulrazzaq, V.Saini, S.Bourdo, E.Dervishi and A. S. Biris Organic solar cells: a review of materials, limitations, and possibilities for improvement. Part. Sci. Technol. 31 (2013)427-442.*
- [20] *J.J.M.Halls, K. Pichler, R. H. Friend, S. C. Moratti and A. B. Holmes. Exciton diffusion and dissociation in a poly(p-phenylenevinylene)/C-60 heterojunction photovoltaic cell. Appl Phys Lett. 68(1996)3120.*
- [21] *V.S.Gevaerts, L.J.A. Koster, M.M. Wienk, R.A.J. Janssen, Discriminating between bilayer and bulk heterojunction polymer: fullerene solar cells using the external quantum efficiency, ACS Appl. Mater. Interfaces 3 (2011) 3252-3257.*
- [22] *S.H.Park, A.Roy, S.Beaupre, S.Cho, N.Coates, J.S.Moon, D.Moses, M.Leclerc, K.Lee, and A.J. Heeger, Bulk heterojunction solar cells with internal quantum efficiency approaching 100%. Nat Photonics. 2009;3(5):297-302.*
- [23] *W.Wang, C.J. Schaffer, L.Song, V.Körstgens, S.Pröllner, E.D.Indari, T. Wang, A.Abdelsamie, S.Bernstorff, and P.M.-Buschbaum, In operando morphology investigation of inverted bulk heterojunction organic solar cells by GISAXS. J. Mater. Chem. A 3 (2015)8324-8331.*
- [24] *J.Peet, J.Y.Kim, N.E.Coates, W.L.Ma, D.Moses, A.J.Heeger, et al. Efficiency enhancement in low-bandgap polymer solar cells by processing with alkane dithiols. Nat Mater. 7 (2007)497-500.*
- [25] *T.Salim, L.H.Wong, B.Brauer, R.Kukreja, Y.L.Foo, Z.N.Bao, et al. Solvent additives and their effects on blend morphologies of bulk heterojunctions. J Mater Chem. 21(2011)242-50.*
- [26] *Chen, F.-C., Wu, J.-L., & Hung, Y. (2010). Spatial redistribution of the optical field intensity in inverted polymer solar cells. Applied Physics Letters, 96(19), 95.*
- [27] *Gilot, J., Barbu, I., Wienk, M. M., & Janssen, R. A. (2007). The use of ZnO as optical spacer in polymer solar cells: theoretical and experimental study. Applied Physics Letters, 91(11), 113520.*

- [28] Kim, J. Y., Kim, S. H., Lee, H. H., Lee, K., Ma, W., Gong, X., & Heeger, A. J. (2006). New architecture for high-efficiency polymer photovoltaic cells using solution-based titanium oxide as an optical spacer. *Advanced materials*, 18(5), 572-576.
- [29] Roy, A., Park, S. H., Cowan, S., Tong, M. H., Cho, S., Lee, K., & Heeger, A. J. (2009). Titanium suboxide as an optical spacer in polymer solar cells. *Applied Physics Letters*, 95(1), 179.
- [30] P. P. Khlyabich, A. E. Rudenko, R. A. Street, and B. C. Thompson, *ACS Appl. Mater. Interfaces* 6 (2014) 9913-9919.
- [31] T. Ameri, P. Khoram, J. Min, and C. J. Brabec, *Adv. Mater.* 25 (2013) 4245-4266.
- [32] Tvingstedt, K., Andersson, V., Zhang, F., & Inganäs, O. (2007). Folded reflective tandem polymer solar cell doubles efficiency. *Applied Physics Letters*, 91(12), 123514.
- [33] Zhou, Y., Zhang, F., Tvingstedt, K., Tian, W., & Inganäs, O. (2008). Multi-folded polymer solar cells on flexible substrates. *Applied Physics Letters*, 93(3), 257.
- [34] Cocoyer, C., Rocha, L., Sicot, L., Geffroy, B., De Bettignies, R., Sentein, C., Fiorini-Debuisschert, C., & Raimond, P. (2006). Implementation of submicrometric periodic surface structures toward improvement of organic-solar-cell performances. *Applied Physics Letters*, 88(13), 133108.
- [35] Na, S. I., Kim, S. S., Jo, J., Oh, S. H., Kim, J., & Kim, D. Y. (2008). Efficient polymer solar cells with surface relief gratings fabricated by simple soft lithography. *Advanced Functional Materials*, 18(24), 3956-3963.
- [36] Mandal, P., & Sharma, S. (2016). Progress in plasmonic solar cell efficiency improvement: A status review. *Renewable and sustainable energy reviews*, 65, 537-552.
- [37] Tang, M., Sun, B., Zhou, D., Gu, Z., Chen, K., Guo, J., Feng, L., & Zhou, Y. (2016). Broad-band plasmonic Cu-Au bimetallic nanoparticles for organic bulk heterojunction solar cells. *Organic Electronics*, 38, 213-221.
- [38] Y. Tian, and T. Tatsuma, *Mechanisms and Applications of Plasmon-Induced Charge Separation at TiO<sub>2</sub> Films Loaded with Gold Nanoparticles*, *J. Am. Chem. Soc.*, 127(2005) 7632-7637.
- [39] N.Zhou, V.L.-Puente, Q.Wang, L.Polavarapu, I.P.-Santos, and Q.-H.Xu, *Plasmon-enhanced light harvesting: applications in enhanced photocatalysis, photodynamic therapy and photovoltaics* *RSC Advances* 5(37)29076-29097.
- [40] A.Tanaka, S.Sakaguchi, K.Hashimoto and H.Kominami, *Preparation of Au/TiO<sub>2</sub> with Metal Cocatalysts Exhibiting Strong Surface Plasmon Resonance Effective for Photoinduced Hydrogen Formation under Irradiation of Visible Light*, *ACS Catal.*, 3(2012)79-85.

- [41] *S.T.Kochuveedu, Y.H.Jang, and D.H.Kim, A study on the mechanism for the interaction of light with noble metal-metal oxide semiconductor nanostructures for various photophysical applications. Chem. Soc. Rev.42(2013)8467-8493.*
- [42] *H.A.Atwater, and A.Polman, Plasmonics for improved photovoltaic devices. Nat Mater 9(2010)205-213.*
- [43] *Y.-H.Su, Y.-F.Ke, S.-L.Cai, and Q.-Y.Yao, Surface plasmon resonance of layer-by-layer gold nanoparticles induced photoelectric current in environmentally-friendly plasmon-sensitized solar cell, Light: Sci. Appl. 1(2012) 14.*
- [44] *U. Kreibig, M. Vollmer, Optical Properties of Metal Clusters, Springer Science & Business Media, Springer-Verlag, Berlin, Heidelberg 2013*
- [45] *K. L. Kelly, E. Coronado, L. L. Zhao, G. C. Schatz, J. Phys. Chem. B. 2003, 107, 668*
- [46] *S. M. Amini, J. Therm. Biol. 2019, 79, 81*
- [47] *Y. Liu, Z. Liu, D. Huang, M. Cheng, G. Zeng, C. Lai, C. Zhang, C. Zhou, W. Wang, D. Jiang, H. Wang, B. Shao, Coord. Chem. Rev. 2019, 388, 63*
- [48] *X. Duan, S. Kamin, N. Liu, Nat. Commun. 2017, 8, 14606*
- [49] *C. Zong, M. Xu, L.-J. Xu, T. Wei, X. Ma, X.-S. Zheng, R. Hu, B. Ren, Chem. Rev. 2018, 118, 4946.*
- [50] *J. Clayden, N. Greeves, S. Warren, P. Wothers. Organic Chemistry. 1st Edition. Oxford: Oxford University Press; (2001)*
- [51] *Moliton, A., Hiorns, R. C. Review of electronic and optical properties of semi-conducting  $\pi$ -conjugated polymers: applications in optoelectronics. Polymer International 53, 1397-1412, (2004).*
- [52] *Fahlman, M., Salaneck, W. R. Surfaces and interfaces in polymer-based electronics. Surf. Sci. 500, 904-922 (2002).*
- [53] *Semiconducting Polymers, Vol. 1(Eds: G. Hadziioannou, G. G. Malliaras), Wiley-VCH, Weinheim 2007.*
- [54] *Jonathan Griffin, Transition Metal Oxides and Their Use as Hole Extraction Materials in Organic Photovoltaic Devices, Thesis, University of Sheffield, UK (2014)*
- [55] *V. D. Mihailetschi, P. W. M. Blom, J. C. Hummelen, M. T. Rispen. Cathode Dependence on the Open-Circuit Voltage of Polymer:Fullerene Bulk Heterojunction Solar Cells. Journal of Applied Physics. 94, 6849-6854 (2003)*
- [56] *D. Rauh, A. Wagenpfahl, C. Deibel, V. Dyakonov. Relation of Open-Circuit Voltage to Charge Carrier Density in Organic Bulk Heterojunction Solar Cells. Applied Physics Letters. 98, 133301 (2011)*

- [57] V. Coropceanu, J. Cornil, D. A. D. S. Filho, Y. Olivier, R. Silbey, J. L. Bredas., *Charge Transport in Organic Semiconductors. Chemical Reviews.* 107, 926-952 (2007)
- [58] W. R. Salaneck, R. H. Friend, J. L. Bredas. *Electronic Structure of Polymers. Physical Reports.* 319, 231-251 (1999)
- [59] Scharber, M. C. D. Muhlbacher, M. Koppe, P. Denk, C. Waladauf, A. J. Heeger, C. J. Brabec. *Design rules for donors in bulk-heterojunction solar cells – Towards 10 % energy conversion efficiency. Adv. Mater.* 18, 789-794 (2006)
- [60] Harri Aarnio, Parisa Sehati, Slawomir Braun, Mathias Nyman, Michel P. de Jong, Mats Fahlman, and Ronald Österbacka, *Spontaneous charge transfer and dipole formation at the interface between P3HT and PCBM. Adv. Energy Mater,* 1, 792-797 (2011)
- [61] Qinye Bao, Oskar Sandberg, Daniel Dagnelund, Simon Sandén, Slawomir Braun, Harri Aarnio, Xianjie Liu, Weimin M. Chen, Ronald Österbacka, Mats Fahlman; *Trap-assisted recombination via integer charge transfer states in organic bulk heterojunction photovoltaics. Adv. Funct. Mater.* 24, 6309-6316 (2014)
- [62] Hwang, J., Wan, A., Kahn, A. *Energetics of metal-organic interfaces: New experiments and assessment of the field. Mat. Sci. Eng. R.* 64, 1-31 (2009)
- [63] Shoaee, S. et al. *Charge photogeneration in donor/acceptor organic solar cells. J. Photon Energy* 2, 021001 (2012)
- [64] Maurano, A. et al. *Recombination dynamics as a key determinant of open circuit voltage in organic bulk heterojunction solar cells: a comparison of four different donor polymers. Adv. Mater.* 22, 4987 (2010)
- [65] K.G. Jespersen, F. Zhang, A. Gadisa, V. Sundström, A. Yartsev, and O. Inganäs, *Org. Electron.* 7, 235-242 (2006).
- [66] S. M. Sze and K. K. Ng, *Physics of semiconductor devices, John Wiley & Sons 3rd edition (2007) New Jersey.*
- [67] J. T. Bell and G. T. Mola, *Physica B: Condensed Matter,* 437 (2014) 63-66.
- [68] G. Chidichimo and L. Filippelli, *Organic Solar Cells: Problems and Perspectives, International Journal of Photoenergy.* (2010).
- [69] C.J.Brabec, C.Winder, S.Sariciftci, J.C. Hummelen, A.Dhanabalan, P.A. Hal, and R.A. J. Janssen, *A low-bandgap semiconducting polymer for photovoltaic devices and infrared emitting diodes. Adv Funct Mater* 12(2002)709-712.
- [70] N.Yeh, P.Yeh, *Organic solar cells: their developments and potentials. Renewable and Sustainable Energy Reviews* 21 (2013) 421-431.
- [71] P.W.M.Blom, V.D. Mihaileti, L. J.A.Koster, and D.E. Markov. *Device physics of polymer: fullerene bulk heterojunction solar cells. Adv Mater* 2007;19:1551-66.

- [72] C. Deibel, V. Dyakonov, *Rep. Prog. Phys.* 73 (2010) 096401(39pp).
- [73] J. L. Bredas, J. E. Norton, J. Cornil, and V. Coropeanu, *Accounts of Chemical Research* 42(11) (2009) 1691-1699.
- [74] J.Nelson, *The Physics of Solar Cells*, Imperial College Press, London, (2003).
- [75] Q.An, F.Zhang, J.Zhang, W.Tang, Z.Deng, B.Hu, *Versatile ternary organic solar cells: a critical review*, *Energy Environ. Sci.*, 9(2016)281-322.
- [76] C.J.Brabec, A.Cravino, D.Meissner, N. S.Sariciftci, T.Fromherz, M.T. Rispens, L.Sanchez, J.C. Hummelen, *Origin of the Open Circuit Voltage of Plastic Solar Cells*, *Adv. Funct. Mater.* 11( 2001)374-380.
- [77] J.-T.Chen, and C.-S.Hsu, *Conjugated polymer nanostructures for organic solar cell applications*, *Polym. Chem.*, 2(2011) 2707-2722.
- [78] V.Shrotriya, Wu, E. H. E., Li, G, Y.Yao, Y.Yang, *Efficient light harvesting in multiple device stacked structure for polymer solar cells*, *Applied physics letters*, 88(2006), 064104.
- [79] S.E.Shaheen, C.J.Brabec, N.S.Sariciftci, F.Padinger, T.Fromherz, J.C.Hunnelen, *2.5% Efficient organic plastic solar cells*. *Appl Phys Lett* 78(2001)841-843.
- [80] M.Jrgensen and F. C. Krebs, *Valence band edges and optical band gaps of alternating substituted poly(phenylenevinylenes)* *Polym. Bull.*, 51(2003) 20-23.
- [81] H.Sirringhaus, N.Tessler, R.H.Friend, *Integrated optoelectronic devices based on conjugated polymers*. *Science* 280.5370 (1998)1741-1744.
- [82] Z.C.He, C.M. Zhong, S.J. Su, M. Xu, H.B. Wu, Y. Cao, *Enhanced power conversion efficiency in polymer solar cells using an inverted device structure*, *Nat. Photon.* 6 (2012) 591-595.
- [83] P.Li, T. Jiu, G. Tang, G. Wang, J. Li, X. Li, J. Fang, *Solvents induced ZnO nanoparticles aggregation associated with their interfacial effect on organic solar cells*, *ACS Appl. Matter. Interfaces* 6 (2014) 18172-18179.
- [84] L.Burgi, M.Turbiez, R.Pfeiffer, F.Bienewald, H.J.Kirner, C.Winnewisser, *Highmobility ambipolar near-infrared light-emitting polymer field-effect transistors*. *Adv Mater* 20(2008)2217-2224.
- [85] J.Hou, M.H.Park, S.Zhang, Y.Yao, L.MChen, J.H.Li, Y.Yang, *Bandgap and molecular energy level control of conjugated polymer photovoltaic materials based on benzo[1,2-b:4,5-b']dithiophene*. *Macromolecules* 41(2008)6012-6018.
- [86] S.Shao, K. Zheng, T. Pullerits, F. Zhang, *Enhanced performance of inverted polymer solar cells by using poly (ethylene oxide)-modified ZnO as an electron transport layer*, *ACS Appl. Matter. Interfaces* 5 (2013) 380-385.
- [87] J.C.Hummelen, B.W. Knight, F. Lepeq, F. Wudl, *J. Org. Chem.Preparation and characterization of fulleroid and methanofullerene derivatives* 60 (1995) 532.

- [88] G.J. Zhao, Y.J. He, Y.F. Li, 6.5% Efficiency of Polymer Solar Cells Based on poly(3-hexylthiophene) and Indene-C60 Bisadduct by Device Optimization *Adv. Mater.* 22 (2010) 4355.
- [89] Mola, G. T., Ahmed, A. Y., Ike, J. N., Liu, M., Hamed, M. S., & Zhang, Y. (2022). Engineering Non-fullerene Acceptors as a Mechanism to Control Film Morphology and Energy Loss in Organic Solar Cells. *Energy & Fuels*.
- [90] Liu, L., Zhou, S., Zhao, C., Jiu, T., Bi, F., Jian, H., Zhao, M., Zhang, G., Wang, L., Li, F., Xiao, X., TTA as a potential hole transport layer for application in conventional polymer solar cells. *J. Energy Chem.* 2020, 42, 210-216.
- [91] Liu, T., Guo, Y., Yi, Y., Huo, L., Xue, X., Sun, X., Fu, H., Xiong, W., Meng, D., Wang, Z., Liu, F., Russell, T. P., Sun, Y., Ternary organic solar cells based on two compatible nonfullerene acceptors with power conversion efficiency 10%. *Adv. Mater.* 2016, 28 (45), 10008-10015.
- [92] Lucenno-Sanchez, J. A., Díez-Pascual, A. M., Pena Capilla, R., Materials for photovoltaics: State of art and recent developments. *Int. J. Mol. Sci.* 2019, 20 (4), 976.
- [93] Chen, C. C., Chang, W. H., Yoshimura, K., Ohya, K., You, J., Gao, J., Hong, Z., & Yang, Y. (2014). An efficient triple-junction polymer solar cell having a power conversion efficiency exceeding 11%. *Advanced materials*, 26(32), 5670-5677.
- [94] Lin, Y., & Zhan, X. (2014). Non-fullerene acceptors for organic photovoltaics: an emerging horizon. *Materials Horizons*, 1(5), 470-488.
- [95] Cui, Y., Yao, H., Zhang, J., Zhang, T., Wang, Y., Hong, L., Xian, K., Xu, B., Zhang, S., Peng, J., Wei, Z., Gao, F., Hou, J., Over 16% efficiency organic photovoltaic cells enable by a chlorinated acceptor with increased open-circuit voltages. *Nat. Commun.* 2019, 10 (1), 2515.
- [96] Yuan, J., Zhang, Y., Zhou, L., Zhang, G., Yip, H.L., Lau, T.K., Lu, X., Zhu, C., Peng, H., Johnson, P. A., Leclerc, M., Cao, Y., Ulanski, J., Li, Y., Zou, Y., Single-Junction Organic Solar Cell with over 15% Efficiency Using Fused-Ring Acceptor with Electron-Deficient Core. *Joule* 2019, 3 (4), 1140-1151.
- [97] C.C. Chen, W.H. Chang, K. Yoshimura, K. Ohya, J. You, J. Gao, Z. Hong and Y. Yang, *Adv. Mater.* 26 (2014) 5670-5677.
- [98] Y. Liu, J. Zhao, Z. Li, C. Mu, W. Ma, H. Hu, K. Jiang, H. Lin, H. Ade and H. Yan, *Nat. Commun.* 4 (2014) 6293.
- [99] L. Nian, W. Zhang, N. Zhu, L. Liu, Z. Xie, H. Wu, F. Wurthner and Y. Ma, *J. Am. Chem. Soc.* 137 (2015) 6995-6998.
- [100] I. Constantinou, T-H. Lai, D. Zhao, E. D. Klump, J. J. Deiningner, C. K. Lo, J. R. Reynolds, and F. So, *Appl. Mater. Interfaces* 7 (2015) 4826-4832.
- [101] N. Li and C.J. Brabec, *Energy Environ. Sci.* 8 (2015) 2902-2909.

- [102] Wu, J. L., Chen, F. C., Hsiao, Y. S., Chien, F. C., Chen, P., Kuo, C. H. & Hsu, C. S. (2011). Surface plasmonic effects of metallic nanoparticles on the performance of polymer bulk heterojunction solar cells. *ACS nano*, 5(2), 959-967.
- [103] Fleetham, T., Choi, J.-Y., Choi, H. W., Alford, T., Jeong, D. S., Lee, T. S., Lee, W. S., Lee, K.-S., Li, J., & Kim, I. (2015). Photocurrent enhancements of organic solar cells by altering dewetting of plasmonic Ag nanoparticles. *Scientific reports*, 5(1), 1-9.
- [104] Kalfagiannis, N., Karagiannidis, P., Pitsalidis, C., Panagiotopoulos, N., Gravalidis, C., Kassavetis, S., Patsalas, P., & Logothetidis, S. (2012). Plasmonic silver nanoparticles for improved organic solar cells. *Solar Energy Materials and Solar Cells*, 104, 165-174.
- [105] Mandal, P., & Sharma, S. (2016). Progress in plasmonic solar cell efficiency improvement: A status review. *Renewable and sustainable energy reviews*, 65, 537-552.
- [106] Enrichi, F., Quandt, A., & Righini, G. C. (2018). Plasmonic enhanced solar cells: Summary of possible strategies and recent results. *Renewable and sustainable energy reviews*, 82, 2433-2439.
- [107] Na, S. I., Kim, S. S., Jo, J., Oh, S. H., Kim, J., & Kim, D. Y. (2008). Efficient polymer solar cells with surface relief gratings fabricated by simple soft lithography. *Advanced Functional Materials*, 18(24), 3956-3963.
- [108] S.T.Kochuveedu, T.Son, Y.Lee, M.Lee, D.Kim, and D.H.Kim, Revolutionizing the FRET-Based Light Emission in Core-Shell Nanostructures via Comprehensive Activity of Surface Plasmons. *Sci.Rep.* 4(2014)4735.
- [109] X.D.Hoa, A.G. Kirk, M.Tabrizian. Towards Integrated and sensitive Surface Plasmon Resonance Biosensors: A Review of recent progress. *Biosens. Bioelectron.*23(2007)151-160.
- [110] J.Boken, P.Khurana, S.Thatai, D.Kumar and S.Prasad, Plasmonic nanoparticles and their analytical applications: A review, *Applied Spectroscopy Reviews*, 9(2017) 774-820.
- [111] N.Li, D.Liu, and H.Cui, Metal-nanoparticle-involved chemiluminescence and its applications in bioassays ,*Analytical and bioanalytical chemistry* 23 (2014): 5561-5571.
- [112] C.-H.Chou, and F.-C.Chen, Plasmonic nanostructures for light trapping inorganic photovoltaic devices, *Nanoscale*, 6(2014)8444-8458.
- [113] R.Veenkamp, S.Ding, I.Smith, and W. N. Ye, Silicon Solar Cell Enhancement by Plasmonic Silver Nanocubes. In *Physics, Simulation, and Photonic Engineering of Photovoltaic Devices III*, SPIE OPTO, San Francisco, USA, Feb 3-6, 2014 Freundlich, A., Guillemoles, J.-F., Eds.; SPIE, Bellingham, WA, 2014; 89811B.

- [114] C.Burda, X. Chen, R. Narayanan and M. A. El-Sayed, *Chemistry and Properties of Nanocrystals of Different Shapes* Chem. Rev., 105(2005)1025-1102.
- [115] J.Mertz, *Radiative absorption, fluorescence, and scattering of a classical dipole near a lossless interface: a unified description.* J. Opt. Soc. Am. B 17(2000) 1906-1913.
- [116] P.Spinelli, M.Hebbink, R.de Waele, L.Black, F. Lenzmann, and A.Polman, *Optical Impedance Matching Using Coupled Plasmonic Nanoparticle Arrays,* Nano Lett. 11 (2011)1760-1765.
- [117] W.R. Erwin, H.F. Zarick, E.M. Talbert and R.Bardhan, *Light trapping in mesoporous solar cells with plasmonic nanostructures,* Energy Environ. Sci., 9(2016)1577-1601.
- [118] M.Pelton, J. Aizpurua, and G. Bryant, *Metal-nanoparticle plasmonics* Laser Photonics Rev, 136(2008)136-159.
- [119] S.Pillain, M.A. Green, *Plasmonics for photovoltaic applications,* Solar Energy Materials & Solar Cells 94 (2010) 1481-1486.
- [120] C.-H.Chou, and F.-C.Chen, *Plasmonic nanostructures for light trapping inorganic photovoltaic devices,* Nanoscale, 6(2014)8444-8458.
- [121] L.-W.Jang, H.Park, S.-H.Lee, A.Y. Polyakov, R. Khan, J.-K.Yang, and I.-H.Lee, *Device performance of inverted polymer solar cells with Ag@SiO<sub>2</sub> nanoparticles in active layer,* Optics Express, 23(2015) A211-A218.
- [122] G.D.Spyropoulos, M.M.Stylianakis, E.Stratakis, and E.Kymakis, *Organic bulk heterojunction photovoltaic devices with surfactant-free Au nanoparticles embedded in the active layer.* Appl. Phys. Lett.100(2012)213904.
- [123] D.T.Gangadharan, Z.Xu, Y.Liu, R.Izquierdo, D.Ma, *Recent advancements in plasmon-enhanced promising third-generation solar cells,* Nanophotonics, 6(2017)153-175.
- [124] K.L.Kelly, E.Coronado, L.L.Zhao, and G.C. Schatz, *J. Phys. Chem. B The optical properties of metal nanoparticles the influence of size, shape, and dielectric environment* 107 (2003) 668.
- [125] C.F.Bohren, *How can a particle absorb more than the light incident on it?* Am.J. Phys. 51(1983) 323-327.
- [126] K.R.Catchpole, A.Polman, *Plasmonic solar cells,* Opt. Express 16 (2008) 21793-21800.
- [127] G.Xu, M. Tazawa, P. Jin, S. Nakao, and K. Yoshimura, *"Wavelength tuning of surface plasmon resonance using dielectric layers on silver island films,"* Appl. Phys. Lett. 82(2003) 3811-3813.
- [128] H.Mertens, J. Verhoeven, A. Polman, and F. D. Tichelaar, *"Infrared surface plasmons in two-dimensional silver nanoparticle arrays in silicon,"* Appl. Phys. Lett. 85(2004)1317-1319.

- [129] V.E.Ferry, L.A. Sweatlock, D.Pacifici, H.A. Atwater, *Plasmonic Nanostructure Design for Efficient Light Coupling into Solar Cells*. *Nano Lett.* 8(2008) 4391-4397.
- [130] V.E.Ferry, L.A.Sweatlock, D.Pacifici, H.A. Atwater. *Supporting Information: Plasmonic Nanostructure Design for efficient Light Coupling into Solar Cells* *Nano Lett.* 8 (2008) 4391.
- [131] H.Raether, in *surface Plasmons*, Springer Tracts in Modern Physics Vol.111, edited by G. Höhler Springer, Berlin, (1988), 4-18.
- [132] M.W.Dlamini, G.T.Mola, *Near-field enhanced performance of organic photovoltaic cells*, *Physica B: Condensed Matter* 552 (2019)78-83.
- [133] H.Kaçuş, S.Aydoğan, M .Biber, Ö.Metin ,and M.Sevim, *The power conversion efficiency optimization of the solar cells by doping of (Au:Ag) nanoparticles into P3HT:PCBM active layer prepared with chlorobenzene and chloroform solvents*, *Materials Research Express*, 9(2019)095104.
- [134] H.Choi, J.-P.Lee, S.-J.Ko, J.-W.Jung, H.Park, S.Yoo, O.Park, J.-R. Jeong, S.Park, and J.Y.Kim, *Multipositional Silica-Coated Silver Nanoparticles for High-Performance Polymer Solar Cells*, *Nano letters*, 13(2013)2204-2208.
- [135] B.Chen, W.Zhang, X.Zhou, X.Huang, X.Zhao, H.Wang, M.Liu, Y.Lu, SYang, *Surface plasmon enhancement of polymer solar cells by penetrating Au@SiO<sub>2</sub> core/shell nanoparticles into all organic layers*, *Nano Energy*, 2(2013)906-915.
- [136] E.Kymakis, G.D.Spyropoulos, R.Fernandes, G.Kakavelakis, A.G.Kanaras, and E.Stratakis, *Plasmonic Bulk Heterojunction Solar Cells: The Role of Nanoparticle Ligand Coating*, *ACS Photonics*, 2(2015) 714-723.
- [137] S.Liu, Y.Hou, W.Xie, S.Schlücker, F.Yan, and D.Y.Lei, *Quantitative Determination of Contribution by Enhanced Local Electric Field, Antenna-Amplified Light Scattering, and Surface Energy Transfer to the Performance of Plasmonic Organic Solar Cells*, *Small*,14(2018) 1800870.
- [138] W.Shen, J.Tang, Y.Wang, J.Liu, L.Huang, W.Chen, L.Yang, W.Wang, Y.Wang, R.Yang, J.Yun, and Laurence A. Belfiore, *Strong Enhancement of Photoelectric Conversion Efficiency of Co-hybridized Polymer Solar Cell by Silver Nanoplates and Core-Shell Nanoparticles.*” *ACS applied materials & interfaces* 9 (2017)5358-5365.
- [139] X.G.Mbuyise, E.A. A. Arbab, and G.T.Mola, *The effect of a trimetallic nanocomposite in the solar absorber layer of organic solar cells*, *RSC Adv.*, 9(2019) 6070-6076.
- [140] S.O.Oseni, G.T.Mola, *Effects of metal-decorated nanocomposite on inverted thin film organic solar cell*, *Journal of Physics and Chemistry of Solids* 130 (2019) 120-126.
- [141] R.Sharma, S.Bhalerao, D.Gupta, *Effect of incorporation of CdS NPs on performance of PTB7: PCBM organic solar cells*, *Organic Electronics* 33 (2016) 274-280

- [142] G.T.Mola, E.A. A. Arbab, *Bimetallic nanocomposite as hole transport co-buffer layer in organic solar cell*, *Applied Physics A* 123 (2017)772.
- [143] S.R.Gollu, R.Sharma, G.Srinivas, S.Kundu, D.Gupta, *Incorporation of silver and gold nanostructures for performance improvement in P3HT: PCBM inverted solar cell with rGO/ZnO nanocomposite as an electron transport layer*, *Organic Electronics* 29 (2016) 79-87.
- [144] Y.He, C.Liu, J.Li, X.Zhang, Z.Li, L.Shen, W.Guo, and S.Ruan, *Improved Power Conversion Efficiency of Inverted Organic Solar Cells by Incorporating Au Nanorods into Active Layer*, *ACS Applied Materials and Interfaces* 29(2015)15848-15854.
- [145] S.L.Mousavi, F.J.-Sheini, M.Sabaeian, R.Yousefie, *Enhanced solar cell performance of P3HT:PCBM by SnS nanoparticles*, *Solar Energy* 199 (2020) 872-884.
- [146] X.Li, Y.Cao, S.Li, W.Li, and Z.Bo, *The preparation of plasmonic Au@SiO<sub>2</sub> NPs and its application in polymer solar cells*, *Materials Letters* 268 (2020) 127599.
- [147] D.Chi, S.Lu, R.Xu, K.Liu, D.Cao, L.Wen, Y.Mi, Z.Wang, Y.Lei, S.Qu and Z.Wang, *Fully understanding the positive roles of plasmonic nanoparticles in ameliorating the efficiency of organic solar cells*. *Nanoscale*,7(2015)15251-15257.
- [148] K.N'Konou, M.Chalh, B.Lucas, S.Vedraine and P.Torchio, *Improving the performance of inverted organic solar cells by embedding silica-coated silver nanoparticles deposited by electron-beam evaporation*, *PolymInt* 68(2019)979-983.
- [149] G.Kakavelakis, I.Vangelidis, A.H.-Jungemann, A.G. Kanaras, E.Lidorikis , E.Stratakis, and E.Kymakis, *Plasmonic Backscattering Effect in High-Efficient Organic Photovoltaic Devices*, *Adv. Energy Mater.*6(2016) 1501640.
- [150] D.D.S.Fung, L.Qiao, W.C.H.Choy, C.Wang, W. E.I. Sha, F. Xiea and S.He, *Optical and electrical properties of efficiency enhanced polymer solar cells with Au nanoparticles in a PEDOT:PSS layer*. *J. Mater. Chem.* 21(2011)16349.
- [151] M.Tang, B.Sun, D.Zhou, Z.Gu, K.Chen, J.Guo, L. Feng, Y.Zhou, *Broad-band plasmonic Cu-Au bimetallic nanoparticles for organic bulk heterojunction solar cells*, *Organic Electronics* 38 (2016) 213-221.
- [152] P.Shen, Y.Liu, Y.Long, L.Shen, and B.Kang, *High-Performance Polymer Solar Cells Enabled by Copper Nanoparticles-Induced Plasmon Resonance Enhancement*, *J. Phys. Chem.* 120, (2016) 8900-8906.
- [153] Q.Li, F.Wang, Y.Bai, L.Xu, Y.Yang, L.Yan, S.Hu, B. Zhang, S.Dai, Z.Tan, *Decahedral-shaped Au nanoparticles as plasmonic centers for high performance polymer solar cells*, *Organic Electronics* 43 (2017) 33-40.
- [154] P.Shao, X.Chen, X.Guo, W.Zhang, F.Chang, Q.Liu, Q.Chen, J.Li, Y.Li, D.He, *Facile embedding of SiO<sub>2</sub> nanoparticles in organic solar cells for performance improvement*, *Organic Electronics* 50 (2017) 77-81.

- [155] C.-P.Chen, I.-C.Lee, Y.-Y.Tsai, C.-L.Huang, Y.-C.Chen, G.-W.Huang, *Efficient organic solar cells based on PTB7/PC71BM blend film with embedded different shapes silver nanoparticles into PEDOT:PSS as hole transporting layers*, *Organic Electronics* 62 (2018) 95-101.
- [156] Z.Liu, S.Y.Lee, and E.-C.Lee, *Copper nanoparticle incorporated plasmonic organic bulk-heterojunction solar cells*, *APPLIED PHYSICS LETTERS* 105 (2014) 223306.
- [157] Y.H.Lee, A.E.Abdu, D.H.Kim, T.W.Kim, *Enhancement of the power conversion efficiency of organic photovoltaic cells due to Au@SiO<sub>2</sub> core shell nanoparticles embedded into a WO<sub>3</sub> hole transport layer*, *Organic Electronics* 68 (2019) 182-186.
- [158] L.Lu, Z.Luo, T.Xu, and L.Yu, *Cooperative Plasmonic Effect of Ag and Au Nanoparticles on Enhancing Performance of Polymer Solar Cells*, *Nano Lett.* 13(2013)59-64.
- [159] E.A.A. Arbab, G.T.Mola, *Metals decorated nanocomposite assisted charge transport in polymer solar cell*, *Materials Science in Semiconductor Processing* 91 (2019) 1-8.
- [160] D.H.Wang , K.H.Park , J.H. Seo, J.Seifter , J.H.Jeon , J.K.Kim, J.H. Park, O.O.Park, and A.J. Heeger , *Enhanced PowerConversion Efficiency in PCDTBT/PC70BM Bulk HeterojunctionPhotovoltaic Devices with Embedded Silver Nanoparticle Clusters*.*Adv. Energy Mater.*1(2011)766-770.
- [161] X.Li, W.C.H.Choy, H. Lu, W. E. I. Sha, and A.H.P.Ho, *Efficiency Enhancement of Organic Solar Cells by Using Shape-Dependent Broadband Plasmonic Absorption in Metallic Nano-particles*.*Adv. Funct.Mater.*23(2013)2728-2735.
- [162] S.Liu, R.Jiang, P.You, X.Zhu, J.Wang, and F.Yan, *Au/Ag core-shell nanocuboids for high-efficiency organic solar cells with broadband plasmonic enhancement*, *Energy Environ. Sci.*, 9(2016) 898-905.
- [163] Notarianni, M., et al., *Plasmonic effect of gold nanoparticles in organic solar cells*. *Solar Energy*, 2014. 106: p.23-37.
- [164] X.Li, X.Ren, F.Xie, Y.Zhang, T.Xu, B.Wei, and W.C. H. Choy, *High-Performance Organic Solar Cells with Broadband Absorption Enhancement and Reliable Reproducibility Enabled by Collective Plasmonic Effects*, *Advanced Optical Materials* 9 (2015)1220-1231.
- [165] S.O.Oseni, G.T.Mola, *Bimetallic nanocomposites and the performance of inverted organic solar cell*,*Composites Part B* 172 (2019) 660-665
- [166] Chandrasekaran, S., Yao, L., Deng, L., Bowen, C., Zhang, Y., Chen, S. & Zhang, P. (2019). *Recent advances in metal sulfides: from controlled fabrication to electrocatalytic, photocatalytic and photoelectrochemical water splitting and beyond*. *Chemical Society Reviews*, 48(15), 4178-4280.
- [167] Y. Shiga, N. Umezawa, N. Srinivasan, S. Koyasu, E. Sakai and M. Miyauchi, *Chem. Commun.*, 2016, 52, 7470-7473.

- [168] Q. H. Wang, K. Kalantar-Zadeh, A. Kis, J. N. Coleman and M. S. Strano, *Nat. Nanotechnol.*, 2012, 7, 699.
- [169] Y. Wang and N. Herron, *J. Phys. Chem.*, 1991, 95, 525–532.
- [170] A. Hoffman, G. Mills, H. Yee and M. Hoffmann, *J. Phys. Chem.*, 1992, 96, 5546–5552.
- [171] D. Voiry, R. Fullon, J. Yang, C. de Carvalho Castro e Silva, R. Kappera, I. Bozkurt, D. Kaplan, M. J. Lagos, P. E. Batson, G. Gupta, Aditya D. Mohite, L. Dong, D. Er, V. B. Shenoy, T. Asefa and M. Chhowalla, *Nat. Mater.*, 2016, 15, 1003.
- [172] M. Chhowalla, H. S. Shin, G. Eda, L. J. Li, K. P. Loh and H. Zhang, *Nat. Chem.*, 2013, 5, 263.
- [173] K. Iwashina, A. Iwase, Y. H. Ng, R. Amal and A. Kudo, *J. Am. Chem. Soc.*, 2015, 137, 604–607.
- [174] X. Rui, H. Tan and Q. Yan, *Nanoscale*, 2014, 6, 9889–9924.
- [175] X. Xu, W. Liu, Y. Kim and J. Cho, *Nano Today*, 2014, 9, 604–630.
- [176] J. Bebie, M. A. Schoonen, M. Fuhrmann and D. R. Strongin, *Geochim. Cosmochim. Acta*, 1998, 62, 633–642.
- [177] Y. Zhao, L. P. Wang, M. T. Sougrati, Z. Feng, Y. Leconte, A. Fisher, M. Srinivasan and Z. Xu, *Adv. Energy Mater.*, 2017, 7, 1601424.
- [178] Y. Li, H. Wang, L. Xie, Y. Liang, G. Hong and H. Dai, *J. Am. Chem. Soc.*, 2011, 133, 7296–7299.

# Chapter 3

## Materials, Methods and Device Simulation Modelling

In this chapter, the list of chemicals used in the various experiments contained in this thesis are presented, with reasons adduced for their usage where necessary. The experimental methods, characterizations and device simulation principles behind the P3HT/PCBM solar cell are also presented.

### 3.1 Materials

#### 3.1.1 The metal-sulphide nano-structures

Two metal sulphide nanoparticles, Silver Sulphide ( $Ag_2S$ ) and Copper Sulphide (CuS) were used in the investigations contained in this thesis. Copper sulphide (CuS) is a common p-type semi-conductor that has been used in gas sensors [1], in lithium-ion batteries as cathode material [2], non-linear optical material and solar radiation absorber [3, 4, 5]. It also has found application in composite materials and thin films. It is a good counter electrode for quantum DSSCs [6, 7, 8]. CuS can be incorporated as nano-particles in photo-active medium of OSC for its plasmonic resonance effects [9]. Lei H. et al recently fabricated a TFOSC with an in-situ p-type copper sulphide prepared via a low cost, low temperature, hydrothermal method [10] as the HTL and obtained a 3.4% PCE. In this investigation, we have incorporated CuS nanoparticles into PEDOT:PSS as a hole transport buffer layer so as to improve the surface contacts and aid charge collection from P3HT/PC61BM TFOSC, in a standard device architecture.

Silver sulfide ( $Ag_2S$ ) is a monoclinic crystal structure with a narrow band gap, a large absorption coefficient and good chemical stability. It has an excellent electronic and photo-conductivity that are suitable for photovoltaic application [11, 12, 13, 14]. This nano-structure was used in both a conventional and inverted device architec-

ture utilizing PEDOT:PSS and Zinc Oxide as the Hole transport and the Electron transport buffer materials respectively.

### 3.1.2 Photo-active layer materials

The photo-active layer materials consisted of blends of donor and acceptor materials. The donor polymers are: poly(3-hexylthiophene) (**P3HT**) and Poly[4,8-bis(5-(2-ethylhexyl)thiophen-2-yl)benzo [1,2-b;4,5-b']dithiophene-2,6-diyl-alt-(4-(2-ethylhexyl)-3-fluorothieno[3,4-b] thiophene-)-2-carboxylate-2-6-diyl)] (**PTB7-Th**).

The acceptors are the fullerene acceptors [6,6]-phenyl-C61-butyric acid methyl ester (**PC60BM**) and [6,6]-phenyl C71-butyric acid methyl ester (**PC71BM**), and the non-fullerene acceptor 3,9-bis(2-methylene-(3-(1,1-dicyanomethylene)-indanone))-5,5,11,11-tetrakis(5-hexylthienyl)-dithieno[2,3-d:2',3'-d']-s-indaceno[1,2-b:5,6-b'] dithiophene (**ITIC-Th**).

### 3.1.3 Charge transport layers

Poly(3,4 ethylene dioxythiophene):poly(styrene sulfonate) (PEDOT:PSS) and Zinc Oxide were used as the hole transport material and electron transport material respectively.

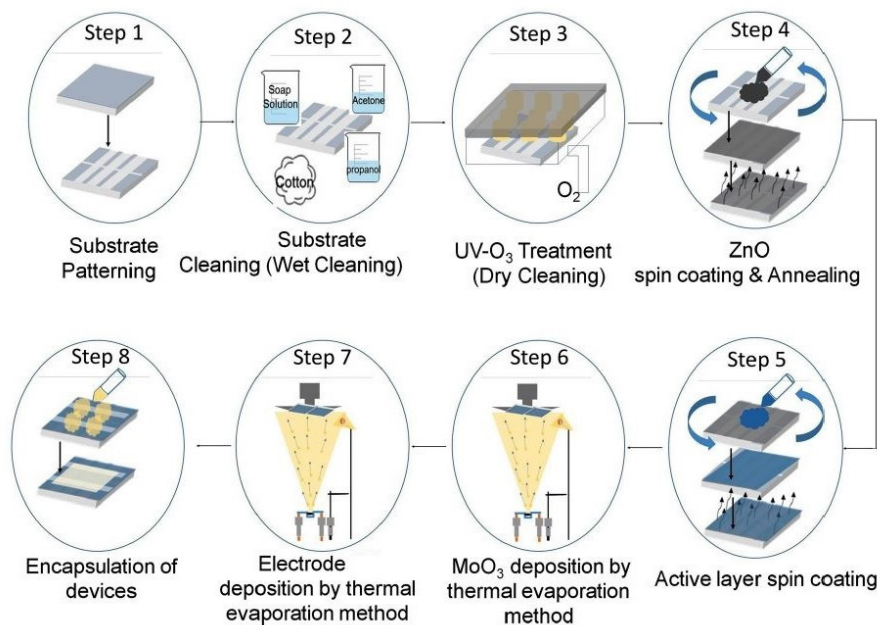


Figure 3.1: Typical device fabrication processes for inverted solar cells[15]

## 3.2 Characterizations and characteristics

**UV-Vis spectroscopy** was measured with a UV-vis Rayleigh 1601 and Perkin Elmer Lambda UV-Visible-NIR spectro-photometers. The nano-structures dispersed in de-ionized water, thin films of the materials and/or blends and fabricated devices (in some cases) absorption spectral scans were done in the 300 - 900 nm range.

**Scanning and Transmission electron microscopy - SEM and TEM** investigations were conducted with a SEM - JEOL JSM6100, Zeiss Evo SEM and a TEM - JEOL JEM 1010. These were used for characterizing the surface morphology and composition of the metal-sulphide nano-structures.

**XRD analysis** was conducted with a Bruker D8 Discover X-Ray Diffractometer, with filtered Cu-K $\alpha$ 1 radiation source and ( $\lambda = 0.15406$  nm) to resolve the structural phases at varying  $2\theta$  values. The XRD data were successfully matched with standard crystallographic data for phase determinations.

**Steady-state Photoluminescence** was acquired with Edinburgh Instruments FS5 spectrofluorometer.

**The J-V characteristics** of the fabricated devices was measured using solar simulator systems comprising of a computer interfaced with a Keithley (HP2420) source meter and a solar simulator (model SS50AAA) under a AM 1.5 illumination and operating at a light intensity of 100 mW/cm<sup>2</sup> [16, 17].

**EQE measurements** were taken with a custom built incident photon-current conversion efficiency.

## 3.3 The Simulation Model

The photo- and electrical response of OSCs can be modeled by accounting for the motion of free charge carriers across the device as well as their trapping and de-trapping dynamics in energy space. A finite-difference drift-diffusion model is therefore adopted to describe these processes. Also by discretizing the HOMO-LUMO energy space, trap levels by which recombination occurs are defined within the model. Although the model accepts input parameters for all layers of the OSC, it adopts an effective medium approximation to simulate transport of free carriers in the device's photo-active only [18, 19].

Poisson's equation is solved to get the voltage profile  $\phi$  within the device (equation 1), between the anode at  $x = 0$  and the cathode at  $x = d$ ,

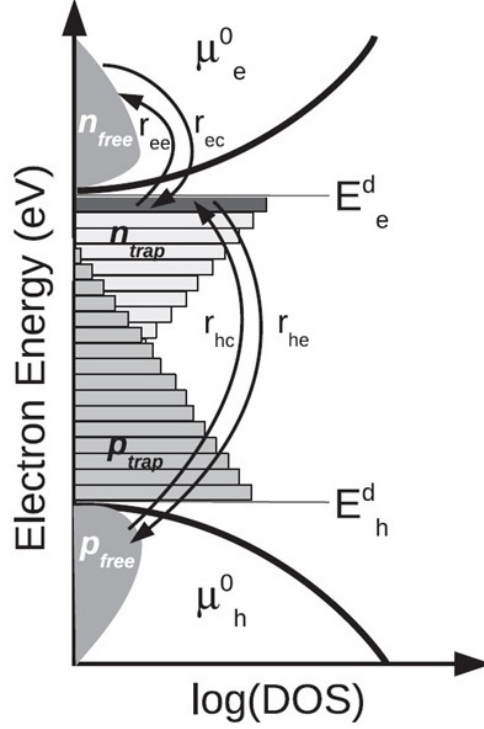


Figure 3.2: DoS diagram adopted in the model. The e/h capture and release processes for one electron trap. Similar processes take place in all electron and hole traps[24]

$$\frac{d}{dx} \cdot \epsilon_0 \epsilon_r \frac{d\phi}{dx} = q(n - p) \quad (3.1)$$

where  $\epsilon_0$ ,  $\epsilon_r$ ,  $q$ ,  $n$  and  $p$  are the permittivity of free space, the relative permittivity of the photo-active layer, the elementary charge quantity, the free electron- and the free hole- populations respectively. The current continuity equations for electrons (equation 2) and holes (equation 3) are solved to determine current flux in the cell.

$$\frac{\partial J_n}{\partial x} = q(R_n - G + \frac{\partial n}{\partial t}) \quad (3.2)$$

$$\frac{\partial J_p}{\partial x} = q(R_p - G + \frac{\partial p}{\partial t}) \quad (3.3)$$

here  $J_{n,p}$ ,  $R_{n,p}$  and  $G$  represent the electron current- and the hole current- flux densities, the electron- and the hole- recombination rates and the free carrier generation rate, respectively. The drift-diffusion equation for electrons eq(4) and holes eq(5) are used as expressed below[20, 21]

$$J_n = q\mu_e n \frac{\partial E_C}{\partial x} + qD_n \frac{\partial n}{\partial x} \quad (3.4)$$

$$J_p = q\mu_h p \frac{\partial E_V}{\partial x} + qD_p \frac{\partial p}{\partial x} \quad (3.5)$$

The Maxwell-Boltzmann statistics is used to describe the free carriers.  $E_C$  and  $E_V$  are the free carrier mobility edges. They are given as  $E_C = -\chi - \phi$  while  $E_V = E_V - E_g$ , where  $\chi$  is vacuum level – LUMO mobility edge difference while the HOMO – LUMO mobility edges difference defines the  $E_g$ .

Electrons and holes capture, escape, and recombination are modeled using the Shockley-Read-Hall (SRH) recombination formalism for both charge species[22]. Figure 1 provides a representation of the density of states (DoS), capture, escape, and recombination in which an exponential DoS was adopted for trapped carriers while a parabolic band was adopted for the free carriers. The number of trapped levels and their characteristic energy width between the HOMO and the LUMO levels can be varied to fit experimental data. For an electron trap as noted in Figure 1, the trap's electron density ( $n_t$ ) is expressed by;

$$\frac{\delta n_t}{\delta t} = r_{ec} - r_{ee} - r_{hc} + r_{he} \quad (3.6)$$

where  $r_{ec}$  is the free electrons trap rate,  $r_{ee}$  is the trapped electrons escape/release rate,  $r_{hc}$  is the free holes trap rate and the  $r_{he}$  is the trapped holes escape/release rate. Similar equation exists for a hole trap. References[22, 23, 24] provide additional descriptions for the rates. Electrons and holes escape rates are respectively expressed as equations 7 and 8

$$e_n = \nu_{th}\sigma_n N_C \exp\left(\frac{E_t - E_C}{kT}\right) \quad (3.7)$$

$$e_p = \nu_{th}\sigma_p N_V \exp\left(\frac{E_V - E_t}{kT}\right) \quad (3.8)$$

$\nu_{th}$ ,  $\sigma_n$ ,  $\sigma_p$ ,  $N_C$  and  $N_V$  are the carriers thermal emission velocity, electron and hole trap cross sections, conduction and valence bands effective DoS for free the free carriers respectively. Hence, the difficulty of carriers to escape from a trap is strongly dependent on how energetically deep the trap is. For the trap states, their DoS is given as;

$$\rho^{e/h}(E) = N^{e/h} \exp\left(\frac{E}{E_u^{e/h}}\right) \quad (3.9)$$

where  $E_u^{e/h}$  stands for the tail slope characteristic energy while  $N^{e/h}$  represents the trap DoS magnitude at the LUMO or HOMO band edge. To calculate  $N_t$  for one trap ( $N_t(E)$ ), the DoS function in equation 9 is averaged over the trap's entire energy range  $\Delta E$ :

$$N_t(E) = \frac{\int_{E-\Delta E/2}^{E+\Delta E/2} \rho^e(E) dE}{\Delta E} \quad (3.10)$$

By finding the difference between total escaped electrons from traps and total captured electrons into traps, which eventually join the free carrier population across traps, the electron recombination rate ( $R_n$ ) in equation 2 may be evaluated. Following similar process, the holes recombination rate ( $R_p$ ) may also be calculated.

The model as discussed is incorporated in the General-purpose Photovoltaic Device Model (GPVDM)[18] simulation software through which the simulations of the P3HT:PC60BM organic solar cells were performed. The GPVDM is a general-purpose tool for simulating light-harvesting devices, developed by Dr. Roderick C. I. MacKenzie at University of Nottingham, United Kingdom. The program was initially developed for organic solar cells simulation but its being used recently to simulate CIGS, a-Si and c-Si solar cells as well.

# Bibliography

- [1] A.A. Sagade, R. Sharma, *Copper sulphide (CuS) as an ammonia gas sensor working at room temperature*, *Sens. Actuat. B: Chem.* 133 (2008) 135-143.
- [2] C.H. Lai, K.W. Huang, J.H. Cheng, C.Y. Lee, B.J. Hwang, L.J. Chen, *Direct growth of high-rate capability and high capacity copper sulfide nanowire array cathodes for lithium-ion batteries*, *J. Mater. Chem.* 20 (2010) 6638.
- [3] Ben Meester, Liesbeth Reijnen, J. Albert Goossens, Schoonman, *atomic layer deposition of  $Cu_xS$  for solar energy conversion*, *Chem. Vapor Deposition* 9 (2003) 15-20.
- [4] B.R. Jia, M.L. Qin, X.Z. Jiang, Z.L. Zhang, L. Zhang, Y. Liu, X.H. Qu, *Synthesis, characterization, shape evolution, and optical properties of copper sulfide hexagonal bipyramid nanocrystals*, *J.Nanopart. Res.* 15 (2013) 1469-1478.
- [5] M. Page, O.Niitsoo, Y.Itzhaik, D.Cahen, G.Hodes, *Coppersulfide as a light absorber in wet-chemical synthesized extremely thin absorber (ETA) solar cells*, *Energy Environ. Sci.* 2 (2009) 220.
- [6] M. Saranya, C. Santhosh, S.P. Augustine, A.N. Grace, *Synthesis and characterization of CuS nanomaterials using hydrothermal route*, *Experiment. Nanosci.* 4 (2014) 329-336.
- [7] L.H. Qing, C. Hu, C.Z. Yong, L.W. Chang, *CuS nanostructures prepared by a hydrothermal method*, *J. Alloy. Comp.* 509 (2011) 6382-6389.
- [8] W. Ke, G. Fang, H. Lei, P. Qin, H. Tao, W. Zeng, J. Wang, X. Zhao, *An efficient and transparent copper sulfide nanosheet film counter electrode for bifacial quantum dot-sensitized solar cells*, *J. Power Sources* 248 (2014) 809-815.
- [9] Mohammed S.G. Hamed, Genene Tessema Mola, *Copper sulphide as a mechanism to improve energy harvesting in thin film solar cells*, *Journal of Alloys and Compounds* 802 (2019) 252-258.
- [10] Hongwei Lei, Guojia Fang, Fei Cheng, Weijun Ke, Pingli Qin, Zengcai Song, Qiao Zheng, Xi Fan, Huihui Huang, Xingzhong Zhao, *Enhanced efficiency inorganic solar cells via in-situ fabricated p-type copper sulfide as the hole transporting layer*, *Solar Energy Materials & Solar Cells* 128 (2014) 77-84.
- [11] V.Krylova, A.Milbrat, A.Embrechts, J.Baltrusaitis,  *$Ag_2S$  deposited on oxidized polypropylene as composite material for solar light absorption*, *Applied Surface Science* 301 (2014) 134-141

- [12] Z.D.Meng, T.Ghosh, L.Zhu, J.G.Choi, C.Y. Park, W.C.Oh, *Synthesis of fullerene modified with Ag<sub>2</sub>S with high photocatalytic activity under visible light*, *J. Mater. Chem.* 22 (2012) 16127-16135.
- [13] C.Chen, Y. Xie, G. Ali, S.H. Yoo, S.O. Cho, *Improved conversion efficiency of Ag<sub>2</sub>S quantum dot-sensitized solar cells based on TiO<sub>2</sub> nanotubes with a ZnO recombination barrier layer*, *Nanoscale Res. Lett.* 6 (2011) 462.
- [14] Emmanuel Stratakis, and Emmanuel Kymakis , *Nanoparticle-based plasmonic organic photovoltaic devices*, *Materials Today*, Vol. 16 (4), (2013) 134-146
- [15] Datt, R., Arya, S., Bishnoi, S., Gupta, R., Gupta, V., & Khosla, A. (2019). *Comparative study of PTB7: PC71BM based polymer solar cells fabricated under different working environments*. *Microsystem Technologies*, 1-6.
- [16] (Photo Emission Tech, Inc; <http://www.photoemission.com/SS50A.html>)
- [17] Emery, K.A.: *Solar simulators and I-V measurement methods*. *Sol Cells* 18 (1986)251-260
- [18] R. C. I. MacKenzie , T. Kirchartz , G. F. A. Dibb , J. Nelson , *Modeling nongeminate recombination in P3HT: PCBM solar cells*, *J. Phys. Chem. C* 2011 , 115 , 9806.
- [19] R MacKenzie , J. J. Lim , S Bull , S Sujecki , A. J. Kent , E. C. Larkins , *The impact of hot-phonons on the performance of 1.3 μm dilute nitride edge-emitting quantum well lasers*, *J. Phys.: Conf. Series* 2007 , 92 , 012068
- [20] L. J. A. Koster , E. C. P. Smits , V. D. Mihailetschi , *Device model for the operation of polymer/fullerene bulk heterojunction solar cells*, P. W. M. Blom , *Phys. Rev. B* 2005 , 72 , 085205 .
- [21] E. M. Azoff , *Generalized energy-momentum conservation equations in the relaxation time approximation*, *Solid-State Electronics* 1987 , 30 , 913.
- [22] W. Shockley , W. T. Read , *Statistics of the recombinations of holes and electrons*, *Phys. Rev.* 1952 , 87 , 835
- [23] B. E. Pieters , *PhD Thesis, Delft University of Technology* , 2008
- [24] Roderick C. I. MacKenzie, Christopher G. Shuttle, Michael L. Chabinye, and Jenny Nelson, *Extracting Microscopic Device Parameters from Transient Photocurrent Measurements of P3HT:PCBM Solar Cells*, *Adv. Energy Mater.* 2012, DOI: 10.1002/aenm.201100709

# Chapter 4

## Light trapping using copper decorated nano-composite in the hole transport layer of organic solar cells

Solar Energy 203 (2020) 83–90



Contents lists available at ScienceDirect

Solar Energy

journal homepage: [www.elsevier.com/locate/solener](http://www.elsevier.com/locate/solener)



Light trapping using copper decorated nano-composite in the hole transport layer of organic solar cell



Michael A. Adedeji, Mohammed S.G. Hamed, Genene Tessema Mola\*

*School of Chemistry & Physics, University of KwaZulu-Natal, Pietermaritzburg Campus, Private Bag X01, Scottsville 3209, South Africa*

### ARTICLE INFO

**Keywords:**  
Bulk heterojunction  
Copper sulphide  
Hole transport layer  
Nanoparticles  
OSCs stability

### ABSTRACT

Copper sulphide (CuS) nano-particles were employed in the hole transport layer (HTL) of thin film organic solar cells (TFOSC), to assist in the charge transport processes and improve the photons harvesting. Solar cells were fabricated in the standard bulk heterojunction device architecture using solar absorber composed of poly (3 hexylthiophene) (P3HT) and [6,6]-phenyl-C61-butyric acid methyl ester (PCBM) blend. The CuS nano-particles were dispersed in the aqueous solution of PEDOT:PSS, at concentrations varied from 0% to 0.15% by weight, to be able to determine the right doping level for the best solar cell performances. The particles exhibited surface plasmon resonance absorption and induced intense electric field that was beneficial to exciton dissociation. The highest power conversion efficiency found, in this investigation, was 4.51% at 0.10% CuS concentration in the HTL. This is an increase of 115% and 35% over the pristine PEDOT:PSS and CuS only HTLs used solar cells, respectively. Moreover, the solar cells fabricated with CuS doped PEDOT:PSS hole transport layers exhibited better environmental stability in ambient condition compared to those sole PEDOT:PSS or CuS HTLs. The newly fabricated devices were studied in terms of electrical and optical properties of the solar absorber layers.

## 4.1 Abstract

Copper sulphide (CuS) nano-particles **were** employed in the hole transport layer (HTL) of thin film organic solar cells (TFOSC), to assist in the charge transport processes and improve the photons harvesting. The solar cells were fabricated in the standard bulk heterojunction device architecture using solar absorber composed

of poly (3 hexylthiophene) (P3HT) and [6,6]-phenyl-C61-butyric acid methyl ester (PCBM) blend. The CuS nano-particles were dispersed in the aqueous solution of PEDOT:PSS, at concentrations varied from 0% to 0.15% by weight, to be able to determine the right doping level for the best solar cell performances. The particles exhibited surface plasmon resonance absorption and induced intense electric field that was beneficial to exciton dissociation. The highest power conversion efficiency found, in this investigation, was 4.51 % at 0.10% CuS concentration in the HTL. This is an increase of 115% and 35% over the pristine PEDOT:PSS and CuS-only HTLs used solar cells, respectively. Moreover, the solar cells fabricated with CuS doped PEDOT:PSS hole transport layers exhibited better environmental stability in ambient condition compared to those sole PEDOT:PSS or CuS HTLs. The newly fabricated devices were studied in terms of electrical and optical properties of the solar absorber layers.

## 4.2 Introduction

It is to be noted that the amount of energy our planet receives from the sun every minute exceeds the total world's energy consumption for a year. This makes the sun the most important and the most abundant energy reservoir which is yet to be fully tapped to satisfy our energy needs. More solar energy uptake is also crucial to saving the planet Earth from environmental catastrophe [1, 2, 3]. So far, the energy tapped from the sun barely covers 1% of the world's daily energy consumption at present while substantial fraction of energy comes from fossil fuels, which are non-renewable and unsustainable energy sources. The emission of CO<sub>2</sub> into the atmosphere due to the burning of fossil fuels pose real danger to life on the planet [4, 5]. The conventional inorganic molecules-based solar cells are relatively costly and are presently mostly assembled on rigid surfaces and this limit the portability of the solar panels. On the other hand, thin film organic solar cells (TFOSCs) are a relatively new solar cell technology that offer cheap solar cell fabrication cost, environmental friendliness and mechanical flexibility. These advantages over inorganic molecules solar cells make them complementary or suitable alternative solar cell technology [6, 7, 8, 9, 10, 11, 12, 13]. Research in organic solar cells has made important strides in improving power conversion efficiencies (PCEs) and device stability in recent years. A few have attained PCEs of >15% well beyond the required threshold for mass production [9, 10, 11]. However, most TFOSCs still suffer from low PCEs and are environmentally unstable in the presence of oxygen and moisture [14]. Rapid developments in the synthesis of new and stable conjugated polymer and small molecules donors and fullerene acceptors along with interface engineering have greatly contributed to the increase in PCEs [15, 16]. The optimization of the device structures, especially the interfaces between the photo-active layers and the electrodes is one of the approaches that could be adopted to realize increased device performances. This method offers several complementary and alternative possibilities along with the search for new photoactive materials with improved optoelectronic properties [15, 17, 18, 19, 20].

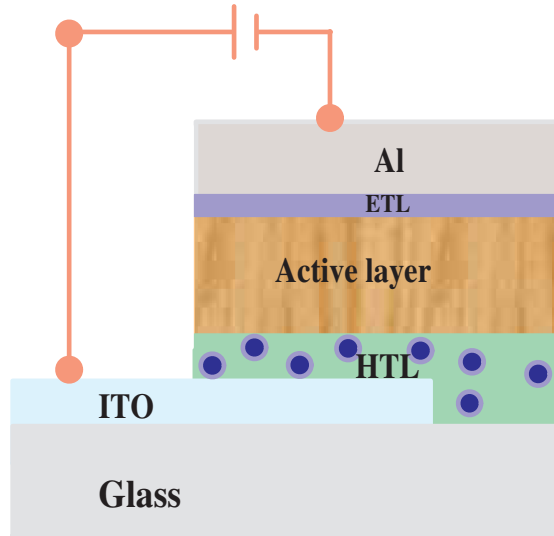


Figure 4.1: Schematics for P3HT:PC61BM photoactive layer BHJ OSC and CuS-nanoparticles doped PEDOT:PSS buffer HTL

The nature of the interface conditions between the photo-active layers and the electrodes is highly important for efficient exciton dissociations and charge extraction in BHJ organic solar cell [15, 16, 17, 18, 19, 20, 21]. Hole and Electron transport layers (HTL & ETL) are usually sandwiched between the photoactive layer and the device electrodes to improve interface conditions and facilitate for more efficient exciton dissociation, charge collection and charge extraction through chemical reactions, geometry modification and/or inducing interfacial charge redistribution processes [15, 16, 19, 21]. Hole transport materials are deposited between the photoactive layer and the anode to selectively transport holes while blocking electrons [22]. Some of these HTL materials are polymers [18, 23, 24, 25], small organic molecules and self-assembled monolayers [26, 27, 28, 29, 30].

The water-soluble polymer molecule, poly(3,4-ethylenedioxythiophene)-poly(styrenesulfonate)(PEDOT:PSS), is the most popular conventional hole transport material (HTM) in organic solar cells [22, 31]. PEDOT:PSS is compatible to solution-based device processing and has a high work function (4.8 - 5.2 eV), enabling ohmic contact formation with numerous small molecules and polymer donors [18, 22, 31, 32, 33, 34, 35, 36, 37, 38]. The presence of an insulating PSS moiety is crucial, thus the pristine PEDOT:PSS HTM film has a relatively low electrical conductivity [18, 22]. The thickness of PEDOT:PSS produces high series resistance in TFOSC devices ( $R_s$ ) and influences the fill factor and short-circuit current ( $J_{sc}$ ) of the devices [39]. The acidic and hygroscopic properties of PEDOT:PSS also make the interface between ITO and PEDOT:PSS to be corrosive and very unstable, leading to reduced power conversion efficiencies and device instability in ambient conditions [40, 41]. Some metal oxides and metal sulphides are used as alternative hole transport materials in TFOSCs, with similar and sometimes better reported efficiencies and device stabilities compared to PEDOT:PSS [42]. Copper sulphide (CuS) is a common p-type semi-conductor that has been used in gas sensors [43], in Lithium-ion batteries as cathode material [44], non-linear optical material and solar

radiation absorber [45, 46, 47]. It also has found application in composite materials and thin films. It is a good counter electrode for quantum DSSCs [48, 49, 50]. CuS can be incorporated as nano-particles in photo-active medium of OSC for its plasmonic resonance effects [42]. Lei H. et al recently fabricated a TFOSC with an in-situ p-type copper sulphide prepared via a low cost, low temperature, hydrothermal method [51] as the HTL and obtained a 3.4% PCE. In this investigation, we have incorporated CuS nanoparticles into PEDOT:PSS as a hole transport buffer layer so as to improve the surface contacts and aid charge collection from P3HT/PC61BM TFOSC, in a standard device architecture. The CuS nanoparticles were well dispersed in aqueous PEDOT:PSS, leading to higher current density in the fabricated devices that resulted in better overall device performances.

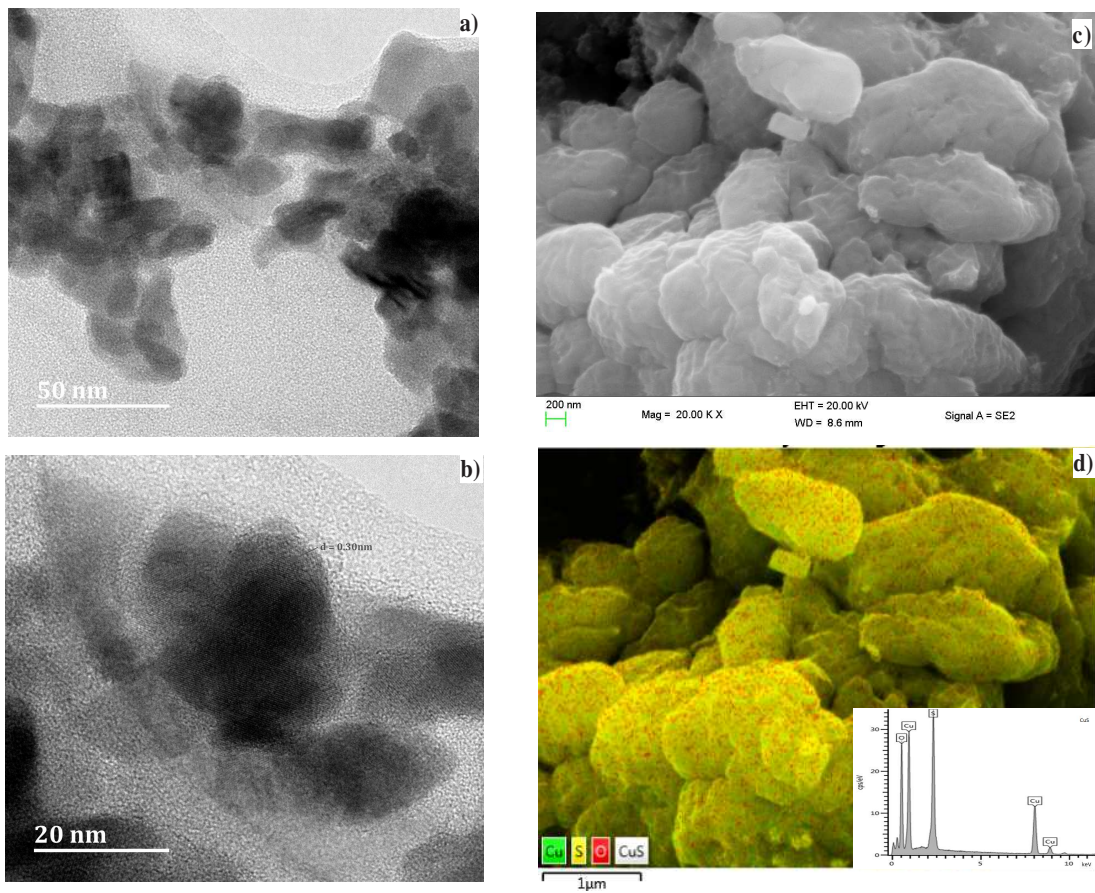


Figure 4.2: CuS powder HRTEM images (a & b), HRSEM (c) and the Energy Dispersive X-ray (EDX) (d).

## 4.3 Experimental and Methods

### 4.3.1 Materials

The polymers poly-(3,4-ethylenedioxythiophene):poly-(styrenesulfonate) (PEDOT:PSS), poly-(3-hexylthiophene) (P3HT):Phenyl-C61-butyric acid methyl ester

(PC61BM) and the substrate, ITO-coated glass (15  $\Omega$ /sq sheet resistance) were obtained from Ossila Ltd, UK and were used as received. The synthesis of CuS was recently reported from our group by Hamed et al [42] and the synthesized CuS was used in this investigation. The ITO-glass substrates were partially etched with acid solution composed of HCl:H<sub>2</sub>O:HNO<sub>3</sub> at 48%:48%:4% concentration ratio by volume. The substrates were thereafter meticulously cleaned in deionized water, acetone and isopropanol ultrasonic baths sequentially for 10 minutes each and then dried in the oven at 100°C for 30 minutes before the HTM was spin-coated on them. Solutions of the HTMs were prepared by blending fine-powdered CuS NPs in PEDOT:PSS solution at concentrations of 0.05%, 0.10% and 0.15% by weight and magnetically stirred overnight at 40°C. The HTMs were spin-coated on the prepared substrates at 3500 rpm for 60 second. Pristine PEDOT:PSS HTM solution was similarly prepared and coated on a substrate as one of the two reference devices. CuS nanoparticles were directly evaporated unto the substrate in a vacuum chamber to obtain the second reference device HTL with a thickness of 20nm. The coated substrates were further annealed in the oven at 100°C for 30 minutes. The organic solar cells thin films were fabricated in the standard device configuration ITO /PEDOT:PSS:CuS / P3HT:PC61BM / LiF / Al in ambient laboratory conditions (Fig 4.1). The photo-absorbing layer contained poly-(3-hexythyophene) (P3HT) and [6-6]phenyl-C61- butyric-acid methyl ester (PCBM) blend at 1:1 ratio by weight, both dissolved in chloroform solvent. The solution has a concentration of 20 mg/ml and was stirred for 4hrs at 40°C to achieve good polymer and molecular miscibility.

The active layer was thereafter spin-coated on the HTL at 1200 rpm for 40 second and dried in a furnace at 100°C for 5 mins in nitrogen atmosphere. The samples were later taken into the vacuum chamber (Edward Auto 306 deposition unit) at a base pressure of 10<sup>6</sup> mbar. A shadow mask was used to define the effective area of the devices, Lithium Fluoride (LiF) was used as the ETL while Aluminium (Al) was used as an electrode. These two were deposited in the vacuum chamber on top of the other layers, with thickness 0.4 nm and 60 nm, respectively. The solar cells were electrically characterized with computer interfaced Keithley HP2400 source-meter and a solar simulator (model SS50AAA) operating at AM1.5 and integrated power intensity of 100 mW/cm<sup>2</sup>. The fabricated diodes have an effective area of 0.6 cm<sup>2</sup>. The photoactive thin film optical properties were studied using UV-vis spectrometer (Rayleigh 1601).

## 4.4 Results and discussion

### 4.4.1 Morphology studies

The as-prepared CuS nanoparticles synthesized through wet chemistry process by Hamed et al was used in this investigation [42]. The nanoparticles had been synthesized and stored in ambient laboratory conditions. Fig. 4.2 contains imageries of the morphology and composition of the Copper Sulphide nanoparticles taken via high resolution scanning and transmission electron microscopy (HRSEM & HRTEM).

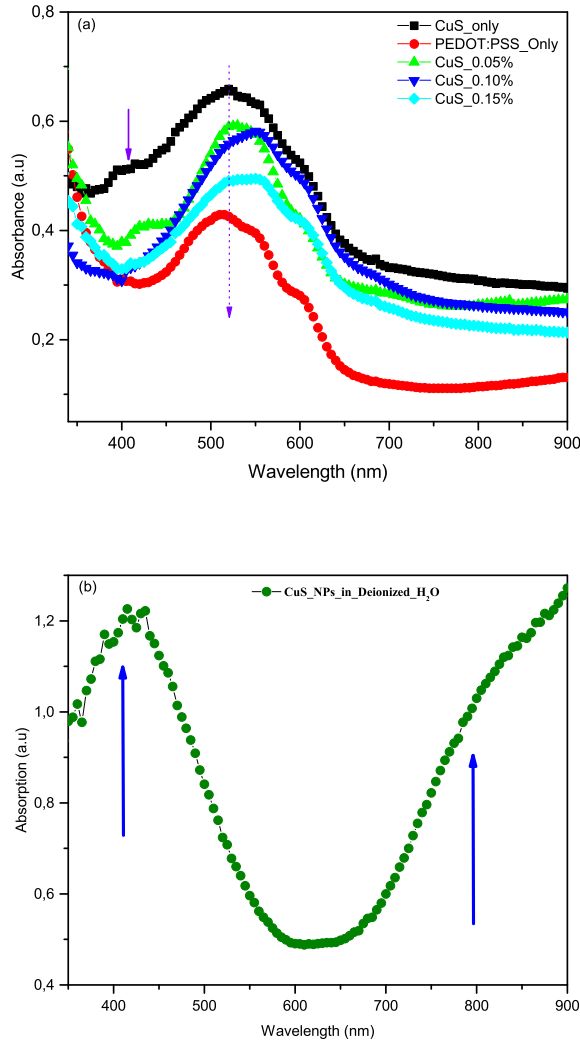


Figure 4.3: Absorption spectra of the solar devices prepared at different CuS concentrations in PEDOT:PSS (b)Optical absorption of CuS NPs suspension in deionized water

Various structures of the CuS NPs can be seen in the HRTEM image of Fig. 2(a) and (b), these were characterized by different shapes and sizes. Oval and spherical shapes with an average diameter of 20 nm clearly dominated the HRTEM images. Moreover, well defined nano crystallites are visible in Fig 2b in terms of several fringes. The lattice constant determined from fringes was 0.30 nm as measured from HRTEM. The HRSEM images provided on Fig. 2c and (d) were taken from the powder of CuS nano-particles which contained various sizes of nano-clusters. The elemental mapping given in Fig. 2(d) displayed uniform distribution of copper and sulphur elements throughout the medium. The EDX elemental analysis (Fig. 2d inset) confirms presence of Cu, S and some O elements, with the significant oxygen level that resulted from the ambient oxidation or the contamination from the sample holder. Detailed analysis on the CuS nanoparticles is given in previous study [42], where further crystallographic representation of the initial X-ray diffraction and

Raman spectroscopic studies were explained.

#### 4.4.2 Optical absorption of HTL films

The hole transport layers were deposited via spin-coating, on cleaned ITO-coated-glass substrates, from solutions of PEDOT:PSS with or without the inclusion of CuS NPs. Solar absorber films were then produced on dried HTL layers from the solution of active layer composed of P3HT:PCBM blend at 1:1 ratio.

The optical characteristics of the various films were examined using UV-Vis spectra as provided in Fig 4.3. The UV-Vis spectra taken from film composed of layers of materials ITO/CuS-doped-PEDOT:PSS/P3HT:PCBM/LiF/Al at various CuS NPs loading is featured in Fig 3a while the absorption spectrum of CuS NPs in deionized water is given in Fig. 4.3b. The absorption of CuS NPs in deionized water has peaks in the low UV region centred around 425 nm as well as in the near infra-red (NIR) region (750 nm – 900 nm) which is in agreement with literatures [52-56]. The absorbance of the CuS NPs decreased from around 425 nm to 700 nm and reached the lowest point around 650 nm, thereafter, the intensity rise once again for longer wavelengths into the near infrared region. According to the literature, the rise at far infra-red is expected to peak around 1300 nm [52]. The first absorption peak in the UV region (around 425 nm) is due to the direct bandgap transition in the semiconductor with bandgap from 1.2 eV to 2.2 eV [52-54]. The absorption around 700 nm in the NIR region resulted from the localized surface plasmon resonance of valence-band free charge carriers [55].

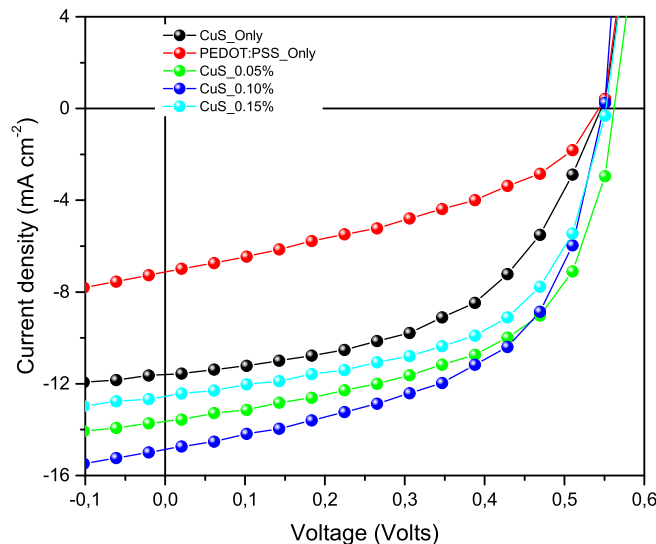


Figure 4.4: J–V plots of devices fabricated with/without CuS-doped PEDOT:PSS as HTLs at various CuS doping levels.

Doping PEDOT:PSS with CuS NPs expectedly altered the optical properties of both CuS and PEDOT:PSS in the aqueous solutions as noted in the optical characteristics of the various fully deposited devices given by the absorbance of the fabricated devices (Fig. 4.3a), which is demonstrated by various characteristics peaks in different regions of the wavelengths considered. The absorption peaks of the photoactive films deposited on CuS-doped PEDOT:PSS layered-devices generally tend to show red-shift compared to the film produced on pristine PEDOT:PSS device. The all-CuS HTL device exhibited the highest absorbance in almost all wavelength regions while the pristine PEDOT:PSS device had the lowest absorption peak as shown in Fig. 4.3a. It is evident that the absorption bump around (350 nm - 450 nm) region is the result of CuS in HTL layers. Similar observation is noticed in the 550 nm - 650 nm region where a broadening of the absorption peaks could be seen in the doped devices, with the 0.10% doped device having the broadest effect amongst the doped devices. This is attributed to the light trapping effects, multiple scattering and absorption [56] of the incident light due to the presence of CuS NPs at the interface between active layer and the anode. Moreover, the CuS NPs exhibited plasmon resonance effect which contributed to absorption in the 750 nm - 900 nm range of the spectrum in the doped solar cells.

The CuS NPs doping concentration in PEDOT:PSS however appeared to have an inverse relationship with light trapping effects that resulted in lower absorption for the highest concentration (0.15%) doped HTL amongst the doped devices both in the UV and in the NIR region. This is due to the fact that the increase in NPs concentration actually creates more scattering centres in the device and thus scatters the incident radiation out of the device rather than into it. Nonetheless, all doped devices demonstrated superior absorption compared with the pristine PEDOT:PSS device as a result of improved charge transport processes.

### 4.4.3 Characterization of TFOSC

Copper Sulphide nanoparticles doped PEDOT:PSS hole transport layers were employed in the fabrication of thin film organic solar cells. The solar absorbing layer of the devices was composed of P3TH:PCBM polymer blend which **was** integrated into a complete device structure as ITO/CuS-doped:PEDOT:PSS/P3TH:PC61BM/LiF/Al. The concentration of CuS in the PEDOT:PSS layer was varied from 0%, 0.05%, 0.10% and 0.15% by weight, specifically, so as to determine the optimal concentration of CuS required in PEDOT:PSS for best device performances. The current-voltage characteristics (J-V) of the solar cells were measured and given in Fig. 4.4 at various concentrations of CuS in HTL.

The solar cell fabricated at 0.10% CuS doping level in HTL has the best power conversion efficiency (PCE) as provided in Table I. This supports the observations that were noted in the optical properties of the films discussed in the previous section. It was found that there were significant differences in device parameters with the concentration of CuS in the various HTLs (Table 4.1).

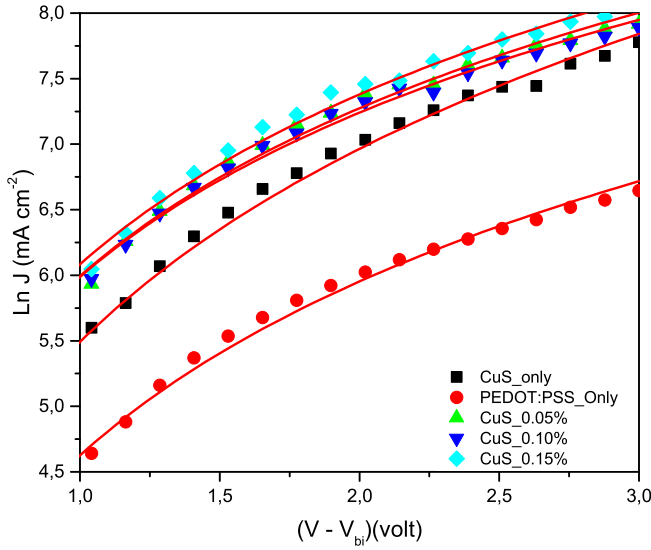


Figure 4.5: SCLC curves of devices fabricated with CuS-doped PEDOT:PSS as HTLs at various CuS doping levels

Table 4.1: The solar cell parameters of the best performed devices.

Device	$V_{oc}$ (V)	$J_{sc}$ ( $\text{mA}\cdot\text{cm}^{-2}$ )	FF (%)	PCE (%)	$R_s$ ( $\Omega\cdot\text{cm}^{-2}$ )
PEDOT:PSS Only	0.55	8.91	42.77	2.01	348
CuS Only	0.55	11.18	54.25	3.34	148
CuS_0.05 %	0.56	13.61	55.34	4.24	63
CuS_0.10 %	0.55	14.78	55.43	4.51	25
CuS_0.15 %	0.55	12.52	56.60	3.91	62

The open circuit voltage ( $V_{oc}$ ), however, appears constant for all doping levels suggesting that the concentration of CuS was very low to be able to make changes on the energy levels at the interface. The highest recorded device PCE was 4.51 % at 0.10 wt % CuS which is significantly higher than the PCEs of the devices prepared without the nanoparticles. The two reference devices, the pristine PEDOT:PSS and all-CuS-buffer layered devices, shows a relatively low PCE of 2.01% and a moderate 3.34% respectively. For the CuS-doped-PEDOT:PSS HTL solar devices, the efficiencies were notably improved compared to the two reference cells, with the improvement ratio depending on the CuS doping amount. When the CuS doping was increased from 0.05% to 0.10% by weight, the overall device performance improved, but a further CuS doping increase to 0.15% by weight resulted in decreased overall device performance. Hence, the optimal CuS doping level was determined to be 0.10% by weight which resulted in the highest PCE of 4.51%. This indeed suggests that the inclusion of CuS in the HTL improved the device performance by promoting photo-generated current collection. Besides, the hydrophobic nature of CuS prevents the diffusion and/or reaction of oxygen and moisture in the photoactive layer that improved the stability of the solar cells which will be discussed later. Moreover, interfacial layers usually decrease the barrier potential between electrodes and the

photoactive layers, improving charge carrier injection into the device [57]. The hydrophobic properties, roughness and surface of HTLs are also important features that influence the active layer's adhesion to the HTLs surface which eventually defines the performance of fabricated solar cell devices. CuS nanoparticles are more hydrophobic than PEDOT:PSS, thus they afford improved surface homogeneity and physical contact at the photoactive layer and HTLs interface. Introducing CuS NPs in the HTL not only assisted in improved hole collection from the photoactive layer but also assisted in expelling humidity from the device since the interaction of the device with moisture was reduced by the CuS presence [57].

#### 4.4.4 Charge transport properties

The collection of photons generated charges in organic solar cells could be influenced by a number of factors, such as light absorption in the photoactive layer, generation and dissociation of excitons, charge transport to the electrodes. The charge transport properties in an organic polymer or small molecules are usually examined with space charge limited current (SCLC) method. Here space charge currents are measured under dark conditions to suppress the photo-generated current in the devices. In this situation, carriers emanate via injection from the electrodes through the external circuit. The high rectification ratio developed by the potential barrier created across the electrode inhibits the transport of free charge carriers across the junction [58, 59, 60, 61, 62, 63]. If there are few or no traps and low electric fields, the current density,  $J$ , has a quadratic relation with the applied bias voltage,  $V$ . Thus, the field dependent space charge limited current is expressed by Mott-Gurney's Law [62]:

$$J = \frac{9}{8} \epsilon \epsilon_0 \mu_0 \frac{V^2}{L^3} \exp(0.89\gamma \sqrt{\frac{V}{L}}) \quad (4.1)$$

$\epsilon$  and  $\epsilon_0$  are the relative dielectric permittivity of the polymer medium and free space, respectively;  $\mu_0$  is the zero-field mobility;  $\gamma$  is the field activation factor,  $L$  is the active layer thickness and  $V$  is the applied voltage across the device corrected for the built-in potential  $V_{bi}$  [64]. The SCLC in Fig. 4.5 fits well with the Mott-Gurney equation. From the results contained in Table 4.2, the zero field mobilities obtained from the CuS-doped PEDOT:PSS devices have higher magnitudes than those from pure PEDOT:PSS and CuS buffer layer devices, by an average approximate factors of 5 and 3 respectively.

This clearly demonstrates that the presence of CuS in the HTL contributed to the enhancement of charge transport in the solar cell device. The devices charge carrier mobility varied slightly with the CuS doping level in the hole transport layer. The value slightly increased in the 0.05% CuS loaded PEDOT:PSS buffer to the 0.10% device and then reduced in the 0.15% CuS loaded solar cell. CuS nanoparticles are considered to possess high electrical conduction when properly distributed in the HTL medium. As good conductors and medium of free charge transport, CuS NPs reduce charge recombination processes at the HTL/photoabsorber interface. CuS

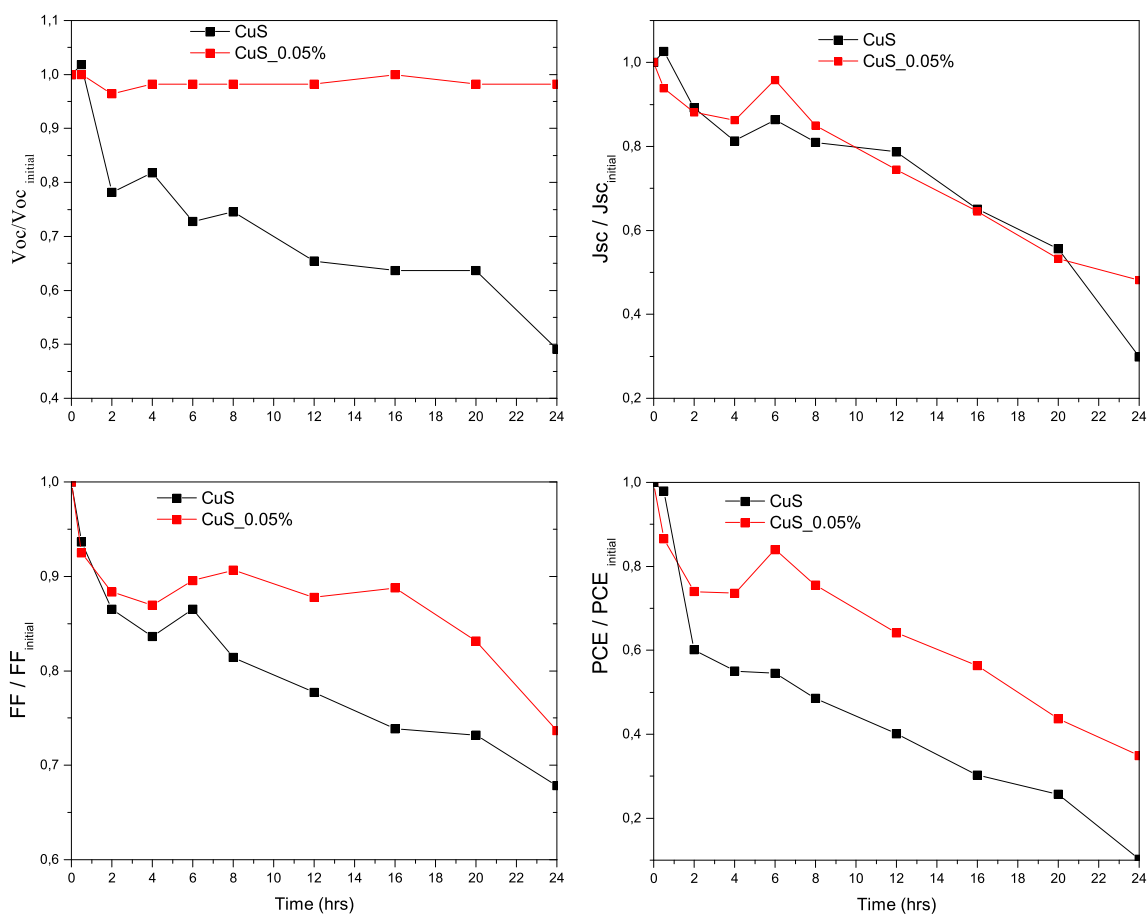


Figure 4.6: Stability of the solar cells fabricated with CuS and 0.05% CuS doped PEDOT:PSS hole transport layers stored in ambient laboratory conditions.

may also function as an interface modifier which could reduce the Schottky barrier formed between the electrodes and the PSS moieties interfaces. PEDOT possesses high metallic properties which often lead to large leakage currents in devices, the presence of CuS in the buffer layer reduces this effect. Doping PEDOT:PSS with CuS NPs creates desirable energy alignment between the photoactive layer and the ITO electrode which is demonstrated in improved device performance. A supplementary or alternative explanation for the charge carrier mobility enhancement of the PEDOT:PSS films by CuS nanoparticles doping could also be expounded in terms of columbic charge screening effects. PEDOT:PSS films contains chains of PEDOT and PSS that are entangled by static interactions, creating PEDOT chains which are positively charged and PSS chains which are negatively charged [65]. Additional charged species are introduced into the system when CuS NPs are added to the PEDOT:PSS aqueous solution. The negatively charged PSS chains may bind with the  $\text{Cu}^{2+}$  cations while similar coulombic interactions may happen simultaneously between the positively charged PEDOT chains and the  $\text{S}^{2-}$  anions thus efficiently screening the charges of the PEDOT and PSS moieties. This charge screening effect

Table 4.2: The charge transport parameters of devices fabricated with CuS-doped PEDOT:PSS as HTLs various CuS doping levels

HTL material	$\mu_0(\text{cm}^2\text{S}^{-1}\text{V}^{-1})$	$\gamma(\text{cmV}^{-1})$
PEDOT:PSS Only	$2.06 \times 10^{-4}$	$-2.33 \times 10^{-5}$
CuS Only	$3.43 \times 10^{-4}$	$-3.88 \times 10^{-5}$
CuS_0.05 %	$9.03 \times 10^{-4}$	$-1.02 \times 10^{-4}$
CuS_0.10 %	$9.58 \times 10^{-4}$	$-1.09 \times 10^{-4}$
CuS_0.15 %	$9.51 \times 10^{-4}$	$-1.08 \times 10^{-4}$

could result in reducing Columbic attractions between the two polymer moieties, and thus assist in the phase separation of the positively charged conducting PEDOT and the non-conducting, negatively-charged PSS chains which ultimately contributes in the conductivity improvement of the PEDOT:PSS film. When the PEDOT:PSS is highly-doped by CuS in the 0.15% device, the excess  $\text{S}^{2-}$  that did not interact with PEDOT chains may hinder efficient stacking of PEDOT chains, leading to a reduction in conductivity[65, 66].

#### 4.4.5 Device degradation

Apart from improved PCEs, the stability of fabricated TFOSC devices is another major requirement for the viable uptake of solar cells based on polymers and organic molecules in the energy market [64, 67, 68, 69, 70]. Despite having several attractive properties such as the ease of device fabrication and mechanical flexibility of TFOSCs, the photo-active layers of the solar cells are still largely unstable under exposure to oxygen and humidity. We studied the performance of some of the fabricated solar cells kept in nitrogen atmosphere at  $100^\circ\text{C}$  without encapsulation for about 6 hours and thereafter removed from the furnace and left them in ambient laboratory conditions for an additional 18 hours. In the pristine PEDOT:PSS HTL device, appreciable solar cell parameters ceased to exist within 2 hours of device fabrication while the CuS-only HTL device retained some of its performance for the duration of monitoring. Within the first hour after device fabrication, the 0.10% and 0.15% CuS-loading PEDOT:PSS doped devices showed good stability, and retained 40% of their initial performance parameters after 48 hours.

The all-CuS HTL and the 0.05 % CuS-loading devices were systematically monitored and their device performances are summarized in Fig 4.6, in which the ratios of the solar cell parameters to their initial values were plotted as a function of time, taking into account the open circuit voltage ( $V_{oc}$ ), short circuit current density ( $J_{sc}$ ), fill factor (FF) and power conversion efficiency (PCE). The solar cell parameters of the device fabricated with the 0.05% CuS-doped HTL decreased monotonically with time at a slower rate than the CuS-only HTL device. The CuS-incorporated PEDOT:PSS buffer layered solar cells maintained 40% of initial PCE, while CuS-only HTL device retained 10% PCE after 24 hours of ambient condition storage. The initial high storage temperature might have assisted in polymer recrystallization and aid in oxygen and water content removal from the polymer matrix. The prolonged thermal annealing could have equally created a new conformational order

which created better interpenetrating network of the polymer and CuS for better charge percolation pathways. While the lifetime of the CuS-doped PEDOT:PSS HTL devices was prolonged from about an hour in ambient conditions to more than 25 hours compared to PEDOT:PSS only devices, the lifetime is still much lower to the lifetime of CuS buffer layer reported by [51]. The different mechanisms for the synthesis of the CuS used for the investigations and subsequent fabrication might have been responsible for the discrepancy. This assertion is supported in previous investigations [71].

## 4.5 Conclusion

CuS nano-particles were synthesized and dispersed in PEDOT:PSS hole transport layer of TFOSCs to successfully improve the performances. The fabricated devices using CuS-doped hole transport material demonstrated significant performance improvement and environmental stability compared to pristine PEDOT:PSS HTL-based solar cells. The optimum CuS loading in PEDOT:PSS was determined to be 0.10 % by weight and produced the highest PCE of 4.51 % under ambient laboratory conditions. The high transmittance of the CuS-doped PEDOT:PSS HTL in the low wavelength and absorption in the near infra-red region contributed to better photon harvesting. Furthermore, the plasmon resonance effect exhibited by CuS nano-particle at the interface between the active layer and anode electrode enhanced light trapping through scattering in the active layer and contributed to improved charge generation and hole collection that was reflected in the measured high photocurrent. Moreover, keeping the solar cells in a warm nitrogen environment assisted device stability to over 25 hours in un-encapsulated laboratory conditions and ambient environment, as some devices retained as much as 40% of their initial PCEs.

## Acknowledgments

This work is supported by the National Research Foundation (NRF) (Grant numbers, 85589, 113831), South Africa. The authors also appreciate the members of staff of Microscopy and Microanalysis Unit(MMU) at UKZN, for several SEM and TEM measurements.

# Bibliography

- [1] G. Luo, X. Ren, S. Zhang, H. Wu, W.C.H. Choy, Z. He, and Y. Cao, Recent Advances in Organic Photovoltaics: Device Structure and Optical Engineering Optimization on the Nanoscale. *Small*, Vol. 12 (2016) 1547-1571.
- [2] A. Dey, O.P. Bajpai, A.K. Sikder, S. Chattopadhyay and M.A.S. Khan, Recent advances in CNT/graphene based thermoelectric polymer nanocomposite: A proficient move towards waste energy harvesting. *Renewable and Sustainable Energy Reviews*, Vol. 53 (2016) 653-671.
- [3] Y. Miyauchi, Photoluminescence studies on exciton photophysics in carbon nanotubes. *J. Mater. Chem. C*, Vol. 1(40) (2013) 6499-6521.
- [4] F. Wang, D. Kozawa, Y. Miyauchi, K. Hiraoka, S. Mouri, Y. Ohno, and K. Matsuda, Considerably improved photovoltaic performance of carbon nanotube-based solar cells using metal oxide layers, *Nat. commun*, 6:6305 doi:10.1038/ncomms7305 (2015).
- [5] M. Kanungo, H. Lu, G. Malliaras, and G.B. Blanchet, Suppression of metallic conductivity of single-walled carbon nanotubes by cycloaddition reactions. *Science*, Vol. 323(5911) (2009) 234-237.
- [6] J. Peet, M.L. Senatore, A.J. Heeger, G.C. Bazan, The role of processing in the fabrication and optimization of plastic solar cells, *Adv. Mater.* 21 (2009) 1521-1527.
- [7] Z. Liu, S.Y. Lee, E.-C. Lee, Copper nanoparticle incorporated plasmonic organic bulk-heterojunction solar cells, *Appl. Phys. Lett.* 105 (2014) 223306.
- [8] K. Kaviyarasu, Genene T. Mola, S.O. Oseni, K. Kanimozhi, C. Maria Magdalane, J. Kennedy, M. Maaza, ZnO doped single wall carbon nanotube as an active medium for gas sensor and solar absorber, *J. Mater. Sci. Mater. Electron.* 30 (2019) 147158.
- [9] S. Zhang, Y. Qin, J. Zhu, J. Hou, Over 14% efficiency in polymer solar cells enabled by a chlorinated polymer donor, *Adv. Mater.* 30 (2018) 1800868.
- [10] S. Li, L. Ye, W. Zhao, H. Yan, B. Yang, D. Liu, W. Li, H. Ade, J. Hou, A wide bandgap polymer with a deep highest occupied molecular orbital level enables 14.2% efficiency in polymer solar cells, *J. Am. Chem. Soc.* 140 (2018) 7159-7167.

- [11] Yong Cui<sup>1</sup>, Huifeng Yao, Jianqi Zhang, Tao Zhang<sup>1</sup>, Yuming Wang, Ling Hong<sup>1</sup>, Kaihu Xian<sup>1</sup>, Bowei Xu<sup>1</sup>, Shaoqing Zhang<sup>1</sup>, Jing Peng, Zhixiang Wei, Feng Gao & Jianhui Hou, Over 16 % efficiency organic photovoltaic cells enabled by a chlorinated acceptor with increased open-circuit voltages, *Nature Communication*, (2019) doi.org/10.1038/s41467-019-10351-5
- [12] Albert O. Juma, Elhadi A.A. Arbab, Cosmas M. Muiva, Lucia M. Lepodise, Genene Tessema Mola: synthesis and characterization of CuO-NiO-ZnO mixed metal oxide nanocomposite, *J. Alloy. Comp.* 723 (2017) 866-872.
- [13] Elhadi Abdalla, Genene Tessema Mola: Metals decorated nanocomposite assisted charge transport in polymer solar cell. *Materials Science in Semiconductor Processing*, Vol 91, (2019)1-8.
- [14] G.F. Wang, X.M. Tao, and R.X. Wang, Fabrication and characterization of OLEDs using PEDOT:PSS and MWCNT nanocomposites. *Composites Science and Technology*, Vol. 68(14) (2008) 2837-2841.
- [15] He, Z. C.; Zhong, C. M.; Su, S. J.; Xu, M.; Wu, H. B.; Cao, Y., Enhanced Power-Conversion Efficiency in Polymer Solar Cells Using an Inverted Device Structure. *Nat. Photonics* 2012, 6, 591-595.
- [16] You, J. B.; Chen, C. C.; Hong, Z. R.; Yoshimura, K.; Ohya, K.; Xu, R.; Ye, S. L.; Gao, J.; Li, G.; Yang, Y. 10.2% Power Conversion Efficiency Polymer Tandem Solar Cells Consisting of Two Identical Sub-Cells. *Adv. Mater.* 2013, 25, 3973-3978.
- [17] Liao, S. H.; Jhuo, H. J.; Cheng, Y. S.; Chen, S. A. Fullerene Derivative-Doped Zinc Oxide Nanofilm as the Cathode of Inverted Polymer Solar Cells with Low-Bandgap Polymer (PTB7-Th) for High Performance. *Adv. Mater.* 2013, 25, 4766-4771.
- [18] Po, R.; Carbonera, C.; Bernardi, A.; Camaioni, N. The Role of Buffer Layers in Polymer Solar Cells. *Energy Environ. Sci.* 2011, 4, 285-310.
- [19] Chen, S.; Manders, J. R.; Tsang, S.-W.; So, F. Metal Oxides for Interface Engineering in Polymer Solar Cells. *J. Mater. Chem.* 2012, 22, 24202-24212.
- [20] Ma, H.; Yip, H. L.; Huang, F.; Jen, A. K. Y. Interface Engineering for Organic Electronics. *Adv. Funct. Mater.* 2010, 20, 1371-1388.
- [21] Qu, S. X.; Li, M. H.; Xie, L. X.; Huang, X.; Yang, J. G.; Wang, N.; Yang, S. F. Noncovalent Functionalization of Graphene Attaching 6,6 -Phenyl-C61-butyrlic Acid Methyl Ester (PCBM) and Application as Electron Extraction Layer of Polymer Solar Cells. *ACS Nano* 2013, 7, 4070-4081.
- [22] Nardes, A. M.; Kemerink, M.; de Kok, M. M.; Vinken, E.; Maturova, K.; Janssen, R. A. J. Conductivity, Work Function, and Environmental Stability of PEDOT: PSS Thin Films Treated with Sorbitol. *Org. Electron.* 2008, 9, 727-734.

- [23] Kim, Y. H.; Sachse, C.; Machala, M. L.; May, C.; Muller-Meskamp, L.; Leo, K. Highly Conductive PEDOT:PSS Electrode with Optimized Solvent and Thermal Post-Treatment for ITO-Free Organic Solar Cells. *Adv. Funct. Mater.* 2011, 21, 1076-1081.
- [24] Hao, Z. H.; Hu, Z. Y.; Zhang, J. J.; Hao, Q. Y.; Zhao, Y. Influence of Doped PEDOT: PSS on Performance of Polymer Solar Cells. *Acta. Phys. Sin.* 2011, 60, 117106.
- [25] Li, G.; Zhu, R.; Yang, Y. Polymer Solar Cells. *Nat. Photonics* 2012, 6, 153-161.
- [26] Lim, T. H.; Oh, K. W.; Kim, S. H. Self-Assembly Supramolecules to Enhance Electrical Conductivity of Polyaniline for a Flexible Organic Solar Cells Anode. *Sol. Energy Mater. Sol. Cells* 2012, 101, 232-240.
- [27] Lu, K. Y.; Yuan, J. Y.; Peng, J.; Huang, X. D.; Cui, L. S.; Jiang, Z. Q.; Wang, H. Q.; Ma, W. L. New Solution-Processable Small Molecules as Hole-Transporting Layer in Efficient Polymer Solar Cells. *J. Mater. Chem. A* 2013, 1, 14253-14261.
- [28] Li, S.-S.; Tu, K.-H.; Lin, C.-C.; Chen, C.-W.; Chhowalla, M. Solution-Processable Graphene Oxide as an Efficient Hole Transport Layer in Polymer Solar Cells. *ACS Nano* 2010, 4, 3169-3174.
- [29] Chao, Y. H.; Wu, J. S.; Wu, C. E.; Jheng, J. F.; Wang, C. L.; Hsu, C. S. Solution-Processed (Graphene Oxide)-(d(0) Transition Metal Oxide) Composite Anodic Buffer Layers toward High-Performance and Durable Inverted Polymer Solar Cells. *Adv. Energy Mater.* 2013, 3, 1279-1285.
- [30] He, Z.; Wu, H.; Cao, Y. Recent Advances in Polymer Solar Cells: Realization of High Device Performance by Incorporating Water/Alcohol-Soluble Conjugated Polymers as Electrode Buffer Layer. *Adv. Mater.* 2014, 26, 1006-1024.
- [31] Groenendaal, B. L.; Jonas, F.; Freitag, D.; Pielartzik, H.; Reynolds, J. R. Poly(3,4-ethylenedioxythiophene) and its Derivatives: Past, Present, and Future. *Adv. Mater.* 2000, 12, 481-494.
- [32] Xia, Y. J.; Zhang, H. M.; Ouyang, J. Y. Highly Conductive PEDOT:PSS Films Prepared Through a Treatment with Zwitterions and Their Application in Polymer Photovoltaic Cells. *J. Mater. Chem.* 2010, 20, 9740-9747.
- [33] Nagata, T.; Oha, S.; Chikyow, T.; Wakayama, Y. Effect of UVOzone Treatment on Electrical Properties of PEDOT:PSS Film. *Org. Electron.* 2011, 12, 279-284.
- [34] Z. Li, Y. Liang, Z. Zhong, J. Qian, G. Liang, K. Zhao, H. Shi, S. Zhong, Y. Yin, W. Tian, A Low-work-function, high-conductivity PEDOT:PSS electrode for organic solar cells with a simple structure, *Synth. Met.* 210 (2015) 363-366.
- [35] M. Tanveer, A. Habib, M.B. Khan, Interface Modification of inverted bulk heterojunction organic solar Cell by ZnO and CuOx layers, *NUST J. Eng. Sci.* 6 (2013) 15-20.

- [36] H.-L. Yip, A.K.-Y. Jen, Recent advances in solution-processed interfacial materials for efficient and stable polymer solar cells, *Energy Environ. Sci.* 5 (2012) 5994-6011.
- [37] C.J. Brabec, A. Cravino, D. Meissner, N.S. Sariciftci, T. Fromherz, M.T. Rispens, L. Sanchez, J.C. Hummelen, Origin of the open circuit voltage of plastic solar cells, *Adv. Funct. Mater.* 11 (2001) 374-380.
- [38] Q. An, F. Zhang, J. Zhang, W. Tang, Z. Deng, B. Hu, Versatile ternary organic solar cells: a critical review, *Energy Environ. Sci.* 9 (2016) 281-322.
- [39] Aernouts, T.; Geens, W.; Poortmans, J.; Heremans, P.; Borghs, S.; Mertens, R. Extraction of Bulk and Contact Components of the Series Resistance in Organic Bulk Donor-Acceptor-Heterojunctions. *Thin Solid Films* 2002, 403, 297-301.
- [40] X. Hu, L. Chen, L. Tan, T. Ji, Y. Zhang, L. Zhang, D. Zhang, and Y. Chen, In situ polymerization of ethylene-dioxythiophene from sulfonated carbon nanotube templates: toward high efficiency ITO-free solar cells. *J. Mater. Chem. A*, Vol. 4(17) (2016) 6645-6652.
- [41] X.G. Mbuyise, E.A.A. Arbab, K. Kaviyarasu, G. Pellicane, M. Maaza, G.T. Mola, Zinc oxide doped single wall carbon nanotubes in hole transport buffer layer, *Journal of Alloys and Compounds* (2017), doi: 10.1016/j.jallcom.2017.02.249.
- [42] Mohammed S.G. Hamed, Genene Tessema Mola, Copper sulphide as a mechanism to improve energy harvesting in thin film solar cells, *Journal of Alloys and Compounds* 802 (2019) 252-258.
- [43] A.A. Sagade, R. Sharma, Copper sulphide (CuS) as an ammonia gas sensor working at room temperature, *Sens. Actuat. B: Chem.* 133 (2008) 135-143.
- [44] C.H. Lai, K.W. Huang, J.H. Cheng, C.Y. Lee, B.J. Hwang, L.J. Chen, Direct growth of high-rate capability and high capacity copper sulfide nanowire array cathodes for lithium-ion batteries, *J. Mater. Chem.* 20 (2010) 6638.
- [45] Ben Meester, Liesbeth Reijnen, J. Albert Goossens, Schoonman, atomic layer deposition of  $Cu_xS$  for solar energy conversion, *Chem. Vapor Deposition* 9 (2003) 15-20.
- [46] B.R. Jia, M.L. Qin, X.Z. Jiang, Z.L. Zhang, L. Zhang, Y. Liu, X.H. Qu, Synthesis, characterization, shape evolution, and optical properties of copper sulfide hexagonal bipyramid nanocrystals, *J. Nanopart. Res.* 15 (2013) 1469-1478.
- [47] M. Page, O.Niitsoo, Y.Itzhaik, D.Cahen, G.Hodes, Coppersulfide as a light absorber in wet-chemical synthesized extremely thin absorber (ETA) solar cells, *Energy Environ. Sci.* 2 (2009) 220.
- [48] M. Saranya, C. Santhosh, S.P. Augustine, A.N. Grace, Synthesis and characterization of CuS nanomaterials using hydrothermal route, *Experiment. Nanosci.* 4 (2014) 329-336.

- [49] L.H. Qing, C. Hu, C.Z. Yong, L.W. Chang, CuS nanostructures prepared by a hydrothermal method, *J. Alloy. Comp.* 509 (2011) 6382-6389.
- [50] W. Ke, G. Fang, H. Lei, P. Qin, H. Tao, W. Zeng, J. Wang, X. Zhao, An efficient and transparent copper sulfide nanosheet film counter electrode for bifacial quantum dot-sensitized solar cells, *J. Power Sources* 248 (2014) 809-815.
- [51] Hongwei Lei, Guojia Fang, Fei Cheng, Weijun Ke, Pingli Qin, Zengcai Song, Qiao Zheng, Xi Fan, Huihui Huang, Xingzhong Zhao, Enhanced efficiency inorganic solar cells via in-situ fabricated p-type copper sulfide as the hole transporting layer, *Solar Energy Materials & Solar Cells* 128 (2014) 77-84.
- [52] A.R. Ashish, E.J. Young, S.P. Seong, Facile synthesis of plate-like CuS nanoparticles and their optical and photo-thermal properties, *Materials Chemistry and Physics* 207 (2018) 465-469
- [53] G. Hu, T. Xu, X. Chen, T.D. James, S. Xu, Solar-driven broad spectrum fungicides based on monodispersed Cu<sub>7</sub>S<sub>4</sub> nanorods with strong near-infrared photothermal efficiency, *RSC Adv.* 6 (2016) 103930–103937.
- [54] U.T.D. Thuy, N.Q. Liem, C.M.A. Parlett, G.M. Lalev, K. Wilson, Synthesis of CuS and CuS/ZnS core/shell nanocrystals for photocatalytic degradation of dyes under visible light, *Catal. Commun.* 44 (2014) 62–67.
- [55] J. Fang, P. Zhang, H. Chang, X. Wang, Hydrothermal synthesis of nanostructured CuS for broadband efficient optical absorption and high-performance photo-thermal conversion, *Solar Energy Materials and Solar Cells* 185 (2018) 456–463
- [56] X. Wang, Y. He, Y. Hu, G. Jin, B. Jiang, Y. Huang, Photothermal-conversion-enhanced photocatalytic activity of flower-like CuS superparticles under solar light irradiation, *Solar Energy* 170 (2018) 568-593
- [57] H. Huang, and J. Huang, *Organic and Hybrid Solar Cells*. Springer (2014) 1-18.
- [58] A.M. Nardes, M. Kemerink, M.M. Kok, K. Maturova, and R.A.J. Janssen, Conductivity, work function, and environmental stability of PEDOT: PSS thin films treated with sorbitol. *Org. Elec.*, Vol. 9(5) (2008) 727-734.
- [59] Z. Zhang, L. Wei, X. Qin, and Y. Li, Carbon nanomaterials for photovoltaic process. *Nano Energy*, Vol. 15 (2015) 490-522.
- [60] V. Coropceanu, D.A. Filho, Y. Olivier, R. Silbey, and J.L. Bredas, Charge transport in organic semiconductors. *Chemical reviews*, Vol. 107(4) (2007) 926-952.
- [61] G. Li, and L. Liu, *Organic Solar Cells Enhanced by Carbon Nanotubes-Chapter 11*. (2012) 183-198.
- [62] Mpilo Wiseman Dlamini, Genene Tessema Mola: Near-field enhanced performance of organic photovoltaic cells, *Physica B: Condensed Matter* Vol. 552 (2019) 78-83.

- [63] P.N. Murgatroyd,, Theory of space-charge-limited current enhanced by Frenkel effect. *J. Phys. D: Applied Physics*, Vol. 3(2)(1970) 151-156.
- [64] Saheed O. Oseni, Genene Tessema Mola, Bimetallic nanocomposites and the performance of inverted organic solar cell, *Composite part B*, 172(2019), 660-665.
- [65] Xia, Y. J.; Ouyang, J. Y., Anion Effect on Salt-Induced Conductivity Enhancement of Poly(3,4-ethylenedioxythiophene): Poly(styrenesulfonate) Films. *Org. Electron.* 2010, 11, 1129-1135.
- [66] Zhiqiang Zhao, Qiliang Wu, Fei Xia, Xiang Chen, Yawei Liu, Wenfeng Zhang, Jun Zhu, Songyuan Dai, Shangfeng Yang; Improving the Conductivity of PEDOT:PSS Hole Transport Layer in Polymer Solar Cells via Copper(II) Bromide Salt Doping; *ACS Appl. Mater. Interfaces* 2015, 7,3, 1439-1448.
- [67] W.F. Pasveer, J. Cottaar, C. Tanase, R. Coehoorn, P.A. Bobbert, P.W.M. Blom, D.M. Leeuw, and M.A.J. Michels, Unified description of charge-carrier mobilities in disordered semiconducting polymers. *Phys. Rev. Lett.*, Vol. 94(20) (2005) 206601.
- [68] R.A. Hatton, N.P. Blanchard, L.W. Tan, G. Latini, F. Cacialli, S. Ravi, and P. Silva, Oxidised carbon nanotubes as solution processable, high work function hole- extraction layers for organic solar cells. *Org. Elect.*, Vol.10(3) (2009) 388-395.
- [69] L. Gomes, A. Branco, T. Moreira, F. Feliciano, C. Pinheiro, and C. Costa, Increasing the electrical conductivity of electrochromic PEDOT: PSS films: A comparative study. *Solar Energy Materials and Solar Cells*, Vol. 144 (2016) 631-640.
- [70] M. Rassi, L. Vignau, E. Cloutet and B. Ratier, Soluble carbon nanotubes/phthalocyanines transparent electrode and interconnection layers for flexible inverted polymer tandem solar cells. *Org. Elect.*, Vol. 21 (2015) 86-91.
- [71] J. Santos Cruz, S. A. Mayén Hernández, F. Paraguay Delgado, O. Zelaya Angel, R. Castanedo Pérez, G. Torres Delgado; Optical and Electrical Properties of Thin Films of CuS Nanodisks Ensembles Annealed in a Vacuum and Their Photocatalytic Activity; *International Journal of Photoenergy*, Volume 2013, Article ID 178017, 9 pages, doi: 10.1155/2013/178017

# Chapter 5

## Numerical investigation of the effects of copper sulfide nanoparticles on hole transport layer of thin-film organic solar cells

Journal of Computational Electronics  
<https://doi.org/10.1007/s10825-021-01843-z>



### Numerical investigation of the effects of copper sulfide nanoparticles on hole transport layer of thin-film organic solar cells

Michael A. Adedeji<sup>1</sup> · Genene Tessema Mola<sup>1</sup>

Received: 17 June 2021 / Accepted: 17 December 2021  
© The Author(s), under exclusive licence to Springer Science+Business Media, LLC, part of Springer Nature 2022

#### Abstract

Incorporation of metal nanoparticles (NPs) into various layers of organic solar cells (OSCs) has become a popular means of enhancing device performances through increased light absorption by way of plasmon resonance effects. A number of NPs properties and device fabrication parameters should be considered when designing NPs-embedded OSCs for achieving optimum photovoltaic performance. Understanding the impact and mechanisms of photo-absorption with NPs in the solar cells becomes important, making numerical simulations for such investigations critical. Adopting the effective medium model in a numerical simulation; we have investigated charge transport and recombination dynamics of copper sulfide nanoparticles (CuS NPs)-doped hole transport layer (HTL) in OSC. The P3HT:PCBM blend bulk heterojunction (BHJ) solar absorber is used in modeling the devices. The CuS NPs-doping of the hole transport layer (HTL) was realized by introducing a thin modified hole selective layer (MHSL) between the HTL and the absorber. Non-ideal factors such as limited mobility, traps states, recombination dynamics and adjusted exciton generation profiles were considered to describe the solar cells. Enhanced conductivity, variations in the Fermi level offset at the interface and thickness of the MHSL were also taken into account to analyze device performances. The results were compared with experimentally measured device parameters, which are found to be in good agreement. These will greatly assist in understanding the physical processes in nanoparticles-doped OSCs.

**Keywords** Bulk Heterojunction · Organic solar cells · Simulation · P3HT/PCBM · Modeling · CuS · Nanoparticles · Plasmon

## 5.1 Abstract

Incorporation of metal nano-particles (NPs) into various layers of organic solar cells (OSCs) have become a popular means of enhancing device performances through increased light absorption by way of plasmon resonance effects. A number of NPs properties and device fabrication parameters should be considered when designing NPs-embedded OSCs for achieving optimum photovoltaic performance. Understanding the impact and mechanisms of photo-absorption with NPs in the solar cells become important, making numerical simulations for such investigations critical. Adopting the effective medium model in a numerical simulation; we have investigated charge transport and recombination dynamics of copper sulphide nano-particles (CuS NPs) doped hole transport layer (HTL) in OSC. The P3HT:PCBM blend bulk heterojunction (BHJ) solar absorber is used in modelling the devices. The CuS NPs-doping of the hole transport layer (HTL) was realized by introducing a thin modified hole selective layer (MHSL) between the HTL and the absorber. Non-ideal factors such as limited mobility, traps states, recombination dynamics and adjusted exciton generation profiles were considered to describe the solar cells. Enhanced conductivity, variations in the Fermi level offset at the interface and thickness of the MHSL were also taken into account to analyse device performances. The results were compared with experimentally measured device parameters, which are found to be in good agreement. These will greatly assist in understanding the physical processes in nano-particles-doped OSCs.

## 5.2 Introduction

The present energy production landscape mainly lean on fossil fuel which is environmentally unfriendly and unsustainable. The demand for clean sources of energy is increasing which calls for more affordable solar cell technology. Thin film organic solar cells (TFOSCs) is one of rapidly growing thin film solar cell technologies with the view to produce low cost solar panel [1-10]. OSC offers cheap and abundant raw materials for production, reduced embedded energy and payback time, mechanical flexibility and easy adaptability for large-scale production via the roll-to-roll processes[4]. Their materials properties are also versatile, tunable and thus can be optimized by virtue of their solution process-ability[4,6-8]. The bulk heterojunction (BHJ) design is the most popular architecture adopted for OSCs, where electron donating and electron accepting materials are mixed to form a photoactive layer. BHJ creates large A/D interfaces that enhances the dissociation of photo-induced exciton in the medium. Ultrafast charge transfer process also takes place in this system due to the large inter-facial area between the acceptor and the donor materials, leading to increased charge-transfer (CT) state formation and better charge separation [3,11]. However, incident photon absorption and exciton diffusion dynamics taking place within the organic solar cell imposes a limit to the thickness of the device's active layer to prevent geminate and non-geminate recombination[12] and to extract as much useful photo-current from the solar device as possible. One

way of improving the efficiency of OSCs is by improving incident light absorption in the solar device [13]. Trapping incident light within the solar cell, via the plasmon resonance effects, therefore becomes viable means of compensating or improving the drawbacks imposed by low charge carriers mobility and small active layer thickness as the plasmon resonance effects provides a viable avenue of reducing active layer thickness while maintaining or improving the optical path length[14-15].

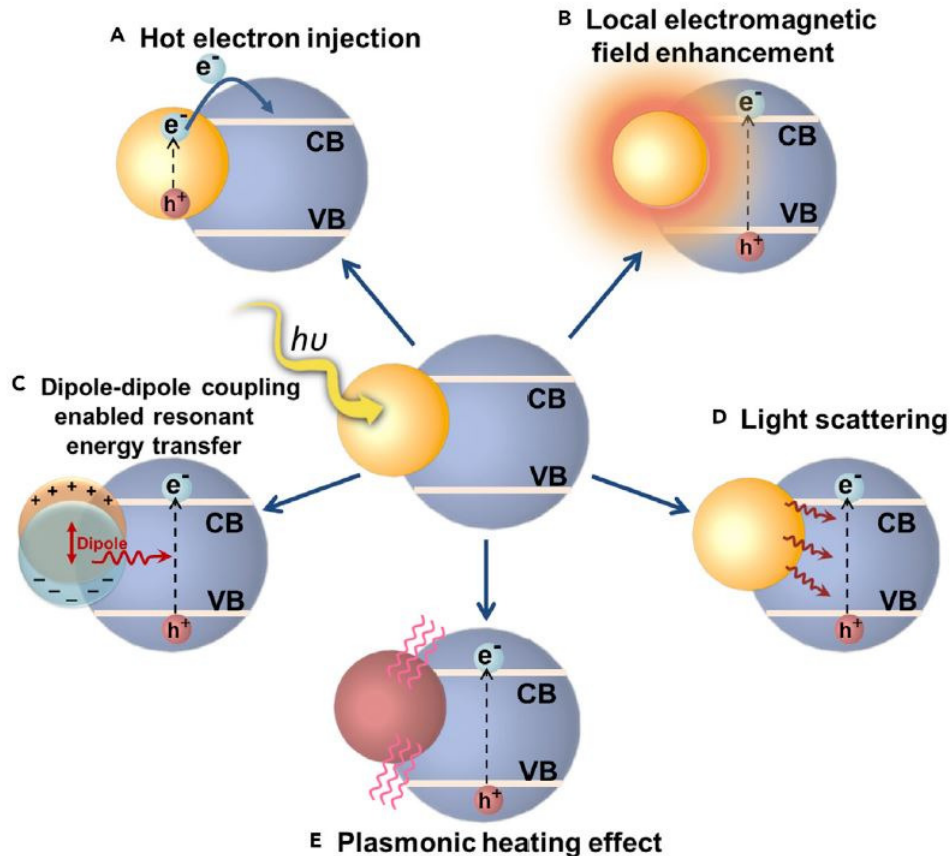


Figure 5.1: Various photoactivity that may be induced by the presence of plasmonic nanomaterials embedded in a semiconducting medium in the presence of electromagnetic field. Reproduced with permission from ref[26]. Copyright Elsevier, 2018.

In a recent publication, Mohammed et al improved the power conversion efficiency (PCE) of a P3HT:PCBM solar cell by as much as 84% over the pristine device after including Cadmium-doped Zinc Oxide (Cd:ZnO) nanoparticles in the active layer of the solar cell[16]. Other such experiments have proven successful in eliciting similar responses from organic solar cells[17-20], demonstrating that suitable nanoparticles incorporation in solar cells improves the overall cell performance. In these instances of adopting plasmonic nanoparticles to elicit enhanced absorption and thus improved power conversion efficiency (PCE) in OSCs, the enhanced PCE can be realized through various mechanisms such as the local electromagnetic field enhancement due to localized surface plasmon resonance (LSPR) and light scattering amongst other mechanisms[14-26] as depicted in Figure 5.1. In LSPR, incident photons excite free electrons in metal nano-particles embedded in the solar cell structure, creating a strong local EM field within the photoactive layer that

enhances excitons generation, dissociation and even migration. The Mie theory[14] provides a physical description for LSPR. LSPR effects are strongly dependent on nanoparticles size, shape, nature of particles and the surrounding medium[15,21-22]. Incident radiation scattering often leads to extension in the propagation length of the light, and consequently the absorption due to the light persisting for longer duration within the solar device. The light may either be forward or back scattered in the solar cell depending on the location of the nano-particles in the device. Plasmonic nano-particles (NPs) embedded in the frontal charge transport layer may induce forward scattering into the active layer while the light may be backscattered into the photo-active layer if the NPs are embedded in the rear transport layer[15,23-24]. The incoming electromagnetic radiation, upon hitting the NPs, may also induce propagating surface waves, the so-called surface plasmon polariton (SPP). These are collective electromagnetic waves and electronic oscillations propagating along the device interfaces – such as the semiconductor/metal and dielectric/metal interfaces. SPPs are extremely interface sensitive, decaying rapidly as they move away from the interface. Thus SPPs created at the interfaces can trap light within the active layer and assist the organic solar cells, especially in relation to the small diffusion length of charge[17,25].

Several investigations have demonstrated improved optical absorptions due to metal[27-29] and metal sulphides[30-32] nanoparticles incorporation in the active layers and transport layers of OSCs, ultimately leading to increment in current densities and other solar cell performance matrices, as well as overall cell efficiencies. Different optoelectrical characterization techniques have been used for the comprehensive study of OSCs. While many investigations have been conducted on the synthesis, incorporation and subsequent fabrication and evaluation of nanoparticles-embedded bulk heterojunction organic solar cells and significant device improvements, the underlying physical mechanisms of the embedded nano-particles have not been extensively reported. Additionally, relatively few simulations have been made to investigate the impact of variation of materials and technological parameters in this class of OSCs on their performance in the quest to arrive at optimized attributes for enhanced device efficiency.

In this report, we investigate the performance of P3HT:PCBM organic solar cells containing copper sulphide nano-particles doped hole transport layer via device numerical simulation. Device simulation presents a great deal of information about the inherent physics of the devices that can assist for optimum photovoltaic effect. Numerical modeling is increasingly becoming essential for realistic description of polymer photovoltaic devices. It involves solving sets of equations that are the mathematical models for the solar devices operation via numerical solution. Material properties and processes within the device are also described with the mathematical models. Simulation programs make simultaneous investigation of different device properties possible as independent model parameters representing each property may be independently set and investigated, leading to quicker results. The analysis and interpretation of the results also provide profound insights for experimental set-ups and often assist in minimizing experimental costs due to the foresight provided by simulations. Various authors have published several simulation models that may be adopted for organic solar cells[33-38]. In this paper, we present simulation results of P3HT/PCBM bulk heterojunction solar cell based on the effective medium

approach.

### 5.3 The simulation parameters

The photo- and electrical response of OSCs can be modeled by accounting for the motion of free charge carriers across the device as well as their trapping and de-trapping dynamics in energy space. A finite-difference drift-diffusion model is therefore adopted to describe these processes. Although the model accepts input parameters for all layers of the OSC, it adopts an effective medium approximation to simulate transport of free carriers in the device's photo-active layer only. A full description of the diffusion model, including the governing equations and build can be found in refs[38,39] and incorporated in the General-purpose Photovoltaic Device Model (GPVDM) simulation software through which the simulations of the organic solar cells were performed.

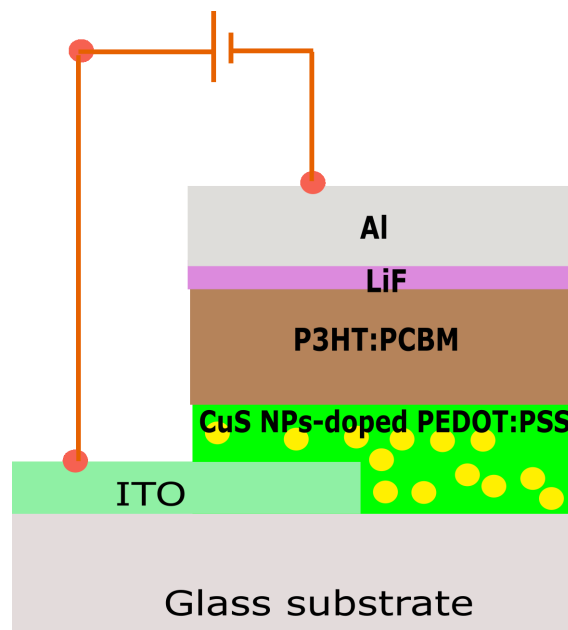


Figure 5.2: Copper sulphide (CuS) nanoparticles-doped hole transport layer (PEDOT:PSS) in a P3HT/PCBM organic solar cell.

GPVDM is a general-purpose tool for simulating light-harvesting devices, developed by Dr. Roderick C. I. MacKenzie at University of Nottingham. The program was initially developed for organic solar cells simulation but its being lately used to simulate CIGS, a-Si and c-Si solar cells as well. As typical of simulation programs, GPVDM describes charge movement within OSCs devices by solving the electron- and hole- drift diffusion equations as well as the carrier continuity equation in position space. To calculate internal electrostatic potential, GPDVM solves the Poisson's equation. The Shockley-Read-Hall (SRH) formalism is employed to describe recombination and carrier trapping in the program[39].

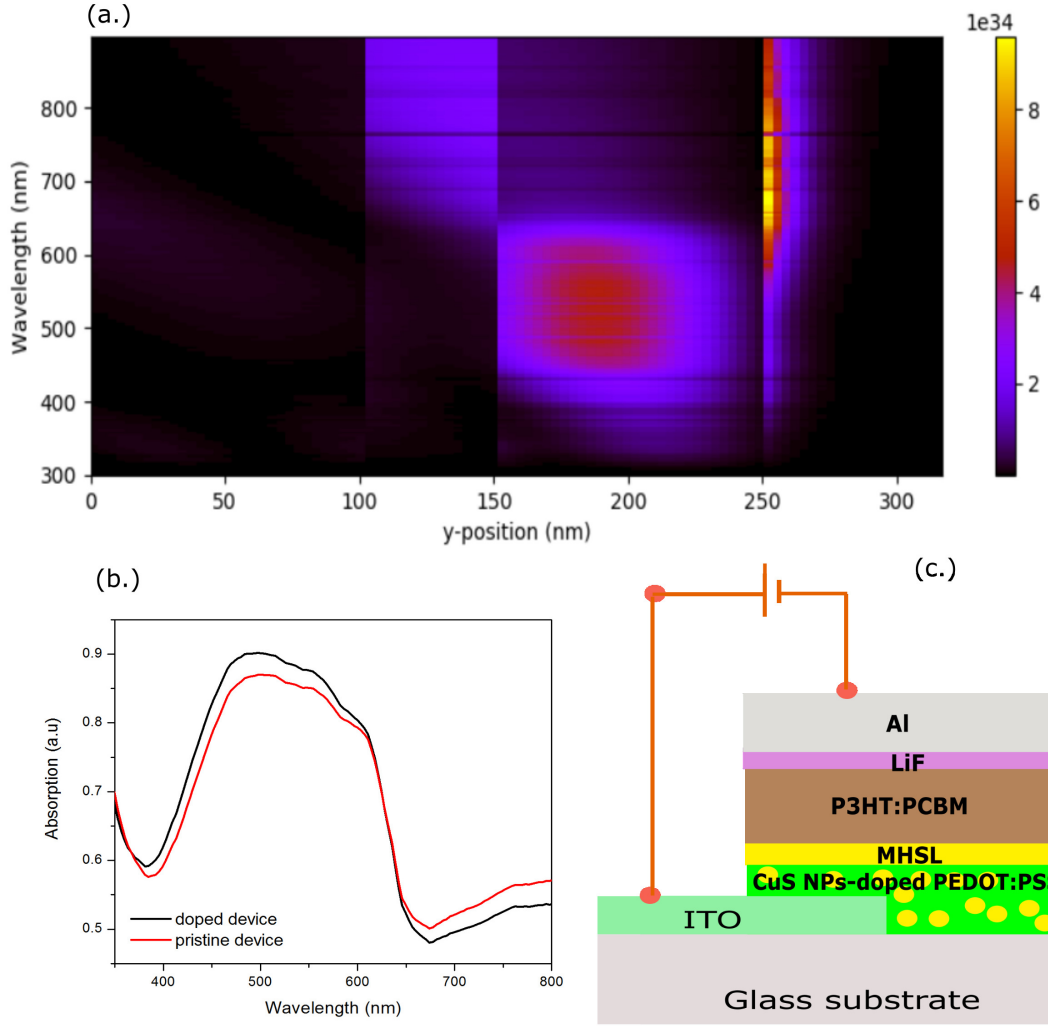


Figure 5.3: (a) Optical absorption profile of the OSC under investigation (b) Measured optical absorptions of the pristine and doped OSC devices (c) The modified device schematics showing the introduced modified hole selective layer (MHSL)

The simulated organic solar cell had a configuration of ITO/PEDOT:PSS/P3HT:PC60BM /LiF/Al, where PEDOT:PSS serves as the hole transport layer, LiF serves as the electron transport layer, ITO and Al serves as the anode and cathode contacts, respectively. The schematic diagram of the simulated device structure is illustrated in Fig. 5.2. The Copper sulphide nano-particles (CuS NPs) are incorporated in the HTL (PEDOT:PSS). Excitons are generated when incoming solar radiation are absorbed in the photo-active layer. By summing the time average of dissipated energy per unit time at a specific location  $x$  and spectral wavelength  $\lambda$  by  $(Q(x,\lambda))$  divided by the energy  $(E_p)$  of a single photon at that wavelength, the exciton generation rate may be calculated[42].

$$\chi(x) = \int_{\lambda_1}^{\lambda_2} \frac{Q(x, \lambda)}{E_p} d\lambda \quad (5.1)$$

But  $E_p = hc/\lambda$  , hence equation 1 becomes

$$\chi(x) = \eta \int_{\lambda_1}^{\lambda_2} \frac{\lambda}{hc} Q(x, \lambda) d\lambda \quad (5.2)$$

$Q(x, \lambda)$  can be expressed as the product of active layer's absorption coefficient  $\alpha(\lambda)$  and the incoming solar radiation power  $I(\lambda)$ , that is  $Q(x, \lambda) = \alpha(\lambda)I(\lambda)$ . Integrating over the width of the photoabsorbing layer enables us to know total photons absorbed and absorbed photons density in one second is

$$\eta_{photons} = \frac{\alpha(\lambda).I(\lambda)cot\lambda}{hc} \quad (5.3)$$

Eventually giving the absorption rate profile as

$$\chi(x) = \eta \int_{\lambda_1}^{\lambda_2} n_{photons} d\lambda \quad (5.4)$$

The absorption profile for both the pristine and doped entire devices are modeled using transfer matrix formalism over all wavelengths and are illustrated in Figure 5.3. The slight change in absorption is noticed in the HSL(Fig. 5.3 b, c).

Physical and material parameters adopted for the active layer of the OSCs in the simulations are as shown in Table 5.1, where parameters symbols used mostly represent their usual physical meaning. For instance, the bandgap is  $E_g$ , electron affinity is  $\chi$ , relative permittivity is  $\epsilon_0$ , electron and hole mobilities are  $\mu_e$  and  $\mu_h$  respectively, acceptor and donor densities are  $N_A$  and  $N_D$  while  $N_C$  and  $N_V$  are conduction and valence band effective DOS. We performed the simulations at AM1.5 solar spectrum.

To model the CuS nano-particles incorporation in the PEDOT:PSS HTL, a thin modified hole selective layer (MHSL) was introduced between pure PEDOT:PSS and the active layer in the device structure. The hole mobility, hole density of trap states within the MHSL and the exciton generation efficiency were varied to reproduce fabricated device upon the assumption that the doped-PEDOT:PSS/Active layer interface properties would be different from the respective bulk of the PEDOT:PSS and the active layer[45-46]. The simulated solar cell performance parameters for the pristine device with unmodified PEDOT:PSS layer are short circuit current ( $J_{sc} = 7.48\text{mA}/\text{cm}^2$ ), open circuit voltage ( $V_{oc} = 0.55\text{V}$ ), fill factor ( $FF = 49.16\%$ ) and power conversation efficiency ( $PCE = 2.02\%$ ). These values are comparable to experimental results from [30] indicating that the adopted simulation parameters closely relates to the functioning of real devices. The J-V characteristics of the fabricated and simulated devices are plotted in Figure 5.4 to further match the simulation parameters to real device values. The solar cells were thereafter simulated under varying conditions to describe various charge transport and recombination processes in the devices under varying non-ideal conditions.

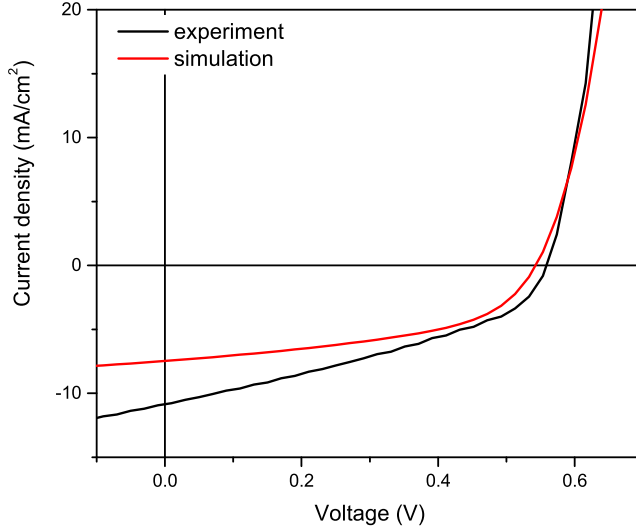


Figure 5.4: J-V characteristics of laboratory fabricated and simulated devices

Table 5.1: Baseline parameters

Parameters	P3HT:PCBM	HSL
Thickness (nm)	100	15
$E_g$ (eV)	1.10	1.20
$\chi$ (eV)	3.80	3.85
$\epsilon_0$	3.80	3.85
$\mu_e$ ( $cm^2/Vs$ )	$2.00 \times 10^{-3}$	$2.48 \times 10^{-2}$
$\mu_h$ ( $cm^2/Vs$ )	$4.00 \times 10^{-4}$	$4.48 \times 10^{-2}$
$N_A$ ( $cm^{-3}$ )	$3.80 \times 10^{21}$	$3.80 \times 10^{20}$
$N_D$ ( $cm^{-3}$ )	$1.45 \times 10^{20}$	$1.45 \times 10^{17}$
$N_C$ ( $cm^{-3}$ )	$1.28 \times 10^{21}$	$1.28 \times 10^{20}$
$N_V$ ( $cm^{-3}$ )	$2.86 \times 10^{19}$	$6.60 \times 10^{17}$
electron exponential tail's energy (meV)	40	$40 \times 10^{-1}$
hole exponential tail's energy (meV)	60	$60 \times 10^{-1}$

## 5.4 Results and Discussion

Plasmonic nano-particles have been shown to improve device internal electric field, increase exciton dissociation efficiency, charge migration and ultimately charge collection at the electrodes, thus calculations were conducted on OSCs composed of OSCs with CuS-doped HTL. The simulations are based on CuS nano-particles-modified PEDOT:PSS HTL coded as a thin (15 nm) modified hole selective layer (MHSL) inserted between the active layer and the PEDOT:PSS layer while keeping the rest of the PEDOT:PSS layer in the pristine state. The solar cell was initially analyzed by studying the conductivity enhancement due to the nanoparticles interaction with the PEDOT: PSS via various combination of the several plasmonic processes previously explained. The valence band's effective DOS in the MHSL was varied between  $10^{16} cm^{-3}$  and  $10^{18} cm^{-3}$  to account for variation in the nanoparticle

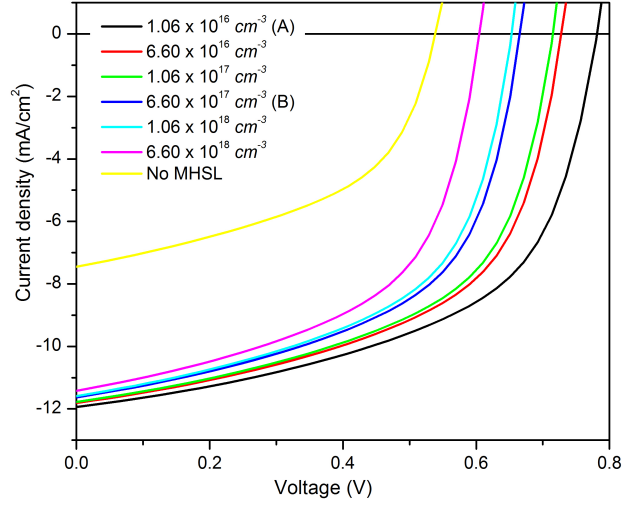


Figure 5.5: J–V curves taken from simulated OSCs at different valence band’s DOS in the Modified Hole Selective Layer (MHSL) with values A, B and No MSHL giving results that are in close agreement to actual fabricated Cus-doped devices

Table 5.2: Device performance parameters for varying  $N_V$  in the MHSL.

$N_V$ /Device	$V_{OC}$	$J_{SC}$	FF	PCE
$1.06 \times 10^{16}$	0.78	11.94	55.29	3.82
$6.60 \times 10^{16}$	0.73	11.81	54.97	3.53
$1.06 \times 10^{17}$	0.72	11.78	54.79	3.45
$6.60 \times 10^{17}$	0.67	11.63	54.44	3.16
$1.06 \times 10^{18}$	0.66	11.59	54.37	3.09
$6.60 \times 10^{18}$	0.61	11.43	53.98	2.81
No MSHL	0.55	7.48	49.16	2.02

doping profiles. The output JV curves for the various doping levels are as presented in Figure 5.5, while their device characteristics are summarized in Table 5.2. The devices’ output solar parameters demonstrated minimal but noticeable steady decline in performance as the MHSL’s  $N_V$  is increased. The  $1.06 \times 10^{16}$  and  $6.60 \times 10^{17} \text{ cm}^{-3}$  devices demonstrated fill factor, current density and efficiency values that are in close agreement to experimental values and are thereafter termed devices A and B respectively. Figure 5.6 represent simulated CELIV plots of some of the devices, in which both doped devices had higher peaks than the undoped device due to the additional MHSL in their configuration. Increase in carriers density shifts the CELIV peaks slightly to the right while growing the magnitude of the CELIV peaks as well. In the plots, the current densities in the three devices remain unchanged in the first  $10 \mu\text{s}$  before their respective current overshoot are noted for the next  $3 - 4 \mu\text{s}$ , after which extracted charge carriers decreased linearly at around  $18 \mu\text{s}$  due to recombination events.

In most bulk heterojunction organic solar cells, device illumination takes place from the HTL/absorber end of the device, hence electron-hole pairs are often created

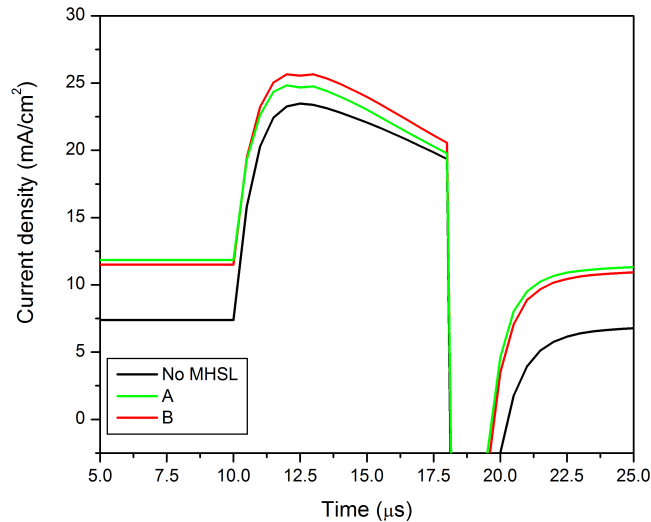


Figure 5.6: CELIV plots for the three devices

around the absorber/hole transport layer interface. Electron-hole pairs creation may increase recombination rate in the active layer on one hand and increase exciton dissociation into free charge carriers on the other hand, especially when such exciton are created near a donor-acceptor interface. Enhanced recombination can reduce extractable current density while heightened exciton dissociation efficiency does the opposite. The interplay between the two processes will determine the overall device performance. The addition of nano-particles into the HTL is expected to induce or increase the surface roughness at the HTL/absorber interface by virtue of the varied nano-sizes of the particles, which may lead to defect grains.

We performed calculations for various surface roughness effects introduced into the HTL due to the presence of the nanoparticles, quantified by varying the thickness of the MHS�. The MHS� thickness was varied from 10 nm to 20 nm in steps of 2.5 nm. Figure 5.7 demonstrates the recombination time constant as a function of the MHS� thickness in device A and B, while Figure 5.8 gives graphical illustration of their corresponding device parameters. The pristine device parameters were adopted for the 'No MHS�' layer situation and hence had a constant output for all device parameters over the range of thickness values simulated. Increase in the MHS� thicknesses led to increase in the recombination time constant, which means that charge carriers had longer lifetimes before recombining and thus increased probability of reaching the electrodes for collection. This led to improved device performance as can be seen in all device parameters in which the fill factor and PCE were increased by roughly 10%, while the  $J_{sc}$  had a more moderate improvement. The  $V_{oc}$  didn't appear to be affected by the change in thickness of the MHS� layer.

To study the effect of CuS-NPs on the ITO which served as the anode, we simulated varying the Fermi offsets within the anode for the devices with and without the MHS� at a constant MSHL thickness. Figure 5.9a is a graph of the average car-

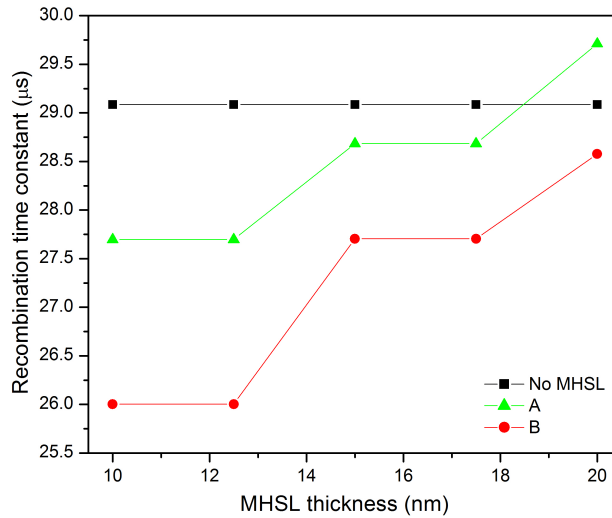


Figure 5.7: Plots of recombination time constants as a function of MHSL thicknesses for the three devices

rier density at maximum power of the devices while figure 5.9b is the recombination time constant as a function of the Fermi offsets at the hole collecting electrodes. As the Fermi offsets increased from -0.1 eV to 0.3 eV, the average carrier density in the doped devices experienced an initial marginal increase before recording significant drop which began at 0.1 eV, while there was continuous increase within the undoped device. The Recombination time constants for all three devices demonstrated similar S-shaped trends with increasing Fermi offsets, with the undoped device having recording the longest recombination time constant. In terms of device performance, Figure 10 gives the corresponding respective performances of the simulated devices due to the fermi offset modulation at the anode. With the exception of the short circuit current densities which demonstrated very slight change over the simulated offset range, the other parameters demonstrated remarkable decline which though started slowly but became pronounced as the fermi offsets increased. The inter-relation between the devices' average carriers the devices and the recombination processes within the devices as noted in Fig 5.9 may be used to explain the obtained parameters in Fig 10. Since the carrier recombination rate  $R$  is a function of carrier density  $n_p$  ( $R = kn_p$ , where  $k$  is a recombination constant), hence increase in the devices' carrier densities will correspondingly increase the recombination rate. The reduced device performances may be additionally attributed to increased resistances to carriers motions due to lowered charge injection from the electrode.

## 5.5 Conclusion

The effective medium model is used to describe charge transport and recombination dynamics in an organic solar cell whose hole transport layer had been doped with copper sulphide nano-particles. The doped solar cell device was modelled by

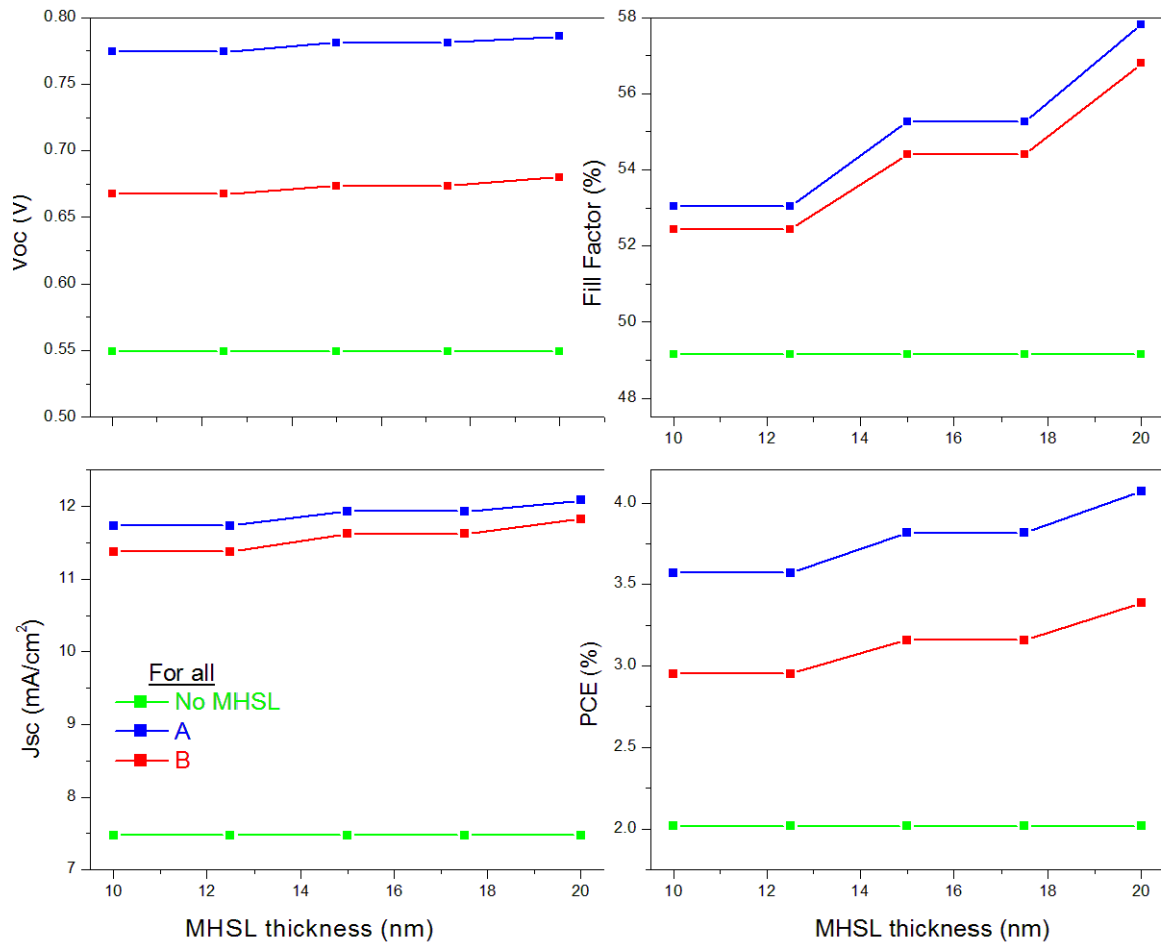


Figure 5.8: Device performances plotted as a function of MHSL thicknesses.

introducing a thin modified hole selective layer (MHSL) between the HTL and the absorber. Charge carriers density of states, recombination characteristics and Fermi offsets amongst other characteristics were investigated to describe device parameters under doped and undoped conditions. The simulations showed that device performances are enhanced with increased MHSL thickness and non-positive Fermi-offset values. Hence, the investigation clearly showed the importance of plasmon nano-particles for effective photons harvesting via thin film organic solar absorber.

## Acknowledgments

This research was supported by the National Research Foundation (NRF) (Grant numbers, 93562, 92786 and 85589), South Africa. The authors also appreciate Dr. Roderick C. I. MacKenzie at the Faculty of Engineering, University of Nottingham, United Kingdom for making the GPDVM software freely available for use.

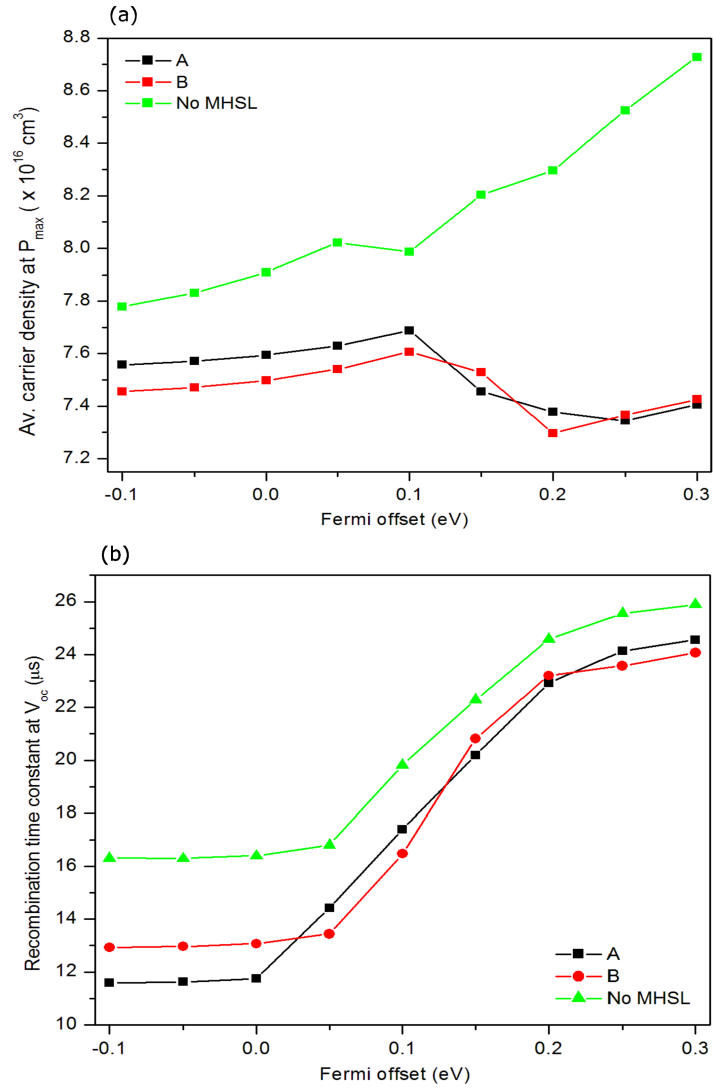


Figure 5.9: (a) Average carriers density at  $P_{max}$  and (b) recombination time constant of doped and undoped devices plotted as a function of fermi offsets at the anode.

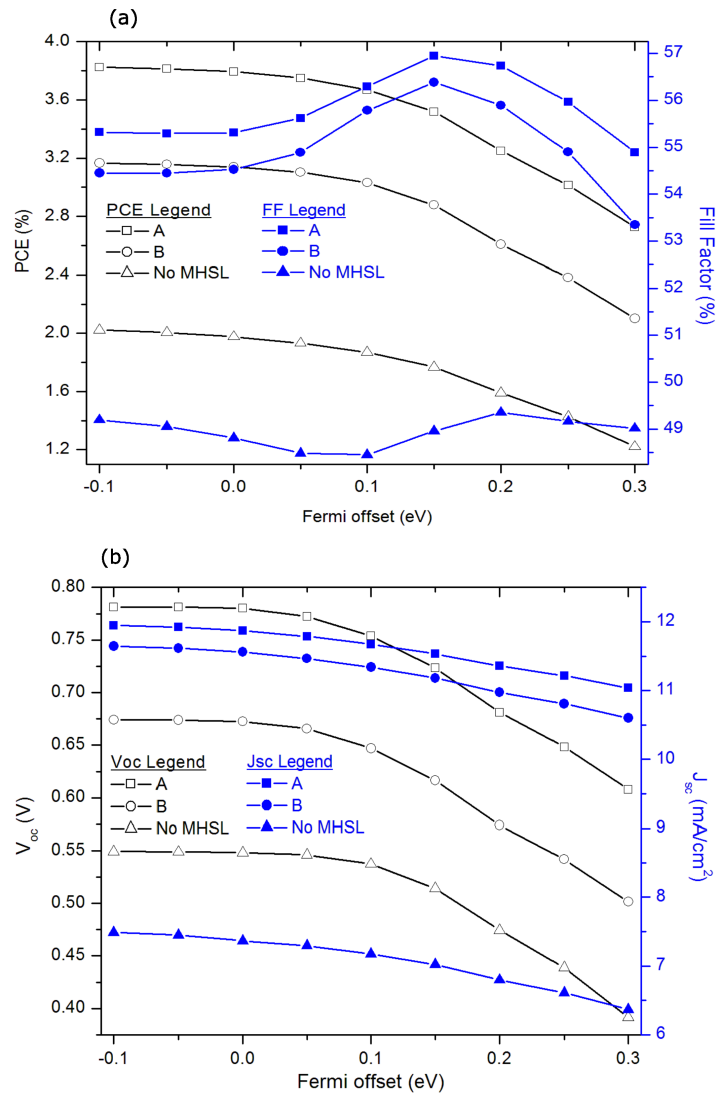


Figure 5.10: Device performance characteristics for the devices as functions of fermi offsets at the anode.

# Bibliography

- [1] C. W. Tang, *Two-layer organic photovoltaic cell*, *Appl. Phys. Lett.*, 1986, 48, 183–185.
- [2] W. L. Ma, C. Y. Yang, X. Gong, K. Lee and A. J. Heeger, *Thermally Stable, Efficient polymer solar cells with control of the Interpenetrating Network Morphology*, *Adv. Funct. Mater.*, 2005, 15, 1617–1622.
- [3] M. C. Scharber, D. Wuhlbacher, M. Koppe, P. Denk, C. Waldauf, A. J. Heeger and C. L. Brabec, *Design Rules for Donors in Bulk-Heterojunction Solar Cells—Towards 10 % Energy-Conversion Efficiency*, *Adv. Mater.*, 2006, 18, 789–794.
- [4] C. J. Brabec, N. S. Sariciftci and J. C. Hummelen, *Plastic Solar Cells*, *Adv. Funct. Mater.*, 2001, 11, 15–26
- [5] C. J. Brabec, *Organic photovoltaics: technology and market*, *Sol. Energy Mater. Sol. Cells*, 2004, 83, 273–292.
- [6] K.M. Coakley and M. D. McGehee, *Conjugated Polymer Photovoltaic Cells*, *Chem. Mater.*, 2004, 16, 4533–4542.
- [7] B. C. Thompson and J. M. J. Frechet, *Polymer-fullerene composite solar cells*, *Angew. Chem., Int. Ed.*, 2008, 47, 58–77.
- [8] B. Kippelen and J. L. Bredas, *Organic photovoltaics*, *Energy Environ. Sci.*, 2009, 2, 251–261.
- [9] S. E. Gledhill, B. Scott and B. A. Gregg, *Organic and nano-structured composite photovoltaics: An overview*, *J. Mater. Res.*, 2005, 20, 3167–3179.
- [10] Jonathan D. Servaites, Mark A. Ratner, and Tobin J. Marks, *Organic solar cells: A new look at traditional models*, *Energy Environ. Sci.*, 2011, 4, 4410–4422
- [11] Wasiu Hamed, Rosiyah Yahya, Abdulra Bola, Habibun Mahmud, *Recent approaches to controlling the nanoscale morphology of polymer-based bulk-heterojunction solar cells*, *Energies* 6 (2013) 5847–5868.
- [12] S. Koul, N. Hakim, *Investigation of Non-ideality Factors for a P3HT: PCBM Based Bulk Heterojunction Organic Solar Cell in Presence of Silver Nanoparticles*, *Trans. Electr. Electron. Mater.* 19, 319 (2018)

- [13] S. Maity, B. Das, R. Maity, N.P. Maity, K. Guha, K.S. Rao, *Sol. Energy* 185, 439 (2019) 15.10. H.A. Atwater, A. Polman, *Plasmonics for improved photovoltaic devices*, *Nat. Mater.* 9, 205 (2010)
- [14] W.C. Choy, X. Ren, *Organic Solar Cells: High Efficiency Organic Solar Cells Achieved by the Simultaneous Plasmon-Optical and Plasmon-Electrical Effects from Plasmonic Asymmetric Modes of Gold Nanostars*, *IEEE J. Sel. Top. Quantum Electron.* 22, (2016)
- [15] L. Feng, M. Niu, Z. Wen, X. Hao, *Recent Advances of Plasmonic Organic Solar Cells: Photophysical Investigations*, *Polymers* 10, 33 (2018)
- [16] Mohammed S G Hamed, Jude N Ike and Genene Tessema Mola; *Plasmonic nano-particles mediated energy harvesting in thin-film organic solar cells*; *J. Phys. D: Appl. Phys.* 55 (2022) 015102 (9pp); doi: 10.1088/1361-6463/ac24c8
- [17] Jude N. Ike, Mohammed S.G. Hamed, Genene Tessema Mola; *Effective energy harvesting in thin film organic solar cells using Ni:Zn as bimetallic nanoparticles*, *Journal of Physics and Chemistry of Solids* 161 (2022) 110405
- [18] Xolani Mbuyise, Mpilo Wiseman Dlamini, Genene Tessema Mola, *Metal nano-composite induced light trapping and enhanced solar cell performances*, *Physica B Condensed Matter* 622 (2021): 413321, DOI: 10.1016/j.physb.2021.413321
- [19] Mohammed S.G. Hamed, Michael A. Adedeji, Genene Tessema Mola, *Rare-earth metal induced plasmon resonances for enhanced photons harvesting in inverted thin film organic solar cell*, *Energy Fuels* 2021, 35, 15010-15017, doi 10.1021/acs.energyfuels.1c01907
- [20] Genene Tessema Mola, Makhosazane C. Mthethwa, Mohammed S.G. Hamed, Michael A. Adedeji, Xolani G. Mbuyise, Amit Kumar, Gaurav Sharma, Yong Zang, *Local surface plasmon resonance assisted energy harvesting in thin film organic solar cells*, *Journal of Alloys and Compounds* 856 (2020) 158172, doi: 10.1016/j.jallcom.2020.158172
- [21] C.H. Chou, F.C. Chen, *Plasmonic nanostructures for light trapping in organic photovoltaic devices*, *Nanoscale* 6, 8444 (2014)
- [22] C.C. Wang, W.C. Choy, C. Duan, D.D. Fung, E.I. Wei, F.X. Xie, F. Huang, Y. Cao, *Optical and electrical study of organic solar cells with a 2D grating anode*, *J. Mater. Chem.* 22, 1206 (2012)
- [23] G. Kakavelakis, I. Vangelidis, A. Heuer-Jungemann, A.G. Kanaras, E. Lidorikis, E. Stratakis, E. Kymakis, *Plasmonic Backscattering Effect in High-Efficient Organic Photovoltaic Devices*, *Adv. Energy Mater.* 6, 1501640 (2016)
- [24] J. Wang, S. Jia, Y. Cao, W. Wang, P. Yu, *Design Principles for Nanoparticle Plasmon-Enhanced Organic Solar Cells*, *Nanoscale Res. Lett.* 13, 211 (2018)
- [25] W.J. Yoon, K.Y. Jung, J. Liu, T. Duraisamy, R. Revur, *Plasmon-enhanced optical absorption and photocurrent in organic bulk heterojunction photovoltaic devices using self-assembled layer of silver nanoparticles*, *Solar energy mater. Solar Cells* 94, 128 (2010)

- [26] Nan Zhang, Chuang Han, Xianzhi Fu, Yi-Jun Xu, *Function-Oriented Engineering of Metal-Based Nanohybrids for Photoredox Catalysis: Exerting Plasmonic Effect and Beyond*, *Chem* 4, 1832–1861, August 9, 2018, doi.org/10.1016/j.chempr.2018.05.005
- [27] A.J. Morfa, K.L. Rowlen, T.H. Reilly, M.J. Romero, J. van de Lagemaat, *Plasmon-enhanced solar energy conversion in organic bulk heterojunction photovoltaics*, *Appl. Phys. Lett.* 9, 013504 (2008)
- [28] S. Liu, F. Meng, W. Xie, Z. Zhang, L. Shen, C. Liu, Y. He, W. Guo, Shengping Ruan, *Performance improvement of inverted polymer solar cells by doping Au nanoparticles into TiO<sub>2</sub> cathode buffer layer*, *Appl. Phys. Lett.* 103, 233303 (2013)
- [29] P.M. Aneesh, C.R. Kumar, P.C.R. Varma, K. Vivek, M.A.G. Namboothiry, *Enhancement in photovoltaic properties of plasmonic nanostructures incorporated organic solar cells processed in air using P3HT: PCBM as a model active layer*, *Org. Photonics Photovolt.* 3, 64 (2015)
- [30] Michael A. Adedeji, Mohammed S.G. Hamed, Genene Tessema Mola, *Light trapping using copper decorated nano-composite in the hole transport layer of organic solar cell*, *Solar Energy* 203 (2020) 83-90
- [31] Mohammed S.G. Hamed, Genene Tessema Mola, *Copper sulphide as a mechanism to improve energy harvesting in thin film solar cells*, *Journal of Alloys and Compounds* 802 (2019) 252-258
- [32] Saheed O. Oseni, Genene Tessema Mola, *Effects of metal-decorated nanocomposite on inverted thin film organic solar cell*, *Journal of Physics and Chemistry of Solids* 130 (2019) 120–126
- [33] L.J.A. Koster, E.C.P. Smits, V.D. Mihailetschi, and P.W.M. Blom, *Device model for the operation of polymer/fullerene bulk heterojunction solar cells*, *Physical Review B* 72, 085205, 2005.
- [34] Jan D. Kotlarski, Paul W.M. Blom, Lambert J.A. Koster, Martin Lenes, and Lenneke H. Slooff, *Combined optical and electrical modeling of polymer:fullerene bulk heterojunction solar cells*, *Journal of Applied Physics* 103, 084502, 2008.
- [35] Douglas W. Sievers, Vishal Shrotriya, and Yang Yang, *Modeling optical effects and thickness dependent current in polymer bulk-heterojunction solar cells*, *Journal of Applied Physics* 100, 114509, 2006.
- [36] H. Hoppe, N. Arnold, N.S. Sariciftci, D. Meissner, *Modeling the optical absorption within conjugated polymer/fullerene-based bulk-heterojunction organic solar cells*, *Solar Energy Materials & Solar Cells* 80, 2003, pp. 105-113.
- [37] Sasa Lacić and Olle Inganäs, *Modeling electrical transport in blend heterojunction organic solar cells*, *Journal of Applied Physics* 97, 124901, 2005.
- [38] R. C. I. MacKenzie, T. Kirchartz, G. F. A. Dibb, J. Nelson, *Modeling nongeminate recombination in P3HT: PCBM solar cells*, *J. Phys. Chem. C* 2011, 115, 9806.

- [39] *R MacKenzie , J. J. Lim , S Bull , S Sujecki , A. J. Kent , E. C. Larkins , The impact of hot-phonons on the performance of 1.3  $\mu\text{m}$  dilute nitride edge-emitting quantum well lasers, J. Phys.: Conf. Series 2007 , 92 , 012068*
- [40] *L. J. A. Koster , E. C. P. Smits , V. D. Mihailetschi , Device model for the operation of polymer/fullerene bulk heterojunction solar cells, P. W. M. Blom , Phys. Rev. B 2005 , 72 , 085205 .*
- [41] *E. M. Azoff , Generalized energy-momentum conservation equations in the relaxation time approximation, Solid-State Electronics 1987 , 30 , 913 .*
- [42] *W. Shockley , W. T. Read , Statistics of the recombinations of holes and electrons, Phys. Rev. 1952 , 87 , 835*
- [43] *B. E. Pieters , PhD Thesis, Delft University of Technology , 2008*
- [44] *Roderick C. I. MacKenzie, Christopher G. Shuttle, Michael L. Chabinye, and Jenny Nelson, Extracting Microscopic Device Parameters from Transient Photocurrent Measurements of P3HT:PCBM Solar Cells, Adv. Energy Mater. 2012, DOI: 10.1002/aenm.201100709*
- [45] *Bizuneh Gebremichael, Genene Tessema Mola, The effect of skin-depth interfacial defect layer in perovskite solar cell, Appl. Phys. B (2016) 122:215, DOI 10.1007/s00340-016-6492-y*
- [46] *Lothar Sims, Ulrich Hörmann, Robert Hanfland, Roderick C.I. MacKenzie, F. René Kogler, Roland Steim, Wolfgang Brütting, Pavel Schilinsky, Investigation of the s-shape caused by the hole selective layer in bulk heterojunction solar cells, Organic Electronics 15 (2014) 2862–2867*

# Chapter 6

## Plasmon enhanced charge transport processes for improved collection of photo-current in polymer solar cell

ACS **APPLIED**  
ENERGY MATERIALS

www.acsaem.org

Article

### Plasmon-Enhanced Charge Transport Processes for Improved Collection of Photo-Current in Polymer Solar Cells

Michael A. Adedeji, Rodrigo Garcia-Rodriguez, Matthew L. Davies, Yong Zhang, and Genevieve Tessema Mola\*

 Cite This: *ACS Appl. Energy Mater.* 2022, 5, 12503–12512

 Read Online

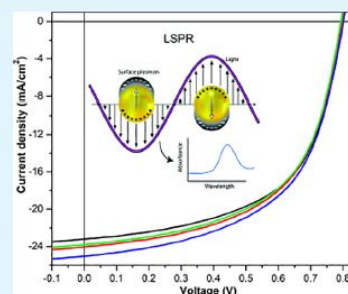
ACCESS |

 Metrics & More

 Article Recommendations

**ABSTRACT:** Silver sulfide ( $\text{Ag}_2\text{S}$ ) nanoparticles were incorporated into the electron transport layer (ETL) of thin-film organic photovoltaic cells to assist in light trapping and improve charge-transport processes. The solar cells were fabricated in an inverted device architecture design using a solar absorber composed of donor polymer poly[4,8-bis(5-(2-ethylhexyl)thiophen-2-yl)benzo[1,2-*b*; 4,5-*b'*]dithiophene-2,6-diyl-alt-(4-(2-ethylhexyl)-3-fluorothieno[3,4-*b*]thiophene)-2-carboxylate-2,6-diyl)] (PTB7-Th) and the non-fullerene acceptor (NFA) 3,9-bis(2-methylene-(3-(1,1-dicyanomethylene)-indanone))-5,5,11,11-tetrakis(5-hexylthienyl)-dithieno[2,3-*d*:2',3'-*d'*]-s-indaceno[1,2-*b*:5,6-*b'*]dithiophene (ITIC-Th). The  $\text{Ag}_2\text{S}$  nanoparticles were dispersed in the zinc oxide nano-ink suspension, at varying concentrations from 0.00 to 0.55% by weight, to be able to determine the optimum doping level for the best solar cell performances. The nanoparticles exhibit local surface plasmon resonance absorption and produce intense local electric field in the polymer matrix, which is beneficial to efficient exciton dissociation. Consequently, improved device performances were recorded at various effective device areas. The measured electrical and optical properties of the NP-doped polymer films showed improved characteristics for energy harvesting. This investigation demonstrates the effective collection of photo-generated charges using  $\text{Ag}_2\text{S}$  nanoparticle-doped ETLs in NFA-based thin-film organic solar cells.

**KEYWORDS:** organic solar cells, non-fullerene acceptors, electron transport layer, plasmon resonance, silver sulfide, nanoparticles



## 6.1 Abstract

Silver sulfide ( $\text{Ag}_2\text{S}$ ) nano-particles were incorporated in the electron transport layer (ETL) of thin film organic photovoltaic (TFOPV) cell to assist in light trapping and improve charge transport processes. The solar cells were fabricated in an inverted device architecture design using solar absorber composed of donor polymer poly[4,8-bis(5-(2-ethylhexyl)thiophen-2-yl)benzo[1,2-b;4,5-b']dithiophene-2,6-diyl-alt-(4-(2-ethylhexyl)-3-fluorothieno[3,4-b]thiophene-)-2-carboxylate-2,6-diyl] (PTB7-Th), and the non-fullerene acceptor (NFA) 3,9-bis(2-methylene-(3-(1,1-dicyanomethylene)-indanone))-5,5,11,11-tetrakis(5-hexylthienyl)-dithieno[2,3-d:2',3'-d']-s-indaceno[1,2-b:5,6-b']dithiophene (ITIC-Th). The  $\text{Ag}_2\text{S}$  nano-particles were dispersed in zinc oxide nano-ink suspension, at varying concentrations from 0.00% to 0.55% by weight, to be able to determine the optimum doping level for the best solar cell performances. The nano-particles exhibit local surface plasmon resonance (LSPR) absorption and produce intense local electric field in polymer matrix, which is beneficial to efficient exciton dissociation. Consequently, improved device performances were recorded at various effective device areas. The measured electrical and optical properties of the NPs doped polymer films showed improved characteristics for energy harvesting. This investigation demonstrates the effective collection photo-generated charges using  $\text{Ag}_2\text{S}$  nano-particles doped ETL in non-fullerene acceptor based thin film organic solar cells.

## 6.2 Introduction

Thin film organic photovoltaic (TFOPVs) cells are increasingly becoming desirable alternatives for renewable energy generation and harnessing by virtue of their desirable qualities like low production cost, low embodied energy, solution processability, possibility to be fabricated on flexible and multiple surfaces as well as semi-transparency. Most high-performing TFOPVs are usually made with the bulk heterojunction (BHJ) design[1, 2] in which donor and acceptor polymers are mixed in a suitable solvent to form a 3-dimensional polymers blend matrix having large-area phase-separated interfaces for dissociating excitons efficiently[3, 4]. Donor polymers and fullerene derivatives-based acceptors[5, 6] have been classically employed as the absorption medium in TFOPVs with power conversion efficiencies (PCEs) close to 13%[7] being reported in the literature. However, these solar cells have weak absorption in the visible region and have limited possibilities for energy bandgap tuning. Non-fullerene acceptors (NFAs), on the other hand, possess several advantages such as tunable energy levels and broader absorption range that covers as far as the near infra-red (NIR) regions[8] and have consequently achieved PCEs above 19%[9, 10, 11].

Charge transport is an important component of solar energy harvesting in TFOPV, which is dependent on the film conductivity, morphology of the absorber medium, energy level alignment of the molecules at the interfaces. The nature of the transport layers critically determines the effective collection of photo-generated free charge carriers in the solar cell devices. Fine tuning the properties of the transport

layers using impurity doping has brought significant successes in device performance from the limited choices of charge transport materials available today in the preparation organic photovoltaic[12]. This compliments with the efforts of retaining some of the absorption losses as a consequence of using very thin absorber layers in TFOPVs (approx. less than 200 nm)[13, 14]. Thus, modifications of the transport layer with plasmon metal nano-particles is expected to cause a light trapping mechanism, which yields positive impact on improving photons harvesting[14, 15].

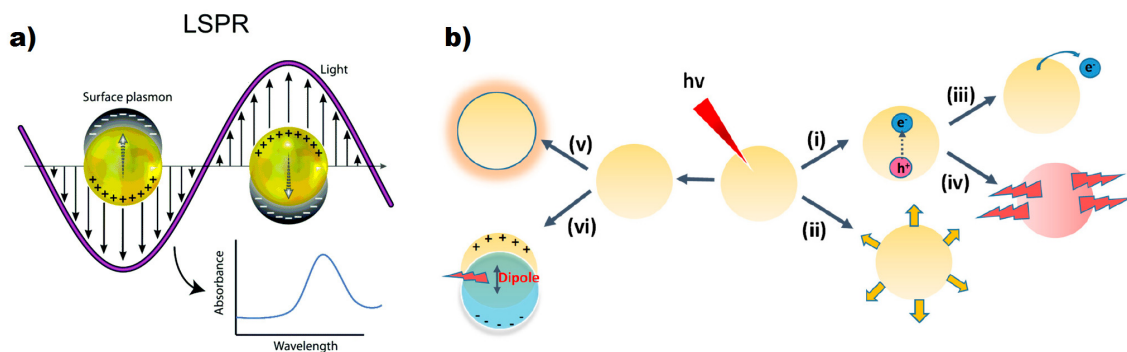


Figure 6.1: (a) Collective displacement of electron cloud due to interaction of metal nanoparticle with the incident electric field. (b) Possible plasmonic processes that may occur in a semiconducting medium when plasmonic materials interact with incident electromagnetic fields (i) charge carriers excitation (ii) light scattering (iii) hot electron injection (iv) heat transfer (v) local electric field enhancement (iv) dipole resonance energy transfer. Reproduced with permission from refs[26, 27]. Copyrights MDPI, 2016 and RSC, 2020.

Plasmon metal nano-composites can be employed within various layers of the device structure, such as the light absorbing layer and/or the charge transport layers[16, 17, 18]. Hence, the interaction between nano-composite with the incident electromagnetic radiation could cause the occurrence of one or more of the processes presented in Figure 6.1, which includes light scattering, hot electron injection, dipole resonance energy transfer and local electric field enhancement. LSPR occurs due to the interaction of the electric field component of the incident photon with surface charges on a metal that oscillate collectively with the frequency of the photon at resonance[15] (Fig. 6.1a). The significant contrast between the metal refractive index and the polymer blend medium behaves like a waveguide which couples light into the absorber through forward scattering[19, 20]. These plasmonic excitations due to metal nano-particles incorporation are useful for harvesting more photons because of resonance absorption as well as near/or far field scattering that changes the path length of the incident radiation that contribute to light trapping[21]. The collective effect of NPs results into improved optical absorption, thereby improving the overall performance of the devices[14, 15]. The use of metal nano-particles in the device structures of various solar cells have shown remarkable results in the past few years[17, 18, 22, 23]. Similarly, the effect of quantum confinement in quantum dots have been employed to boost absorption and PCE of the non-fullerene acceptors based solar cells[24, 25]. However, the incorporation of metallic nano-composites in ETL of non-fullerene acceptors (NFAs) based OSC have not been demonstrated

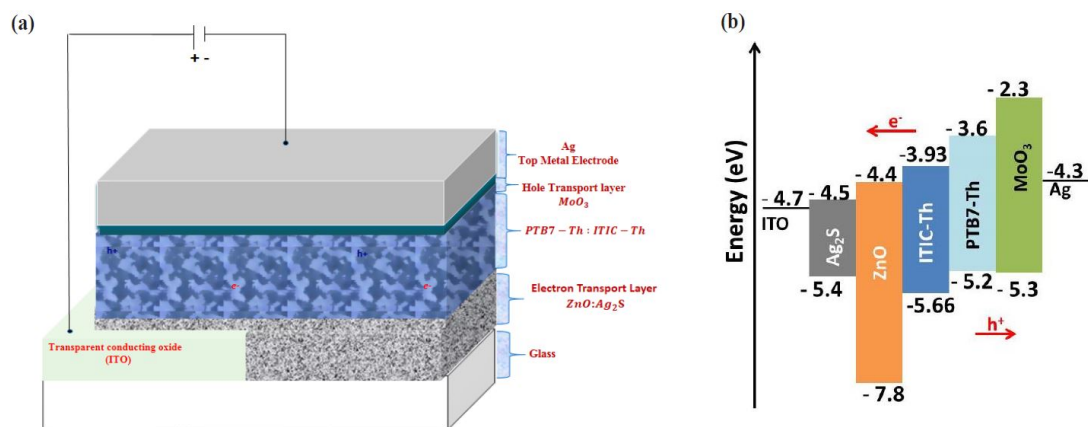


Figure 6.2: Schematics device diagram (a) and energy levels alignment (b) for organic solar cell whose ZnO ETL has been incorporated with silver sulfide NPs.

to the best of our knowledge. We herein report the successful incorporation of a metallic nano-structure in a NFA-based TFOPV.

## 6.3 Materials and methods

### 6.3.1 Materials

All polymers, chemicals and nanoparticles used in this investigation were commercially purchased and were used as delivered without chemical modification. The donor polymer, poly[4,8-bis(5-(2-ethylhexyl)thiophen-2-yl)benzo[1,2-b;4,5-b']dithiophene-2,6-diyl-alt-(4-(2-ethylhexyl)-3-fluorothieno[3,4-b]thiophene)-2-carboxylate-2,6-diyl] (PTB7-Th), and the non-fullerene acceptor, 3,9-bis(2-methylene-(3-(1,1-dicyanomethylene)-indanone))-5,5,11,11-tetrakis(5-hexylthienyl)-dithieno[2,3-d:2',3'-d']-s-indaceno[1,2-b:5,6-b']dithiophene (ITIC-Th), were obtained from Ossila Ltd in the UK. Silver sulfide ( $\text{Ag}_2\text{S}$ ) powders and zinc oxide nano-powder ink suspension in isopropanol were purchased from SigmaAldrich, UK. Pre-patterned ITO-coated glass substrate and silver (Ag) pellets were used as electrodes.

### 6.3.2 Methods

The thin film organic photovoltaic cells were fabricated in an inverted device architecture. The solar cell structure was composed of layers of different materials as ITO/ZnO:Ag<sub>2</sub>S/PTB7-Th:ITIC-Th/MoO<sub>3</sub>/Ag. The device schematics and the energy level diagram are illustrated in Figure 6.2. Pre-patterned ITO glass substrates were ultrasonically sequentially cleaned with soap solution, deionized water, acetone and isopropanol, respectively, for 10-15 min for each operation. The substrates were thereafter dried with nitrogen gun and on hotplate. UV-ozone treatment was further applied on the substrates for 5 min and 'pumped-down' for 25 min, bringing the combined UV-ozone treatment time to 30 min, prior to the depositions. Solu-

tions of the electron transport layers (ETLs) were prepared by blending appropriate masses of the  $\text{Ag}_2\text{S}$  powders in  $\text{ZnO}$  nanoparticles suspension at 0.11 wt%, 0.33 wt% and 0.55 wt% concentration. The mixtures were continuously sonicated for 1 h before commencing the spin coating and continued until all the substrates have all been coated. The coating of the ETL was carried out at 4500 rpm, 7500 rpm spin rate for 40 s holding time. Undoped buffer layers were also coated at the same rpm. The coated substrates were annealed on hotplate at 150 °C for 15 min and allowed another 5 min to cool before transferring them to the  $\text{N}_2$ -filled glovebox for active layer coating,  $\text{MoO}_3$  and Ag deposition and encapsulation. The active layer comprised of PTB7-Th: ITIC-Th mixed at 1:1.3 weight ratio and blended together in chlorobenzene solvent at 17 mg/ml concentration. The blend was continuously stirred overnight with a magnetic stirrer at room temperature. The active layer spin coating was carried out at 1500 rpm, 2000 rpm (spin rate), respectively, for 60 s. The coated substrates were left to dry overnight in the glovebox without thermal annealing under continuous  $\text{N}_2$  environment.  $\text{MoO}_3$  and Silver (Ag), which served as hole transport layer and electrode, respectively, were finally thermally evaporated in vacuum on the samples upto the thickness 10 nm and 100 nm, respectively. Suitable shadow masks were used to define the effective cell areas as 0.1  $\text{cm}^2$ , 0.15  $\text{cm}^2$  and 1  $\text{cm}^2$ . Encapsulation was achieved by means of cleaned cover glasses carefully placed on the devices, glued by means of epoxy resin and cured by monochromatic UV radiation for 7 min, causing the resins to set.

The TFOPV cells were electrically characterized with a computer-interfaced Class AAA Newport Oriel Solar Simulator combined with a Keithley 2400 sourceme-ter operating at 1 sun illumination and power intensity of 100  $\text{mW}/\text{cm}^2$ . Furthermore, the following equipment were used for measuring different parameters of the photoactive thin films, devices and/or silver sulfide powders: Perkin Elmer Lambda UV-Visible-NIR and Rayleigh UV 1601 spectrophotometers (Optical absorption), Bruker D8 Discover X-ray diffractometer (XRD), Edinburgh Instruments FS5 spectrofluorometer (steady-state photoluminescence), custom built incident photon-current conversion efficiency system (IPCE) and Zeiss Evo scanning electron microscope (SEM).

## 6.4 Results and discussion

### 6.4.1 Silver sulphide characterization

The morphology and average particle sizes of the  $\text{Ag}_2\text{S}$  nano-composites were studied with scanning electron microscopy, x-ray diffraction and absorption spectroscopy. The SEM and XRD were taken from powder samples, while the absorption spectrum was measured by dispersing the powder in deionized water. Figure 6.3 shows the XRD patterns and the SEM image of the  $\text{Ag}_2\text{S}$  nanoparticles. The SEM image presented in the figure shows spherical-shaped particles that are relatively uniformly sized. The shape, size and uniformity of the nano-particles are similar to those reported in literature[28, 29]. Crystallites sizes analysis from XRD measurements supports the possibility of the particles being uniformly sized as their calculated

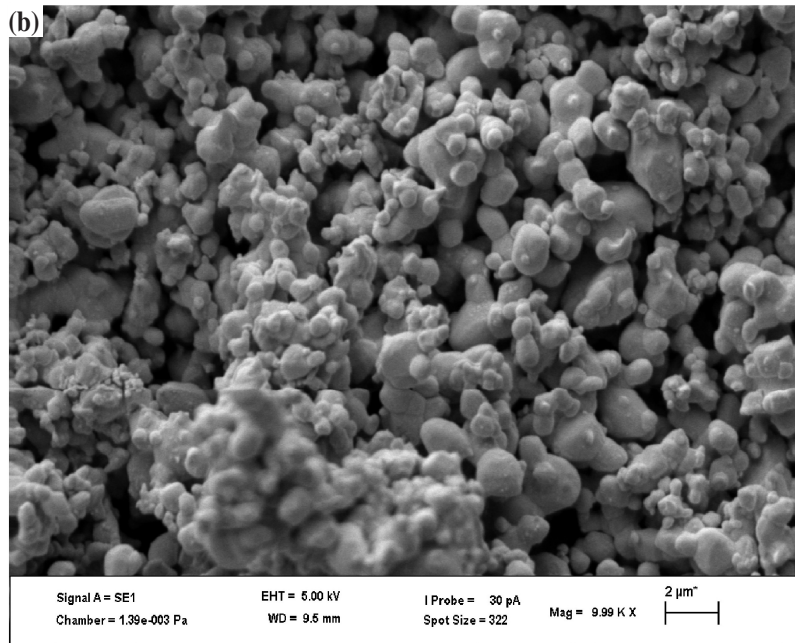
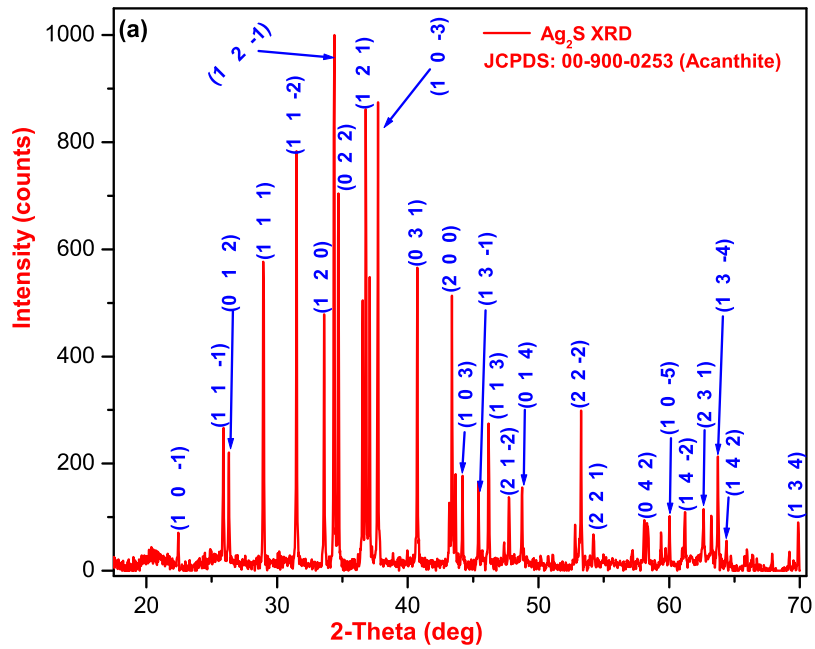


Figure 6.3: (a) XRD and (b) SEM of the silver sulfide powders.

crystallites sizes only ranges from 38 nm to 51 nm with the average crystallite being 44.46 nm ( $\pm 3.77$  nm). These particle sizes are capable of forward light-scattering[**30**, **31**, **32**] when employed in thin film organic solar cells.

The XRD analysis of the silver sulfide ( $\text{Ag}_2\text{S}$ ) nanoparticles was conducted to obtain information about its crystallographic structure. Several prominent peaks are detected on the measured XRD spectrum provided in Figure 6.3a. The XRD data were compared with standard diffraction pattern (JCPDS Card No. 00-900-0253) to be able to determine the structure of the nano-particles. The diffraction patterns indicate acanthite/monoclinic structured  $\text{Ag}_2\text{S}$  with parameters  $a = 4.22900$ ,  $b = 6.93100$  and  $c = 7.86200$  Å and belong to space group P 121/n1 1. The broadness of the peaks indicates nano-crystals formation. The average crystallites size of the particles was determined to be 44.46 nm ( $\pm 3.77$  nm) using Debye-Scherers equation provided in eq.(1)[33]:

$$D = k\lambda/\beta\cos\theta \quad (6.1)$$

where  $\lambda$  is the wavelength of the X-ray (1.5405 Å),  $k$  is the Scherrer constant ( $k = 0.89$ ),  $\beta$  is the full width at half maximum (FWHM) of the diffraction peak in radians and  $\theta$  is the corresponding Bragg angle at the maximum peak. The XRD analysis is summarized in Table 6.1, showing several lattice planes to which the several lattice reflections were matched.

Figure 6.4a shows the optical absorption of  $\text{Ag}_2\text{S}$  powder suspension in deionized water. The absorption peak is evident in the wavelengths range from 350 to 500 nm, followed by broad absorption tail which falls off monotonically towards larger wavelength regions. The broad band absorption is attributed to light scattering by the particles being in a water medium. The non-uniformity in the sizes of the nanoparticles may also be responsible for the broad band absorption. The energy bandgap of  $\text{Ag}_2\text{S}$  was calculated using the Tauc equation eq. (2) presented as follows and using Fig. 6.4a (inset):

$$(\alpha h\nu)^2 = \beta(h\nu - E_g) \quad (6.2)$$

where  $h$  is Planck's constant,  $\beta$  is a constant,  $\alpha$  is the absorption co-efficient and  $E_g$  is the band gap[34, 35]. The nano-particle energy band gap was determined to be 1.25 eV, which is similar to values reported in the literature[28, 29, 36].

## 6.4.2 Optical characteristics of the thin films

The electron transport layers were deposited via spin coating on cleaned ITO-coated glass substrates, from solutions of ZnO doped or undoped with silver sulfide nanoparticles. On these substrates, active layer solutions were deposited and characterized to study the effect of the  $\text{Ag}_2\text{S}$  incorporation on the neat films. Absorption and photo-luminescence (PL) spectra were measured for the various doped thin films

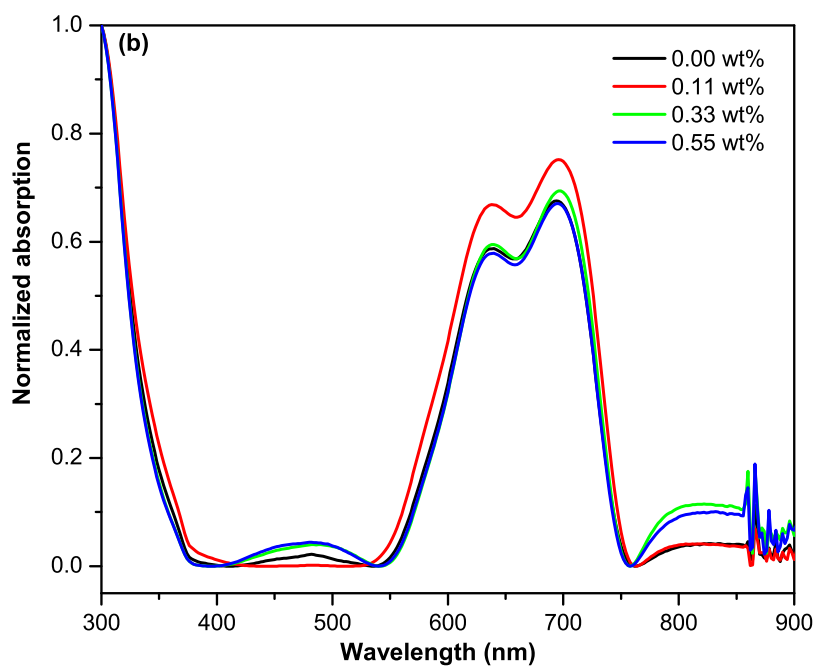
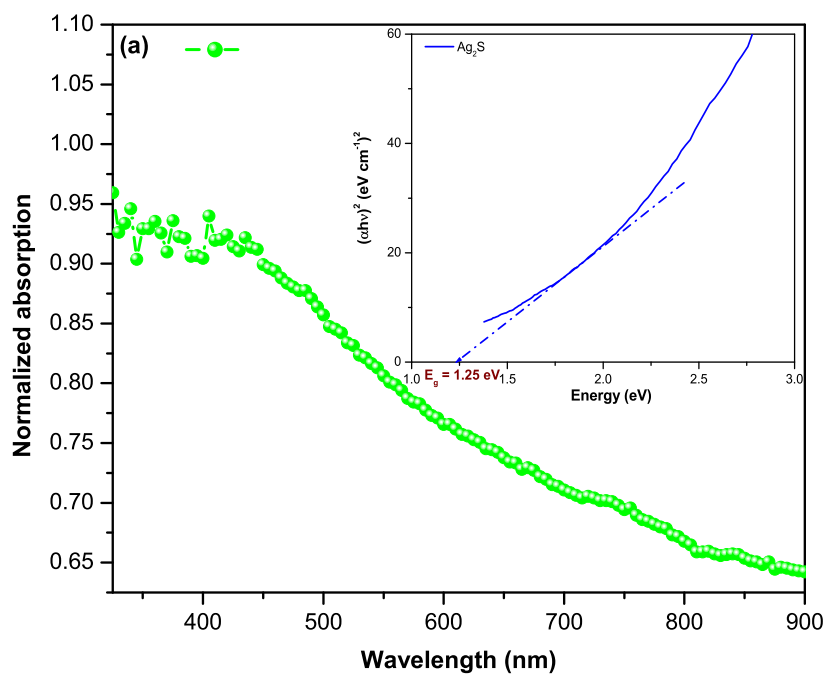


Figure 6.4: (a) Normalized absorption (inset: bandgap extrapolation) of the silver sulfide powders. (b) Absorbency of the TFOPV films with/without NPs incorporation.

Table 6.1: Silver sulfide NPs XRD analysis

Peak No	$2\theta$	FWHM	(h k l)	D (nm)
1	22.44	0.179	1 0 -1	44.742
2	25.90	0.209	1 1 -1	38.569
3	26.32	0.179	0 1 2	45.071
4	28.94	0.209	1 1 1	38.819
5	31.48	0.209	1 1 -2	39.052
6	33.60	0.179	1 2 0	45.844
7	34.37	0.209	1 2 -1	39.345
8	34.70	0.209	0 2 2	39.380
9	36.55	0.179	1 1 2	46.219
10	37.72	0.179	1 0 -3	46.376
11	40.73	0.179	0 3 1	46.813
12	43.38	0.179	2 0 0	47.232
13	44.19	0.209	1 0 3	40.567
14	45.41	0.179	1 3 -1	47.574
15	46.19	0.179	1 1 3	47.711
16	47.74	0.209	2 1 -2	41.103
17	48.75	0.209	0 1 4	41.266
18	53.26	0.179	2 2 -2	49.095
19	54.21	0.179	2 2 1	49.303
20	58.30	0.179	0 4 2	50.252
21	60.03	0.209	1 0 -5	43.409
22	61.19	0.209	1 4 -2	43.668
23	62.63	0.179	2 3 1	51.370
24	63.73	0.209	1 3 -4	44.257
25	64.39	0.209	1 4 2	44.416

(Figures 6.4b and 6.5, respectively). Doping ZnO with Ag<sub>2</sub>S NPs slightly altered the optical properties of both Ag<sub>2</sub>S and ZnO, as noted in the optical characteristics of the various deposited thin films devices given by the absorption and PL intensity.

The absorption spectra show that doped films had slightly higher absorbance peaks than the undoped film. There was a slight bump in absorption in some of the doped films from 450 nm to 550 nm, as well as above the 750 nm wavelength. Within the main absorption window of the blend (600 - 750) nm, the doped films displayed relatively higher absorption intensity of the incoming radiation than the undoped film with the 0.11 wt% doped film being more prominent. The new absorption bumps (450 - 550) nm could be due to a band to band transition of Ag, while the enhancement on the main absorbance peak (550-750) nm could be attributed to the occurrence of LSPR absorption coupled with more light trapping in the absorber layer. The bump near infra-red regions could be the result of multiple scattering processes that could result in large wavelength absorption.

Moreover, the occurrence of enhanced local electromagnetic field (EM) around the metal NPs could be an additional mechanism for exciton dissociations, which is strongly dependant on field intensity and could boost photo-current[37, 38]. Furthermore, the influence of the metal nano-composite on the photo-generated current was studied by measuring the photo-luminescence measurements of the blend thin films. The PL spectra (Fig. 6.5) was taken from films of solar absorber coated on top of the electron transport layer with/without doping Ag<sub>2</sub>S nano-particles. The PL spectra was obtained using an excitation source with a wavelength of 520 nm. The

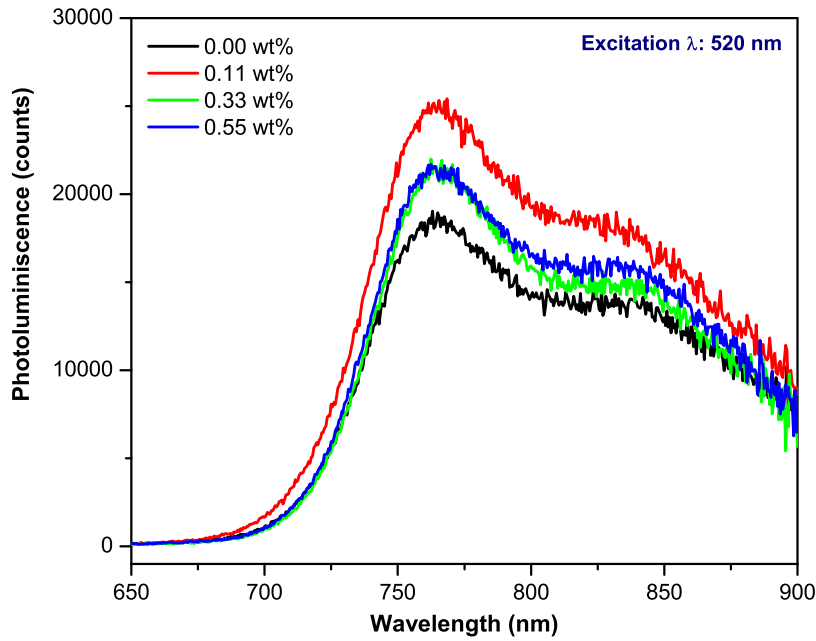


Figure 6.5: Photo-luminescence of thin film solar cells using ETL incorporated with  $\text{Ag}_2\text{S}$  nanoparticles.

excitation wavelength was chosen to be situated within the nano-particles resonance regions. Consequently, blend thin films deposited on doped buffer layers showed improved PL response compared to the reference buffer layer, demonstrating improved charge transfer processes between the donor and the acceptor materials. Here, fluorescence is contingent on the light excitation rate and the quantum yield, which also results from the interplay between radiative and non-radiative decay processes[43].

### 6.4.3 Photovoltaic characteristics

Thin film organic photovoltaic cells were fabricated with and without  $\text{Ag}_2\text{S}$  NPs doped in ZnO electron transport layer. The solar cells were prepared on different device effective areas to study their size dependent performances, which yields important information for large area device production. The measured device parameters are summarized in Table 6.2. Figure 6.6a show the current density - voltage (J-V) characteristics of the devices fabricated at different NPs concentration in the ZnO ETL for the  $0.1 \text{ cm}^2$  devices while Figure 6.6b is the J-V curves for the  $0.33 \text{ wt}\%$  NPs incorporated devices fabricated at the different effective device areas. The performance of the solar cells is generally increased with  $\text{Ag}_2\text{S}$  concentration in the electron transport layers. This is particularly true for small effective areas solar cells, namely  $0.1 \text{ cm}^2$  and  $0.15 \text{ cm}^2$ . The improved device performance is mainly due to increased collections of photo-current using doped ETL, which are reflected on the measured  $J_{sc}$ s. Considering a  $0.1 \text{ cm}^2$  effective area devices, which is the best in this investigation, the  $J_{sc}$ s increased from  $23.21 \text{ mA/cm}^2$  (undoped ETL) to

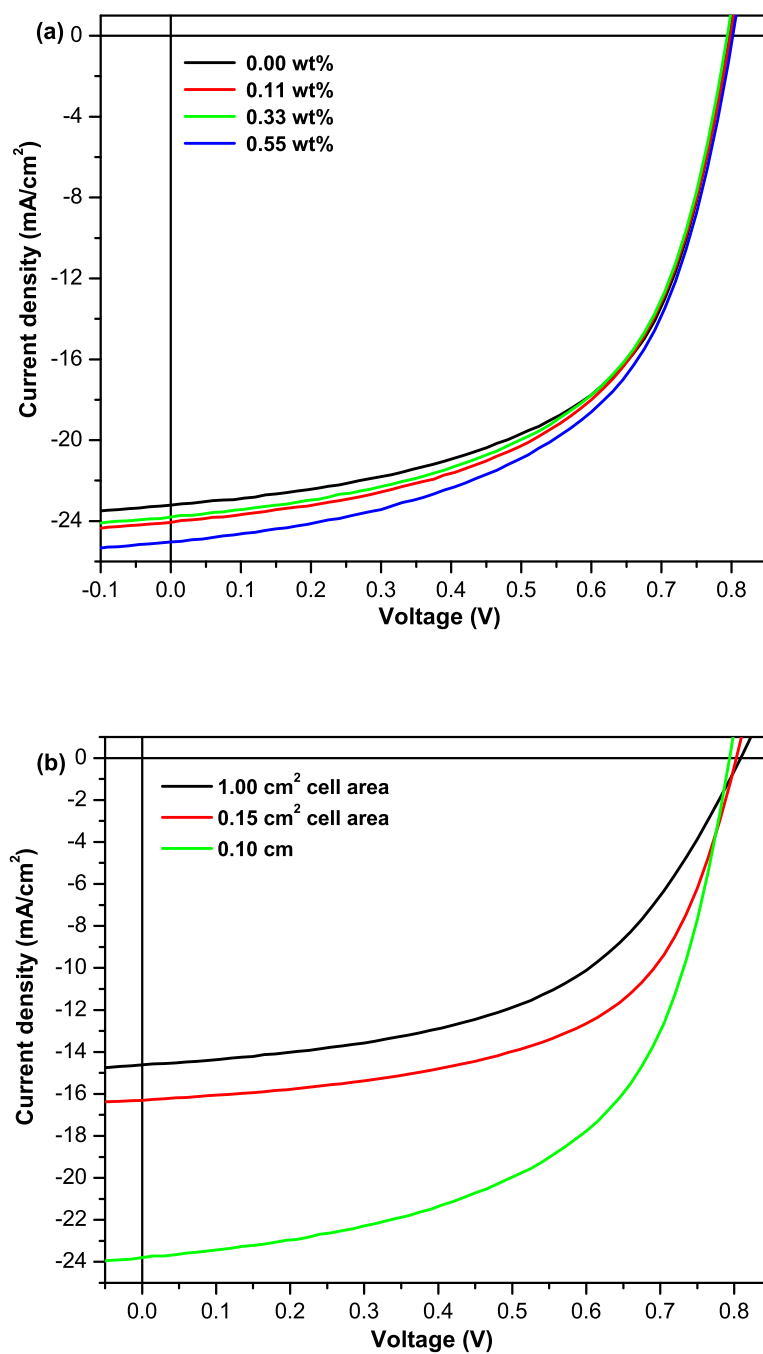


Figure 6.6: J-V plots of PTB7-Th:ITIC-Th solar cells fabricated at (a) different concentration of NPs incorporation in the ZnO ETL for the 0.1 cm<sup>2</sup> devices and (b) different device effective areas at 0.33 wt% nanoparticle incorporation.

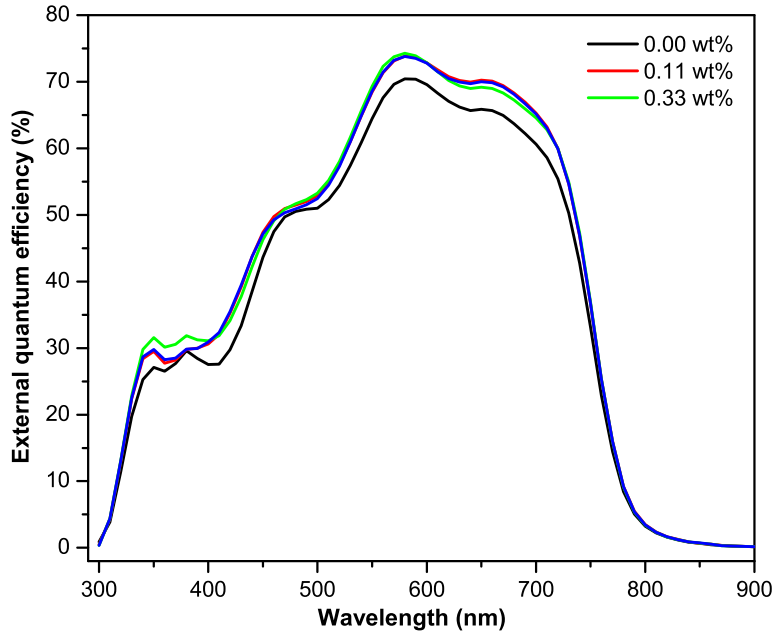


Figure 6.7: External quantum efficiency measured from solar cells that use ETL with/without  $\text{Ag}_2\text{S}$  nano-particles.

25.02  $\text{mA}/\text{cm}^2$  at 0.55 wt% doping concentration. Consequently, the power conversion efficiency rose by 7.7% from 10.69% to 11.17%. However, the increase in device performance sharply decreases as the effective area of the devices increased. This is due to the fact that large area devices contain large concentration of defects that sink free charge carriers and reduce the collection of photo-current. The reference solar cells fabricated with a 0.15  $\text{cm}^2$  cell area exhibited similar characteristics to those reported in previous investigations[39]. However, the current experiment differ from others because of the doped ETL used to promote charge collection in a non-fullerene acceptor based organic solar cell.

The observed performance enhancements of the solar cells could be associated with improved photon harvesting, as evidenced by enhanced optical absorptions. Furthermore, near-field enhancement of electromagnetic radiation around the plasmonic  $\text{Ag}_2\text{S}$  NPs possibly led to better exciton dissociation and ultimately leading to better overall device performance. The slight decreases in measured fill factor could suggest dwindling diode rectification. This can be improved upon with better film and device preparation in future investigations. The 0.55 wt% doped device at 1  $\text{cm}^2$  device area showed a noticeable drop in fill factor and PCE relative to the others but a sharp increase in  $R$  at  $V_{oc}$ , suggesting that excess incorporation of the nano-particles in the solar cells may induce leakage currents which may have caused the reduction of diodes rectification. High shunt and low series resistances are often simultaneously desired in a solar cell[40, 41]. The shunt resistance provides an indication of leakage current in the cell and depends on the films quality, while series resistance results from the device ohmic loss due to a combination of resistances from various sources such as from the active layer, the heterojunction

Table 6.2: Device performance parameters for solar cells fabricated with/without silver sulfide-incorporated ZnO as the ETLs at various NPs loading levels and at various effective device areas.

0.1 $cm^2$ devices	$V_{oc}$ (V)	$J_{sc}$ mA/ $cm^2$	FF (%)	PCE (%)	$R_s$ ( $\Omega cm^2$ )	$R_{sh}$ ( $\Omega cm^2$ )
0.00 wt%	0.80	23.21	57.92	10.69	42.62	3224
0.11 wt%	0.80	24.05	56.50	10.82	45.34	3060
0.33 wt%	0.80	23.79	56.57	10.67	52.75	3114
0.55 wt%	0.80	25.02	55.76	11.17	50.88	2922
<b>0.15 <math>cm^2</math> de-</b>						
<b>vices</b>						
0.00 wt%	0.81	15.79	58.27	7.42	55.12	3142
0.11 wt%	0.80	16.18	56.52	7.27	52.16	2778
0.33 wt%	0.80	16.29	58.32	7.61	48.54	3372
0.55 wt%	0.80	15.96	57.58	7.38	50.44	3138
<b>1 <math>cm^2</math> devices</b>						
0.00 wt%	0.81	14.50	52.45	6.15	15.09	436
0.11 wt%	0.80	14.06	52.43	5.92	13.66	420
0.33 wt%	0.81	14.62	51.97	6.14	14.56	439
0.55 wt%	0.80	14.28	42.07	4.81	25.91	285

(metal-organic) contacts, device electrodes and charge carriers extraction layers[42].

Figure 6.7 presents the external quantum efficiency curves for the solar cells produced in this investigation. The external quantum efficiency is a measure of how effective incident photons of different wavelengths are at generating photocurrents within the semiconducting device. The ratio of output photocurrent densities at different wavelengths and the incident power at the wavelengths are obtained for all wavelengths, integrated and expressed as a percentage of the total input power. All the devices exhibited broad photoresponse extending from 350 to 800 nm. Generally, the doped devices have exhibited enhanced spectral response relative to the reference device. The photon to electron conversion rose from nearly 70% in pristine ETL device to 75% in doped solar cells. The 5% increase in EQE could be attributed to enhanced optical absorption due to light trapping and improved dissociation of exciton at the photo-active layer and ETL interfaces. The increased EQE, coupled with the PL responses, may be attributed to the effective dissociation and collection of the charge carriers by the presence of the nano-particles in ETL medium. The elevated excitation rate in turn possibly increased photo-generated excitons density in the blend to enhance fluorescence intensity[44, 45]. Moreover, the improved EQE may be due to better movement of the photo-generated electrons from the  $Ag_2S$ -incorporated ZnO ETL layer due to the favourable energy band alignment between the  $Ag_2S$  NPs and the ZnO as noted in Figure 6.2, while the holes migrate to the VB of  $MoO_3$  and are collected at the Ag electrode. This improved charge carriers motion may enhance faster electron-hole pair separation and reduce recombination[46].

#### 6.4.4 Device simulation

Device simulation is an increasingly complimentary research tool for device physics studies and designing of optimal approach(es) for obtaining optimum device efficiency. Hence, in order to get more information about our fabricated solar cells,

Table 6.3: Simulation device parameters

Parameters	MoO <sub>3</sub>	PBT7-Th/ITIC-Th	ZnO
Thickness (nm)	10	100	40
Bandgap (eV)	3.0	1.27 <sup>a</sup>	3.30
Electron affinity (eV)	2.5	3.93 <sup>b</sup>	4.0
Relative permittivity	9	3.5	9
CB effective DOS (cm <sup>-3</sup> )	2 x 10 <sup>18</sup>	5 x 10 <sup>20</sup>	2.2 x 10 <sup>18</sup>
VB effective DOS (cm <sup>-3</sup> )	1.8 x 10 <sup>19</sup>	1 x 10 <sup>21</sup>	1.8 x 10 <sup>19</sup>
Electron mobility (cm <sup>2</sup> /V s)	25	3.1 x 10 <sup>-4</sup>	100
Holes mobility (cm <sup>2</sup> /V s)	100	3.2 x 10 <sup>-4</sup>	25
Donor density - ND (cm <sup>-3</sup> )	0	0	1 x 10 <sup>18</sup>
Acceptor density - NA (cm <sup>-3</sup> )	1 x 10 <sup>16</sup>	0	0

<sup>a</sup> [53], <sup>b</sup> Equal to the negative LUMO of ITIC-Th[54] [56, 55]

we performed numerical simulations using the Solar Cells Capacitance (SCAPS) software (version 3.3.07). The program is a 1D solar devices simulator that was developed by Prof. Burgelman at the University of Gent, Belgium[47, 48]. The simulation was based on the effective medium model[49, 50], in which the active layer (composed of the donor and acceptor materials) is described by a single semi-conducting layer. Selective contacts or buffer layers are introduced to provide the migration driving force for the photo-generated electron-hole pairs generated[51, 52]. The materials properties for the effective medium are obtained from either PTB7-Th, ITIC-Th or an average of both and are summarized in Table 6.3.

The configuration of the simulated device is Glass/ITO/ZnO w/wo Ag<sub>2</sub>S/PTB7-Th:ITIC-Th/MoO<sub>3</sub>/Ag. ZnO serves as the ETL, MoO<sub>3</sub> is the HTL, ITO as the cathode (front contact) and Ag as the anode (back contact). Parameters that were not included in the table are set to be identical in each layer or across devices. The flatband setting is adopted for the front and back contact workfunctions. Interface defects between the ETL/Active and Active/HTL were defined and set to 1 x 10<sup>9</sup> cm<sup>-2</sup>. The NFA used in this investigation has a high relative permittivity and consequently a high exciton dissociation probability (approximately 0.945) under short circuit conditions[57]. This also reduces the exciton binding energy (to roughly 10 meV), making the excitons dissociation and transport efficiencies close to one[55]. In order to effectively calibrate the simulation, suitable series and shunt resistances were applied to reproduce the 0.15 cm<sup>2</sup> device parameters at 0.00 wt% and 0.33 wt% doping levels. The solar spectrum transmission was set to 90-95%. The simulation results were compared with experimental measurements in Table 6.4. The simulated device characteristics closely matches the experimental results, validating the baseline settings adopted for the simulation. At these settings, further characterizations were performed on the doped and undoped devices to explain within a reasonable approximation the effects of the silver sulfide nanoparticles on the overall device performance.

Device performance can be influenced by the working temperature as there is often change in environmental temperature. The PV device performance under varying temperature condition was investigated. The variation of the four device parameters for both the doped and undoped solar cells are illustrated in Fig. 6.8. As the temperature increased from 300 K to 450 K, the device parameters for both solar

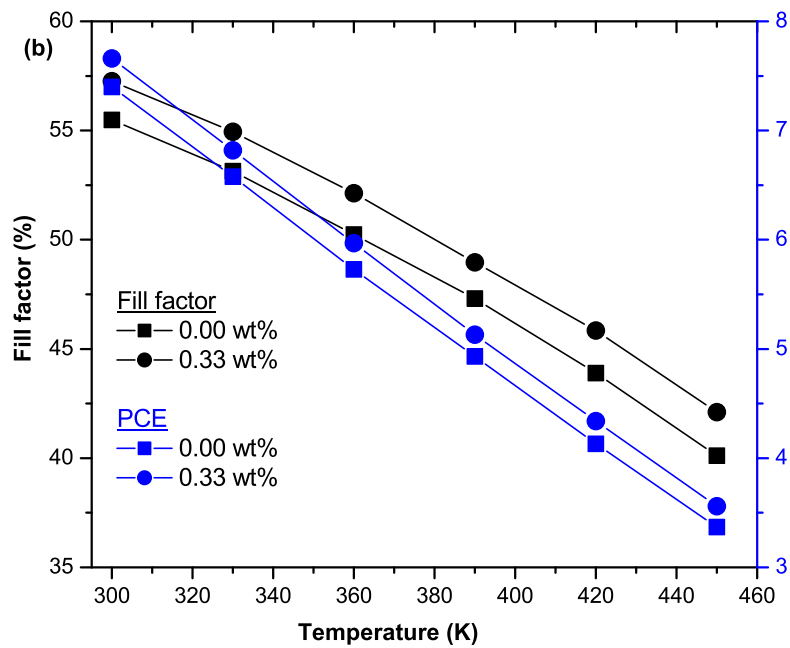
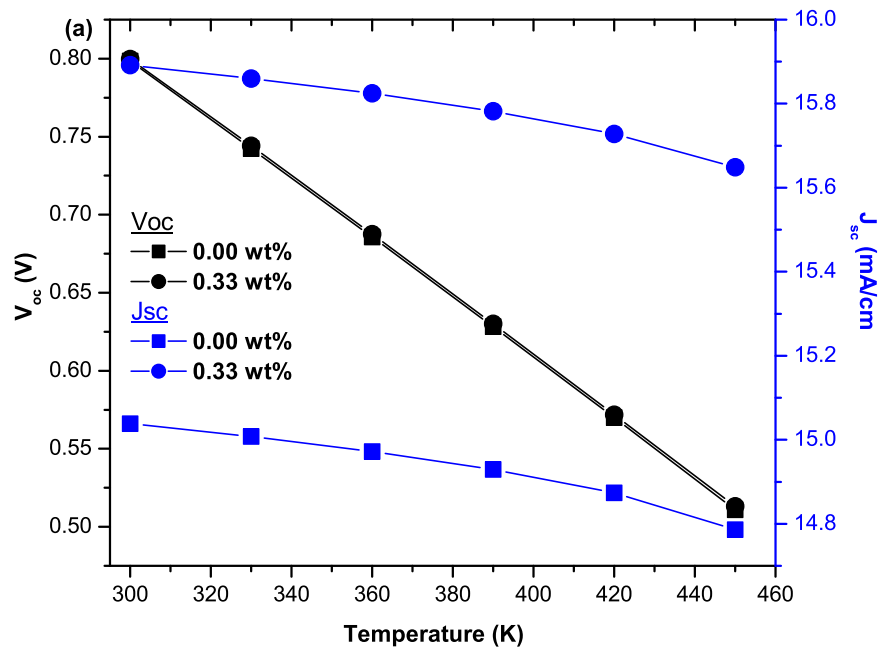


Figure 6.8: Numerical investigation of the temperature dependence of device parameters via device simulation for NPs-doped and pristine HTL devices (a) Voc and Jsc versus temperature (b) Fill factor and PCE, respectively.

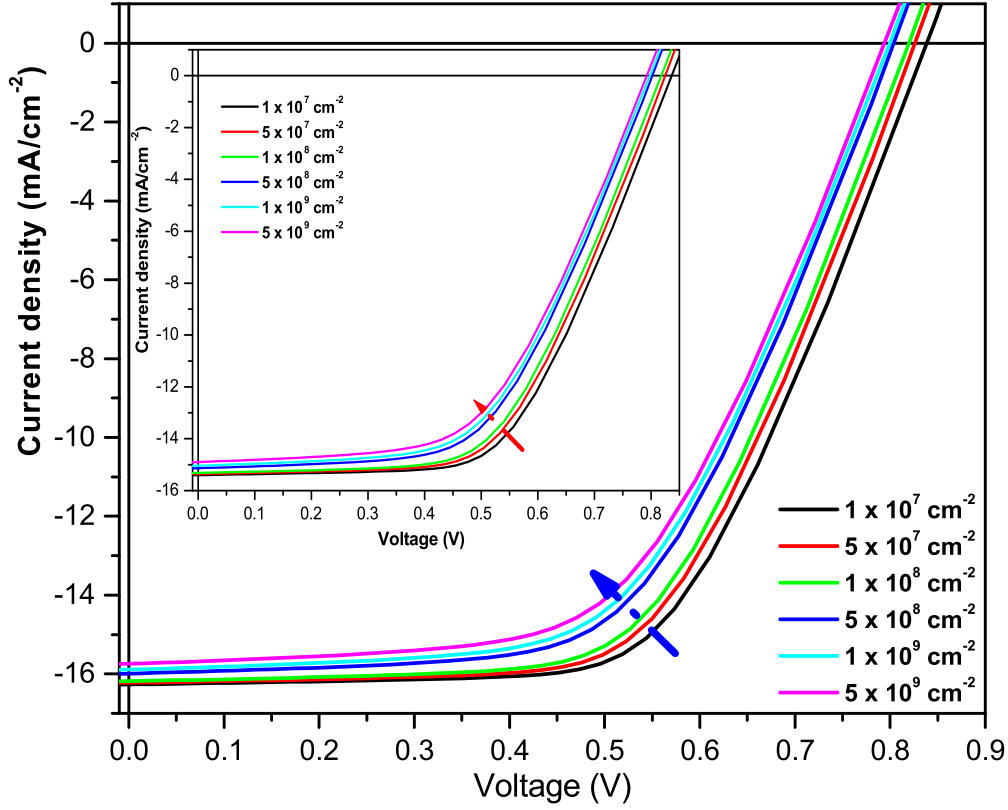


Figure 6.9: J-V curves of the simulated Ag<sub>2</sub>S-doped devices with different doped-ETL/Active layer interface defect densities (inset: similar simulation with the pristine devices).

Table 6.4: Experimental and simulated solar cells parameters for the 0.15 cm<sup>2</sup> devices

	0.00 wt%	simulated	0.33 wt%	simulated
$V_{oc}$ (V)	0.81	0.80	0.80	0.80
$J_{sc}$ (mA/cm <sup>2</sup> )	15.79	15.04	16.29	15.89
FF (%)	58.27	55.49	58.32	57.26
PCE (%)	7.42	7.40	7.61	7.66

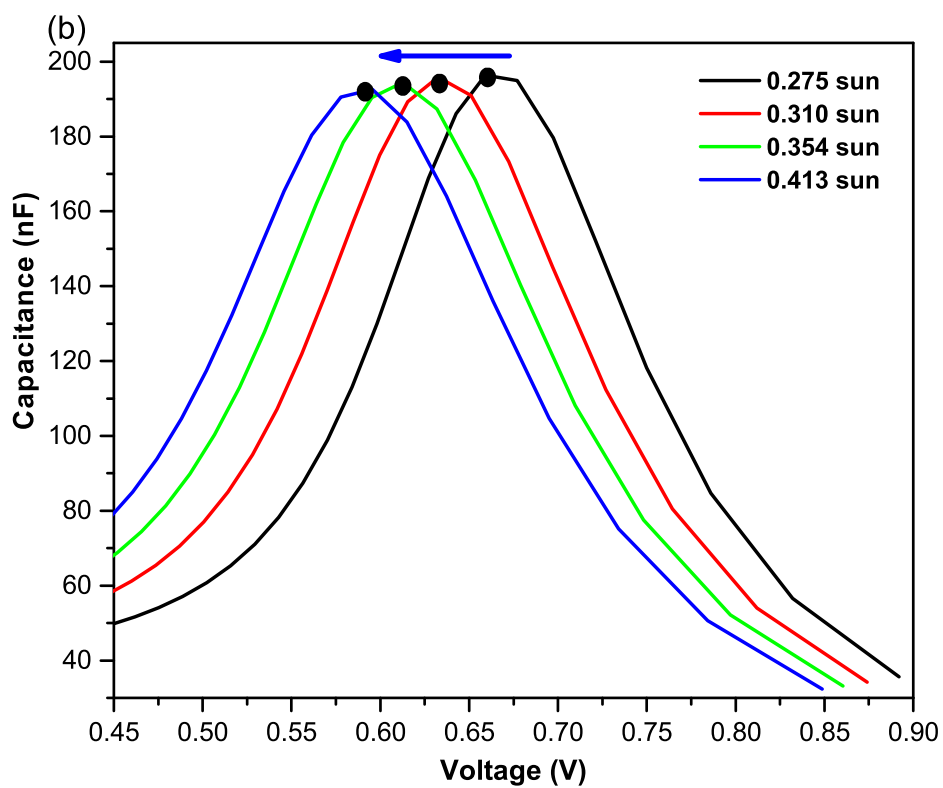
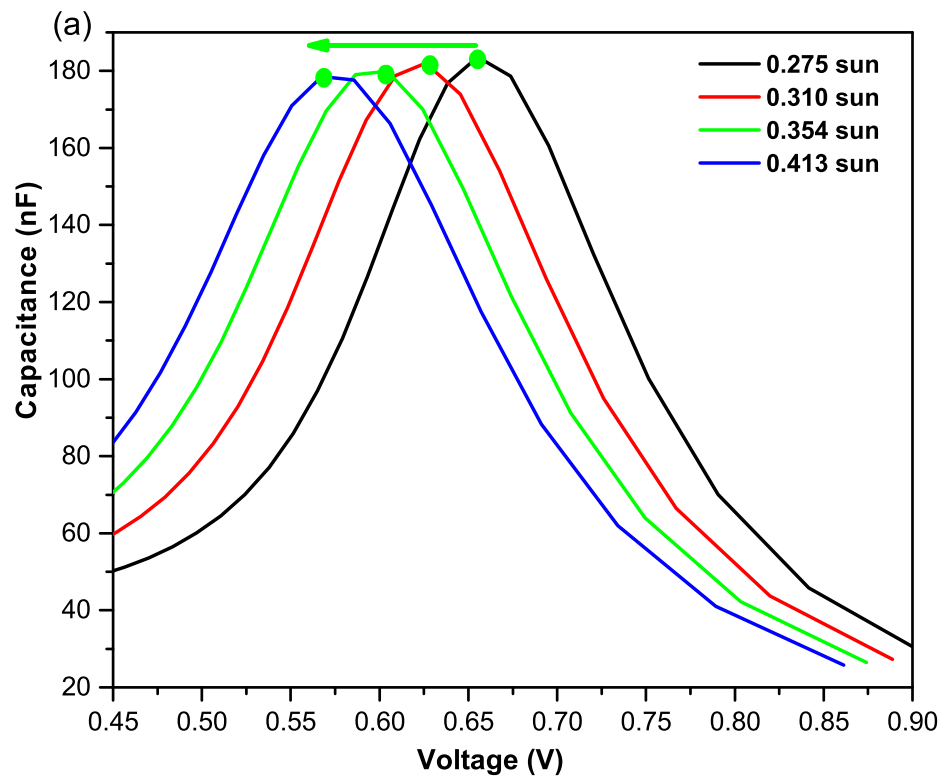


Figure 6.10: The photo-assisted capacitance–voltage characteristics of the a) pristine ETL and the b) NPs-incorporated ETL devices at various illumination intensities.

cells degraded slightly differently. The Voc reduction from both devices followed similar patterns while Jsc drops of  $252 \text{ mAcm}^{-2}$  and  $243 \text{ mAcm}^{-2}$  were recorded for the pristine and NPs-incorporated devices, respectively. A rise in the saturation current and increased recombination rate due to the increased temperature led to the Voc decline. Although the temperature rise may cause more thermal carriers to be generated, however, thermal resistance to the carriers motion may simultaneously increase leading to the reduced short circuit current density[55]. Since there is a decline in both the Voc and the Jsc, the efficiency and the fill factor of the devices decreased as well.

Next, we simulate the influence of recombination arising from interface defects due to the doping of the ETL. An ETL/active layer interface was defined with the interface defects varied from  $1 \times 10^7$  to  $5 \times 10^9 \text{ cm}^{-2}$ . The J-V curves of the simulated cells are illustrated in Fig. 6.9. The ETL/Active layer interface defects have a remarkable influence on the devices performance. As expected, the higher defect densities present increased traps and recombination centers, leading to depreciating device output. The rate of performance decline from both the doped and undoped devices remained roughly similar. Since our devices were fabricated with the inverted architecture, the device was illuminated through the front contact (glass/ITO/Zno/Active layer), hence the density of the photo-generated electron-hole pairs is expected to be higher at the ETL side of the devices than at the HTL side (Active layer/MoO<sub>3</sub>/Ag), thus the excess carrier density at the front contact of the device would likely be less than the excess carrier density at the back contact and the recombination rate, which is a function of the excess carrier density, will be higher at the front contact. Hence, the interface defects at the Zno/Active layer interface will expectedly have a greater influence on the device performance at the Active layer/MoO<sub>3</sub> interface. We therefore did not perform simulation for the Active layer/MoO<sub>3</sub> interface.

Finally, to explore the effect of photo-induced dipoles of the Ag<sub>2</sub>S on the charge extraction at ETL/Active layer interface, photo-assisted capacitance–voltage (C-V) measurements at various photo-excitation illumination intensities were simulated following methods adopted by refs[58, 59]. Low illumination values were used because higher illumination generates more charges and thus more charge accumulation. Shifts in the devices voltage peak in reverse bias with respect to the illumination intensity is a measure of interfacial charge accumulation[58, 60]. Figure 6.10 shows the C–V characteristics of the undoped and doped devices at different photo-illumination intensities. The voltage peak values shifted by 88.6 mV and 74.5 mV for the undoped and doped devices, respectively, when the illumination was adjusted from 0.413 sun to 0.275 sun, indicating slightly higher charge accumulation in the undoped devices. Thus, the photo-induced dipoles at the ETL/Active layer interface in the doped devices demonstrated improved interfacial charge transfer reducing charge accumulation over the undoped device.

## 6.5 Conclusion

Effective absorption of light is a critical process in thin film organic photovoltaic cells, where the active layer thickness is low. In this report, we have demonstrated the possibility and effectiveness of enhanced light absorption through plasmonic-induced processes in electron transport layer of organic solar cells by incorporating silver sulfide nanoparticles in the ZnO to achieve improved device PCEs. The improved optical absorption due to enhanced light trapping could be attributed to near and/or far field scattering of the metal NPs dopant in the electron transport layer. Plasmons and photo-generated excitons interactions led to better exciton dissociation, thereby limiting geminate recombination. This is in fact supported by the 5% increase in external quantum efficiency. Being one of the first few reports on the incorporation of nano-particles in non-fullerene acceptor based organic solar cells, this is a highly recommended route to enhancing the performance of this class of TFOPV devices. It is worth to mention that the metal NPs are environmentally friendly and stable, which make it more desirable for roll to roll device fabrication.

## Acknowledgments

This research was supported by the National Research Foundation (NRF) (Grant numbers, 93562, 132786), South Africa. We thank members of staff of Microscopy and Microanalysis Unit (MMU) at UKZN for the SEM analysis. The authors also appreciate the Commonwealth Scholarships Commission (CSC) in the United Kingdom for awarding a split-site scholarship to Michael A.A. which enabled him to travel to Swansea University to conduct several aspects of this research. Efforts of colleagues at Materials Science Group (UKZN) and Applied Photochemistry Group (Swansea University) are also appreciated

# Bibliography

## References

- [1] Liang, Y., Xu, Z., Xia, J., Tsai, S. T., Wu, Y., Li, G., Ray, C., & Yu, L. (2010). For the bright future—bulk heterojunction polymer solar cells with power conversion efficiency of 7.4%. *Advanced materials*, 22(20), E135-E138.
- [2] Li, G., Shrotriya, V., Huang, J., Yao, Y., Moriarty, T., Emery, K., & Yang, Y. (2011). High-efficiency solution processable polymer photovoltaic cells by self-organization of polymer blends. In *Materials For Sustainable Energy: A Collection of Peer-Reviewed Research and Review Articles from Nature Publishing Group* (pp. 80-84). World Scientific.
- [3] Sariciftci, N. S., Smilowitz, L., Heeger, A. J., & Wudl, F. (1992). Photoinduced electron transfer from a conducting polymer to buckminsterfullerene. *Science*, 258(5087), 1474-1476.
- [4] Yu, G., Gao, J., Hummelen, J. C., Wudl, F., & Heeger, A. J. (1995). Polymer photovoltaic cells: enhanced efficiencies via a network of internal donor-acceptor heterojunctions. *Science*, 270(5243), 1789-1791
- [5] Adedeji, M. A., Hamed, M. S., & Mola, G. T. (2020). Light trapping using copper decorated nano-composite in the hole transport layer of organic solar cell. *Solar Energy*, 203, 83-90.
- [6] Anthony, J. E., Facchetti, A., Heeney, M., Marder, S. R., & Zhan, X. (2010). *n*-Type organic semiconductors in organic electronics. *Advanced materials*, 22(34), 3876-3892.
- [7] He, Y., & Li, Y. (2011). Fullerene derivative acceptors for high performance polymer solar cells. *Physical chemistry chemical physics*, 13(6), 1970-1983.
- [8] Chen, C. C., Chang, W. H., Yoshimura, K., Ohya, K., You, J., Gao, J., Hong, Z., & Yang, Y. (2014). An efficient triple-junction polymer solar cell having a power conversion efficiency exceeding 11%. *Advanced materials*, 26(32), 5670-5677.
- [9] Lin, Y., & Zhan, X. (2014). Non-fullerene acceptors for organic photovoltaics: an emerging horizon. *Materials Horizons*, 1(5), 470-488.
- [10] Cui, Y., Xu, Y., Yao, H., Bi, P., Hong, L., Zhang, J., Zu, Y., Zhang, T., Qin, J., & Ren, J. (2021). Single-Junction Organic Photovoltaic Cell with 19% Efficiency. *Advanced materials*, 33(41), 2102420.

- [11] Mola, G. T., Ahmed, A. Y., Ike, J. N., Liu, M., Hamed, M. S., & Zhang, Y. (2022). Engineering Non-fullerene Acceptors as a Mechanism to Control Film Morphology and Energy Loss in Organic Solar Cells. *Energy & Fuels*, 36, 4691-4707.
- [12] Wu, J. L., Chen, F. C., Hsiao, Y. S., Chien, F. C., Chen, P., Kuo, C. H. & Hsu, C. S. (2011). Surface plasmonic effects of metallic nanoparticles on the performance of polymer bulk heterojunction solar cells. *ACS nano*, 5(2), 959-967.
- [13] Fleetham, T., Choi, J.-Y., Choi, H. W., Alford, T., Jeong, D. S., Lee, T. S., Lee, W. S., Lee, K.-S., Li, J., & Kim, I. (2015). Photocurrent enhancements of organic solar cells by altering dewetting of plasmonic Ag nanoparticles. *Scientific reports*, 5(1), 1-9.
- [14] Kalfagiannis, N., Karagiannidis, P., Pitsalidis, C., Panagiotopoulos, N., Gravalidis, C., Kassavetis, S., Patsalas, P., & Logothetidis, S. (2012). Plasmonic silver nanoparticles for improved organic solar cells. *Solar Energy Materials and Solar Cells*, 104, 165-174.
- [15] Na, S. I., Kim, S. S., Jo, J., Oh, S. H., Kim, J., & Kim, D. Y. (2008). Efficient polymer solar cells with surface relief gratings fabricated by simple soft lithography. *Advanced Functional Materials*, 18(24), 3956-3963.
- [16] Tang, M., Sun, B., Zhou, D., Gu, Z., Chen, K., Guo, J., Feng, L., & Zhou, Y. (2016). Broad-band plasmonic Cu-Au bimetallic nanoparticles for organic bulk heterojunction solar cells. *Organic Electronics*, 38, 213-221.
- [17] Notarianni, M., Vernon, K., Chou, A., Aljada, M., Liu, J., & Motta, N. (2014). Plasmonic effect of gold nanoparticles in organic solar cells. *Solar Energy*, 106, 23-37.
- [18] Amiri, O., Salavati-Niasari, M., Mir, N., Beshkar, F., Saadat, M., & Ansari, F. (2018). Plasmonic enhancement of dye-sensitized solar cells by using Au-decorated Ag dendrites as a morphology-engineered. *Renewable energy*, 125, 590-598.
- [19] Amiri, O., Salavati-Niasari, M., Rafiei, A., & Farangi, M. (2014). 147% improved efficiency of dye synthesized solar cells by using CdS QDs, Au nanorods and Au nanoparticles. *RSC Advances*, 4(107), 62356-62361.
- [20] Ferry, V. E., Munday, J. N., & Atwater, H. A. (2010). Design considerations for plasmonic photovoltaics. *Advanced materials*, 22(43), 4794-4808.
- [21] Fung, D. D., Qiao, L., Choy, W. C., Wang, C., Wei, E., Xie, F., & He, S. (2011). Optical and electrical properties of efficiency enhanced polymer solar cells with Au nanoparticles in a PEDOT-PSS layer. *Journal of Materials Chemistry*, 21(41), 16349-16356.
- [22] Liao, H.-C., Tsao, C.-S., Lin, T.-H., Jao, M.-H., Chuang, C.-M., Chang, S.-Y., Huang, Y.-C., Shao, Y.-T., Chen, C.-Y., & Su, C.-J. (2012). Nanoparticle-tuned self-organization of a bulk heterojunction hybrid solar cell with enhanced performance. *ACS nano*, 6(2), 1657-1666.

- [23] Grzelczak, M., Pérez-Juste, J., Mulvaney, P., & Liz-Marzán, L. M. (2008). Shape control in gold nanoparticle synthesis. *Chemical Society Reviews*, 37(9), 1783-1791.
- [24] Hsu, H.-L., Juang, T.-Y., Chen, C.-P., Hsieh, C.-M., Yang, C.-C., Huang, C.-L., & Jeng, R.-J. (2015). Enhanced efficiency of organic and perovskite photovoltaics from shape-dependent broadband plasmonic effects of silver nanoplates. *Solar Energy Materials and Solar Cells*, 140, 224-231.
- [25] Lin, X., Wang, Y., Wu, J., Tang, Z., Lin, W., Nian, L., & Yi, G. (2021). Black Phosphorus Quantum Dots Based Heterostructure Boosting Electron Extraction for Non-Fullerene Organic Solar Cells Surpassing 15% Power Conversion Efficiency. *ACS Applied Energy Materials*, 4(6), 5905-5912.
- [26] Subramanian, P., Meziane, D., Wojcieszak, R., Dumeignil, F., Boukherroub, R., & Szunerits, S. (2018). Plasmon-induced electrocatalysis with multi-component nanostructures. *Materials*, 12(1), 43.
- [27] Masson, J. F. (2020). Portable and field-deployed surface plasmon resonance and plasmonic sensors. *Analyst*, 145(11), 3776-3800.
- [28] Huang, H. J., Wu, J. C.-S., Chiang, H.-P., Chou Chau, Y.-F., Lin, Y.-S., Wang, Y. H., & Chen, P.-J. (2019). Review of experimental setups for plasmonic photocatalytic reactions. *Catalysts*, 10(1), 46.
- [29] Mukherjee, N., Jana, S., Gopal Khan, G., & Mondal, A. (2012). Photo-induced exciton generation in polyvinylpyrrolidone encapsulated Ag<sub>2</sub>S core-shells: Electrochemical deposition, regular shape and high order of particle size distribution. *Journal of Applied Physics*, 112(12), 124324.
- [30] Muheeb Ahmad Alkhalayfeh, Azlan Abdul Aziz, Mohd Zamir Pakhuruddin, An overview of enhanced polymer solar cells with embedded plasmonic nanoparticles, *Renewable and Sustainable Energy Reviews* 141 (2021) 110726
- [31] Baek S-W, Noh J, Lee C-H, Kim B, Seo M-K, Lee J-Y, Plasmonic forward scattering effect in organic solar cells: a powerful optical engineering method. *Sci Rep* 2013; 3:1726.
- [32] Mokkapati S, Beck F, De Waele R, Polman A, Catchpole K. Resonant nano-antennas for light trapping in plasmonic solar cells. *J Phys Appl Phys* 2011; 44: 185101.
- [33] Jang, J., Cho, K., Lee, S. H., & Kim, S. (2008). Synthesis and electrical characteristics of Ag<sub>2</sub>S nanocrystals. *Materials Letters*, 62(8-9), 1438-1440.
- [34] Moore, P. (1968). : *Elements of X-Ray Crystallography*. *Journal of Geology*, 76(5), 611-612.
- [35] Yadav, A., & Masumdar, E. (2010). Preparation and characterization of indium doped CdSO. 2Se0. 8 thin films by spray pyrolysis. *Materials Research Bulletin*, 45(10), 1455-1459.

- [36] *Hassanien, A. S., & Akl, A. A. (2016). Effect of Se addition on optical and electrical properties of chalcogenide CdSSe thin films. Superlattices and Microstructures, 89, 153-169.*
- [37] *Martínez-Ruvalcaba, I., Hernández-Paz, J., Mancilla, J. F., Ruiz, P. P., Pérez, C. M., García-Casillas, P., & Rodríguez-González, C. (2014). Optical properties of bio-inspired silver sulfide structures. Journal of alloys and compounds, 586, S526-S530.*
- [38] *Monestier, F., Simon, J.-J., Torchio, P., Escoubas, L., Flory, F., Bailly, S., de Bettignies, R., Guillerez, S., & Defranoux, C. (2007). Modeling the short-circuit current density of polymer solar cells based on P3HT: PCBM blend. Solar Energy Materials and Solar Cells, 91(5), 405-410.*
- [39] *Pettersson, L. A., Roman, L. S., & Inganäs, O. (1999). Modeling photocurrent action spectra of photovoltaic devices based on organic thin films. Journal of Applied Physics, 86(1), 487-496.*
- [40] *Clarke, A. J., Luke, J., Meitzner, R., Wu, J., Wang, Y., Lee, H. K., Speller, E. M., Bristow, H., Cha, H., & Newman, M. J. (2021). Non-fullerene acceptor photostability and its impact on organic solar cell lifetime. Cell Reports Physical Science, 2(7), 100498.*
- [41] *Li, J., Liu, J., Gao, C., & Chen, G. (2011). Nanocomposite hole-extraction layers for organic solar cells. International Journal of Photoenergy, ID 392832*
- [42] *Yu, H.-Z., & Peng, J.-B. (2007). Influence of the solvent and device structure on the performance of the MEH-PPV: PCBM solar cell. Acta Physico—Chimica Sinica, 23(10), 1637-1641.*
- [43] *Muth, M.-A., Mitchell, W., Tierney, S., Lada, T. A., Xue, X., Richter, H., Carrasco-Orozco, M., & Thelakkat, M. (2013). Influence of charge carrier mobility and morphology on solar cell parameters in devices of mono- and bis-fullerene adducts. Nanotechnology, 24(48), 484001.*
- [44] *Anger, P., Bharadwaj, P., & Novotny, L. (2006). Enhancement and quenching of single-molecule fluorescence. Physical review letters, 96(11), 113002.*
- [45] *Mahmoud, M. A., Poncheri, A. J., Phillips, R. L., & El-Sayed, M. A. (2010). Plasmonic field enhancement of the exciton-exciton annihilation process in a poly (p-phenyleneethynylene) fluorescent polymer by Ag nanocubes. Journal of the American Chemical Society, 132(8), 2633-2641.*
- [46] *Ghorui, U. K., Mondal, P., Satra, J., Adhikary, B., & Mondal, A. (2022). In situ metallic copper incorporation into novel g-C<sub>3</sub>N<sub>4</sub>/ZnWO<sub>4</sub> nanocomposite semiconductor for efficient thin film solar cell application. Materials Science in Semiconductor Processing, 143, 106559.*
- [47] *Bauer, A., Sharbati, S., & Powalla, M. (2017). Systematic survey of suitable buffer and high resistive window layer materials in CuIn<sub>1-x</sub>Ga<sub>x</sub>Se<sub>2</sub> solar cells by numerical simulations. Solar Energy Materials and Solar cells, 165, 119-127.*

- [48] Verschraegen, J., & Burgelman, M. (2007). Numerical modeling of intraband tunneling for heterojunction solar cells in SCAPS. *Thin Solid Films*, 515(15), 6276-6279.
- [49] Adedeji, M.A., & Mola, G.T. (2022). Numerical investigation of the effects of Copper sulphide nanoparticles on hole transport layer of thin film organic solar cells. *Journal of Computational Electronics*, 21, 128-136.
- [50] Minnaert, B., & Burgelman, M. (2007). Empirical study of the characteristics of current-state organic bulk heterojunction solar cells. *The European Physical Journal Applied Physics*, 38(2), 111-114.
- [51] Hacene, S. B., & Benouaz, T. (2014). Influence of charge carrier mobility and surface recombination velocity on the characteristics of P3HT:PCBM organic solar cells. *physica status solidi (a)*, 211(4), 862-868.
- [52] Arbab, E.A.A., Taleatu, B., Mola, G.T. (2014). Environmental stability of PTB7:PCBM bulk heterojunction solar cell. *Journal of Modern Optics*, 61(21), 1749.
- [53] Luo, H., Lai, J., Wang, C., & Chen, Q. (2018). Understanding the effects of the energy band alignment at the donor/acceptor interface on the open circuit voltage of organic photovoltaic devices. *Chemical Physics Letters*, 711, 113-117.
- [54] Li, S., Hamada, F., Nishikubo, R., & Saeki, A. (2022). Quantifying the optimal thickness in polymer: fullerene solar cells from the analysis of charge transport dynamics and photoabsorption. *Sustainable Energy & Fuels*, 6, 756.
- [55] Abdelaziz, W., Shaker, A., Abouelatta, M., & Zekry, A. (2019). Possible efficiency boosting of non-fullerene acceptor solar cell using device simulation. *Optical Materials*, 91, 239-245.
- [56] Mozafari, B., & Shahhoseini, A. (2020). using Molybdenum trioxide as a TCO layer to improve performance of CdTe-CdS thin film solar cell. *Signal processing and renewable energy*, 4(3), 57-65.
- [57] Liu, X., Xie, B., Duan, C., Wang, Z., Fan, B., Zhang, K., & Cao, Y. (2018). A high dielectric constant non-fullerene acceptor for efficient bulk-heterojunction organic solar cells. *Journal of Materials Chemistry A*, 6(2), 395-403.
- [58] Ahmadi, M., Hsiao, Y. C., Wu, T., Liu, Q., Qin, W., & Hu, B. (2017). Effect of Photogenerated Dipoles in the Hole Transport Layer on Photovoltaic Performance of Organic-Inorganic Perovskite Solar Cells. *Advanced Energy Materials*, 7(4), 1601575.
- [59] Aqoma, H., Mubarak, M. A., Lee, W., Hadmojo, W. T., Park, C., Ahn, T. K. & Jang, S. Y. (2018). Improved processability and efficiency of colloidal quantum dot solar cells based on organic hole transport layers. *Advanced Energy Materials*, 8(23), 1800572.
- [60] Cho, S., Kim, K. D., Heo, J., Lee, J. Y., Cha, G., Seo, B. Y. & Lim, D. C. (2014). Role of additional PCBM layer between ZnO and photoactive layers in inverted bulk-heterojunction solar cells. *Scientific reports*, 4(1), 1-6.

# Chapter 7

## The effect of silver-sulfide on charge transport buffer layers in fullerene based polymer solar cell



### Submission Confirmation

---

From: Solar Energy (em@editorialmanager.com)

To: pelukunmi4@yahoo.com

Date: Wednesday, November 9, 2022 at 07:35 PM GMT+1

---

Dear Mr Michael Adedeji,

Your submission entitled "The effect of silver-sulfide on charge transport buffer layers in fullerene based polymer solar cell" has been received by Solar Energy Research paper

You may check on the progress of your paper by logging on to the Editorial Manager as an author. The URL is <https://www.editorialmanager.com/sej/>.

Your username is: pelukunmi4

If you can't remember your password please click the "Send Password" link on the Login page.

Your manuscript will be given a reference number once an Editor has been assigned.

Thank you for submitting your work to this journal.

Kind regards,

Editorial Manager  
Solar Energy

#AU\_SEJ#

To ensure this email reaches the intended recipient, please do not delete the above code

---

In compliance with data protection regulations, you may request that we remove your personal registration details at any time. (Use the following URL: <https://www.editorialmanager.com/sej/login.asp?a=r>). Please contact the publication office if you have any questions.

## 7.1 Abstract

Silver sulfide ( $\text{Ag}_2\text{S}$ ) nano-particles of sizes 35–50 nm were incorporated in the charge transport buffer layers to improve the collection of photo-generated current in thin film polymer solar cell (TFPSC). Both conventional and inverted device architectures were employed in the preparation of TFPSC devices using solar absorber medium composed of PTB7-Th:PC71BM blend. Zinc oxide (ZnO) and PEDOT:PSS were used as electron transport layer (ETL) and hole transport layer (HTL) in an inverted and conventional device structures, respectively. The solar cells fabricated with  $\text{Ag}_2\text{S}$  doped transport buffer layers have shown a remarkable improvement in terms of power conversion efficiency (PCE), and it is dependent on the concentration of the nano particles (NPs) in the medium. In an inverted design, the PCE have shown growth by 71.6% at concentration 0.33 wt%  $\text{Ag}_2\text{S}$  in the ETL compared to the 21 % increase in the conventional device structure. This is an important development for PSC fabricated in ambient laboratory conditions. The improved device parameters is possibly due to enhanced light absorption arising from the plasmonic effects and improved interface conditions between the active layer and the transport buffer layers, aiding better charge carrier collection. These altogether has led to noticeably enhanced short circuit current density ( $J_{sc}$ ) and slightly increased fill factor (FF). Hence, a power conversion efficiency(PCE) growth of 71.6% is recorded in the current investigation compared to a reference cell in an inverted structure. Much improved device performance was observed in conventional device structure using PEDOT:PSS hole transport layer. Possible mechanisms for the observed improved device performance due to the incorporation of silver sulfide into a PEDOT:PSS layer was thereafter proposed.

## 7.2 Introduction

Thin film polymer solar cells are among the highly sought and researched alternative renewable energy sources by virtue of their desirable qualities like low production cost, solution processability, ability to be fabricated on flexible and multiple surfaces and transparency. Bulk heterojunction (BHJ) is the most successful solar absorber design [1, 2, 3, 4, 5, 6] in which donor and acceptor polymers are mixed in a suitable solvent to form a 3-dimensional matrix blend having large-area phase-separated interfaces for dissociating excitons efficiently [7, 8]. The bid to improve the device performance of BHJ OPV devices have led to the synthesis of several donor polymers and small molecules like P3HT, PTB7, PTB7-Th, PBDTBDD, and DPP-containing materials. These are usually blended with PC61BM, PC71BM acceptors which are fullerene-based and ITIC, ITIC-Th, Y6, DTPC-IC and a host of other non-fullerene acceptors[9, 10, 11, 12, 13, 14, 15, 16].

The conventional and the inverted device architectures have also been explored to improve solar cell performances and device stability [17, 18, 19]. Interfaces and electrodes modification are critical factors that influence device operation due to their important roles in extracting charges and alleviating non-geminate recombina-

tion in the devices[20, 21]. As a result, interfacial materials, commonly called buffer or selective charge layers (HTL/ETL) are now routinely introduced during device fabrications for smoothing the device operations. Hence, after photo-absorption, exciton generation and dissociation, the dissociated charge carriers are transported to their respective electrodes through these interfacial layers. The presence of these layers also increase the internal electric field within the device which aid selective charge extraction[22], through chemical reactions, geometry modification and/or inducing interfacial charge redistribution processes [23, 24, 25, 26, 27]. Zinc oxide

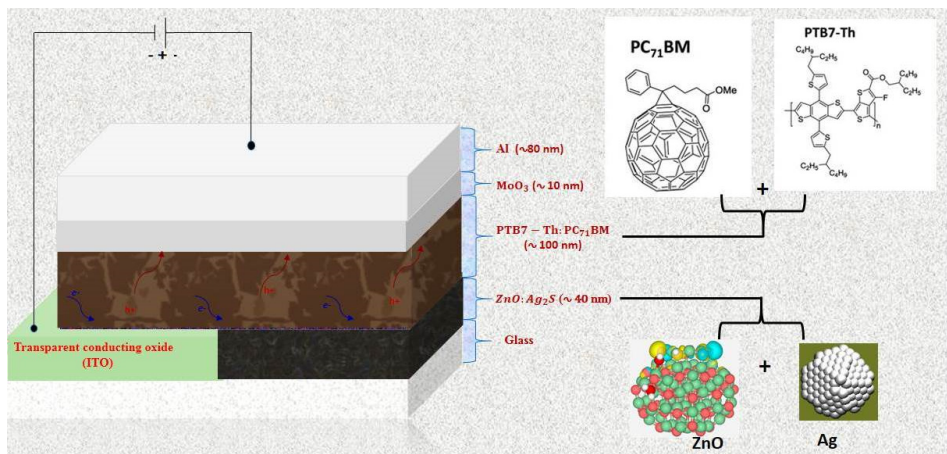


Figure 7.1: Schematic device structure of TFPSC

(ZnO) is often used in TFPSC by virtue of its favourable properties like benign synthesis process, high charge mobility, good stability and offers excellent match with energy levels. It is a widely used electron extraction/transport material[28] and effectively blocks holes in the devices leading to improved device rectification. The wide bandgap (3.4 eV)[29] of ZnO makes it an ideal optical transmitting medium for use as a transparent electrode in devices[30]. The zinc oxide films are often produced via the sol-gel processes [31, 32] in the preparation of polymer solar cell (PSC). However, the quality of the film is dependent on annealing temperature. Highly crystalline zinc oxide nanoparticles suspended in alcohol is an alternative means of making the ZnO films for device fabrication without a rigorous post-annealing procedure [33, 34]. The presence of zinc interstitials and/or oxygen vacancies makes ZnO to be n-type and hence the material exhibit a high electron mobility[35]. ZnO NPs are also widely used in manufacturing rubber, in medicine and in the food industries due to its beneficial anti-microbial and UV resistant properties[36, 37].

The incorporation of metal nano-composites into different functional layers of PSCs is an important mechanism to assist in light absorption in thickness-limited organic solar cells. The advantages can extend to improve the charge transport and collection processes through plasmon resonance phenomenon [38]. Plasmonic resonance is the oscillations of the surface electron cloud of metals or metallic composites placed in a suitable dielectric medium due to the interaction of the electron cloud to incoming electromagnetic field. These oscillations leads to local electromagnetic (EM) enhancements, scattering and local heating effects around the particles. This in turn enhance light absorption within the medium by elongating the

optical path length and increase the EM energy flow. Silver sulfide ( $Ag_2S$ ) is an n-type material that has been applied in different investigations such as in electronic devices[39, 40, 41] and photo-catalysis[42, 43]. It has been used as a photo-absorbing material in solar cells because it is non-toxic, has good absorption in the near-infrared (NIR)[44], stable against moisture and capable of multiple exciton generation (MEG)[45]. In solar cells, silver sulfide has been applied in quantum dot sensitized solar cells (QDSSCs)[39, 44, 46] and in hybrid solar cells[40] where it was employed as the electron acceptor with P3HT as the donor. Silver sulfide ( $Ag_2S$ ) has a wide spectral response due to its narrow bandgap with good opto-electronic properties. In this article, experiments were conducted to investigate the effect of  $Ag_2S$  NPs into charge transport buffer layers both in conventional and inverted structures to understand the role of the metal NPs on p- and n-type semiconductor media.

## 7.3 Materials and methods

### 7.3.1 Materials

The donor polymer, the fullerene acceptor, silver sulfide NPs, zinc oxide NPs suspension and other chemicals used in this investigation were obtained from commercial vendors and used as delivered without further chemical modification. The donor polymer, poly[4,8-bis(5-(2-ethylhexyl)thiophen-2-yl)benzo[1,2-b;4,5-b']dithiophene-2,6-diyl-alt-(4-(2-ethylhexyl)-3-fluorothieno[3,4-b]thiophene)-2-carboxylate-2-6-diyl] (PTB7-Th), and the fullerene acceptor, [6,6]-Phenyl-C71-butyric acid methyl ester (PC71BM), were supplied by Ossila Ltd, UK. The silver sulfide ( $Ag_2S$ ) powder, and the zinc oxide nanograde particles suspension in isopropanol came from SigmaAdrich, UK. Other materials like the un-patterned ITO-coated substrates, molybdenum trioxide ( $MoO_3$ ) and aluminum wire used as electrodes were obtained from other vendors. The device schematics is illustrated in Figure 7.1.

### 7.3.2 Methods

Both conventional and inverted device architectures were used in this investigation and details are available [23, 47]. The inverted devices consists of layers of materials in the sequence of ITO/ZnO w/wo  $Ag_2S$ /PTB7-Th:PC71BM/ $MoO_3$ /Al. While the conventional PSC devices have ITO/PEDOT:PSS: $Ag_2S$ /PTB7-Th:PC71BM/PFN-Br/Ag. In both cases, ITO serves as a cathode and an anode for inverted and conventional structure, respectively. ZnO layer works as ETL in this investigation where prepared with and without the inclusion of silver sulfide NPs.

ZnO is used in the form of suspension in alcohol and 1 ml ZnO were prepared in different vials for  $Ag_2S$  powders at oncentration of 0.11 wt%, 0.33 wt% and 0.55

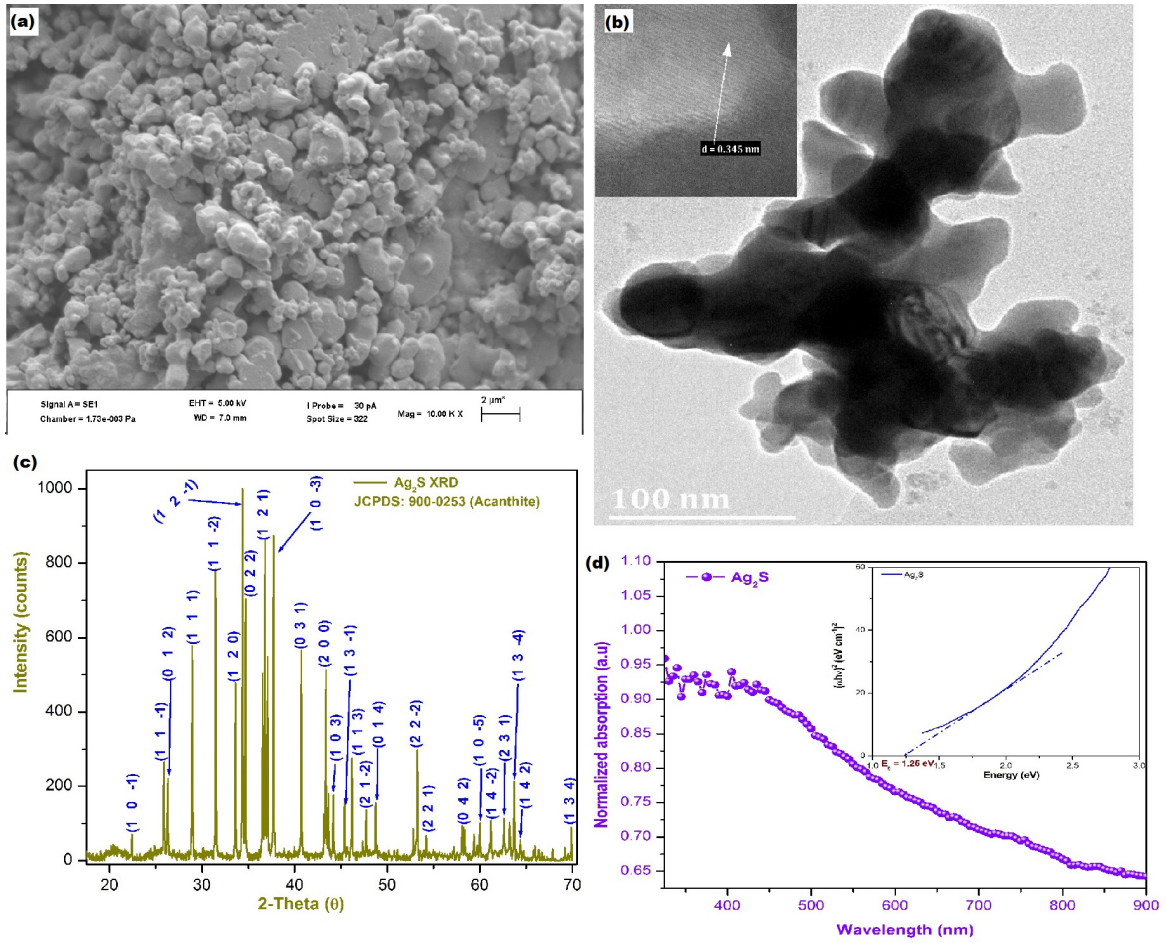


Figure 7.2: (a) The SEM (b) The HR-TEM (Inset: HR-TEM showing fringes and lattice spacing) (c) The XRD of the silver sulfide nanoparticles and (d) Optical absorption of the silver sulfide nanoparticles in de-ionized water (inset: bandgap estimation from the tauc's plot)

wt% NPs by weight. The suspension was sonicated for 1 h followed by magnetically stirred at room temperature for 3 h before commencing the spin coating of the resulting solution. After spin coating the film was dried at  $120 \text{ }^\circ\text{C}$  for 15 min. Active layer material and upper electrode deposition were carried out according to the procedure reported [23].

Water soluble PEDOT:PSS film was deposited on ITO-coated glass substrates to serve as HTL in the conventional device structure. A 1 ml PEDOT:PSS solution was prepared in different vials and different amount of  $\text{Ag}_2\text{S}$  powders were added in each vials to make 1 wt%, 3 wt% and 5 wt% nano-particles concentration followed by sonication for 1 h before the start of spin coating, and continued till all the substrates were spin-coated. Undoped HTL layers were also coated to serve as reference. The PEDOT:PSS films were thermally annealed at  $150 \text{ }^\circ\text{C}$  on hotplate for 15 min, after which the remaining upper layers were deposited according to the procedures reported in [47]. Here, poly(9,9-bis(3'-(N,N-dimethyl)-N-ethylammonium-propyl-2,7-fluorene)-alt-2,7-(9,9-dioctylfluorene))dibromide (PFN-Br) was used as the elec-

tron transport layer. 0.5 mg of PFN-Br was dissolved in 1 ml of methanol and stirred overnight. The dissolved ETL solution was then spincoated on the dried active layers and left to dry for 2 h in the glovebox before thermally evaporating silver (Ag) as the electrode under vacuum to complete the fabrication.

## 7.4 Results and discussion

### 7.4.1 Nano-particles (NPs) characterization

The morphology and average particle sizes of the  $\text{Ag}_2\text{S}$  NPs were studied with scanning electron microscopy (SEM), high resolution transmission electron microscopy (HR-TEM), x-ray diffraction (XRD) and absorption spectroscopy. The SEM, HR-TEM and XRD were taken from powder samples while the absorption spectrum was measured by dispersing the powder in deionized water. Figure 7.2 shows the SEM, HR-TEM images, the XRD patterns and the normalized absorption of the  $\text{Ag}_2\text{S}$  NPs. The SEM image (Fig 7.2a) shows spherical-shaped particles that are relatively uniformly sized. Figure 7.2b is the HR-TEM of the silver sulphide NPs, where the predominantly spherical shape and different sizes of the NPs can be seen. The NPs shapes and sizes play important roles in enhancing light-scattering processes from the buffer layers into the active layer, thereby improving the short-circuit current ( $J_{sc}$ ) due to enhanced absorption of the incident solar radiation in TFOPVs. Crystalline fringes are captured in the Fig. 7.2b inset, indicating presence of well-defined crystalline planes having a spacing of  $d = 0.345$  nm.

The XRD analysis of the Silver sulfide ( $\text{Ag}_2\text{S}$ ) nanoparticles was conducted to obtain information about its crystallographic structure. Several prominent peaks are detected on the measured XRD spectrum provided in Fig 7.2c. The XRD data were compared with standard diffraction pattern (JCPDS Card No. 900-0253) to be able to determine the structure of the NPs, with the peaks being perfectly matched with the (1 0 -1), (1 1 -1), (0 1 2), (1 1 1), (1 1 -2), (1 2 0), (1 2 -1), (0 2 2), (1 1 2), (1 0 -3), (0 3 1), (2 0 0), (1 0 3), (1 3 -1), (1 1 3), (2 1 -2), (0 1 4), (2 2 -2), (2 2 1), (0 4 2), (1 0 -5), (1 4 -2), (2 3 1), (1 3 -4), and (1 4 2) lattice planes. The diffraction patterns indicate acanthite/monoclinic structured  $\text{Ag}_2\text{S}$  with parameters  $a = 4.22900$ ,  $b = 6.93100$  and  $c = 7.86200$  Å and belongs to space group P 121/n1 1. The broadness of the peaks indicates nano-crystals formation. The average crystallites size of the particles was determined to be 44.46 nm ( $\pm 3.77$  nm) using Debye-Scherers equation provided in eq.(7.1)[48]:

$$D = k\lambda/\beta\cos\theta \quad (7.1)$$

where  $\lambda$  is the wavelength of the X-ray (1.5405 Å),  $k$  is the Scherrer constant ( $k = 0.89$ ),  $\beta$  is the full width at half maximum (FWHM) of the diffraction peak in radians and  $\theta$  is the corresponding Bragg angle at the maximum peak. Crystallites sizes ranging from 38 nm - 51 nm with the average crystallite size being 44.46 nm ( $\pm 3.77$  nm) supports the proposition that the particles are uniformly sized. These particle sizes are capable of forward light-scattering[49, 50, 51] when incorporated in thin film OPVs. Finally, the shape, size and uniformity of the NPs are similar to

those reported in literature[52, 53].

Figure 7.2d showed the optical absorption of  $\text{Ag}_2\text{S}$  powder suspension in deionized water. The absorption peak is evident in the wavelengths range from 350 to 500 nm followed by broad absorption tail which falls off monotonically towards larger wavelength regions. The broad band absorption is attributed to light scattering by the particles being in a water medium. The non-uniformity in the sizes of the nanoparticles may also be responsible for the broad band absorption. The energy bandgap of  $\text{Ag}_2\text{S}$  Fig. 7.2d (inset) was calculated using the Taucs equation (equ. 7.2) presented as follows:

$$(\alpha h\nu)^2 = \beta(h\nu - E_g) \quad (7.2)$$

where  $h$  is Planck's constant,  $\beta$  is a constant,  $\alpha$  is the absorption co-efficient and  $E_g$  is the band gap[54, 55]. The nano-particle energy band gap was determined to be 1.25 eV which is similar to values reported in the literature[52, 53, 56].

#### 7.4.2 Silver sulfide NPs in the HTL

Silver sulfide nanoparticles are incorporated in the PEDOT:PSS hole transport layer (HTL) of PBT7-Th:PC71BM solar cell and studied the effect of the nanoparticles on the overall device performance. The results were collected from the experiment performed in a controlled environment (Nitrogen-filled glovebox). This experiment, which was conducted more of out scientific curiosity than proving a scientific theory, had interesting results that were quite revealing. Poly(3,4-ethylenedioxythiophene)-poly-(styrenesulfonate) (PEDOT:PSS), is the most common and popular hole transport layer used in conventional devices due to its wide availability, non-toxicity and ease of use[57, 58, 59]. It's high work function enables PEDOT:PSS to form ohmic contact with several polymer donors and small molecules, giving it wide applicability. The poly-(styrenesulfonate) (PSS) moiety enables the material to be water soluble, however, its being an insulator simultaneously slightly reduces the electrical conductivity[58, 59]. Overall, the conductivity of the PEDOT:PSS in its pristine state is p-type. There is scarcity of literature on the incorporation of  $\text{Ag}_2\text{S}$  - a n-type material, into PEDOT:PSS - a p-type material, possibly due to the opposing conductivity. However, the  $\text{Ag}_2\text{S}$ -incorporated PEDOT:PSS HTLs used in the organic solar cells, demonstrated improved charge conductivity and better device performance than their undoped counterparts, with the doped devices PCEs improving by as much as 29% over the undoped devices, opening-up a new possibility for PEDOT:PSS doping in organic electronics.

#### Thin film optical characteristics

Figure 7.3 is the normalized absorption spectrum of the silver sulfide incorporated PEDOT:PSS HTL devices. Generally, the thin films absorption exhibited similar

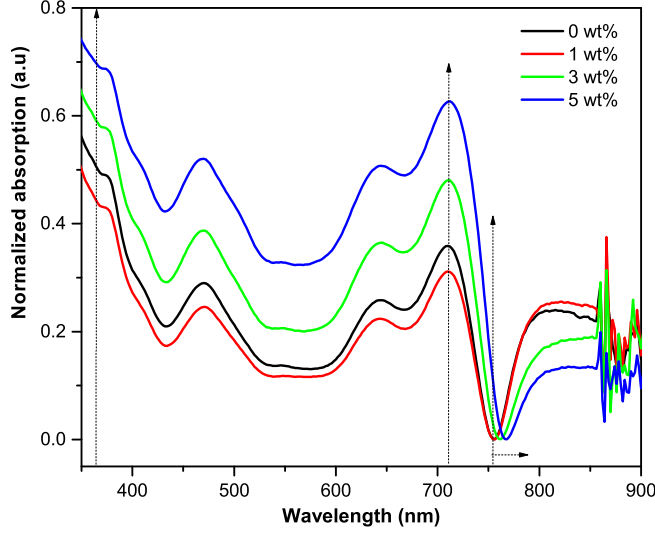


Figure 7.3: Absorption spectrum of the devices thin films at varying silver sulfide NPs doping concentration of the PEDOT:PSS HTL

Table 7.1: Device performance parameters for devices fabricated with/without  $\text{Ag}_2\text{S}$ -doped PEDOT:PSS as the hole transport layers at various doping levels, the effective device area is  $0.15 \text{ cm}^2$

Device	$V_{oc}$ (V)	$J_{sc}$ ( $\text{mA}/\text{cm}^2$ )	FF (%)	PCE (%)	$R_s$ ( $\Omega.\text{cm}^2$ )	$R_{sh}$ ( $\Omega.\text{cm}^2$ )
0 wt% doping	0.76	15.72	49.83	5.94	99.46	1731
1 wt% doping	0.71	16.38	43.37	5.11	85.34	991
3 wt% doping	0.75	16.50	52.13	6.47	73.35	2318
5 wt% doping	0.78	16.51	59.76	7.70	59.50	4568

absorption profiles with few artifacts. The incorporation of the  $\text{Ag}_2\text{S}$  in the PEDOT:PSS had noticeable effects on the absorption intensity as the doped HTL films exhibited both reduced and enhanced photo-absorption intensity than the undoped film, with the 1 wt% doped film exhibiting lower absorption than the pristine film, while the 3 wt% and 5 wt% doped films had higher absorption than the pristine film. The shoulder at approx. 365 nm wavelength appear to be slightly more pronounced in the 3 wt% and in the 5 wt% doped films but less pronounced in the 1 wt% film in comparison to the pristine film. Moreover, the pristine and the 1 wt% doped films had a 'valley' at the 754 nm wavelength, while the 'valleys' of the 3 wt% and the 5 wt% films are red-shifted by a few nanometers. Interesting, there was a reversal in the absorption intensity after the respective 'valleys' were exceeded. These observations may be attributed to interaction of the incident radiation with the nano-structures. The observed enhanced photo-absorption in the doped films may be attributed to the increase in optical path length consequent upon the light trapping and light scattering enabled by the presence of the nano-particles on the path of the incident radiation.

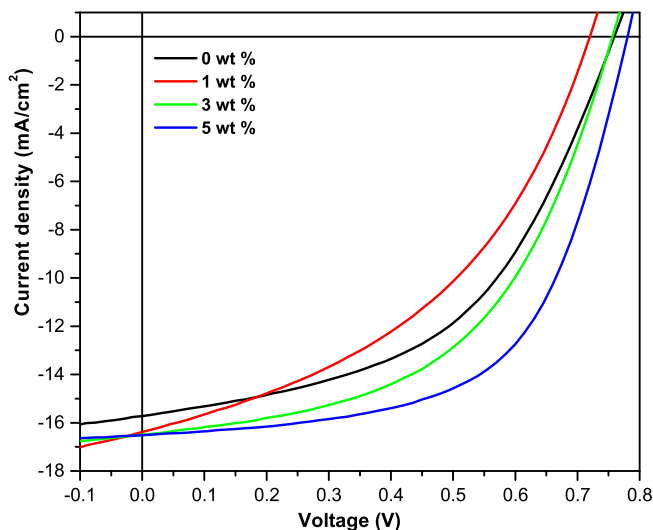


Figure 7.4: Current density - Voltage characteristics of the devices containing varying conc. of  $\text{Ag}_2\text{S}$  NPs doping in the PEDOT:PSS HTL

### Photovoltaic characteristics

Figure 7.4 is the corresponding current density - voltage (J-V) characteristics of the silver sulfide NPs doped-HTL OPV cells while Table 7.1 is the measured device characteristics. The devices' characteristics mirrored the patterns noticed for their corresponding thin films absorption as the 1 wt% doped device exhibited reduced device performance in comparison to the pristine device, while the 3 wt% and the 5 wt% doped devices exhibited superior device characteristics than the reference device. While the reference device had a 5.94% PCE, the NPs-incorporated devices had 5.11%, 6.47% and 7.70% PCEs for the 1 wt%, 3 wt% and 5 wt% devices respectively. The drop in  $V_{oc}$  in the 1 wt% device is a possible indication of energy level mis-match and an initial interfacial re-alignment which improved as the nanoparticles concentration increased[60]. The increased  $V_{oc}$  level in the higher doped devices might be indication of other chemical processes occurring in the devices. The noticed improvement in the 3 wt% and the 5 wt% doped devices' short circuit current densities may be attributed to improved charge transport and improved absorption of the solar radiation leading to a rise in photo-generated exciton. The near-field enhancement of electromagnetic radiation around the plasmonic  $\text{Ag}_2\text{S}$  NPs possibly led to better exciton dissociation and ultimately leading to overall device performance. The devices series resistance decreased from the undoped to the doped devices while the shunt resistances increased with the exception of the 1 wt% doped device. The decline in the FF of the 1 wt% device may be due to the lower shunt resistance which is an indication of leakage currents and increased non-geminate recombination in the device[61]. The external quantum efficiency of the devices is shown in Figure 7.5. All the devices exhibited broad photo-response extending from 350 to 800 nm. The 3 wt% and the 5 wt% doped devices however exhibited enhanced spectra relative to the reference device. The 1 wt% doped

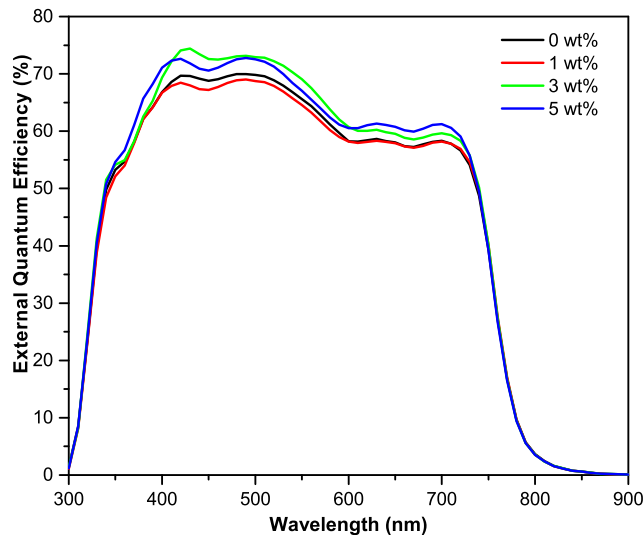


Figure 7.5: Incident photon-to-current conversion efficiency (IPCE) curves for the PEDOT:PSS-doped devices

device had slightly lower photo-response with respect to the pristine around the 400 - 550 nm wavelength range. This pattern was consistent with the measured device characteristics as well as the thin film absorption.

### 7.4.3 Silver sulfide NPs in the ETL

#### Thin film Optical characteristics

Silver sulfide doped ZnO films were used as an electron transport material to fabricate inverted PSC. The ZnO films were deposited on ITO coated glass substrate with/without Ag<sub>2</sub>S nano particles. This is followed by the deposition of photo-active layers and characterized to study the effect of the Ag<sub>2</sub>S incorporation on the absorption of the films which are as plotted in Figure 7.6. All the material depositions and fabrication were carried out under ambient laboratory conditions, except for the photo-active material thermal annealing at 50 °C in a N<sub>2</sub>-filled furnace for 1 hr, with the relative humidity being approximately 35%. Furthermore, the devices were not encapsulated. Generally, the thin films absorption exhibited similar absorption profiles with few artifacts. The incorporation of the Ag<sub>2</sub>S in the zinc oxide had noticeable effects on the absorption intensity as the doped ETL films exhibited more absorption intensity than the undoped film, with the 0.55 wt% doped film demonstrating the highest absorption intensity until around the 750 nm wavelength before being overtaken by the 0.33 wt% film after the 750 nm wavelength into the near infra-red (NIR) region. In terms of the absorption behaviour at above the 750 nm wavelength, the 0.11 wt% and the 0.33 wt% films had the least and the most interactions respectively. These overall increased absorption by the doped films may

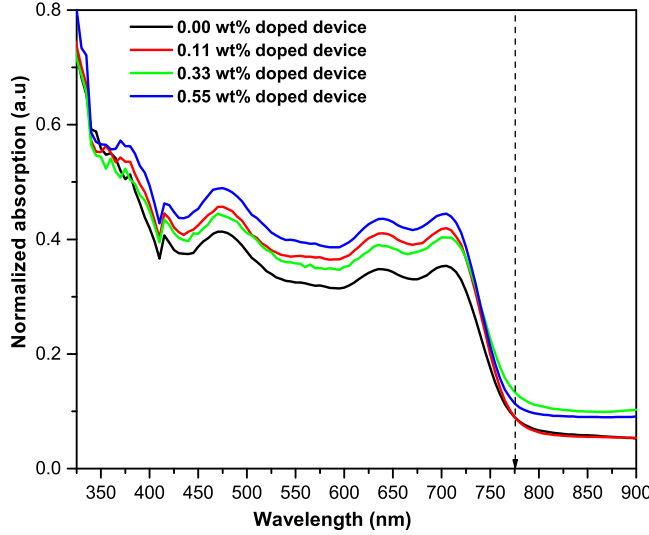


Figure 7.6: Normalized UV-Vis absorption of PTB7-Th:PC71BM active layers coated on ZnO films that had been incorporated w/w silver sulfide NPs

Table 7.2: Device performance parameters for devices fabricated with/without  $\text{Ag}_2\text{S}$ -doped Zinc oxide as the electron transport layers at various doping levels, the effective device area is  $0.035 \text{ cm}^2$

Device	$V_{oc}$ (V)	$J_{sc}$ ( $\text{mA}/\text{cm}^2$ )	FF (%)	PCE (%)	$R_s$ ( $\Omega.\text{cm}^2$ )	$R_{sh}$ ( $\Omega.\text{cm}^2$ )
0.00 wt% doping	0.74	11.13	45.72	3.77	509.6	5432
0.11 wt% doping	0.72	12.00	49.60	4.25	157.1	6186
0.33 wt% doping	0.72	18.22	49.47	6.47	112.9	4070
0.55 wt% doping	0.72	17.76	42.00	5.34	204.5	2692

be attributed to interaction of the incident radiation with the nano-structures as there might be an increase in the optical path length consequent upon the light trapping and forward light-scattering enabled by the presence of the nanoparticles on the path of the incident radiation. The increasing and then decreasing trend of absorption towards the NIR region suggests that the optimum particle concentration for absorption in this wavelength range is the 0.33 wt%, after which the excess nano-particles begin to scatter the light out of the device rather than into it.

### Photovoltaic characteristics

Figure 7.7 is the current density - voltage (J-V) characteristics of the OPV cells prepared using ZnO electron transport layers incorporated with and without  $\text{Ag}_2\text{S}$  nano-particles, while Table 7.2 is the measured device characteristics. The device characteristics for the undoped device is similar to reports from other groups where similar device configuration was fabricated in ambient environment[62, 63, 64]. The open circuit voltage of the doped devices remain unchanged after their marginal

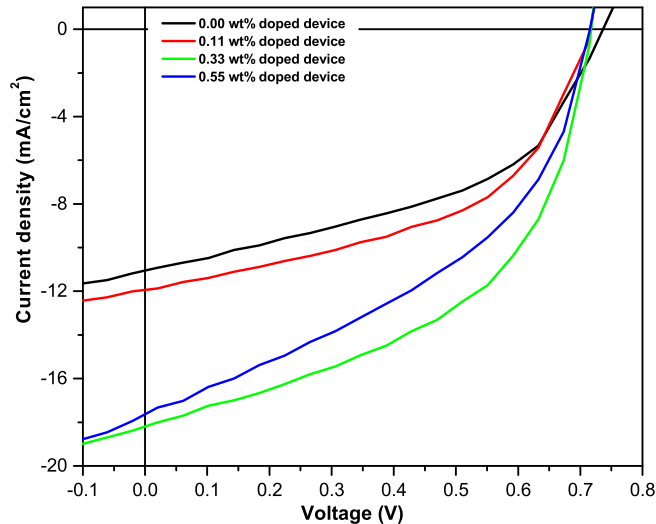


Figure 7.7: Current density - Voltage curves for the devices containing varying concentration of nano-particle doping in the Zinc oxide ETL

drop in comparison to the pristine device's  $V_{oc}$ . The slight drop may be attributed to initial energy-level re-alignment at the interfaces and/or the electrodes due to the presence of the sulfide nanoparticles[60]. All the doped devices had improved overall performance in comparison to the pristine device, with the 0.33 wt% device recording the highest power conversion efficiency (PCE) of 6.47%, a value that is over 70% higher than the undoped device PCE. Despite the generally higher absorption intensity noticed in the 0.55 wt% device, the 0.33 wt% device still exhibited a superior performance in comparison to the 0.55 wt% device, possibly due to better utilization of its internal LSPR processes. It is suspected that the increased nanoparticle concentration in the 0.55 wt% device impeded efficient charge collection thereby increasing the series resistance and reducing the shunt resistance, evidenced by the comparatively reduced short circuit current density and reduced fill factor of the 0.55 wt% device. The noticed improvement in the doped devices' short circuit current densities may be attributed to improved charge transport and improved absorption of the solar radiation leading to a rise in photo-generated excitons. The near-field enhancement of electromagnetic radiation around the plasmonic  $Ag_2S$  NPs possibly led to better exciton dissociation and ultimately leading to improved overall device performance. High shunt and low series resistances are often simultaneously desired in a solar cell[65, 66]. The shunt resistance is an indication of leakage current in the cell and depends on the films quality while series resistance results from the device's ohmic loss due to a combination of resistances from various sources such as from the active layer, the heterojunction (metal-organic) contacts, device electrodes and charge carriers extraction layers[67]. The devices series resistance decreased from the undoped to the doped devices while the shunt resistances increased with the exception of the 0.55 wt% doped device. The decline in the FF of the 0.55 wt% device may be due to the lower shunt resistance which is an indication of leakage currents and increased non-geminate recombination in the device[61].

The charge transport parameters extracted from the current under dark condition (Table 7.3) suggest that the mobilities of the doped devices were noticeably higher than that of the undoped devices, with the 0.33 wt% device exhibiting the highest mobility and field activation factor values. The generally higher mobility in the doped devices is consequence upon improved exciton dissociation and enhanced charge carriers transport in the devices, made possible by the presence of the silver sulfide nano-particles in the electron transport layer.

Table 7.3: Charge transport properties of the doped-ETL thin film organic solar cell devices.

Devices	$\mu_0$ ( $\text{cm}^2\text{S}^{-1}\text{V}^{-1}$ )	$\gamma$ ( $\text{cmV}^{-1}$ )
0.00 wt% device	$1.16 \times 10^{-5}$	$-1.93 \times 10^{-6}$
0.11 wt% device	$4.10 \times 10^{-5}$	$-6.82 \times 10^{-6}$
0.33 wt% device	$1.10 \times 10^{-4}$	$-1.83 \times 10^{-5}$
0.55 wt% device	$5.51 \times 10^{-5}$	$-9.17 \times 10^{-6}$

#### 7.4.4 Device simulation

Computer-assisted numerical simulations were further performed on the solar cells with a view to either extracting more charge transport information from the devices or further understanding and explaining the observed experimental features. Adopting an effective medium approximation in describing the OPVs, their photo-electrical characteristics was modeled with the finite-difference drift-diffusion model as implemented in the popular simulation program General-purpose Photovoltaic Device Model (GPVDM)[68, 69, 70]. The software describes the movement of charge carriers in solar cells by solving the drift diffusion (equations 7.3 and 7.4) and the charge carrier continuity (equations 7.5 and 7.6) equations in position space. The program calculates the internal electrostatic potential by solving the Poisson's equation (equation 7.7) between the anode at  $x = 0$  and the cathode at  $x = d$ . To describe the charge recombination and/or trapping, the GPVDM adopts the Shockley-Read-Hall (SRH) formalism. The software uses the transfer matrix formalism over all wavelengths to model the solar radiation absorption profiles for the devices.

$$J_n = q\mu_e n \frac{\partial E_C}{\partial x} + qD_n \frac{\partial n}{\partial x} \quad (7.3)$$

$$J_p = q\mu_h p \frac{\partial E_V}{\partial x} + qD_p \frac{\partial p}{\partial x} \quad (7.4)$$

$$\frac{\partial J_n}{\partial x} = q(R_n - G + \frac{\partial n}{\partial t}) \quad (7.5)$$

$$\frac{\partial J_p}{\partial x} = q(R_p - G + \frac{\partial p}{\partial t}) \quad (7.6)$$

$$\frac{d}{dx} \cdot \epsilon_0 \epsilon_r \frac{d\phi}{dx} = q(n - p) \quad (7.7)$$

where  $J_{n,p}$ ,  $R_{n,p}$  and  $G$  represent the electron current- and the hole current-flux densities, the electron- and the hole- recombination rates and the free carrier generation rate, respectively. Similarly,  $\epsilon_0$ ,  $\epsilon_r$ ,  $q$ ,  $n$  and  $p$  are the permittivity of free space, the relative permittivity of the photo-active layer, the elementary charge quantity, the free electron- and the free hole- populations respectively. The Maxwell-Boltzmann statistics is used to describe the free carriers.  $E_C$  and  $E_V$  are the free carrier mobility edges. They are given as  $E_C = -\chi - \phi$  while  $E_V = E_V - E_g$ , where  $\chi$  is vacuum level – LUMO mobility edge difference while the HOMO – LUMO mobility edges difference defines the  $E_g$ . More information about the software and how it describes charge carriers transport can be found in these references[68, 69, 70].

The configuration of the simulated devices is ITO/ZnO w/wo  $Ag_2S$  NPs/PTB7-Th:PC71BM/ $MoO_3$ /Ag. The ZnO serves as the ETL,  $MoO_3$  is the HTL, ITO as the cathode (front contact) and Ag as the anode. The material properties used in the simulation are listed in Table 7.4. In order to effectively reproduce the fabricated pristine and NPs-incorporated devices, as well as reflect the impact of the considerable surface roughness difference that the NPs incorporation might introduce into the active layer, the device parameters were slightly adjusted by varying the charge carriers mobilities, the conduction and the valence band densities of state (DOS) to model the various NPs doping profiles. Results of the device simulations and experimental measurements for the 0.00 wt%, 0.11 wt% and 0.33 wt% doped devices are compared in Table 7.5 and are further illustrated in Figure 7.8. The parameters for the most part are in close agreement and validates the baseline settings adopted for the simulation. Further numerical calculations were thereafter performed at these settings under varying conditions to explore within a reasonable approximation the effects of the  $Ag_2S$  NPs on the devices operation.

Figure 7.9 represents the simulated CELIV plots of the 0.00 wt%, 0.11 wt% and 0.33 wt% doped devices. The NPs-incorporated devices had higher current density peaks than the pristine device due to the increased charge carrier mobility and increased DOS which are consequences of the nanoparticles addition. The increased carriers density not only increased extracted currents but also shifted the CELIV peaks a little to the left indicating that the current density peaks were attained earlier by the doped devices. The devices current densities remain constant in the first 10  $\mu s$  before their overshoots are recorded in the next 5 - 7  $\mu s$ , after which the extracted charge carriers decreased at around the 19  $\mu s$  due to recombination events.

In the majority of disordered-BHJ OSCs, the devices are illuminated from the

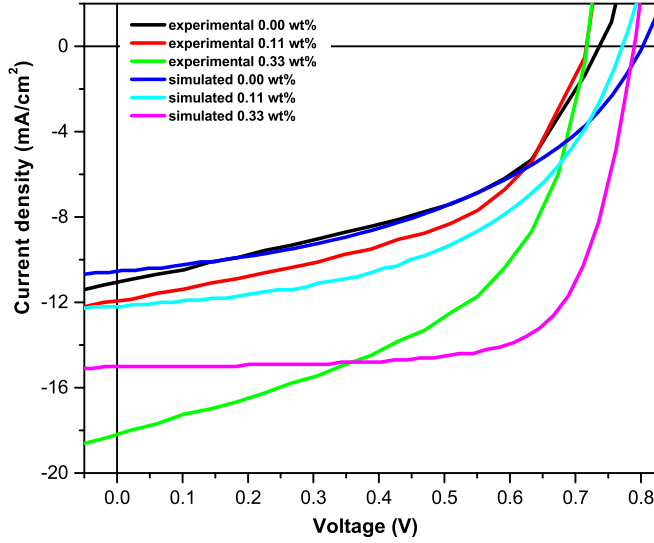


Figure 7.8: Comparison of the experimental and simulated current density - voltage (J-V) characteristics of the devices containing varying conc. of  $Ag_2S$  NPs doping in the zinc oxide ETL

substrate/ITO/transport-layer/absorber side of the device, which in the case of inverted device architecture is the ITO/ETL/absorber end and hence, electron-hole pairs are mostly created near the ITO/ETL/absorber layer interfaces. The electron-hole pairs generation often raises the recombination rate while simultaneously enhancing the rate of exciton dissociation into free charge carriers, particularly if such dissociation occur near a D/A interface. The two phenomena, recombination and exciton dissociation, play opposing roles on the magnitude of the devices extractable current density and the device performance will then depend on their net effect. The introduction of the silver sulphide NPs into the ZnO is expected to affect both the ITO and the active layer (absorber), thus, to examine the effect of the  $Ag_2S$  NPs on the ITO (the cathode), by way of the resulting recombination dynamics happening in the devices as a whole, the Fermi offsets within the cathode of the devices were varied in the simulation. The left (black) panel of Figure 7.10 is a graph of the average carrier density at maximum power ( $P_{max}$ ) of the devices while the right (blue) panel of the same figure gives the corresponding recombination time constants as a function of the Fermi offsets at the electron collecting electrode. The average carrier density for the devices exhibited a laterally inverted S-shaped pattern as the Fermi offsets increased from -0.3 eV to 0.3 eV, with the 0.33 wt% device having noticeable higher carrier density than the other two devices. The closeness in shape and magnitude of the other two devices is roughly evident in the their extracted device characteristics both experimentally and in the simulation. The appreciable jump in the experimentally observed current density (J) of the 0.33 wt% (and 0.55 wt%) device when compared with the current densities of the 0.00 wt% and 0.11 wt% devices may be partially explained by the graph of the recombination time constant as a function of the Fermi offsets. The recombination time constants of all three devices followed similar trajectory as the Fermi offsets increased from -0.3 eV

Table 7.4: Baseline parameters for the simulation of NPs-incorporated ETL solar cell

Parameters	Pristine device	NPs incorporated device
Thickness (nm)	100	100
Bandgap <sup>a</sup> $E_g$ (eV)	1.10	1.10
Electron affinity <sup>b</sup> $\chi$ (eV)	3.90	3.90
relative permittivity <sup>c</sup> $\epsilon_0$	3.90	3.90
Electron mobility <sup>c</sup> $\mu_e$ ( $cm^2/Vs$ )	$5.00 \times 10^{-4}$	varied
Hole mobility <sup>c</sup> $\mu_h$ ( $cm^2/Vs$ )	$5.00 \times 10^{-4}$	varied
Acceptor density $N_A$ ( $cm^{-3}$ )	$2.45 \times 10^{18}$	$2.45 \times 10^{18}$
Donor density $N_D$ ( $cm^{-3}$ )	$3.80 \times 10^{19}$	$3.80 \times 10^{19}$
Free electron to trapped electron ( $cm^{-2}$ )	$2.50 \times 10^{-16}$	$2.50 \times 10^{-16}$
Trapped electron to free hole ( $cm^{-2}$ )	$1.32 \times 10^{-18}$	$1.32 \times 10^{-18}$
Trapped hole to free electron ( $cm^{-2}$ )	$4.67 \times 10^{-18}$	$4.67 \times 10^{-18}$
Free hole to trapped hole ( $cm^{-2}$ )	$4.86 \times 10^{-16}$	$4.86 \times 10^{-16}$
Conduction band effective DOS <sup>c</sup> $N_C$ ( $cm^{-3}$ )	$1.00 \times 10^{18}$	$3.00 \times 10^{18}$
Valence band effective DOS <sup>c</sup> $N_V$ ( $cm^{-3}$ )	$1.00 \times 10^{18}$	$3.00 \times 10^{18}$
electron exponential tail's energy (meV)	$40 \times 10^{-1}$	$40 \times 10^{-1}$
hole exponential tail's energy (meV)	$60 \times 10^{-1}$	$60 \times 10^{-1}$

<sup>a</sup>[71], <sup>b</sup>Equals negative of the acceptor's LUMO (PC71BM), <sup>c</sup>[72]

Table 7.5: Experimental and simulated solar cells parameters for the 0.00 wt%, 0.11 wt% and 0.33 wt% doped-ETL devices.

	0.00 wt%	simulated	0.11 wt%	simulated	0.33 wt%	simulated
$V_{oc}$ (V)	0.74	0.80	0.72	0.77	0.72	0.77
$J_{sc}$ (mA/cm <sup>2</sup> )	11.13	10.55	12.00	12.18	18.22	15.04
FF (%)	45.72	44.64	49.60	50.75	49.47	72.62
PCE (%)	3.77	3.78	4.25	4.34	6.47	6.80

to 0.0 eV. Upon further increasing the Fermi offset from 0.00 eV to 0.3 eV however, the 0.00 wt% and 0.11 wt% devices continued on the trajectory and actually seem to reduce, but the 0.33 wt% device experienced a sudden and appreciable jump in the recombination time constant. The enhanced recombination time constant in the 0.33 wt% device signifies longer lifetimes before dissociated charge carriers may recombine, thus boosting their chances of getting to the electrodes for collection before recombination. The increased charge collection is thus reflected in the jump in the current density.

Solar cells are often subjected to various working temperature due to non-constant environmental conditions. The incoming radiation at different environmental temperatures induce various LSPR processes due to the nanoparticles presence and the plasmonic effects of the NPs may induce additional heating within the device. Therefore, the varying temperatures that may be attained within the devices was simulated by activating the thermal model in the GPVDM software. The temperature was varied from 290K to 400K. The right (black) panel in Figure 7.11 provides the maximum power ( $P_{max}$ ) obtainable from the solar cells while the left (blue) panel is the graph of the average carrier density at ( $P_{max}$ ) as a function of temperature. Although the 0.33 wt% device consistently had appreciable  $P_{max}$ ,

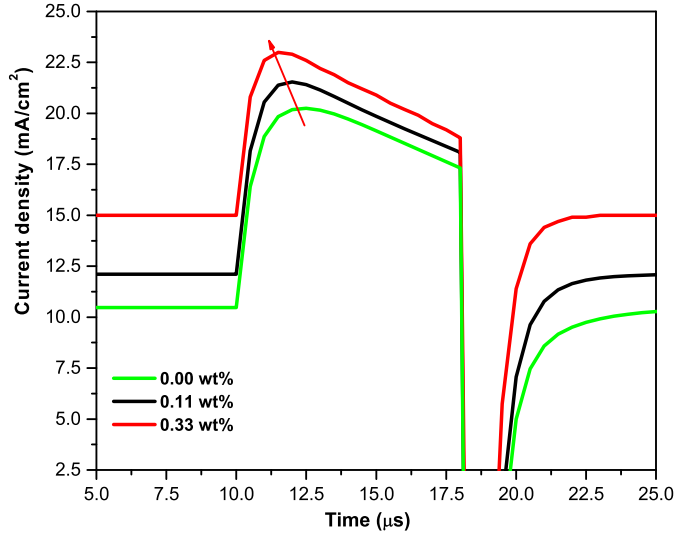


Figure 7.9: CELIV plots for the  $\text{Ag}_2\text{S}$  NPs-incorporated ETL devices

it also had the highest rate of maximum power drop as judged from the slopes of the graphs, as the three devices monotonously declined in power maximum over the entire temperature range. In contrast, the 0.33 wt% device had the lowest average carriers density at  $P_{max}$  as well as lower spread in the fluctuations of its average carriers density in comparison to the other devices. Devices average carriers density and recombination processes may be used to explain the features noted in Figure 7.11. The carriers recombination rate  $R$  is related to the carriers density  $n_p$  by the relation  $R = kn_p$ , where  $k$  is a recombination constant. Thus, increasing the carriers densities simultaneously increases the recombination rate and ultimately the extractable device characteristics exemplified by ( $P_{max}$ ) in this case. As noted in the figure, devices with the higher carrier densities had the lower  $P_{max}$ . Moreover, increase in temperature often leads to larger reverse saturation current density and a heightened recombination rate at the interfaces[73, 74] which may also contribute to the fluctuations (spread) of average carrier densities in the graph.

#### 7.4.5 Discussion on the doped-HTL devices

In summary, while the exact mechanism(s) by which the observed overall improvement in the observed doped-HTL devices wasn't investigated in this report, the authors propose few explanations as follows. First, the observed mixed responses of PEDOT:PSS to the silver sulfide incorporation may be attributed to simultaneously occurring charge sinking and charge promoting processes. Silver sulfide is a n-type material as reported by several groups, while PEDOT:PSS is popularly known as a p-type material. The incorporation of the silver sulfide NPs in the PEDOT:PSS HTL possibly led to the initial trapping (and the consequent recombination) of the separated photo-generated charge carriers at the 1 wt% doping of the HTL when the nano-particles EM field-enhancing plasmonic effects were yet to overcome the

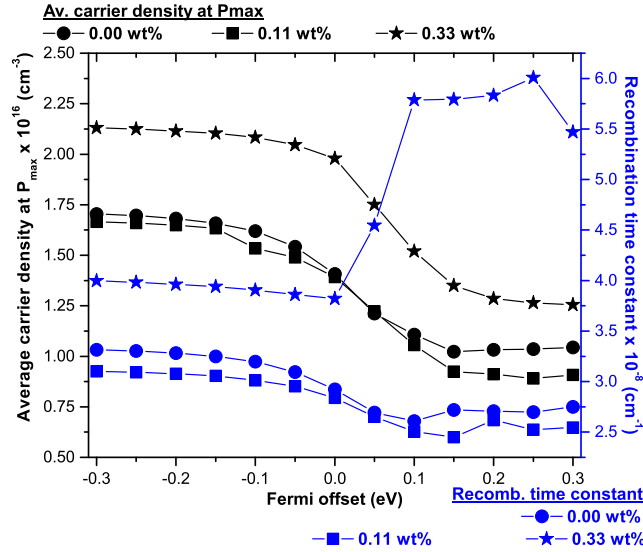


Figure 7.10: (left panel) Average carriers density at  $P_{max}$  and (right panel) Recombination time constant of  $\text{Ag}_2\text{S}$  NPs-incorporated ETL devices plotted as a function of Fermi offsets at the cathode

simultaneously occurring charge trapping/recombination events due to the opposing nature of the conductivity of the two materials in the  $\text{Ag}_2\text{S}$  NPs modified-HTL. However, as the concentration of the NPs increased, there was more plasmon-induced electromagnetic field to enhance the absorption, transport and collection of the photo-generated charge carriers, eventually overcoming the initially heightened charge trapping and recombination events. It is also suspected that other processes such as multiple exciton generation (MEG) and energy cascading events may be simultaneously occurring with the LSPR processes, which could have enhanced charge extraction events in the modified-HTLs. This is feasible because MEG have been reported in quantum dots sensitized solar cells (QDSSCs)[39, 44, 46, 75, 76, 77].  $\text{Ag}_2\text{S}$  QDs might have been produced during the sonication of the NPs+PEDOT:PSS mixture prior to spincoating as it has been reported that sonication breaks down particles to smaller sizes[78] hinting on the possibility of having some  $\text{Ag}_2\text{S}$  QDs in the HTLs. The energy cascading events[79, 80] may be possible due to the favourable energy levels of the silver sulfide in relation to the primary electron acceptor (PC71BM), indirectly turning the device into a ternary OPV device with an acceptor-donor-acceptor (A-D-A) configuration, thereby promoting electrons from exciton dissociation that were collected by the PFN-Br ETL. The feasibility of this mechanism is further based on reports in which silver sulfide was employed as the sole electron acceptor in polymer-inorganic hybrid solar cells[40, 39, 81]. The merit in this mechanism may not be unconnected with the observation that as the concentration of the nanoparticles in the PEDOT:PSS was increased, the devices parameters improved as well, in contrast to observations for most purely LSPR-enhanced performances which mostly tend to decline after some reaching certain 'optimum' concentration, as evidenced in the doped-ZnO devices earlier discussed, in which the device performance declined after the optimum 0.33 wt% was exceeded. Moreover, as the concentration of the nanoparticles increased, the likelihood of the nanoparticles getting into the active layer of the device during further processing

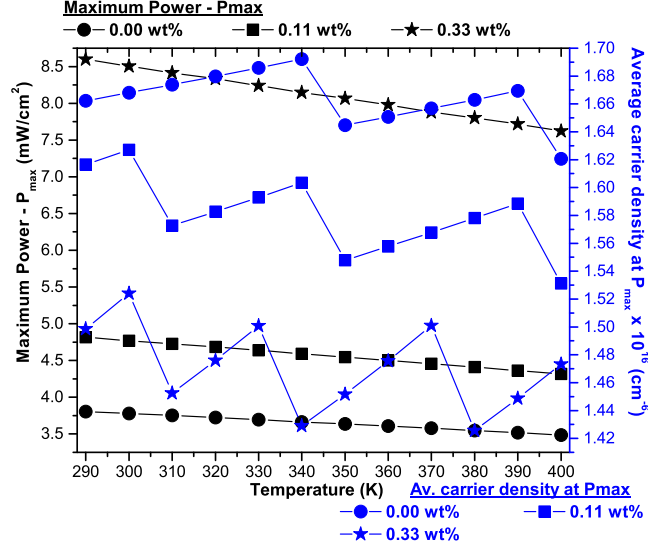


Figure 7.11: (left panel) Maximum Power -  $P_{max}$  and (right panel) Average carriers density at  $P_{max}$  of  $Ag_2S$  NPs -incorporated ETL devices plotted as a function of Temperature

(active-layer spincoating, drying, PFN-Br spincoating etc) to actually form the proposed A-D-A device configuration increases. Lastly, silver sulfide may be suitable for ambipolar applications just as black phosphorous quantum dots are [82, 83, 78], as silver sulfide nanocrystals have been demonstrated to exhibit electrical bi-stability in a bistable device fabrication [84].

## 7.5 Conclusion

In this chapter, the effect of silver sulfide nano particles on transport buffer layers of thin film polymer solar cell is investigated. The incorporation of  $Ag_2S$  on either HTL or ETL is found to have a positive impact on the performances of both conventional and inverted structured PSC. Though  $Ag_2S$  is an n-type semiconductor, however, it's positive influence in HTL of the conventional PSC was not expected; this suggest that the effects of plasmon resonance and enhanced conductance of the HTL are superior over possible charge recombination in the medium. Plasmons and photo-generated excitons interactions led to better exciton dissociation thereby limiting geminate recombination. Device simulation was used to explain noticed jump in the current densities of some of the devices. The results of the device simulations agree very well with experimental results and significant surge in the photo-current densities have been observed. Similarly,  $Ag_2S$  concentration dependent performance of PSC were recorded in an inverted structure where the NPs were used in ETL. In all cases, NPs doped transport buffer layer outperformed over the un-doped ones. Plausible mechanisms for the observed increased performances were proposed to include simultaneously occurring charge trapping/recombination and charge enhancing LSPR processes, multiple exciton generation (MEG) and charge

cascading events, and possibility of silver sulfide to be employed in ambipolar applications due to its bistable nature. This investigation has the tendency of opening up new studies possibilities for improving the 'conducting' properties of commonly used charge transport materials in solar cells.

## **Acknowledgments**

This research was supported by the National Research Foundation (NRF) (Grant numbers, 93562, 92786 and 85589), South Africa. We thank members of staff of Microscopy and Microanalysis Unit(MMU) at UKZN for several SEM and TEM studies and analysis. The authors also appreciate the Commonwealth Scholarships Commission (CSC) in the United Kingdom for awarding a split-site scholarship to M.A.Adedeji which enabled him to travel to Swansea University to conduct some aspects of this research. Efforts of colleagues at Chemistry and Materials Science Group (UKZN) and Applied Photochemistry Group (Swansea University) are also appreciated. Dr. Roderick C. I. MacKenzie at the Faculty of Engineering, University of Nottingham, United Kingdom is also warmly appreciated for making the GPVDM software freely available for our use.

# Bibliography

- [1] Chen, H.-Y., Hou, J., Zhang, S., Liang, Y., Yang, G., Yang, Y., Yu, L., Wu, Y., & Li, G. (2009). Polymer solar cells with enhanced open-circuit voltage and efficiency. *Nature photonics*, 3(11), 649-653.
- [2] Hou, J., Chen, H.-Y., Zhang, S., Chen, R. I., Yang, Y., Wu, Y., & Li, G. (2009). Synthesis of a low band gap polymer and its application in highly efficient polymer solar cells. *Journal of the American Chemical Society*, 131(43), 15586-15587.
- [3] Park, S. H., Roy, A., Beaupre, S., Cho, S., Coates, N., Moon, J. S., Moses, D., Leclerc, M., Lee, K., & Heeger, A. J. (2009). Bulk heterojunction solar cells with internal quantum efficiency approaching 100%. *Nature photonics*, 3(5), 297-302.
- [4] Liang, Y., Xu, Z., Xia, J., Tsai, S. T., Wu, Y., Li, G., Ray, C., & Yu, L. (2010). For the bright future—bulk heterojunction polymer solar cells with power conversion efficiency of 7.4%. *Advanced materials*, 22(20), E135-E138.
- [5] Mihailetchi, V. D., Xie, H., de Boer, B., Koster, L. A., & Blom, P. W. (2006). Charge transport and photocurrent generation in poly (3-hexylthiophene): methanofullerene bulk-heterojunction solar cells. *Advanced Functional Materials*, 16(5), 699-708.
- [6] Li, G., Shrotriya, V., Huang, J., Yao, Y., Moriarty, T., Emery, K., & Yang, Y. (2011). High-efficiency solution processable polymer photovoltaic cells by self-organization of polymer blends. In *Materials For Sustainable Energy: A Collection of Peer-Reviewed Research and Review Articles from Nature Publishing Group* (pp. 80-84). World Scientific.
- [7] Sariciftci, N. S., Smilowitz, L., Heeger, A. J., & Wudl, F. (1992). Photoinduced electron transfer from a conducting polymer to buckminsterfullerene. *Science*, 258(5087), 1474-1476.
- [8] Yu, G., Gao, J., Hummelen, J. C., Wudl, F., & Heeger, A. J. (1995). Polymer photovoltaic cells: enhanced efficiencies via a network of internal donor-acceptor heterojunctions. *Science*, 270(5243), 1789-1791
- [9] Cheng, Y.J., Yang, S.H., Hsu, C.S., 2009. Synthesis of conjugated polymers for organic solar cell applications. *Chem. Rev.* 2009 (109), 5868-5923. <https://doi.org/10.1021/cr900182s>.

- [10] Li, W., Ye, L., Li, S., Yao, H., Ade, H., Hou, J., 2018. A high-efficiency organic solar cell enabled by the strong intramolecular electron push-pull effect of the non-fullerene acceptor. *Adv. Mater.* 30, 1-8. <https://doi.org/10.1002/adma.201707170>
- [11] Liu, H., Li, J., Xia, L., Bai, Y., Hu, S., Liu, J., Liu, L., Hayat, T., Alsaedi, A., Tan, Z., 2018. Perfect complementary in absorption spectra with fullerene, nonfullerene acceptors and medium band gap donor for high-performance ternary polymer solar cells. *ACS Appl. Mater. Interfaces* 10, 29831-29839. <https://doi.org/10.1021/acsami.8b07993>
- [12] Qian, D., Ye, L., Zhang, M., Liang, Y., Li, L., Huang, Y., Guo, X., Zhang, S., Tan, Z., Hou, J., 2012. Design, application, and morphology study of a new photovoltaic polymer with strong aggregation in solution state. *Macromolecules* 45, 9611-9617. <https://doi.org/10.1021/ma301900h>
- [13] Wang, B., Fu, Y., Yan, C., Zhang, R., Yang, Q., Han, Y., Xie, Z., 2018. Insight into the role of PC 71 BM on enhancing the photovoltaic performance of ternary organic solar cells. *Front. Chem.* 6, 1-8. <https://doi.org/10.3389/fchem.2018.00198>.
- [14] Yu, R., Yao, H., Hong, L., Qin, Y., Zhu, J., Cui, Y., Li, S., Hou, J., 2018. Design and application of volatilizable solid additives in non-fullerene organic solar cells. *Nat. Commun.* 9, 1-9. <https://doi.org/10.1038/s41467-018-07017-z>.
- [15] Yao, Z., Liao, X., Gao, K., Lin, F., Xu, X., Shi, X., Zuo, L., Liu, F., Chen, Y., Jen, A.K.Y., 2018. Dithienopicenocarbazole-based acceptors for efficient organic solar cells with optoelectronic response over 1000 nm and an extremely low energy loss. *J. Am. Chem. Soc.* 140, 2054-2057. <https://doi.org/10.1021/jacs.7b13239>.
- [16] Usmani, B., Ranjan, R., Gupta, S. K., Gupta, R. K., Nalwa, K. S., & Garg, A. (2021). Inverted PTB7-Th: PC71BM organic solar cells with 11.8% PCE via incorporation of gold nanoparticles in ZnO electron transport layer. *Solar Energy*, 214, 220-230.
- [17] Jorgensen, M., Norrman, K., Gevorgyan, S.A., Tromholt, T., Andreasen, B., Krebs, F.C., 2012. Stability of polymer solar cells. *Adv. Mater.* 24, 580-612. <https://doi.org/10.1002/adma.201104187>.
- [18] Kim, J.Y., Lee, K., Coates, N.E., Moses, D., Nguyen, T.Q., Dante, M., Heeger, A.J., 2007. Efficient tandem polymer solar cells fabricated by all-solution processing. *Science* (80.) 317, 222-225. <https://doi.org/10.1126/science.1141711>.
- [19] Li, G., Chu, C.W., Shrotriya, V., Huang, J., Yang, Y., 2006. Efficient inverted polymer solar cells. *Appl. Phys. Lett.* 88 <https://doi.org/10.1063/1.2212270>.
- [20] He, Z., Zhong, C., Huang, X., Wong, W.Y., Wu, H., Chen, L., Su, S., Cao, Y., 2011., Simultaneous enhancement of open-circuit voltage, short-circuit current density, and fill factor in polymer solar cells. *Adv. Mater.* 23, 4636-4643. <https://doi.org/10.1002/adma.201103006>.

- [21] Park, J., Jung, C.S., 2017. Efficiency enhancement in organic polymer solar cells with ferroelectric films. *J. Korean Inst. Electr. Electron. Mater. Eng.* 30, 126-132. <https://doi.org/10.4313/jkem.2017.30.2.126>.
- [22] Aqoma, H., Park, S., Park, H.Y., Hadmojo, W.T., Oh, S.H., Nho, S., Kim, D.H., Seo, J., Park, S., Ryu, D.Y., Cho, S., Jang, S.Y., 2018. 11% Organic photovoltaic devices based on PTB7-Th: PC 71 BM photoactive layers and irradiation-assisted ZnO electron transport layers. *Adv. Sci.* 5 <https://doi.org/10.1002/advs.201700858>.
- [23] Adedeji, M. A., Hamed, M. S., & Mola, G. T. (2020). Light trapping using copper decorated nano-composite in the hole transport layer of organic solar cell. *Solar Energy*, 203, 83-90.
- [24] He, Z. C.; Zhong, C. M.; Su, S. J.; Xu, M.; Wu, H.B.; Cao, Y., Enhanced Power-Conversion Efficiency in Polymer Solar Cells Using an Inverted Device Structure. *Nat. Photonics* 2012, 6, 591-595.
- [25] You, J. B.; Chen, C. C.; Hong, Z. R.; Yoshimura, K.; Ohya, K.; Xu, R.; Ye, S. L.; Gao, J.; Li, G.; Yang, Y. 10.2% Power Conversion Efficiency Polymer Tandem Solar Cells Consisting of Two Identical Sub-Cells. *Adv. Mater.* 2013, 25, 3973-3978.
- [26] Chen, S.; Manders, J. R.; Tsang, S.W.; So, F. Metal Oxides for Interface Engineering in Polymer Solar Cells. *J. Mater. Chem.* 2012, 22, 24202-24212.
- [27] Qu, S. X.; Li, M. H.; Xie, L. X.; Huang, X.; Yang, J.G.; Wang, N.; Yang, S. F. Noncovalent Functionalization of Graphene Attaching 6,6 -Phenyl-C61-butyrac Acid Methyl Ester (PCBM) and Application as Electron Extraction Layer of Polymer Solar Cells. *ACS Nano* 2013, 7, 4070-4081.
- [28] H. Xu, F. Yuan, D. Zhou, X. Liao, L. Chen, Y. Chen, *J. Mater. Chem.* A2020, 8, 11478.
- [29] H. Liu, Z. Liu, S. Wang, J. Huang, H. Ju, Q. Chen, J. Yu, H. Chen, C. Li, *Adv. Energy Mater.* 2019, 9, 1900887.
- [30] Huang, J., Yin, Z., & Zheng, Q. (2011). Applications of ZnO in organic and hybrid solar cells. *Energy & Environmental Science*, 4(10), 3861-3877.
- [31] Y. Sun, J. H. Seo, C. J. Takacs, J. Seifter and A. J. Heeger, *Adv. Mater.*, 2011, 23, 1679-1683.
- [32] L. Znaidi, *Mater. Sci. Eng., B*, 2010, 174, 18-30.
- [33] W. J. Beek, M. M. Wienk, M. Kemerink, X. Yang and R. A. Janssen, *J. Phys. Chem. B*, 2005, 109, 9505-9516.
- [34] M. A. Ibrahem, H.Y. Wei, M.H. Tsai, K.C. Ho, J.J. Shyue and C. W. Chu, *Sol. Energy Mater. Sol. Cells*, 2013, 108, 156-163.
- [35] A. L. Roest, J. J. Kelly, D. Vanmaekelbergh and E. A. Meulenkaamp, *Phys. Rev. Lett.*, 2002, 89, 036801.

- [36] P. J. P. Espitia, N. D. F. F. Soares, J. S. D. R. Coimbra, N. J. de Andrade, R. S. Cruz and E. A. A. Medeiros, *Food Bioprocess Technol*, 2012, 5, 1447–1464.
- [37] J. Jiang, J. Pi and J. Cai, *Bioinorg. Chem. Appl.*, 2018, 2018, 1062562.
- [38] Stratakis, E., Kymakis, E., 2013. Nanoparticle-based plasmonic organic photovoltaic devices. *Mater. Today* 16, 133–146. <https://doi.org/10.1016/j.mattod.2013.04.006>
- [39] C. Chen, Y. Xie, G. Ali, S.H. Yoo, S.O. Cho, Improved conversion efficiency of Ag<sub>2</sub>S quantum dot-sensitized solar cells based on TiO<sub>2</sub> nanotubes with a ZnO recombination barrier layer, *Nanoscale Res. Lett.* 6 (2011) 462.
- [40] Y. Lei, H.M. Jia, W.W. He, Y.G. Zhang, L.W. Mi, H.W. Hou, G.S. Zhu, Z. Zheng, Hybrid solar cells with outstanding short-circuit currents based on a room temperature soft-chemical strategy: the case of P3HT:Ag<sub>2</sub>S, *J. Am. Chem. Soc.* 134 (2012) 17392-17395.
- [41] A. Tubtimtae, K.Y. Cheng, M.W. Lee, Ag<sub>2</sub>S quantum dot-sensitized WO<sub>3</sub> photoelectrodes for solar cells, *J. Solid State Electrochem.* 18 (2014) 1627-1633.
- [42] W. Jiang, Z.M. Wu, X.N. Yue, S.J. Yuan, H.F. Lu, B. Liang, Photocatalytic performance of Ag<sub>2</sub>S under irradiation with visible and near-infrared light and its mechanism of degradation, *RSC Adv.* 5 (2015) 24064-24071.
- [43] Z.C. Li, S. Xiong, G.J. Wang, Z. Xie, Z.J. Zhang, Role of Ag<sub>2</sub>S coupling on enhancing the visible-light-induced catalytic property of TiO<sub>2</sub> nanorod arrays, *Sci. Rep.* 6 (2016) 19754.
- [44] H.P. Shen, X.J. Jiao, D. Oron, J.B. Li, H. Lin, Efficient electron injection in non-toxic silver sulfide (Ag<sub>2</sub>S) sensitized solar cells, *J. Power Sources* 240 (2013) 8-13.
- [45] X.L. Zhang, J.H. Liu, E.M.J. Johansson, Efficient charge-carrier extraction from Ag<sub>2</sub>S quantum dots prepared by the SILAR method for utilization of multiple exciton generation, *Nanoscale* 7 (2015) 1454-1462.
- [46] A. Tubtimtae, K.L. Wu, H.Y. Tung, M.W. Lee, G.J. Wang, Ag<sub>2</sub>S quantum dot-sensitized solar cells, *Electrochem. Commun.* 12 (2010) 1158-1160.
- [47] Michael A. Adedeji, Rodrigo Garcia-Rodriguez, Matthew L. Davies, Yong Zhang, and Genene Tessema Mola, (2022), Plasmon-Enhanced Charge Transport Processes for Improved Collection of Photo-Current in Polymer Solar Cells, *ACS Appl. Energy Mater.* 5, 1250312512.
- [48] Jang, J., Cho, K., Lee, S. H., & Kim, S. (2008). Synthesis and electrical characteristics of Ag<sub>2</sub>S nanocrystals. *Materials Letters*, 62(8-9), 1438-1440.
- [49] Muheeb Ahmad Alkhalayfeh, Azlan Abdul Aziz, Mohd Zamir Pakhuruddin, An overview of enhanced polymer solar cells with embedded plasmonic nanoparticles, *Renewable and Sustainable Energy Reviews* 141 (2021) 110726

- [50] Baek S-W, Noh J, Lee C-H, Kim B, Seo M-K, Lee J-Y, Plasmonic forward scattering effect in organic solar cells: a powerful optical engineering method. *Sci Rep* 2013; 3:1726.
- [51] Mokkaḡati S, Beck F, De Waele R, Polman A, Catchpole K. Resonant nano-antennas for light trapping in plasmonic solar cells. *J Phys Appl Phys* 2011; 44: 185101.
- [52] Huang, H. J., Wu, J. C.-S., Chiang, H.-P., Chou Chau, Y.-F., Lin, Y.-S., Wang, Y. H., & Chen, P.-J. (2019). Review of experimental setups for plasmonic photocatalytic reactions. *Catalysts*, 10(1), 46.
- [53] Mukherjee, N., Jana, S., Gopal Khan, G., & Mondal, A. (2012). Photo-induced exciton generation in polyvinylpyrrolidone encapsulated Ag<sub>2</sub>S core-shells: Electrochemical deposition, regular shape and high order of particle size distribution. *Journal of Applied Physics*, 112(12), 124324.
- [54] Moore, P. (1968). : *Elements of X-Ray Crystallography*. *Journal of Geology*, 76(5), 611-612.
- [55] Yadav, A., & Masumdar, E. (2010). Preparation and characterization of indium doped CdSO. 2Se0. 8 thin films by spray pyrolysis. *Materials Research Bulletin*, 45(10), 1455-1459.
- [56] Hassanien, A. S., & Akl, A. A. (2016). Effect of Se addition on optical and electrical properties of chalcogenide CdSSe thin films. *Superlattices and Microstructures*, 89, 153-169.
- [57] Nardes, A. M.; Kemerink, M.; de Kok, M. M.; Vinken, E.; Maturova, K.; Janssen, R. A. J. Conductivity, Work Function, and Environmental Stability of PEDOT:PSS Thin Films Treated with Sorbitol. *Org. Electron.* 2008, 9, 727-734.
- [58] Groenendaal, B. L.; Jonas, F.; Freitag, D.; Pielartzik, H.; Reynolds, J. R. Poly(3,4-ethylene-dioxythiophene) and its Derivatives: Past, Present, and Future. *Adv. Mater.* 2000, 12, 481-494.
- [59] Po, R.; Carbonera, C.; Bernardi, A.; Camaioni, N. The Role of Buffer Layers in Polymer Solar Cells. *Energy Environ. Sci.* 2011, 4, 285-310.
- [60] Oseni, S. O., Kaviyarasu, K., Maaza, M., Sharma, G., Pellicane, G., & Mola, G. T. (2018). ZnO: CNT assisted charge transport in PTB7: PCBM blend organic solar cell. *Journal of Alloys and Compounds*, 748, 216-222.
- [61] Mola, G. T., Oseni, S. O., Kaviyarasu, K., & Maaza, M. (2017). Co-solvent additives influence on the performance of PTB7: PCBM based Thin film organic solar cell. *Materials Today: Proceedings*, 4(14), 12558-12564.
- [62] Lee, S., Seo, J., Jeong, J., Lee, C., Song, M., Kim, H., & Kim, Y. (2017). Effect of Thermal Treatment on the Performance and Nanostructures in Polymer Solar Cells with PTB7-Th: PC71BM Bulk Heterojunction Layers. *Current Photovoltaic Research*, 5(3), 69-74.

- [63] Usmani, B., Ranjan, R., Gupta, S. K., Gupta, R. K., Nahwa, K. S., & Garg, A. (2021). Inverted PTB7-Th: PC71BM organic solar cells with 11.8% PCE via incorporation of gold nanoparticles in ZnO electron transport layer. *Solar Energy*, 214, 220-230.
- [64] Datt, R., Arya, S., Bishnoi, S., Gupta, R., Gupta, V., & Khosla, A. (2019). Comparative study of PTB7: PC71BM based polymer solar cells fabricated under different working environments. *Microsystem Technologies*, 1-6.
- [65] Clarke, A. J., Luke, J., Meitzner, R., Wu, J., Wang, Y., Lee, H. K., Speller, E. M., Bristow, H., Cha, H., & Newman, M. J. (2021). Non-fullerene acceptor photostability and its impact on organic solar cell lifetime. *Cell Reports Physical Science*, 2(7), 100498.
- [66] Li, J., Liu, J., Gao, C., & Chen, G. (2011). Nanocomposite hole-extraction layers for organic solar cells. *International Journal of Photoenergy*, 2011.
- [67] Yu, H.-Z., & Peng, J.-B. (2007). Influence of the solvent and device structure on the performance of the MEH-PPV: PCBM solar cell. *Acta Physico-Chimica Sinica*, 23(10), 1637-1641.
- [68] R. C. I. MacKenzie , T. Kirchartz , G. F. A. Dobb , J. Nelson , Modeling nongeminate recombination in P3HT: PCBM solar cells, *J. Phys. Chem. C* 2011 , 115 , 9806.
- [69] R MacKenzie , J. J. Lim , S Bull , S Sujecki , A. J. Kent , E. C. Larkins , The impact of hot-phonons on the performance of 1.3  $\mu\text{m}$  dilute nitride edge-emitting quantum well lasers, *J. Phys.: Conf. Series* 2007 , 92 , 012068
- [70] Adedeji, M. A., & Mola, G. T. (2022). Numerical investigation of the effects of copper sulfide nanoparticles on hole transport layer of thin-film organic solar cells. *Journal of Computational Electronics*, 21(1), 128-136.
- [71] Luo, H., Lai, J., Wang, C., & Chen, Q. (2018). Understanding the effects of the energy band alignment at the donor/acceptor interface on the open circuit voltage of organic photovoltaic devices. *Chemical Physics Letters*, 711, 113-117.
- [72] Bendenia, C., Merad-Dib, H., Bendenia, S., Bessaha, G., & Hadri, B. (2021). Theoretical study of the impact of the D/A system polymer and anodic interfacial layer on inverted organic solar cells (BHJ) performance. *Optical Materials*, 121, 111588.
- [73] Abdelaziz, W., Shaker, A., Abouelatta, M., & Zekry, A. (2019), Possible efficiency boosting of non-fullerene acceptor solar cell using device simulation, *Optical Materials*, 91, 239-245.
- [74] Y.P. Varshni, Temperature dependence of the energy gap in semiconductors, *Physica* 34 (1) (1967) 149–154
- [75] Ka, I., Le Borgne, V., Fujisawa, K. et al. Multiple exciton generation induced enhancement of the photoresponse of pulsed-laser-ablation synthesized single-wall-carbon-nanotube/PbS-quantum-dots nanohybrids. *Sci Rep* 6, 20083 (2016). doi:org/10.1038/srep20083

- [76] Subhash Chand, A. Dahshan, Nagesh Thakur, Vineet Sharma, Pankaj Sharma, Alloyed  $\text{Ag}_2\text{SexS}_{1-x}$  quantum dots with red to NIR shift: The band gap tuning with dopant content for energy harvesting applications, *Infrared Physics & Technology*, Volume 105, 2020, 103162, doi:10.1016/j.infrared.2019.103162.
- [77] Fatemeh Doosthosseini, Abbas Behjat, Sakineh Hashemizadeh, and Naeimeh Torabi "Application of silver nanoparticles as an interfacial layer in cadmium sulfide quantum dot sensitized solar cells," *Journal of Nanophotonics* 9(1), 093092(2015). <https://doi.org/10.1117/1.JNP.9.093092>
- [78] Lin, S., Liu, S., Yang, Z., Li, Y., Ng, T. W., Xu, Z. & Lau, S. P. (2016). Solution-processable ultrathin black phosphorus as an effective electron transport layer in organic photovoltaics. *Advanced Functional Materials*, 26(6), 864-871.
- [79] Zhang, X., Shen, W., Ma, K., Huang, L., Belfiore, L. A. & Tang, J. (2021). Two dependent working mechanisms enables efficient ternary polymer solar cells with broad compositional tolerance. *Solar Energy*, 221, 512-520.
- [80] An, Q., Zhang, F., Yin, X., Sun, Q., Zhang, M., Zhang, J. & Deng, Z. (2016). High-performance alloy model-based ternary small molecule solar cells. *Nano Energy*, 30, 276-282.
- [81] Lei, Y., Jia, H., He, W., Zhang, Y., Mi, L., Hou, H. & Zheng, Z. (2012). Hybrid solar cells with outstanding short-circuit currents based on a room temperature soft-chemical strategy: the case of P3HT: Ag<sub>2</sub>S. *Journal of the American Chemical Society*, 134(42), 17392-17395.
- [82] Wang, Y., Li, J., Li, T., Wang, J., Liu, K., Jiang, Q. & Zhan, X. (2019). Black phosphorous quantum dots sandwiched organic solar cells. *Small*, 15(47), 1903977.
- [83] Lin, X., Wang, Y., Wu, J., Tang, Z., Lin, W., Nian, L. & Yi, G. (2021). Black Phosphorus Quantum Dots Based Heterostucture Boosting Electron Extraction for Non-Fullerene Organic Solar Cells Surpassing 15% Power Conversion Efficiency. *ACS Applied Energy Materials*, 4(6), 5905-5912.
- [84] Li, J., Tang, A., Li, X., Cao, Y., Wang, M., Ning, Y. & Teng, F. (2014). Negative differential resistance and carrier transport of electrically bistable devices based on poly (N-vinylcarbazole)-silver sulfide composites. *Nanoscale research letters*, 9(1), 1-5.

# Chapter 8

## Conclusion and Recommendation

Copper sulphide (CuS) and Silver sulphide ( $Ag_2S$ ) nano-particles have been used in various organic photovoltaic devices to increase the devices performance by eliciting plasmonic resonance effects in the devices. The nano-structures were incorporated into the charge transport layers of thin-film organic solar cells to aid photo-absorption and charge collection. In some of the experiments, stability studies was conducted to observe the effects of the nano-structures incorporation under prolonged shelf life time. Numerical simulation was also used to provide further insights into some of the photo-physical processes that made these enhancements possible. Six research articles have already been published in the course of this PhD work with three of the publications used in this thesis. A seventh research manuscript included in this thesis has been submitted to a journal (Solar Energy) and is presently being peer reviewed as stated in the publications pages.

p-type and n-type nano-structures have been employed in the hole transport- and in the electron transport- layers of organic devices in various investigations. The nano-particles chosen are environment friendly, inexpensive, easy to work with and can be adapted for mass production via roll-to-roll processing which is desirable for the uptake of organic solar cell technologies in the renewable energy mix.

In the first experiment, copper sulfide nano-structures were incorporated into the HTL of P3HT:PCBM solar cell, which resulted in improved device performance from 2.01% to 4.51% power conversion efficiency (PCE). The shelf-life of the CuS NPs-enhanced solar cells were significantly improved as well. The recombination and charge transport dynamics of the devices were further described using device numerical simulation. In other experiments, silver sulfide nano-particles were used in the ETL of a non-fullerene acceptor solar device, the nano-particles exhibit local surface plasmon resonance (LSPR) absorption, as well as induce intense local electromagnetic field in the polymer matrix, which is useful for exciton dissociation, leading to increased device performances at various effective device areas. Device simulation studies further showed that photo-induced dipoles at the ETL/Active layer interface in the doped devices demonstrated improved interfacial charge trans-

fer reducing charge accumulation indicating better charge transport in the doped devices. Silver sulfide nano-particles were used in a final experiment in the HTL and in the ETL of fullerene-based devices. There was significant device improvements in both cases and while the ETL-doped devices demonstrated improved performances due to the classic LSPR processes, the improvements observed for the HTL- devices were explained through a variety of charge transport processes. The behaviour of the current density characteristics of the ETL-devices was explained with device simulations studies.

## 8.1 Recommendations

Further investigation is suggested to better understand the mechanism(s) by which Silver sulphide could improve the device performance when added to PEDOT:PSS. Transient photo-voltage, Raman- and Impedance spectroscopy studies may be conducted in further experiments to better understand the photo-physical processes going on this unique device. Kelvin probe (UPS) may also be used to study the interfaces in greater detail to investigate the interfaces and the electrodes. The Silver sulphides' characteristics might also be due to the fact that silver sulphide has been demonstrated as a possible candidate for electrically bi-stable applications due to its negative differential resistance and carrier transport[1]. Stability studies of the devices were not carried out at this time. This is also an important study area to investigate the stability of the device by virtue of the p-type PEDOT:PSS, having been doped with n-type material.

Computationally, the interaction of the PEDOT:PSS and the Silver-sulphide nanoparticles in the presence of electromagnetic radiation may be studied using an appropriate density functional theory formalism to look at the interaction at the atomistic/molecular level, while specifying an appropriate solvent. Using the right exchange-correlation functionals to describe the force-fields may be the dominant challenge in running the computations due to their different levels of accuracy and computational cost[2]. Tools such as Quantum espresso, Gaussian09 or Wien2k may be deployed on a computer-cluster to run the analysis, while the time-domain dynamics may be studied with single-scale or multi-scale molecular dynamics using LAMPS, gromacs and allied tools

Silver-sulphide nano-particles was investigated in the buffer layer of a non-fullerene acceptor solar cell. A follow-up investigation with the nano-structures embedded within the active layer may equally been conducted. Agglomeration leading to traps and increased non-geminate recombinations may be the challenge in this approach, however, the use of suitable co-solvents or solvent-additives may improve the dispersion.

# Bibliography

- [1] *Li, J., Tang, A., Li, X., Cao, Y., Wang, M., Ning, Y. & Teng, F. (2014). Negative differential resistance and carrier transport of electrically bistable devices based on poly (N-vinylcarbazole)-silver sulfide composites. Nanoscale research letters, 9(1), 1-5.*
- [2] *R.O. Agbaoye, P.O. Adebambo, J.O. Akinlami, T.A. Afolabi, Smagul Zh., Karazhanov, Davide Ceresoli, G.A.Adebayo, Elastic constants and mechanical properties of PEDOT from first principles calculations, Computational Materials Science 139 (2017) 234-242.*